USARTL-TR-78-27

LEVEL II

OH-58 COMPOSITE MAIN ROTOR BLADE PRELIMINARY DESIGN INVESTIGATION

J. S. Hoffrichter
BOEING VERTOL COMPANY
A Division of the Boeing Company
P. O. Box 16858
Philadelphia, Penn. 19142

November 1978

Final Report

Approved for public release;
distribution unlimited.

Prepared for

APPLIED TECHNOLOGY LABORATORY
U. S. ARMY RESEARCH AND TECHNOLOGY LABORATORIES (AVRADCOM)
Fort Eustis, Va. 23604

APPLIED TECHNOLOGY LABORATORY POSITION STATEMENT

The preliminary design and analysis in this report provides insight into the feasibility and technical gains associated with the application of a composite main rotor blade to the OH-58 helicopter. Results from this program will be of benefit when establishing requirements and objectives for any follow-on Product Improvement Program for the OH-58 helicopter.

Mr. Harold K. Reddick, Jr., Structures Technical Area, Aeronautical Technology Division, served as project engineer for this effort.

Unclassified

SECURITY CLASSIFICATION OF THIS PAGE (When Data Entered)

REPORT DOCUMENTATION PAGE

READ INSTRUCTIONS BEFORE COMPLETING FORM

1. REPORT NUMBER: USARTL-TR-78-27
2. GOVT ACCESSION NO.:
3. RECIPIENT'S CATALOG NUMBER:
4. TITLE (and Subtitle): OH-58 COMPOSITE MAIN ROTOR BLADE PRELIMINARY DESIGN INVESTIGATION
5. TYPE OF REPORT & PERIOD COVERED: Final Report
6. PERFORMING ORG. REPORT NUMBER:
7. AUTHOR(s): J. S. Hoffrichter
8. CONTRACT OR GRANT NUMBER(s): DAAJ02-77-C-0074
9. PERFORMING ORGANIZATION NAME AND ADDRESS: Boeing Vertol Company, A Division of the Boeing Company, P. O. Box 16858 Philadelphia, Penn. 19142
10. PROGRAM ELEMENT, PROJECT, TASK AREA & WORK UNIT NUMBERS: 62209A 1L262209AH76 00 225 EK
11. CONTROLLING OFFICE NAME AND ADDRESS: Applied Technology Laboratory, U.S. Army Research & Technology Laboratories (AVRADCOM) Fort Eustis, Va. 23604
12. REPORT DATE: November 1978
13. NUMBER OF PAGES: 241
14. MONITORING AGENCY NAME & ADDRESS (if different from Controlling Office): 246p.
15. SECURITY CLASS. (of this report): Unclassified
15a. DECLASSIFICATION/DOWNGRADING SCHEDULE:
16. DISTRIBUTION STATEMENT (of this Report)

Approved for public release; distribution unlimited.

17. DISTRIBUTION STATEMENT (of the abstract entered in Block 20, if different from Report)

18. SUPPLEMENTARY NOTES

Appendix B to this report was published under separate cover with limited distribution.

19. KEY WORDS (Continue on reverse side if necessary and identify by block number)

OH-58 C/A Rotor Blade
Scout Helicopter
Composite Rotor Blade

20. ABSTRACT (Continue on reverse side if necessary and identify by block number)

This report presents the results of a design study to replace the existing OH-58 C/A Main Rotor Blade with a Composite Rotor Blade. The effort consisted of a trade study phase and a preliminary design phase. The composite construction rotor blade defined in this report in whole or in part meets the defined improvement objectives in the a[illegible] of life cycle cost, performance, reliability and maintainabil[illegible], radar reflectivity, and ballistic survivability.

DD FORM 1473 1 JAN 73 EDITION OF 1 NOV 65 IS OBSOLETE

Unclassified

SECURITY CLASSIFICATION OF THIS PAGE (When Data Entered)

403 683

SUMMARY

The OH-58C/A composite main rotor blade design is dynamically similar to the OH-58C/A metal blade in flap and chord modes, but significantly softer in the torsion mode. The section properties of the composite blade airfoil section are compared to those of the existing metal blade shown in Figure 1. The large decrease in torsional stiffness, GJ, results in a reduction in first torsional frequency to 3.8. This value is in the range of Boeing Vertol experience, and is well placed relative to other frequencies. Load, stability and blade elastic behavior effects are predicted to be satisfactory.

A spar pin wrap concept was selected as the construction method to achieve root end retention. Although estimated to be more costly to fabricate than the simple bearing design, the confidence in the inherent safety of this design drove the decision. Unidirectional Kevlar, which builds up on the leading and trailing edges of the inboard spar, is extended inboard of the pin to engage the hub latch.

The selected airfoil section shown in Figure 1 is a fiberglass/Kevlar composite "D" spar. It is a constant 13.16-inch chord, VR-7 (12%) airfoil section from the inboard transition to 90% radius. A field-replaceable Estane leading edge is provided for erosion protection which can also be configured to provide pneumatic deicing capability. Chordwise balance is attained by a wedge shaped piece of high-density radar absorbent material, CR-124, in the nose.

Because of the transparent nature of the blade and the internal geometry, only a minimum of additional radar treatment may be necessary. However, the blade is readily treatable without geometry changes to whatever extent may be deemed warranted by the increased cost. By treating materials within the basic configuration, it is felt that an 11 to 15 db reduction in RCS can be attained.

A 3° washout is added to the basic 10.6° linear twist schedule from 85% radius. Outboard of the 90% radius, the blade is tapered (3-1 taper ratio). By restricting the taper to outboard of 90% radius, stall flutter is avoided. An airfoil transition also starts at 90% radius, ending at a VR-8 (8%) airfoil at the tip. It is calculated that this tip treatment in conjunction with the change to a VR-7 airfoil will result in a 5.1% and 6.1% reduction in hover SHP, relative to the mandated baseline airfoil and the OH-58 aircraft airfoil, respectively, with insignificant degradation in forward flight performance.

The overall composite blade weight is 92 pounds as compared to the metal blade weight of 95 pounds. Centrifugal force is unchanged as the reduced weight occurs in the root end area. Because of the centrifugal force restriction, as related to the ground-air-ground cycle fatigue life of the tie-bar assembly, no additional rotor inertia is provided. However, additional rotor inertia could be provided at the expense of the tie-bar assembly retirement life.

The thick leading Kevlar nose pack provides the capability for sustaining the specified impact conditions. A copper wire imbedded behind the CR-124 material provides the path for grounding lightning. The fiberglass outer skins are the best selection for moisture resistance and repairability. There is sufficient distribution of fibers present in the 42% chord "D" spar to meet the ballistic damage criteria. The teeter weight pocket will have a 2-pound capacity. It is planned to carry 1.2 pounds of nominal weight as compared to the existing .8 pound in order to expand the capacity for repairability.

The manufacturing plan includes the automatic layup of 1-inch wide prepreg unidirectional fiber tapes, the use of prepreg broad goods to form cross-ply, and Nomex honeycomb core in the blade box. The possibility of a one cook cure was examined at length, but was not felt to be state-of-the-art with respect to a high-volume manufacturing process.

The life-cycle cost analysis was conducted using the target $3400/blade recurring cost. This projects a moderate savings of $6.7 Million dollars with a planned average service life of 10 years, and a $20.9 Million savings with a 15-year service life. These savings principally result from the large improvement in reliability and maintainability characteristics with the composite blades as compared to the existing metal blades. However, the $3400/blade recurring cost appears to be an unattainable target. At a more realistic level of blade recurring cost, a life-cycle cost savings would only be attained with a 15-year service life or an increased level of utilization beyond the projected 13 hours/month.

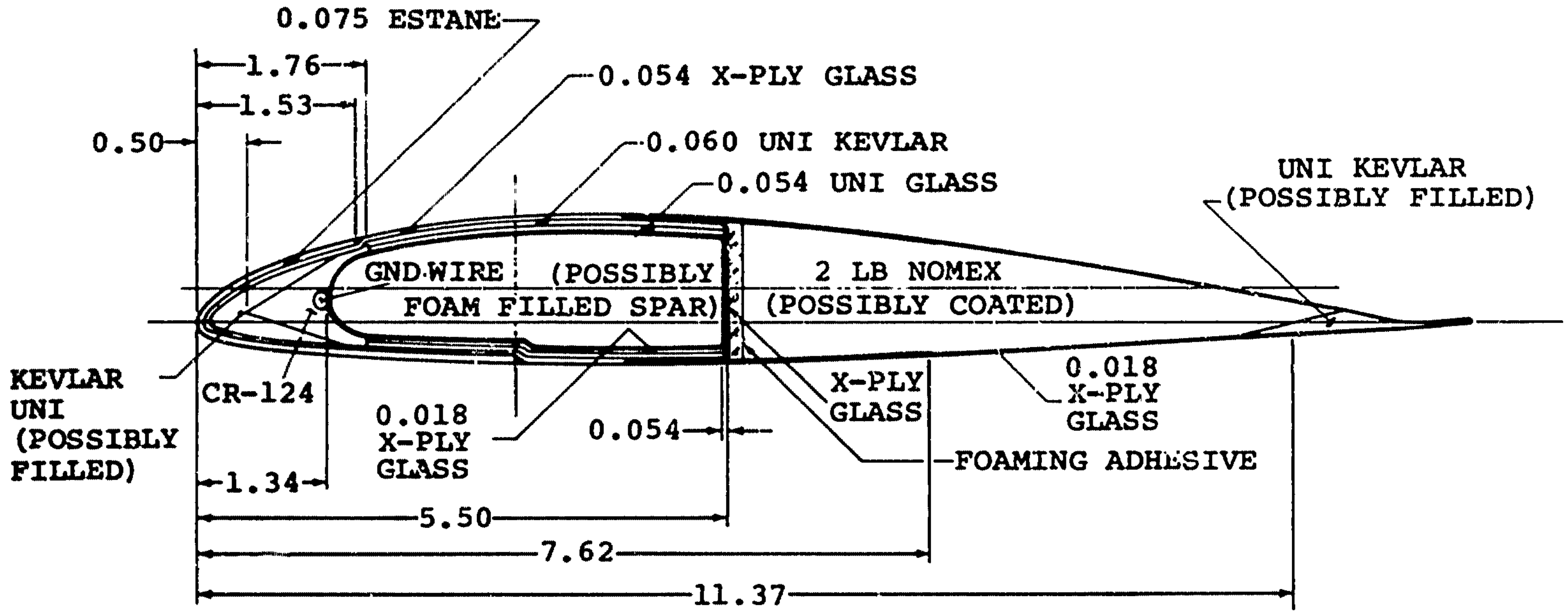

	OH-58C/A METAL	OH-58C/A COMPOSITE
WT	0.288	0.288
CG	0.25	0.25
I	2.69	3.14
EI_F	5.82	4.18
EI_C	233	233
NA	-0.05	0.97
GJ	6.98	2.34
SC	0.05	-0.03

Figure 1. OH-58C/A Composite Rotor Airfoil Cross Section and Comparative Section Properties

PREFACE

This report was prepared by the Boeing Vertol Company under U.S. Army Contract DAAJ02-77-C-0074. The work was administered under the direction of the Applied Technology Laboratory, U.S. Army Research & Technology Laboratories (AVRADCOM), Fort Eustis, Virginia, with H. K. Reddick Jr. as Project Engineer.

The Boeing Vertol Company Program Manager and Project Engineer was J. S. Hoffrichter. The Blade Designer was R. T. DeRosa. Technology support was provided by E. C. Durchlaub, Structures; M. A. McVeigh, Aerodynamics; M. W. Sheffler, Dynamics; J. D. Kelly (Boeing Seattle), Radar Reflectivity; J. J. Dougherty, Reliability and Maintainability; E. T. Keast, Ballistic Survivability; S. J. Blewitt, Life-Cycle Cost; and D. A. Richardson, Mechanical Systems. Manufacturing support was supplied by M. J. Rohner, R. J. Ford and G. H. Guckes.

TABLE OF CONTENTS

LIST OF ILLUSTRATIONS

Figure		Page

Figure		Page
47	Typical Double Plug Patch Repair.	119
48	Trim Tab Repair	119
49	Alternate 1 Schedule.	122
50	The Effect on Cost Savings of Varying the Life Cycle.	124
51	Total Cost for Varying Life Cycles (Scheduled Incorporation)	125
52	Total Costs for Two Incorporation Policies (15 Years).	127
53	Total Costs of Two Incorporation Policies (20 Years).	128
54	The Effect on Cost Savings of Varying Utilization	130
55	Radar Treated Airfoil Cross-Section . (bound separately in Appendix B)	
56	23mm API Damage Tolerance Structural Analysis . . .	134
57	Convergence of Angle of Attack for a Ballistically Damaged OH-58C/A Blade.	137
58	Effect of Damage on Root Loads.	138
59	Effect of Damage on Fixed Hub Vertical Forces . . .	139
60	Schematic of Impact Test Fixture.	144
61	Spanwise Distribution of Running Weight	146
62	Spanwise Distribution of Flapwise Stiffness	147
63	Spanwise Distribution of Chordwise Stiffness. . . .	148
64	Spanwise Distribution of Torsional Stiffness. . . .	149
65	Spanwise Distribution of C.G. Location.	150
66	Spanwise Distribution of Neutral Axis	151
67	Spanwise Distribution of Pitch Inertia.	152
68	Spanwise Distribution of Shear Center	153

Figure		Page

Figure		Page

LIST OF TABLES

1.0 INTRODUCTION

This report presents the results of a design study conducted by the Boeing Vertol Company to replace the existing OH-58 C/A aluminum main rotor blade with a composite construction blade. The helicopter thus configured is to be used for an interim scout helicopter mission over an approximate 10-year period. The desired characteristics of the OH-58 C/A replacement blade are summarized in Table 1.

The study was divided into two phases, a 2-1/2-month trade study phase and a 1-1/2-month preliminary design study phase. In the trade study phase, alternative designs were evaluated relative to the following parameters:

Life-Cycle Cost	30%
Performance	25%
Reliability and Maintainability	20%
Radar Reflectivity	15%
Ballistic Survivability	10%

The priorities of these parameters were established by the Army Technical representative. The weighting factors were submitted by Boeing Vertol and subsequently approved by the Army Technical representative. Following completion of the trade study and selection of the desired root end, outboard and tip configurations, the preliminary design study was conducted.

TABLE 1. REPLACEMENT BLADE DESIRED CHARACTERISTICS

• Compatible with Existing Hub Hardware
• No Degradation in Vibration, Stability, or Flying Qualities
• \$3400/Blade (1976 Dollars) - 3000 Blade Buy
• 3600-Hour Fatigue Life for Specified Mission Profile
• 30-Minute Survivability to 23 mm API
• 1 M^2 Peak and .001 M^2 Median ($\pm 30°$) Radar Signature
• Deicing Consideration
• 200,000-Amp Lightning Strike Capability
• 1200-Hour (Field Replaceable) Leading Edge (Sand, Dust, and Rain)
• 2.5 to -0.5 g Limit Design Load
• 6% Reduction in SHP in Hover
• 10% Increase in Rotor Inertia
• 1-Inch Pine or 0.25-Inch Copper Wire Impact Capability

2.0 FINAL BLADE DEFINITION

The details of the OH-58C/A composite blade configuration are shown in Figures 2 and 3. The blade geometry drawing is condensed and shown as Figure 4. The blade is configured at its root end to attach directly to the OH-58C/A hub without need of any adaptor devices. The existing 212-inch main rotor radius is maintained. The blade section is a constant 13.16-inch chord, VR-7 airfoil (12% thickness ratio) from the inboard end of the airfoil section to 90% radius. Outboard of 90%, the blade has a three-to-one chordwise taper and simultaneously transitions to a VR-8 airfoil (8% thickness ratio) at the tip. A 3° twist washout is added to the basic 10.6° linear twist schedule, starting from 85% radius.

The basic structural materials of the blade are unidirectional fiberglass and Kevlar, ±45° bias fiberglass and Nomex honeycomb core. The main pin attachment wrap and part of the upper and lower spar packs are of unidirectional fiberglass. All of the unidirectional fiberglass fibers present in the spar packs are continuous around the attachment pin loop. Unidirectional Kevlar is used in the upper and lower spar packs and in the leading and trailing edges. The leading- and trailing-edge Kevlar is extended inboard of the attachment pin to react chordwise moment against the hub latch. The inner and outer spar wraps and the blade box skin are of ±45° bias fiberglass.

Chopped fiberglass is used as a structural fill in both the attachment pin area and the outboard blade areas. Outboard, it is used to retain the teeter balance weight and as a filler in the nose of the tip section. A 6-pound density foam is used in the aft fairing section of the tip.

Preformed tungsten segments form the inertia and tuning weights located inside the spar, on the leading-edge side, from Stations 176.75 to 190.8 and 95.4 to 116.6 respectively. Sweep balance weights, potentially of aluminum, steel or tungsten, are attached to studs embedded in the trailing edge of the inboard blade. A teeter weight pocket is located at Station 201.5. The pocket has a greater capacity than the existing pocket in order to expand the capacity for blade repair. The pocket will have a 2-pound capacity and carry 1.2 pounds of nominal weight as compared to the current blades 0.8 pound nominal teeter weight.

The leading-edge balance weight is provided by a shaped, molded piece of CR-124, radar-absorbent material. There are additional potential radar treatments that may be added without changing spar geometry including lossy fiber treatment of resins, dielectric coating of the honeycomb core, and filling of the spar cavity with a lightweight polyurethane/carbon foam.

A .075-inch-thick Estane boot extends from Station 26.48 to within 9 inches of the tip, Station 203.5, for erosion protection. The 3:1 taper ratio results in an airfoil so small near the tip that the use of a 0.075-inch-thick Estane abrasion strip is impractical. The Estane would be half the section thickness at the tip, and any erosion would result in a significant change in the airfoil contour. Consequently, an electroformed nickel nose cap is utilized at the tip. A nickel tip cover will also be used for erosion protection. The Estane boot can optionally be configured to provide pneumatic deicing capability.

The outboard 18 inches of the blade is covered with a wire mesh screen for lightning protection. This area is the most susceptible to lightning strike as a result of static electricity buildup. Ground is provided by a 20,000 circular mill copper wire located in the leading edge of the blade.

A single stainless steel trailing-edge trim tab is provided at 75% radius. Also, stainless steel abrasion plates are bonded to the upper and lower surfaces of the fiberglass pin wraps and to the leading- and trailing-edge surfaces of the Kevlar at the hub latch.

The blade is coated with both a layer of conductive paint and a layer of acrylic lacquer. This will provide weathering protection and facilitate static electricity discharge to permit proper operation of onboard avionics equipment.

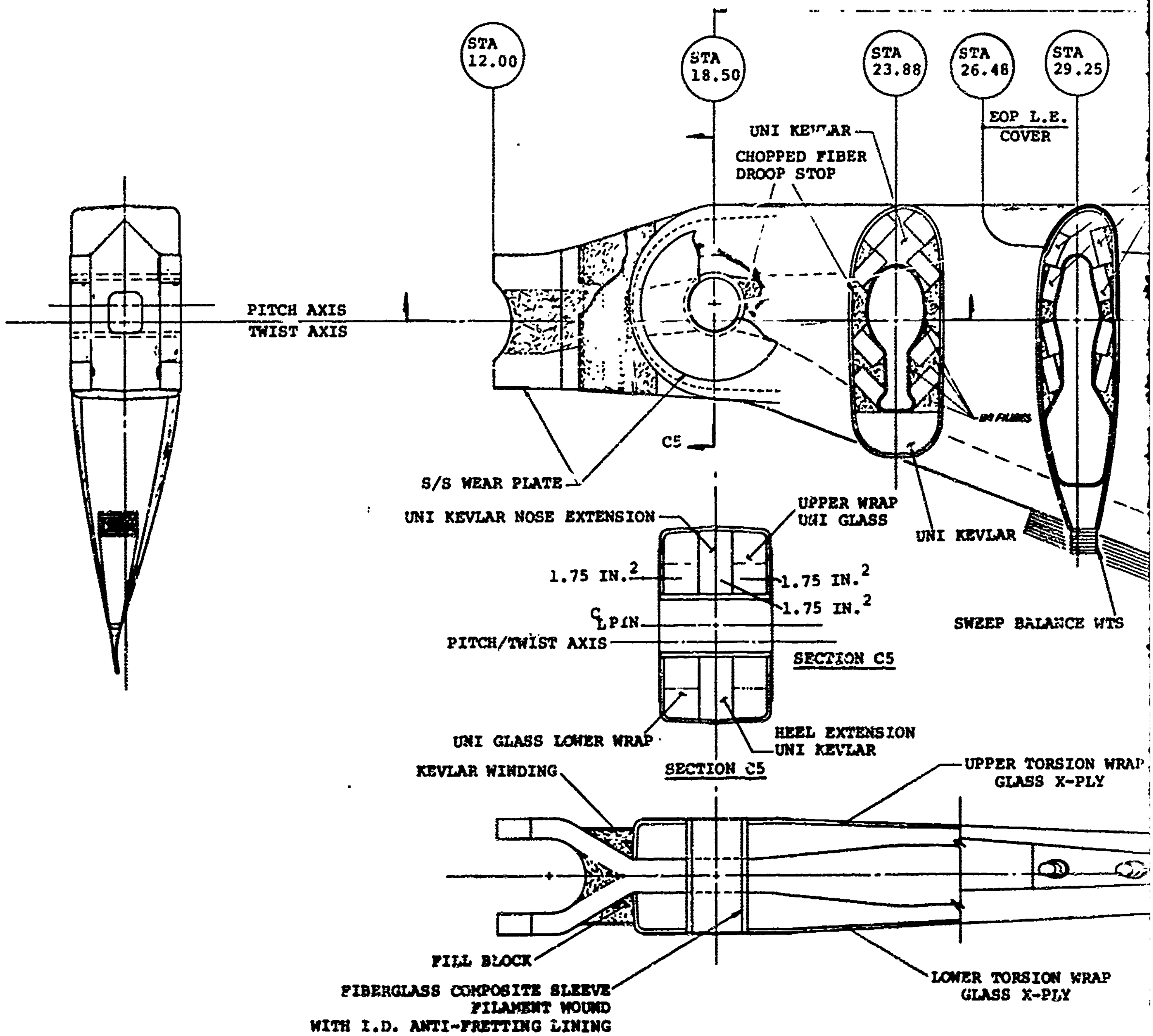

Figure 2. Details of Inboard OH-58C/A Composite Blade

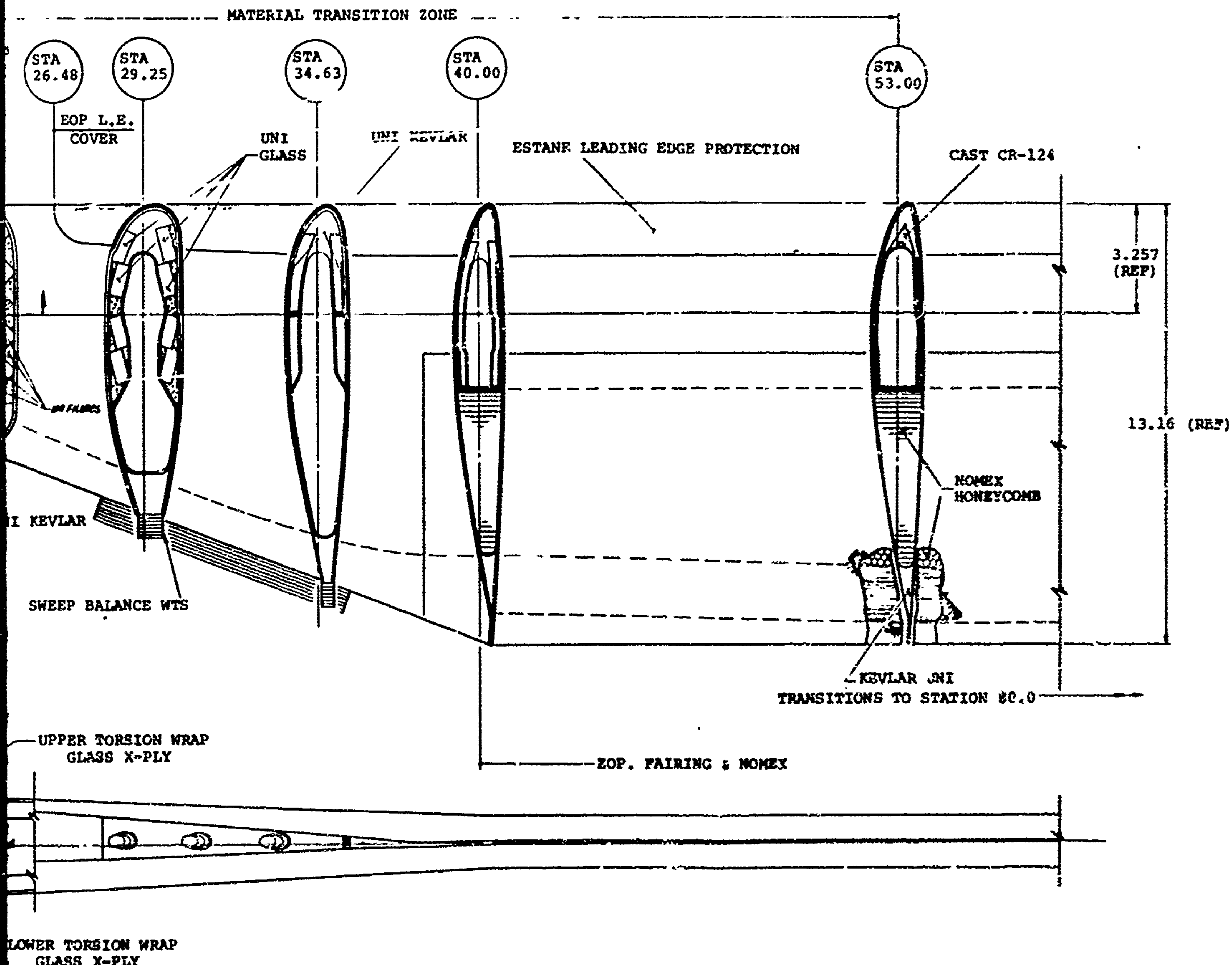

TWIST OMITTED

2

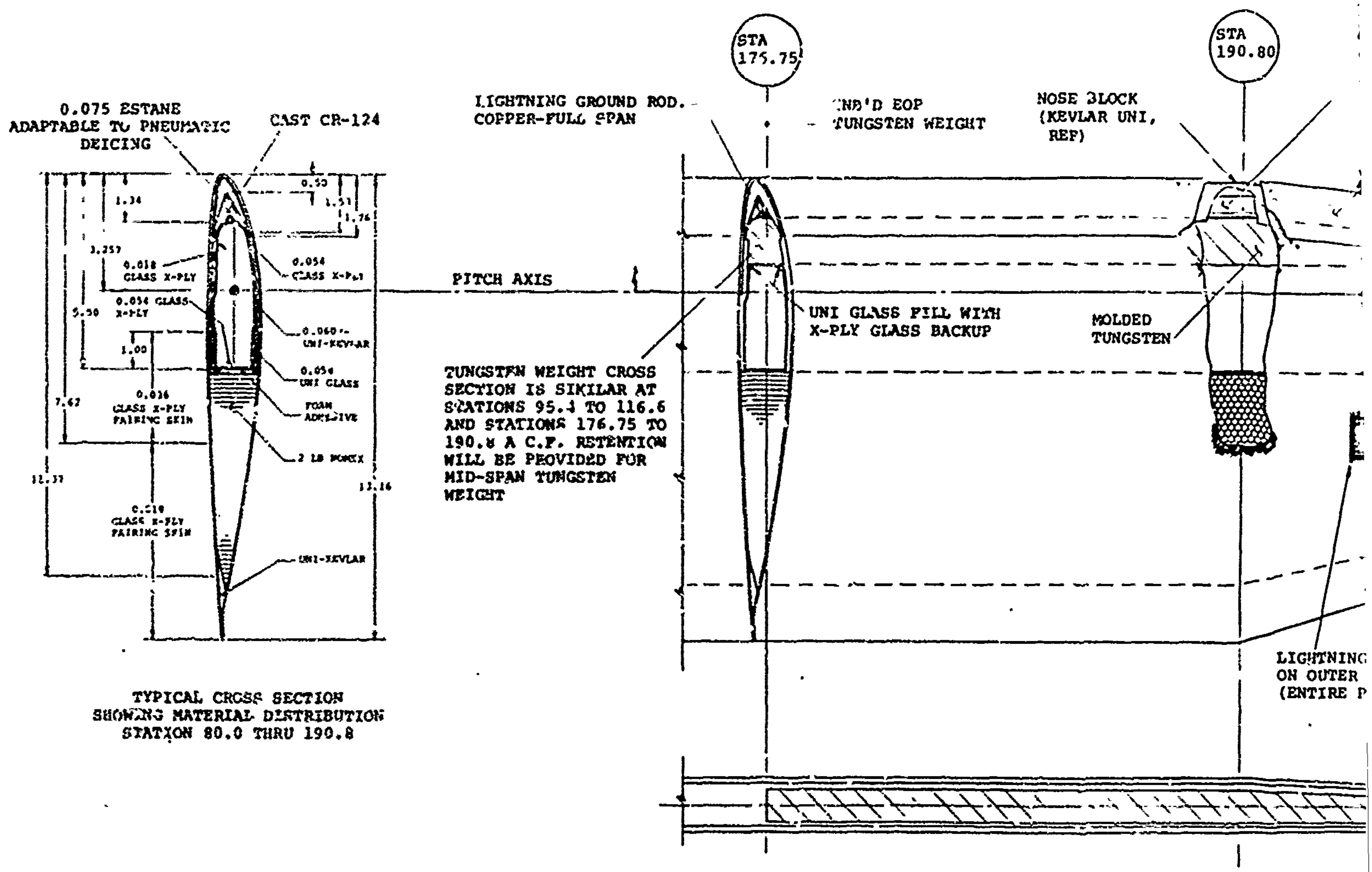

Figure 3. Details of Outboard OH-58C/A Composite Blade

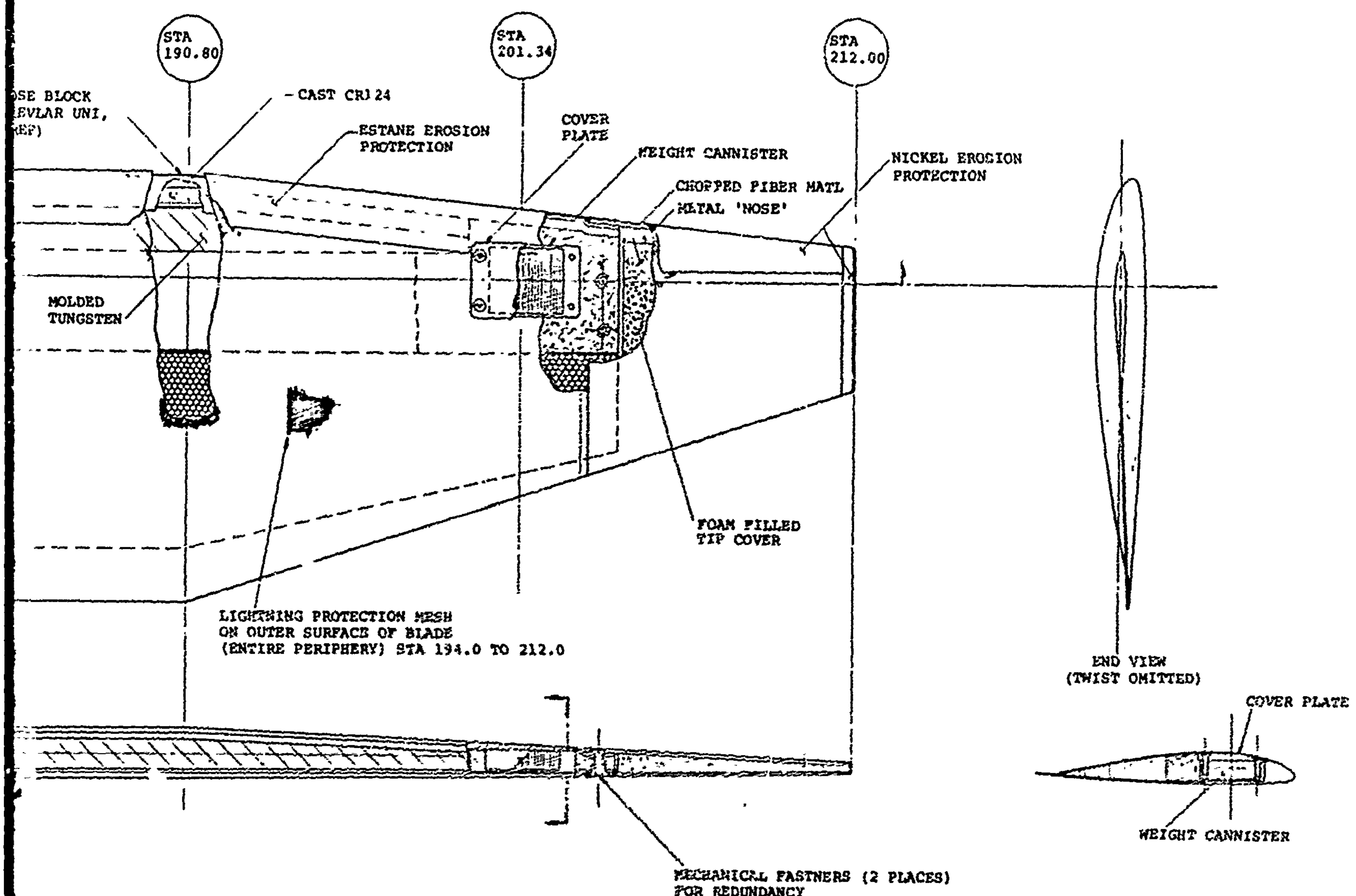

STA 190.80
STA 201.34
STA 212.00
OSE BLOCK
EVLAR UNI,
EF)
CAST CRJ 24
ESTANE EROSION PROTECTION
COVER PLATE
WEIGHT CANNISTER
CHOPPED FIBER MATL
METAL 'NOSE'
NICKEL EROSION PROTECTION
MOLDED TUNGSTEN
FOAM FILLED TIP COVER
LIGHTNING PROTECTION MESH ON OUTER SURFACE OF BLADE (ENTIRE PERIPHERY) STA 194.0 TO 212.0
END VIEW (TWIST OMITTED)
COVER PLATE
WEIGHT CANNISTER
MECHANICAL FASTNERS (2 PLACES) FOR REDUNDANCY

2

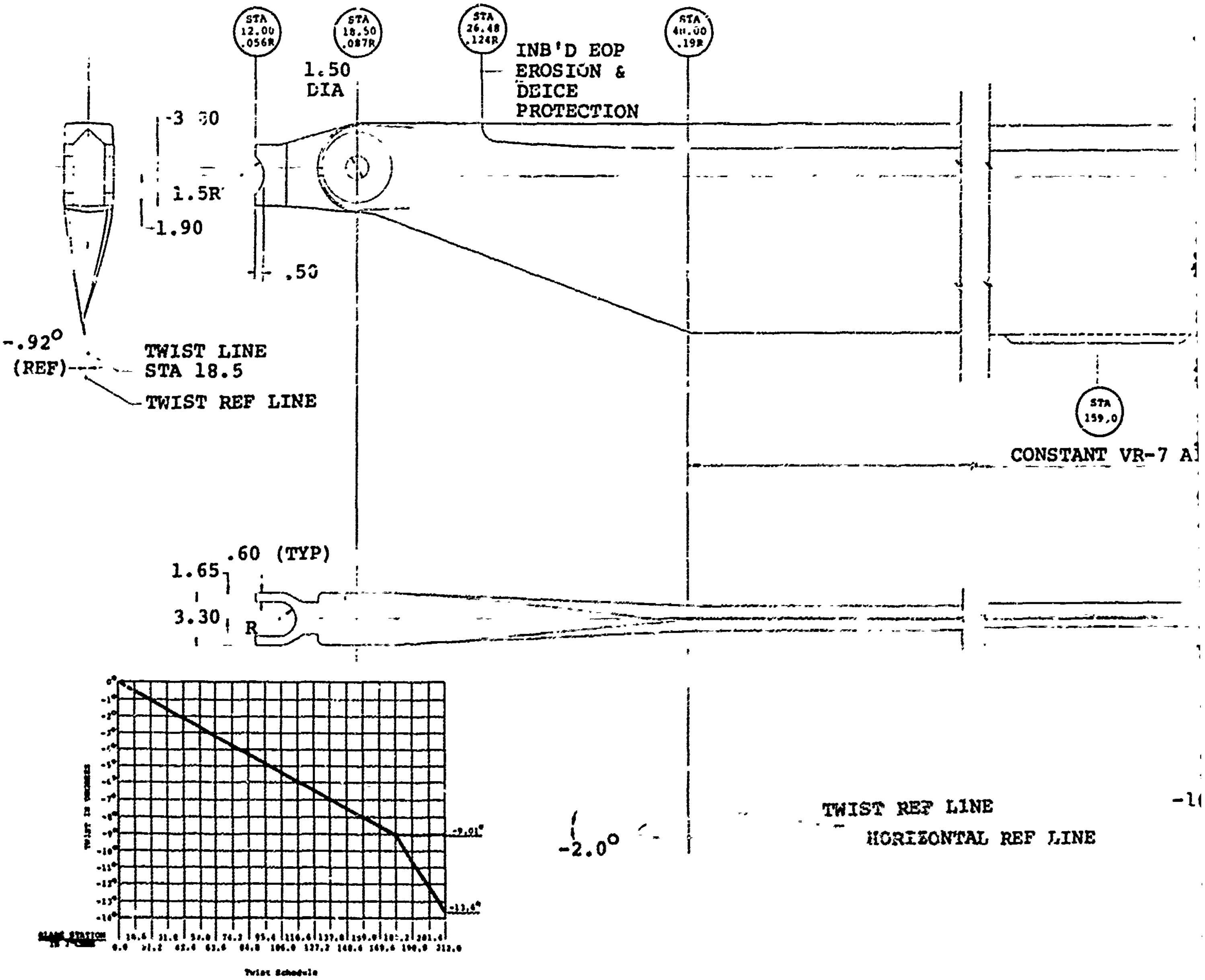

Figure 4. OH-58C/A Composite Blade Geometry

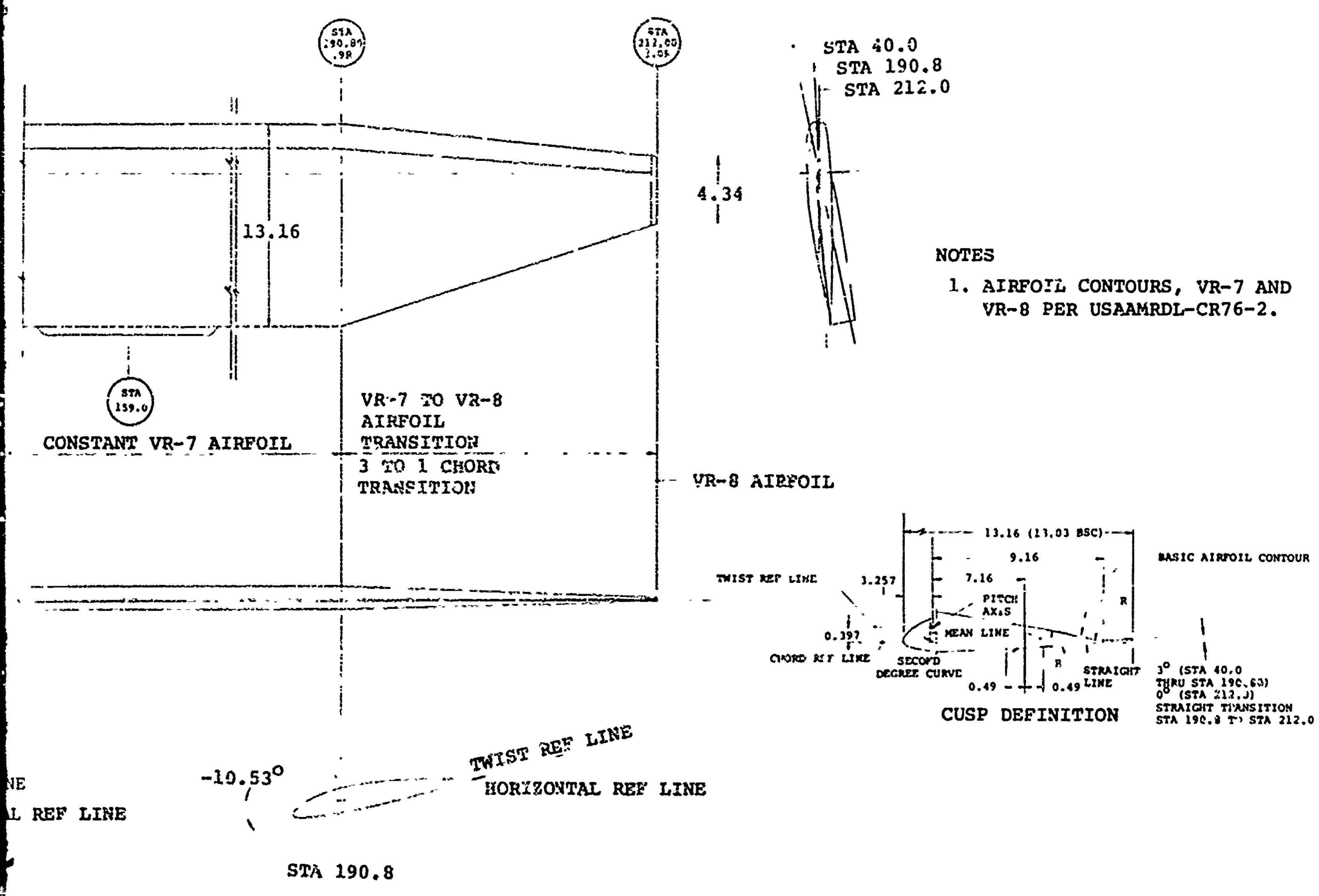
STA 40.0
STA 190.8
STA 212.0
4.34
13.16
STA 159.0
CONSTANT VR-7 AIRFOIL
VR-7 TO VR-8 AIRFOIL TRANSITION
3 TO 1 CHORD TRANSITION
VR-8 AIRFOIL
NOTES
1. AIRFOIL CONTOURS, VR-7 AND VR-8 PER USAAMRDL-CR76-2.
13.16 (13.03 BSC)
9.16
7.16
BASIC AIRFOIL CONTOUR
TWIST REF LINE
3.257
PITCH AXIS
MEAN LINE
R
0.397
CHORD REF LINE
SECOND DEGREE CURVE
STRAIGHT LINE
0.49
0.49
CUSP DEFINITION
-10.53°
TWIST REF LINE
HORIZONTAL REF LINE
L REF LINE
STA 190.8

3.0 TRADE-OFF ANALYSIS

This section presents the rationale and results of the trade-off analysis as defined by Task I of the OH-58 aircraft composite main rotor blade preliminary design investigation. The trade-off analysis was conducted relative to the evaluation parameters of Table 2. The priorities of these parameters were established by the Army technical representative. The weighting factors were then submitted by Boeing Vertol as part of the plan of performance and subsequently approved.

TABLE 2. EVALUATION PARAMETERS

1.	Life-Cycle Cost	30%
2.	Performance	25%
3.	R&M	20%
4.	Radar Reflectivity	15%
5.	Ballistic Survivability	10%

An additional category "technical risk" was proposed by Boeing Vertol as a trade study parameter, to be used principally in consideration of differences from the physical properties of the baseline metal blades. Following discussions with the Army technical representative, the use of this parameter was rejected. It was rejected on the basis that changes in physical properties were acceptable, if necessary, to accomplish the other design goals and did not in themselves present technical risks.

The variables of blade chord, twist, and airfoils were examined in the performance analysis with the objective of attaining a 6% reduction in hover SHP with little or no degradation of forward flight performance. The options that were used to achieve this target were increased twist (or local tip washout), changes to the airfoil, and chord variation by tip taper.

Four configurations of blade construction in the airfoil region were detailed and examined: all-fiberglass, fiberglass/kevlar, fiberglass with a stainless steel leading edge, and graphite/fiberglass. Each was potentially in a "C" or "D" spar configuration.

Varying methods of root end retention were examined, including a simple bearing design and three pin wrap designs. In conjunction with these variations of pin attachment, the problem of the blade inboard extension required to react chordwise moment was examined.

The design of the tip section of the blade is strongly influenced by the planform taper required for improved hover performance. An accessible teeter weight pocket and the provision for bag removal following curing are also major considerations.

It is noted that absolute values used in the life-cycle cost study are rough estimates. In this phase of the study, interest was in a comparative analysis only.

3.1 Outboard Section

3.1.1 Concepts

Four configurations of blade construction, of VR-7 profile, were detailed and examined, relative to the criteria listed in Table 3. The specific concepts, each considered as both a "C" or "D" spar, are:

- All Fiberglass
- Fiberglass with Kevlar Stiffening
- Fiberglass with Stainless Steel Nose Cap
- Graphite with Fiberglass

3.1.1.1 All Fiberglass

The all fiberglass configuration was quickly eliminated when it was seen that the stiffness criteria of Table 3 could not be met without greatly exceeding the existing section weight of .288 lb/in.

TABLE 3. STIFFNESS AND FREQUENCY DESIGN CRITERIA

• No Reduction in ωC_1
• No Degradation in Critical Flap Frequencies
• Keep atic Droop Less Than 12 Inches
• Keep $\omega T_1 > 3.5$
• No Increase in Section Weight

3.1.1.2 Fiberglass with Kevlar

The fiberglass/Kevlar candidate (Figure 5) was conceived as a potential radar treatable configuration. Consistent with that thinking, it was given an Estane leading edge, which can include a pneumatic deicing system. Instead of the traditional

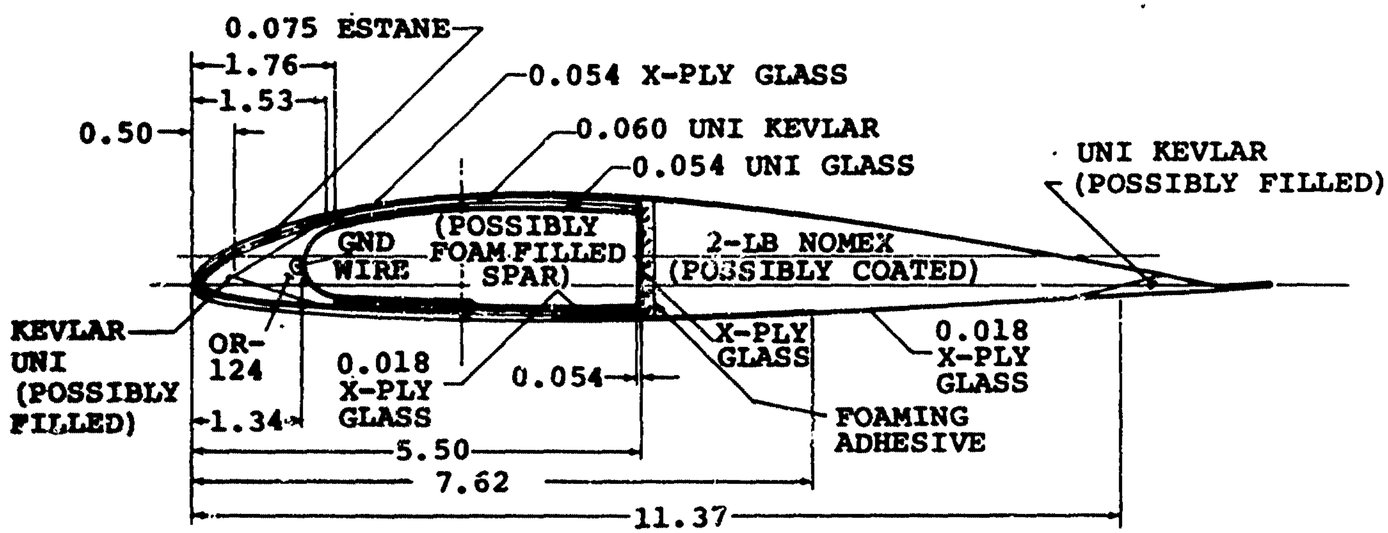

	OH-58C/A METAL	OH-58C/A COMPOSITE
WT	0.288	0.288
CG	0.25	0.25
I	2.69	3.14
EI_F	5.82	4.18
EI_C	233	233
NA	-0.05	0.97
GJ	6.98	2.34
SC	0.05	-0.03

Figure 5. Fiberglass-Kevlar Cross Section

nose weight materials, radar absorbent CR-124 material was used and formed into a favorable shape for radar reflectivity.

The outer skin is of x-ply fiberglass. The leading edge and trailing edge each contain packs of unidirectional Kevlar. Uni-Kevlar is also employed in conjunction with uni-fiberglass in the upper and lower spar packs. The inner skin and spar heel are also of fiberglass x-ply. A copper wire is located behind the CR-124 material for lightning protection. A 2-pound Nomex core is utilized in the aft fairing.

Without changing the airfoil construction, this blade is amenable to considerable development for improved radar reflectivity. This could include treating of the Kevlar resin, coating the core material, or even filling the spar with a lightweight radar absorbent material. The radar benefit of these treatments can only be assessed quantitatively by test. The extent of treatment desired vs. the cost of achieving it can be traded at that time.

The physical properties of this configuration as compared to the OH-58C/A blade are shown in Figure 5. The most noticeable difference is in torsional stiffness, which is reduced from 6.98 to 2.34 x 10^6 lb-in.^{2}. The implication of this change as well as the others will be discussed in Section 3.1.3.

3.1.1.3 Fiberglass w/Stainless Steel Nose Cap

The fiberglass with stainless steel nose cap configuration (Figure 6) has all fiberglass skins and spar, and only Kevlar in the trailing edge wedge. The variable thickness stainless steel nose cap performs the functions of erosion shield, leading edge balance weight, lightning conductor and contributor to the stiffness. An electrical deicing blanket is located under the nose cap. A 2-pound Nomex core is utilized in the aft fairing.

The physical properties of this configuration as compared to the OH-58C/A blade are shown in Figure 6. Some differences exist in torsional stiffness (GJ), pitching inertia (I), and flapwise stiffness (EI_F).

3.1.1.4 Graphite/Fiberglass

The graphite/fiberglass blade configuration, Figure 7, was designed with the objective of matching all OH-58C/A blade physical properties. Inner and outer skins are of graphite cross-ply. The spar consists of graphite and fiberglass uni-packs, as does the nose block. Only a small quantity of graphite uni is required in the trailing edge to achieve the desired chordwise stiffness, and as a result, no leading edge weight is needed to attain an acceptable C.G. An Estane leading edge utilizing a pneumatic deicing system is shown in

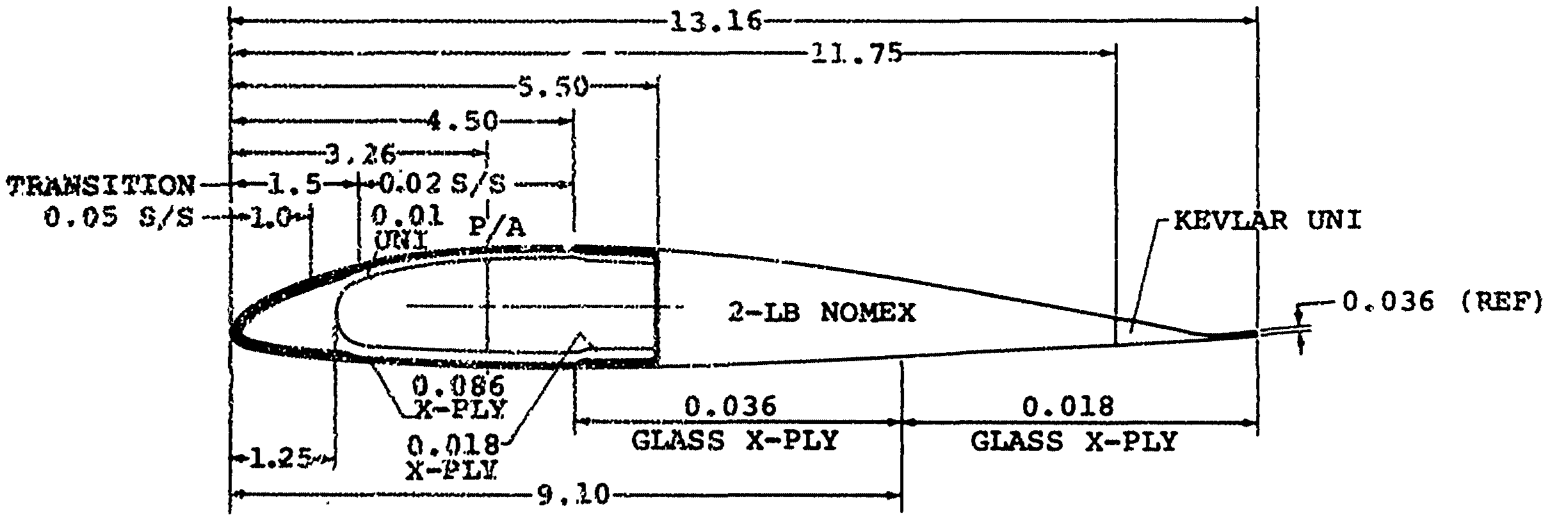

	METAL	COMPOSITE
WT	0.288	0.288
CG	0.25	0.192
I	2.69	2.95
EI_F	5.82	5.48
EI_C	233	246
GJ	6.98	4.84
SC	0.05	-1.38

Figure 6. Fiberglass-Stainless Steel Nose-Cap Cross Section

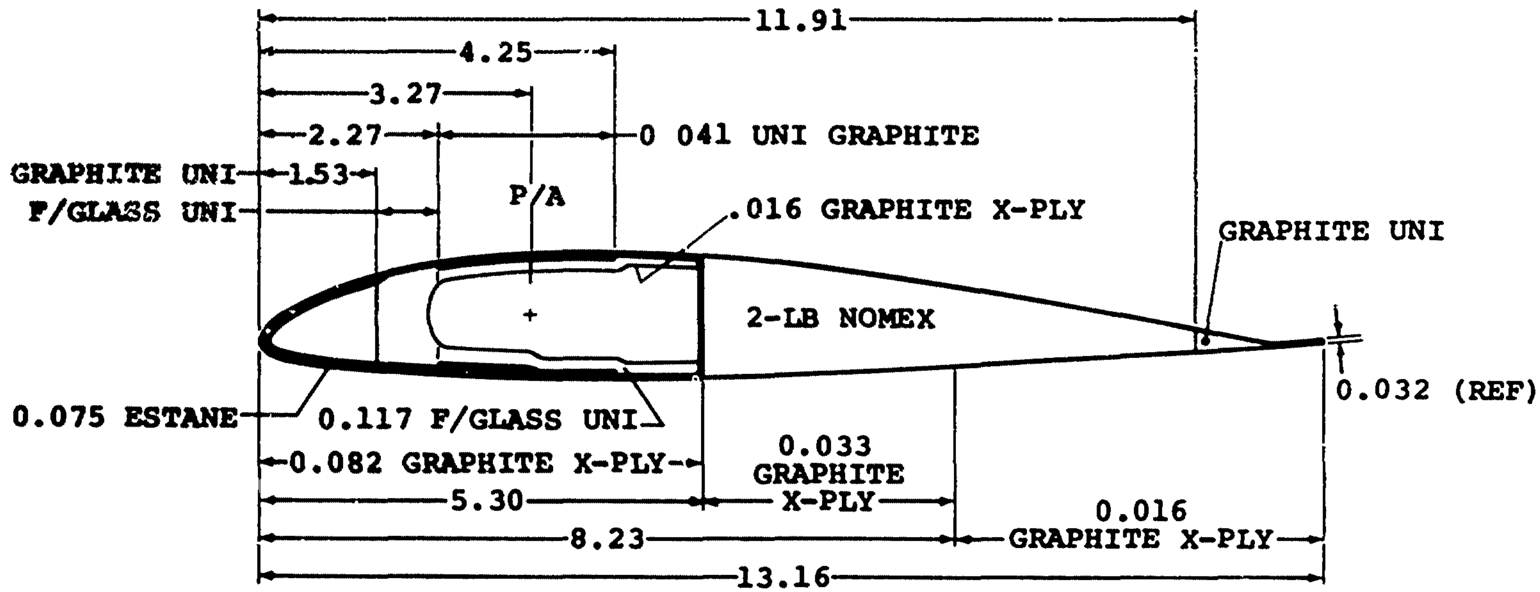

	METAL	COMPOSITE
WT	0.288	0.285
CG	0.25	0.137
I	2.69	2.41
EI_F	5.82	5.84
EI_C	233	216
GJ	6.98	7.12
SC	0.05	-0.31

Figure 7. Graphite-Glass Cross Section

Figure 7; but a thin, stainless steel leading edge of the same chord coverage, with an electrical deicing system could be substituted. Since a graphite airfoil is as untreatable as a metal airfoil for radar reflectivity, a stainless steel nose cap would not further degrade radar reflectivity.

3.1.2 "C" vs "D" Spar

Each of the configurations described could potentially be constructed as either a "C" or "D" spar. The decision was made to use a "D" spar for the following reasons:

1. The "D" spar presents the possibility of a single cure manufacturing process, but certainly requires no more than a two-cure process
2. The core in the "D" spar configuration was less costly
3. Using a bag to cure the spar, rather than relying on core backpressure is more dependable
4. We have more experience with "D" spar fabrication
5. A "D" spar presents slightly better ballistic survivability

3.1.3 Frequencies, Loads, Vibration and Stability

Table 4 displays the comparative frequencies, and Table 5 the comparative high-speed level flight loads predicted for the candidate airfoil sections as compared to the OH-58C/A baseline. No separate column is presented for the graphite/glass configuration, since all physical properties are matched to the baseline. The fixed system hub forces on Table 5 are the indicator of vibration effects. It is noted that this comparison assumes no change in root end or tip physical properties from the existing OH-58C/A blade.

Both the glass/Kevlar and glass w/S.S. nose cap configurations have a reduction in flapwise stiffness (EI_F) as compared to the baseline blade. As seen in Table 4, this results in an increase in static droop (1 g deflection) but it does not have a significant reduction in torsional frequency. First, torsional frequency (ω_{T1}) is reduced from 6.4 on the baseline blade to 4.22 and 5.63 on the candidate configurations respectively. These values are in the range of Boeing Vertol experience: YUH-61A = 3.7, CH-46E = 5.8, YCH-47D = 4.9. The lower torsional frequencies are also placed satisfactorily relative to any adverse coupling effects with other frequencies. Table 5 shows no impact of pitch link loads (PLL) nor is there a large effect on live blade twist. Some change in control input is anticipated, approximately one degree or less of cyclic at the rotor head.

The several different composite rotor blade airfoil constructions being proposed are predicated upon maintaining the same chord bending dynamic characteristics, nearly the same flap bending dynamic characteristics, with only a significant change in the torsional dynamic characteristics from those present in the existing OH-58 metal rotor blades. As a result of this, and because no changes are being proposed in the dynamic characteristics of the existing OH-58 control system, drive system, or airframe, the possibility of experiencing any aeromechanical instability in any flight condition with

TABLE 4. UNCOUPLED FREQUENCIES

		Frequencies (/Rev)		
		Baseline (& Graphite-Glass)	Glass/ Kevlar/ Estane	Steel Nose Cap
Shear Center	%CH	25.4	27.1	24.6
Center of Gravity	%CH	25.9	25.9	25.6
Dynamic Center of Gravity	%CH	24.3	24.3	23.9
Inertia	$Lb\text{-}In.^2$	1.52×10^6	1.52×10^6	1.52×10^6
Centrifugal Force	Lb	38527	38527	38527
1g Deflection	In.	-8.91	-11.30	-9.34
<u>Collective Mode</u>				
ω Flap	1	1.160	1.159	1.160
	2	3.059	3.012	3.050
	3	6.455	6.183	6.389
	4	10.051	9.611	9.956
ω Chord	1	4.711	4.655	4.796
	2	15.586	15.419	15.836
ω Torsion	1	6.248	3.388	5.485
Coupled	1	6.432	4.224	5.626
<u>Cyclic Mode</u>				
ω Flap	1	1.0	1.0	1.0
	2	2.553	2.532	2.549
	3	5.117	4.998	5.091
	4	7.499	7.155	7.424
ω Chord	1	1.299	1.292	1.310
	2	7.020	6.951	7.125
- Uncoupled		6.248	3.388	5.485
- Coupled		6.626	4.123	5.864

TABLE 5. BLADE AND HUB CENTERLINE LOADS

	Baseline (& Graphite-Glass)		Steel Nose Cap		Glass/Kev/Estane	
	Steady	Alt. ±	Steady	Alt. ±	Steady	Alt. ±
M_{CH} (In.-Lb)	23517	94949	23519	92897	23519	96990
M_F (In.-Lb)	8674	9333	8652	9234	8613	9409
P_{LL} (Lb)	122	154	98	149	83	155
HUB						
Fx (Lb)	-23.6	1780	-23.6	1725	-23.7	1816
Fy (Lb)	41.3	1805	41.4	1750	41.5	1851
Fz (Lb)	3562	268	3562	266	3562	264
Mz (In.-Lb)	47040	2155	47040	2092	47040	2191
TWIST (1) (Deg)	-.74	.43	-.58	.57	-.165	1.15

(1) Blade tip with respect to 4.5% Radius

G.W. = 3200 LB
A/S = 113 KT
ALT = 4000 FT
TEMP = 95°F

the proposed rotor blades is considered very improbable, if not impossible. This conclusion is based upon the fact that the aeromechanical instability of a helicopter rotor is largely dictated by the rotor blade chord bending dynamic characteristics and by an adverse control system coupling with the rotor blade chordwise motions, and neither of these items is being changed.

Further, the rotor blade torsional dynamic characteristics have been found to be of no consequence in their effect on this phenomenon. This insensitivity of the rotor aeromechanical stability characteristics to the rotor blade torsional dynamics was found in the UTTAS 1/9 scale dynamic model wind tunnel tests, whose results are reported in Reference 1.

The L-01 Computer Analysis was run to insure that classical flutter was not present at rotor speeds up to 509RPM(1.15 x N_{DL}).

3.1.4 Outboard Section Trade-Off Analysis

3.1.4.1 Summary

The trade-off analysis of the blade outboard section (OBS), station 80.0 thru 190.8, was conducted relative to the evaluation parameters of Table 2. Table 6 summarizes the results of the analysis. The detailed evaluation methodology follows this discussion of the results.

The graphite/glass configuration was last in every category. This reflects the higher material cost, the lesser confidence in its long-term trouble-free performance, the anticipated complexity of repair, and its poor conformability to radar treatment.

The fiberglass with a stainless-steel nose cap configuration showed somewhat better than the fiberglass/Kevlar configuration in all categories except that of radar reflectivity. It was this radar category, with a very one-sided evaluation, which predominated the other categories and resulted in the final selection of the fiberglass/Kevlar configuration. The large stainless steel nose cap is virtually untreatable for improved radar reflectivity and would offer no improvement over the existing OH-58C/A aluminum blade radar signature.

The life cycle cost analysis favored the fiberglass w/S.S.nose cap configuration, but largely as a result of the anticipated

1. MAY 1973 WIND TUNNEL TEST OF A 1/9 SCALE YUH-61A DYNAMIC MODEL FOR AEROELASTIC STABILITY, Boeing Vertol Company, D179-10395-1, August 14, 1973.

high cost of specially treating materials for radar reflectivity. It is doubtful that each of these treatments, incrementally, will improve radar signature sufficiently to warrant the use of them all.

TABLE 6. AIRFOIL SECTION EVALUATION SUMMARY

	R&M	LCC	Ball. Tol	Perf	Radar	Total
Glass with S.S. nose cap	31	31	10	23	5	100
Glass/Kevlar	15	26	9	23	31	104
Graphite/Glass	10	26	9	23	5	73
	56	83	28	69	41	277

The weighting of R&M in favor of the glass w/S.S. nose cap configuration is a function of reliability only and is a reflection of the lack of experience with such features as the composite glass/Kevlar spar pack, and the pneumatic deicing system and the belief that the Estane leading edge will not give as good erosion performance as does a metal leading edge. Because of the field replaceability of the Estane leading edge, the glass/Kevlar configuration is anticipated to be better in overall maintainability

3.1.4.2 Introduction

The key to an effective trade study is the development of a process for multiple criteria decision making. However, until recently, generally accepted rigorous techniques for optimization under multiple objectives have not been available in the literature. Fortunately, there is a new form of Decision Analysis beginning to show up in the Operations Research Management and Social Science fields. We have used this methodology, which is capable of dealing simply, efficiently, and practically with the various (sometimes) conflicting objectives desired of a new OH-58 rotor blade.

In the following paragraphs of this report, we: 1) introduce the basic principles of the theory underlying our analytical process of multi-criterion design prioritization; 2) provide references where the reader can find in-depth justification of the theory of this process, and prior applications of the technique; and 3) apply the process to ranking several candidate OH-58 blade designs.

3.1.4.3 Multicriterion Prioritization - Summary of the Theory

Fundamentally, the approach used in this analysis consists of the identification of the hierarchical structure underlying our objective (determining the "best" OH-58 blade design from several candidate designs), using the necessary mathematical techniques to quantify the importance of the various hierarchical factors in achieving the objective, and assessing the effectiveness of each blade design in achieving the overall objective. Drawing heavily on recent work on analytical hierarchies and systems (References 2, 3, 4), we construct a hierarchical structure as a model for evaluating alternate blade designs, and obtain the desired solution in the form of priorities of the factors or criterion involved by the method of scaling ratios. To calculate these priorities, we use the principal eigenvector of a positive, reciprocal, pairwise comparison matrix. The relative importance of the elements of the hierarchy are calculated through the principal eigenvector solutions of the pairwise comparison matrices.

The following paragraphs introduce the concepts necessary to an understanding of the manner in which the OH-58 blade design trade study was performed.

3.1.4.4 Hierarchies

In its simplest form, a hierarchy consists of several levels of related elements, each level of which is dominated by a neighboring upper level. Furthermore, the proper functioning of the higher level depends upon the proper functioning of the subordinate (lower) levels. Thus, the basic value of a hierarchy as an analytical model is to gather understanding at the highest level through the investigation of interactions at the lower levels.

Although the study of hierarchical structures is not new in the literature, the calculating of priorities of interacting elements in the manner employed in this study is. (A detailed exposition on hierarchical structures and priority determination can be found in Reference 2.)

Figure 8 displays the hierarchy used in this study for determination of the "best outboard section design" and the importance of the various factors as calculated later in this section.

2. Saaty, T.L., A SCALING METHOD FOR PRIORITIES IN HIERARCHICAL STRUCTURES, Journal of Mathematical Psychology 15, 111-111, 1977.

3. Saaty, T.L., HIERARCHIES AND PRIORITIES - EIGENVALUE ANALYSIS, University of Pennsylvania, 1975.

4. Saaty, T.L. and Khouja, M., A MEASURE OF WORLD INFLUENCE, Peace Science, June 1976.

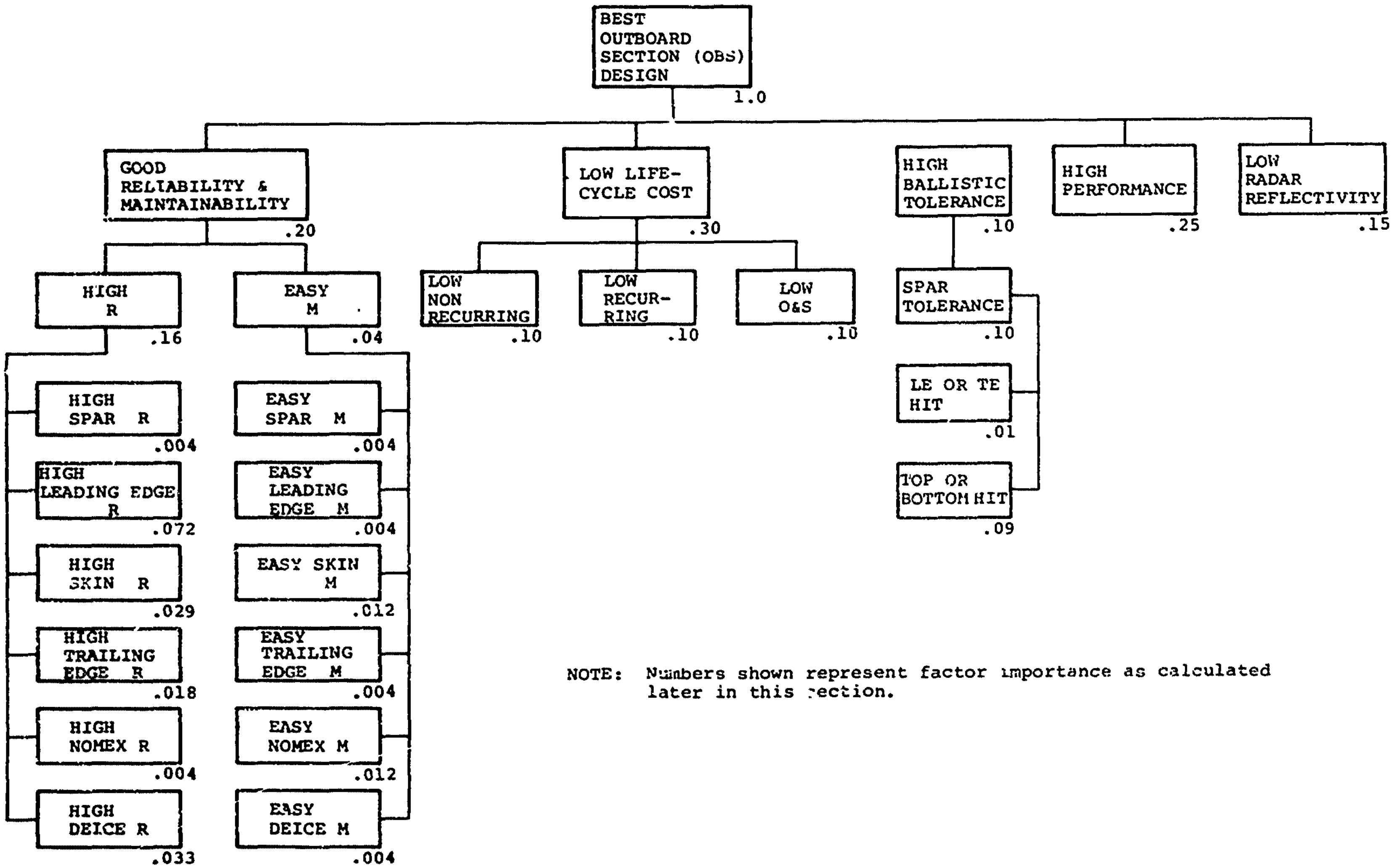

NOTE: Numbers shown represent factor importance as calculated later in this section.

Figure 8. Hierachy for Selecting the Best OBS Design.

3.1.4.5 Pairwise Comparison Matrices

In the comparison of a set of objects or attributes (denoted $A_1, \ldots, A_n$) with weights $w_1, w_2, \ldots, w_n$ (assumed to belong to a ratio scale), the pairwise comparisons are represented by a matrix of the following form:

$$A = \begin{array}{c|cccc} & A_1 & A_2 & \cdots & A_n \\ \hline A_1 & 1 & w_1/w_2 & \cdots & w_1/w_n \\ A_2 & w_2/w_1 & 1 & \cdots & w_2/w_n \\ \vdots & \vdots & \vdots & & \vdots \\ A_n & w_n/w_1 & w_n/w_2 & \cdots & 1 \end{array}$$

As can be seen from the elements of the matrix above, A is a reciprical matrix. That is, for each element a_{ij} of matrix A, the element a_{ji} equals the inverse (or reciprocal) of a_{ij}. The mathematical tractableness of reciprocal matrices is discussed in detail in Reference 2.

Now, in order to develop pairwise comparison matrices for the various hierarchic levels displayed in Figure 8, the following scale of importance has been employed:

IMPORTANCE	DEFINITION	EXPLANATION
1	Equal Importance	Two attributes contribute identically to the objective
3	Weak Dominance	Experience or judgement slightly favors one attribute over another
5	Strong Dominance	Experience or judgement strongly favors one attribute over another
7	Demonstrated Dominance	An attribute dominance is demonstrated in practice
9	Absolute Dominance	The evidence favoring an attribute over another is affirmed to the highest possible order
2,4,6,8	Intermediate Values	Used when further subdivision or compromise is needed

The numbers used in this scale are absolute rather than ordinal, and if numbers larger than those appearing in the scale are needed, clustering methods can be used.

Using this scale, reciprocal, pairwise comparison matrices have been developed for each hierarchic level described in Figure 8. The values contained in the following matrices are subjective. They represent the results of discussion and negotiations conducted among members of the Boeing Vertol Reliability, Maintainability, Manufacturing, and Design Groups. They represent an aggregate of our best judgement regarding the relative importance of the various factors impacting the selection of an optimum blade design.

3.1.4.6 Priority Determination

The five primary factors for evaluating blade designs (R&M, LCC, Ballistic Tolerance, Performance, Radar Reflectivity) shown in Figure 8 were considered to be of significant impact upon the basic objective of choosing a best blade design. As such, no factor was considered to exhibit more than weak dominance (a 3 in the scale described in the section above) over any other factor.

Furthermore, the basic rank of the factors (their order of influence upon the objective) was defined by the Army as shown in Table 7.

TABLE 7. TOP LEVEL PRIORITIES

Factor	Priority
(1) R&M	.20
(2) LCC	.30
(3) Ballistic Tolerance	.10
(4) Performance	.25
(5) Radar Reflectivity	.15

The process used to arrive at the comparison values contained in the matrices is as follows. First, we rank the factors of a comparison matrix in terms of decreasing impact upon the higher level factor to which they are subordinate. Next, we take the factor ranked first and pairwise compare it with each of the other factors, starting with that factor ranked lowest and working upwards. In making the comparisons in this way, we are always comparing a higher valued factor with a lower valued factor, thus generating ratios on the integer portion of the scale. Next, we take the factor ranked second and compare it with all less favored factors in the manner described above. We continue this process on the 3rd, 4th, etc., factors until $M(M-1)/2$ comparisons have been made. This method is of great value when dealing with matrices of order (M) greater than 2 since we are always creating the $M(M-1)/2$ integer values first and then calculating the remaining values by using the relationship $A_{ji} = 1/A_{ij}$.

Using the method of principal eigenvectors, the pairwise comparison matrices are analyzed and priorities corresponding to the normalized (summing to unity) eigenvector components are calculated. These priorities (as shown in Table 7) reflect the relative importance of each factor upon the objective.

This process of making pairwise comparisons and solving the comparison matrix to determine factor priorities was continued on all the remaining hierarchic groups of Figure 8. Thus, for example, the relative priority of reliability compared to maintainability (Reference Table 8) is .80 to .20, representative of a position that poor maintainability is not very important (with reasonable bounds on "poorness") if reliability is high, and simultaneously, even excellent maintainability cannot completely compensate for an unreliable design.

TABLE 8. R&M IMPORTANCE DETERMINATION

	(1)High R	(2)Easy M	Priority	Importance
(1) High Reliability	1	4	.80	.16
(2) Easy Maintainability	1/4	1	.20	.04

Also shown in Table 8 (and in Figure 8) are values labeled "importance". The importance of a factor is the product of the priority of that factor, with the priorities of all higher level hierarchic elements to which it is subordinate. Thus, the importance of reliability is .16, which equals the priority of reliability (.80) times the priority of R&M (.20) times the priority of the Best OBS design (1.0).

In determining the priorities of the blade parts upon reliability (Table 9), estimates of the failure frequencies for the various parts (spar, leading edge, etc.) were taken from the Boeing Vertol CH-46 Fiberglass Blade Failure Modes and Effects Analysis (FMEA), rather than using subjective comparisons, since this data was directly applicable to the kinds of blades being considered.

TABLE 9. R FACTOR IMPORTANCE DETERMINATION

Blade Part	Priority	Importance
Spar	.023	.004
Leading edge	.453	.072
Skin	.182	.029
Trailing edge	.114	.018
Nomex	.023	.004
Deice	.205	.033

Next, each OBS design (fiberglass with a stainless steel nose cap (labeled X), fiberglass and Kevlar (labeled Y), and graphite/fiberglass (labled Z)) was evaluated against each of the lowest level factors in terms of its reliability impact. Table 10 displays the pairwise comparisons and relative priorities of each OBS design. The qualitative data which led to these judgements are contained in Table 11.

A similar analysis was performed to evaluate the maintainability characteristics of the OBS designs, and the priorities and pairwise comparisons are provided in Tables 12 and 13. Again, the rationale for the judgements contained in Table 13 can be found in Table 14.

TABLE 10. PAIRWISE COMPARISONS - R IMPACT OF OUTBOARD SECTION DESIGN

Spar	X	Y	Z	Priority	Leading edge	X	Y	Z	Priority	Skin	X	Y	Z	Priority
X	1	4	5	.669	X	1	5	5	.714	X	1	1	5	.455
Y	1/4	1	2	.217	Y	1/5	1	1	.143	Y	1	1	5	.455
Z	1/5	1/2	1	.114	Z	1/5	1	1	.143	Z	1/5	1/5	1	.091
Trailing edge	**X**	**Y**	**Z**	**Priority**	**Nomex**	**X**	**Y**	**Z**	**Priority**	**Deice**	**X**	**Y**	**Z**	**Priority**
X	1	1	3	.429	X	1	1	1	.333	X	1	3	3	.6
Y	1	1	3	.429	Y	1	1	1	.333	Y	1/3	1	1	.2
Z	1/3	1/3	1	.142	Z	1	1	1	.333	Z	1/3	1	1	.2

X = Fiberglass with stainless-steel nose cap
Y = Glass/Kevlar
Z = Graphite/glass

TABLE 11. OH-58C/A OUTBOARD SECTION RELIABILITY CONSIDERATIONS

	X	Y	Z
SPAR	• All fiberglass-has conventional fabrication and demonstrated reliability	• Glass/Kevlar - no experience • Nose balance weights • Δ Thermal expansion • More stress concentration • More bond lines	• Δ Thermal expansion • Much more stress concentration • More bond lines • Greater lightning damage risk
Leading Edge	• Wear characteristics of steel best in rain	• Wears faster in rain • Bond stress lower • Little service experience	• Wears faster in rain • Bond stress lower • Little service experience
Skin	• Fiberglass has good impact resistance	• Glass is impact resistant	• Graphite is more brittle and vulnerable to impact
Trailing Edge	• Fiberglass has good impact resistance	• Glass is impact resistant	• Graphite is more vulnerable to impact
Nomex	• All designs have Nomex		
Deicing	• Electrical - only proven system	• Pneumatic deice, never built and tested	• Pneumatic deice, never built and tested

X = Fiberglass with stainless-steel nose cap
Y = Glass/Kevlar
Z = Graphite/glass

TABLE 12. M FACTOR IMPORTANCE DETERMINATION

Blade part	Priority	Importance
Spar	.10	.004
Leading edge	.10	.004
Skin	.30	.012
Trailing edge	.10	.004
Nomex	.30	.012
Deice	.10	.004

TABLE 13. PAIRWISE COMPARISONS - M IMPACT OF OUTBOARD SECTION DESIGN

Spar, trailing edge & nomex	X	Y	Z	Priority	Skin	X	Y	Z	Priority
X	1	1	1	.33	X	1	1	5	.45
Y	1	1	1	.33	Y	1	1	5	.45
Z	1	1	1	.33	Z	1/5	1/5	1	.10

Leading edge & deice	X	Y	Z	Priority
X	1	1/5	1/5	.10
Y	5	1	1	.45
Z	5	1	1	.45

X = Fiberglass with stainless-steel nose cap
Y = Glass/Kevlar
Z = Graphite/glass

TABLE 14. OH-58C/A OUTBOARD SECTION MAINTAINABILITY CONSIDERATIONS

	X	Y	Z
SPAR	• Only minor delaminations or cross ply damage can be repaired. • No spar repairs involving unidirectional material are possible on any designs.		
Leading Edge	• Steel probably not replaceable	• Estane easier to replace	• Estane easier to replace
Skin	• Highly repairable	• Highly repairable	• May not be repairable with a return to full strength
Trailing Edge	• Easily repaired	• Easily repaired	• Unknown
Nomex	• All designs have Nomex		
Deicing	• Electric probably not replaceable	• Pneumatic believed to be replaceable	• Pneumatic believed to be replaceable

X = Fiberglass with stainless-steel nose cap
Y = Glass/Kevlar
Z = Graphite/glass

3.1.4.7 Ballistic Tolerance

Previous analyses and wind tunnel tests had shown that, in general, a blade which does not separate from the aircraft due to ballistic damage will continue to be flyable. Therefore, the blades were evaluated on the basis of whether a hit by each threat in any position or angle of entry would cause separation. The ability of a blade to stay intact after ballistic damage is related to the residual strength of the damaged area. Basic calculations of residual strength were made of several marginal cases. It became apparent that all the concepts were invulnerable to 7.62 mm projectiles in either the straight or tumbled attitudes. It was also evident that they would not be vulnerable to straight hits of 12.7 mm rounds. Their vulnerability to tumbled 12.7 mm hits was not quite so apparent.

Looking at the worst case, a 12.7 mm round, hitting directly on the blade nose, exactly centered on the chord plane and perpendicular to it, could provide a condition which might sever a blade. However, after comparing these blades against other components Boeing has tested with 12.7 mm tumbled rounds, it was concluded that such damage, if not impossible, was unlikely because a tumbled round (1) has lost some of its energy and (2) tends to turn or glance off the target, causing less destruction. Thus it was felt that all concepts were virtually invulnerable to this threat, except possibly for such a hit in the last few inches from the tip, which would not cause a hazardous condition.

In evaluating survivability to 23 mm API, as with the other threats, only the spar and root areas were considered. The only types of hit that appeared catastrophic were those which hit the nose directly and then went completely through the top or bottom of the spar in a chordwise direction.

It was felt that all blades were the same for the top or bottom hits, but that the glass with stainless steel (blade X) was superior to the others for maximum damage chordwise spar hits. The pairwise comparisons and priorities associated with ballistic tolerance are contained in Table 15. Top or bottom hits, and hits in the trailing edge or leading edge were considered, with 90% assumed to be top or bottom, and 10% edgewise.

3.1.4.8 Life-Cycle Cost Analysis

In order to evaluate the life-cycle cost (LCC) effectiveness of the various OBS designs, estimates were made of the costs and removal rates associated with each design as follows:

TABLE 15. PAIRWISE COMPARISONS - BALLISTIC TOLERANCE OF OUTBOARD SECTION DESIGN

L.E. or T.E. hit	(Importance = .01) X	Y	Z	Priority	Top or Botton hit	(Importance = .09) X	Y	Z	Priority	Combined priority
X	1	3	3	.6	X	1	1	1	.333	.36
Y	1/3	1	1	.2	Y	1	1	1	.333	.32
Z	1/3	1	1	.2	Z	1	1	1	.333	.32

X = Fiberglass with stainless-steel nose cap
Y = Glass/Kevlar
Z = Graphite/glass

- Nonrecurring - using $50/man-hour, nonrecurring costs were estimated based on nonrecurring man-hour estimates made by Boeing Vertol manufacturing personnel. These values are very rough, but they are considered to be correct when used as relative values from design to design.

- Recurring - The recurring cost goal of this program is $3400/blade. Approximately 70% of the weight of a blade goes into its OBS. As such, we have set the recurring cost of the OBS judged cheapest at 70% of $3400 or $2380. The other two designs (Y and Z) were considered to be approximately 50% and 15% more expensive, respectively than the X design. It is noted that the cost of the glass/Kevlar configuration (Y) includes an estimated $950 of extra material costs for maximum radar treatment.

- Inherent MTBR - It was felt that all three OBS designs were capable of meeting our design objective of 5000 hours inherent MTBR to higher levels. Thus, an MTBR for OBS failures of 5000 hours was established for OBS design Z, which was determined to be the least reliable by analyzing the data contained in Tables 9 and 10. The MTBR's of OBS X and Y were then determined by multiplying the MTBR of OBS Z by the ratio of priorities of OBS X and Y, respectively, to OBS Z.

- MTBR - To calculate an operational (or all failure causes) MTBR for each OBS design, a noninherent removal MTBR to higher levels of 5000 hours was added to the inherent MTBR of each of the OBS designs.

- Average Repair Cost - Historically, blade repair costs at higher levels have run about 30% of acquisition cost. Assuming $3400 as the acquisition cost, the blade determined through Tables 12 and 13 to be most maintainable (OBS Y) was set at a repair cost of 30% of $3400 or $1000. The repair costs of X and Y were then calculated by multiplying the repair cost of Y by the ratio of the priorities of X and Z, respectively to Y.

Table 16 summarizes the data used in the OBS Life-Cycle Cost Analysis.

3.1.4.9 <u>Radar Reflectivity</u>

Table 17 shows the pairwise comparison and priorities for radar reflectivity. It should be noted that only design (Y)

TABLE 16. OBS LIFE CYCLE COST DATA

	Non recurring	Recurring per blade	Total (1) recurring	Inherent MTBRDR	MTBRDR (2)	Avg. rep'r. (3) cost	O&S cost	Total LCC
X	$7,000,000	$2,380	$7,140,000	20,000	4,000	$1,200	$2,592,000	$16,735,000
Y	$7,000,000	$3,570*	$10,710,000	8,000	3,000	$1,000	$2,880,000	$20,590,000
Z	$7,000,000	$2,737	$ 8,211,000	5,000	2,500	$1,350	$4,665,600	$19,876,600

(1) 3,000 Blade buy. 1200 Aircraft., 2400 blades, 600 (25%) spares.

(2) Combines inherent MTBR with 5,000 hr operational MTBR, common to all configurations.

(3) 1200 Aircraft at 20 flight hours (40 blade hours) per aircraft per month, 15 years. 8,640,000 blade hours.

*Include $950 cost of maximum radar treatment.

is treatable to enhance reflectivity, and as such its priority is much higher than the other designs.

TABLE 17. RADAR REFLECTIVITY

	X	Y	Z	Priority	Importance
X	1	1/6	1	.125	.019
Y	6	1	6	.750	.112
Z	1	1/6	1	.125	.019

3.1.4.10 Outboard Section Analysis Conclusion

Taking the LCC data of Table 16 and the radar evaluations of Table 17 and combining them with the R&M and ballistic tolerance previously displayed, it is now possible to rank each OBS based on its composite priority.

In developing this ranking, we have considered all designs as having the capability for equal performance. Thus, the .25 importance of performance has been spread evenly over each design.

The quantitative rating for each design versus each parameter i˙˙ (R&M, LCC, etc.) calculated by multiplying the priority for each design versus each factor times the importance of that factor. Thus, for example, the rating of blade X against R&M is calculated by multiplying the priority of blade X against each R&M factor (ref. Tables 10 and 13) times the importance of each R&M factor (ref. Tables 8 and 12).

Table 18 summarizes the priorities for each design versus each parameter. Design Y (glass/Kevlar) is the preferred design, but just slightly over X (glass with stainless steel); design Z (graphite/glass) is a very distant third.

TABLE 18. SUMMARY OF OUTBOARD SECTION EVALUATION

	R&M	LCC	Bal. Tol	Perf	Radar	Total
Glass with S.S. nose cap	.109	.113	.036	.083	.019	.360
Glass/Kevlar	.056	.092	.032	.083	.112	.375
Graphite/glass	.035	.095	.032	.083	.019	.264

3.2 ROOT END SECTION

3.2.1 Concepts

Four root end retention concepts were examined. These included a simple bearing design and three pin wrap designs. In conjunction with these variations of pin attachment, four concepts to react chordwise moment were also examined.

3.2.1.1 Root End Retention

The four methods of blade retention are shown schematically in Figures 9 through 12. It is noted that only one method of chordwise moment reaction, externally bonded graphite plates, is shown with all four of the blade retention concepts.

Figure 9 displays the spar pin wrap concept. In this concept, one-half of the unidirectional fiber of the upper and lower spar packs are rotated 90°, circle the pin, rotate 90° again, and transcend back into the same upper or lower spar pack from which it originated. The proprietary design was developed by Boeing Vertol and was used on the YUH-61A and YCH-47D.

The nose wrap concept in Figure 10 is similar to the spar wrap concept, however, in this concept it is the unidirectional fiber of the nose block which circles the pin, then rotates 90° to form the unidirectional upper and lower spar packs.

Figure 11 illustrates the simple bearing design. Here, the thickness of the spar is built up with additional layers of interleaved material and then a hole is drilled. Loads are reacted in the bearing with shear-out being the critical failure mode.

Figure 12 is a pin wrap design utilizing a filament winding technique. In this design, both unidirectional and x-ply fibers are wrapped around the main attachment pin in the process of the spar layup operation.

3.2.1.2 Chordwise Moment Reaction

The first design for chord moment reaction utilizing externally bonded graphite doubler plates is shown in Figures 9 through 12. Figure 13 displays a concept of utilizing a machined aluminum fitting bonded internally between the spar packs. The third concept considered was a trapped metal fitting similar to Figure 13. The final concept was an internal Kevlar extension of the leading- and trailing-edge spar material as shown in Figure 14.

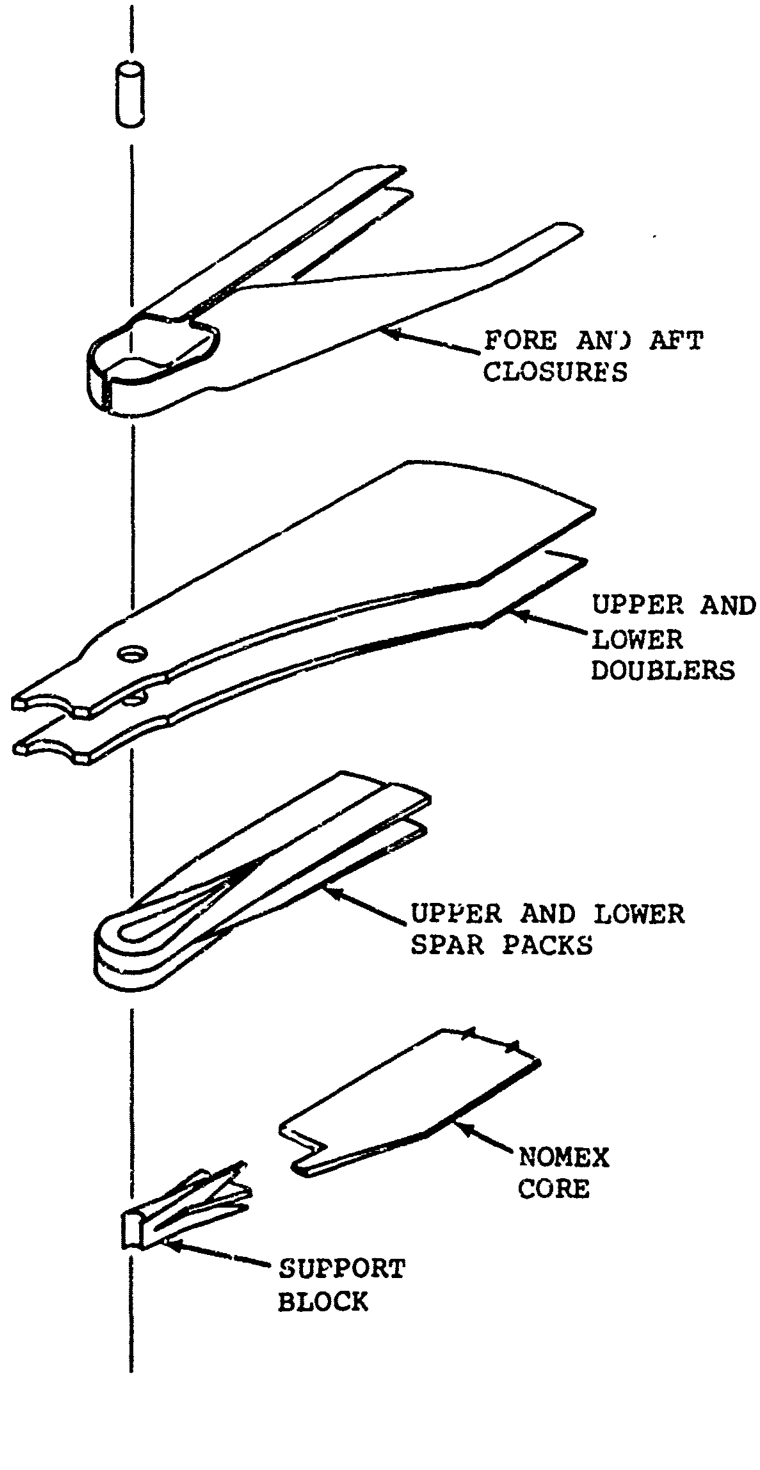

Figure 9. Spar Wrap Root End Design

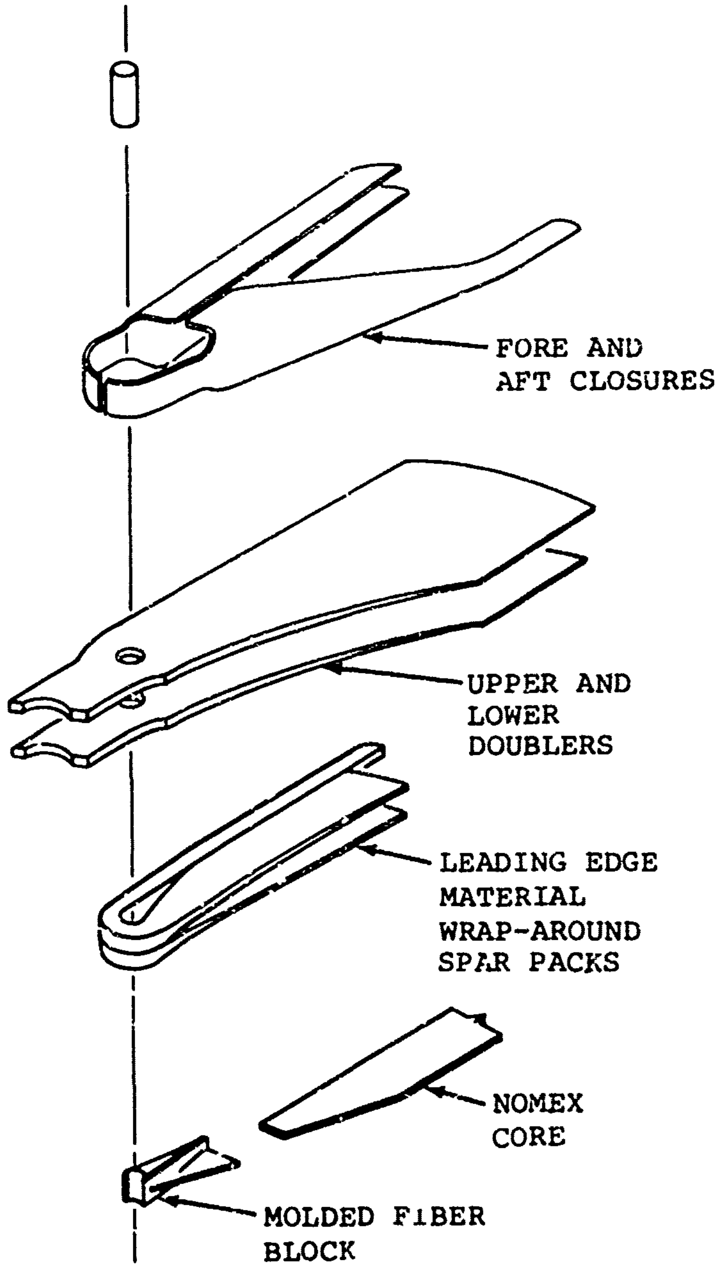

Figure 10. Nose-Wrap Root End Design

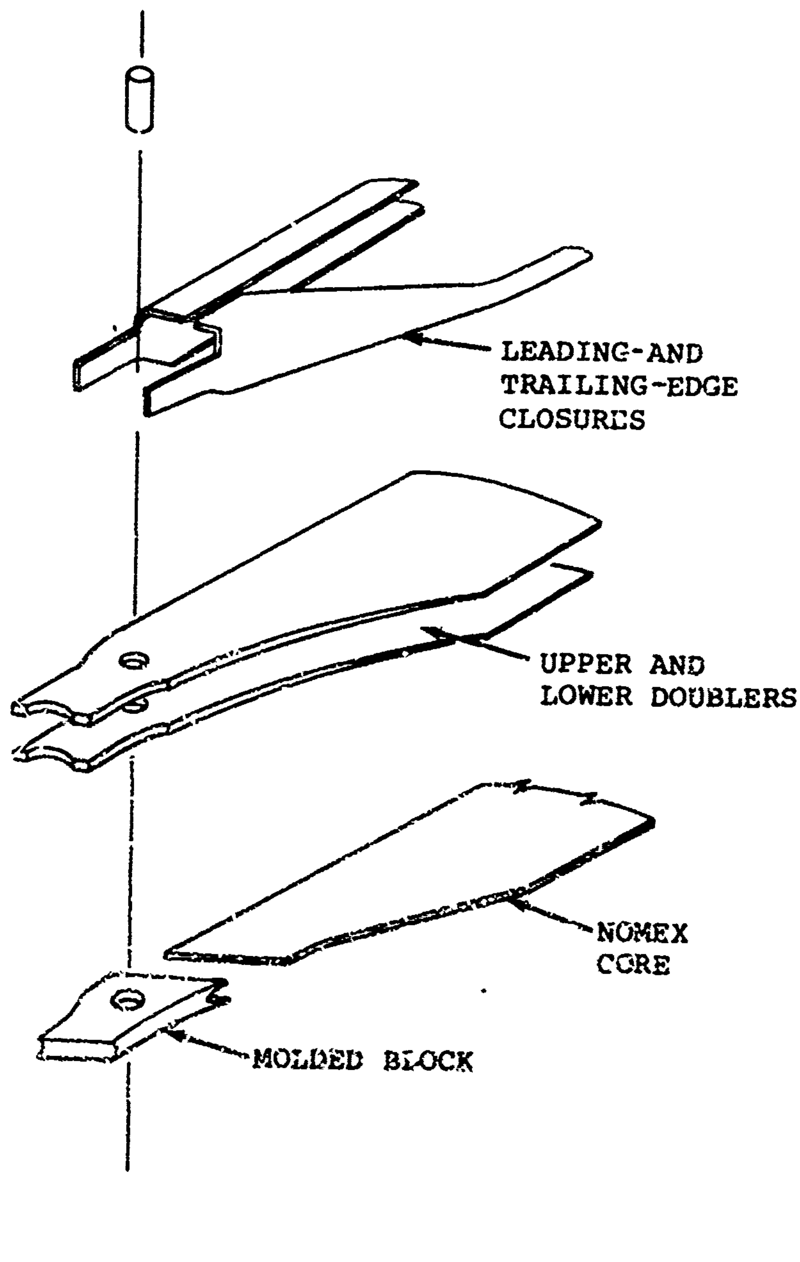

Figure 1[illegible]. Laminate Root End Design

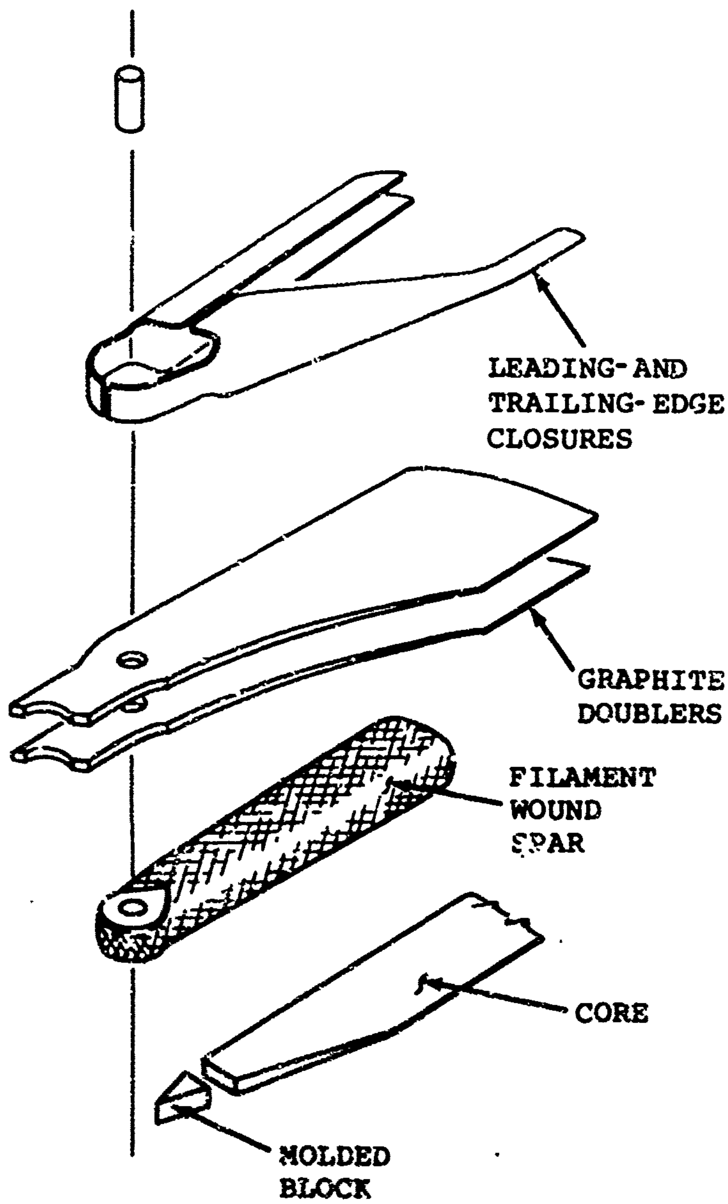

Figure 12. Filament Wound Root End Design

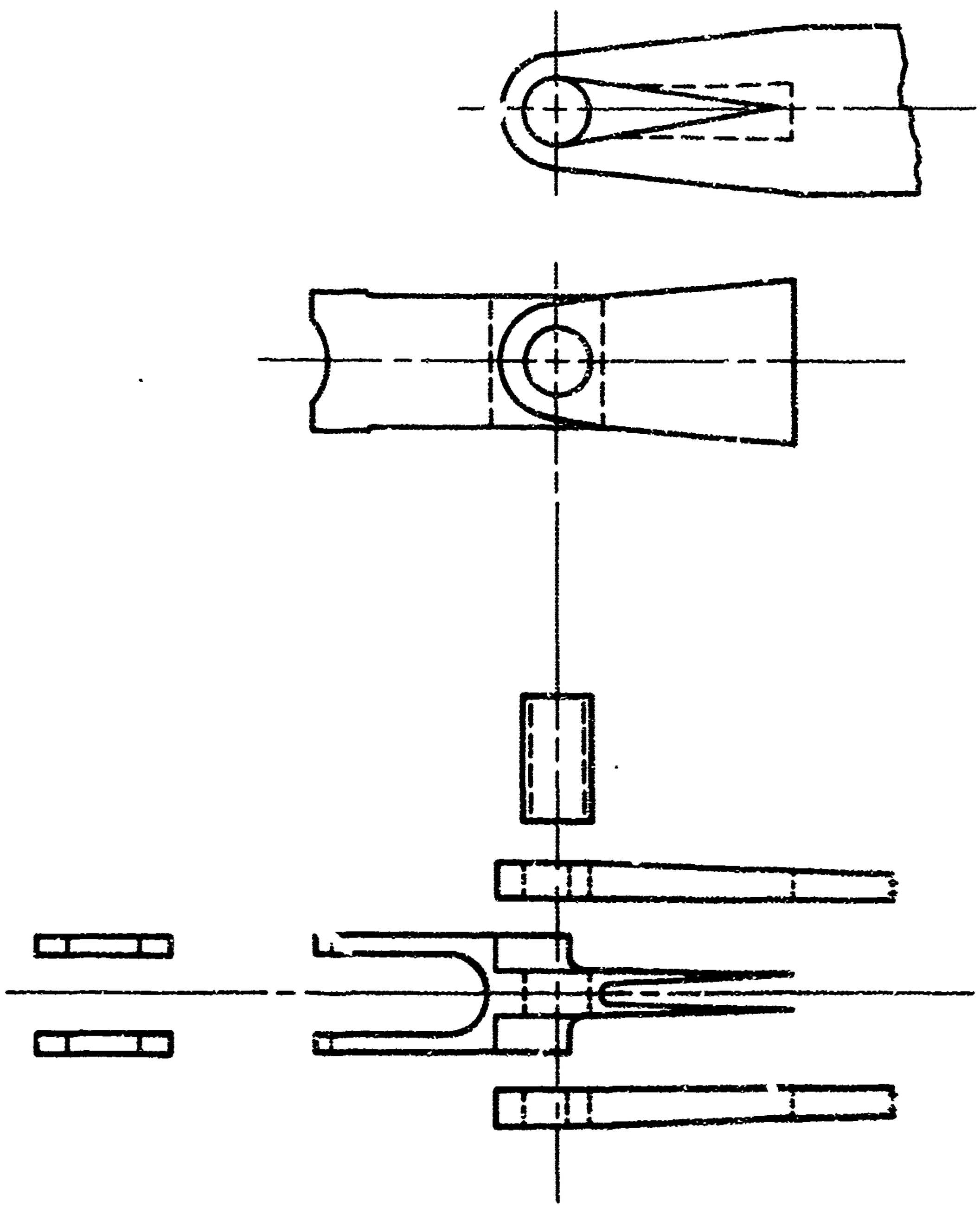

Figure 13. Bonded Metal Fitting Design

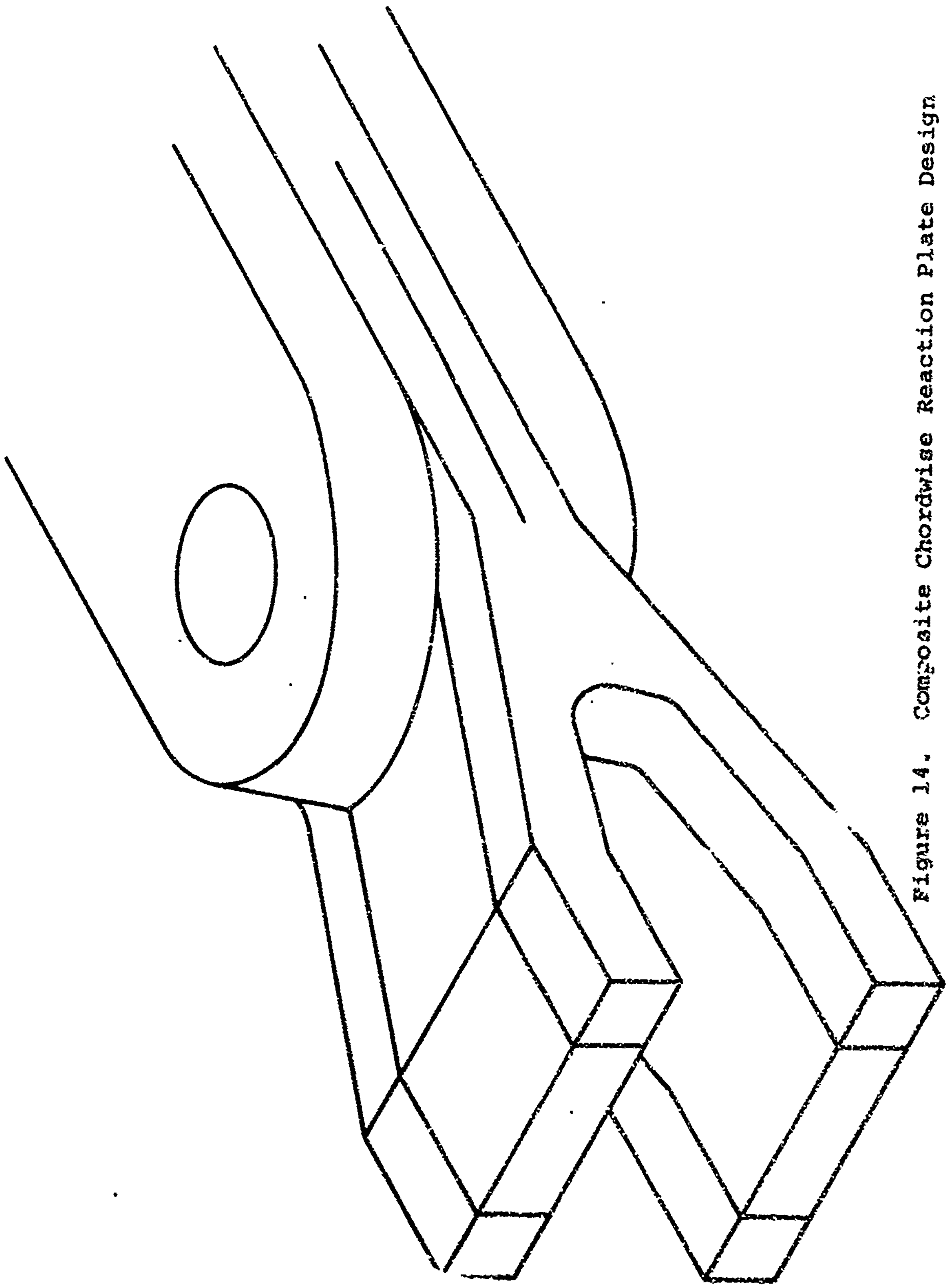

Figure 14. Composite Chordwise Reaction Plate Design

3.2.2 Root End Trade-Off Analysis

3.2.2.1 Summary

The selected root end configuration is that of a spar pin wrap with the internal integral Kevlar chord moment reaction extension. The four pin retention concepts were evaluated in the same format as was the airfoil section. The trade-off analysis is presented later in this section. The results, as summarized in Table 19, show little difference in the final totals. The pin wrap concept was ultimately selected. Although the bearing or punch-through design was judged to be the least costly to fabricate, the confidence of safety inherent in the pin-wrap design was ultimately the decisive factor. The nose-wrap design is not suited to the CR-124/Kevlar nose pack design selected for the airfoil section. Whether the spar wrap design of Figure 9 or the filament wound pin-wrap design of Figure 12 will be utilized is not as yet decided and will depend on the manufacturing sequence defined for the entire blade in Task II.

No formal trade-off analysis was conducted to select the design for chordwise moment reaction. The external graphite doubler design was first derived. This design was objectionable because the doublers also carried all of the flapwise moment reaction and a large share of the centrifugal force, all carried through a bond line. In addition, the design was 6 pounds heavier than the OH-58C/A metal blade and utilized a considerable quantity of costly and radar relective graphite.

The internal metal fitting of Figure 13 was conceived as a way of having the inboard extension react chord moment only. However, there was doubt as to whether the integrity of bond between the fitting and the spar packs above and below could be reliably repeatable on a production basis.

A trapped internal fitting was proposed as an alternative but was too reminiscent of a coke bottle design which has been deemed to be undesirable on a production basis in previous studies. The design concept shown in Figure 14 was conceived to resolve all these objections. It was shown to work structurally and was, therefore, selected.

3.2.2.2 Introduction

An analysis identical to that displayed in rating the outboard section design was performed to rank the various root end designs. As such, the discussion provided in this section is brief, relying on the reader's previously gained familiarity with the hierarchial process.

TABLE 19. ROOT END EVALUATION SUMMARY

	R&M	LCC	BALL. TOL.	PERF.	RADAR	TOTAL
SPAR PACK WRAP AROUND PIN -A	19	30	11	25	15	100
NOSE TO SPAR PACK WRAP AROUND PIN -B	19	27	11	25	15	97
PUNCH THROUGH-C	22	31	8	25	15	101
FILAMENT WRAP AROUND PIN -D	20	32	11	25	15	103
	80	120	41	100	60	401

3.2.2.3 Priority Determination

Figure 15 displays the hierarchical structure used for evaluating the various root end designs and the importance of the various factors. The important factors were derived through pairwise comparisons as discussed in the OBS analysis. The priorities for each blade part that resulted from these pairwise comparisons are shown in Table 20.

Each of the root end designs was then evaluated from an R&M viewpoint against each blade part. Tables 21 and 22 display the qualitiative data used in making the pairwise comparisons for each root end design against the criteria of R&M. Table 23 shows the quantitative results of these comparisons.

The root end concepts were evaluated in the same manner as the outboard sections. All were deemed invulnerable to all threats except the 23 mm API. It was concluded that all the roots would be vulnerable to 23 mm API hits in the section from the vertical pin to Station 26.80 and possibly inboard of the pin, and that the punch through (design C) was slightly worse than the others due to its higher vulnerable area.

Using the same assumptions discussed in the OBS analysis section, the LCC analysis data is displayed in Tables 24 and 25. As can be seen from this data all designs are relatively close in LCC.

3.2.2.4 Root End Section Analysis Conclusions

All root end designs were considered to be identical from a performance and radar reflectivity point of view. As such the priority of these factors was spread uniformly over each design.

Table 26 summarizes the ratings for each design against all the rating criteria. As can be seen, based on the evaluation factors, there is no clear-cut choice. Based on Boeing Vertol experience with the pin-wrap design and its demonstrated fail-safety, this design was selected.

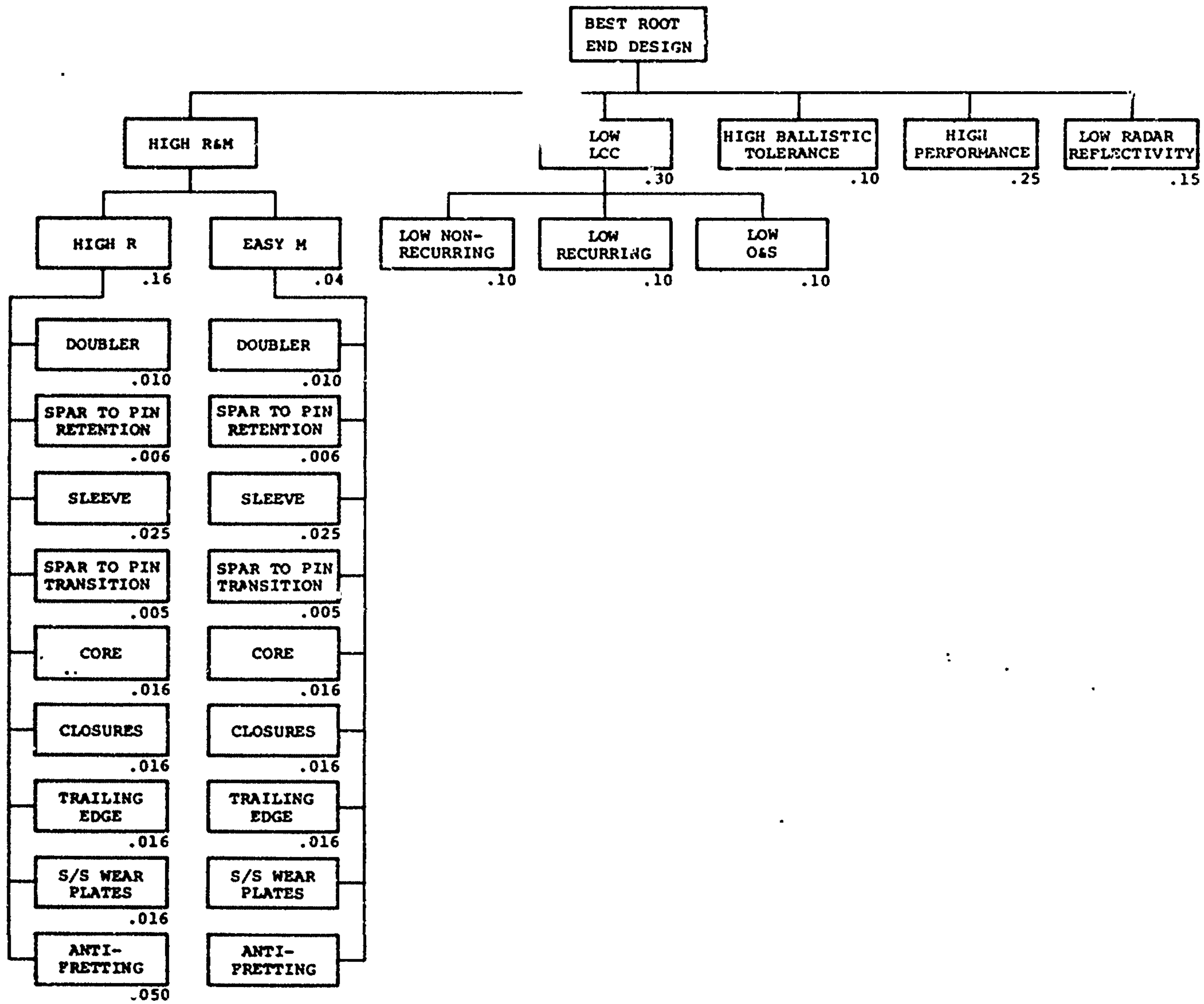

Figure 15. Hierarchy for Root End Selection

TABLE 20. ROOT END R&M FACTOR PRIORITIES

BLADE PARTS	PRIORITY	
	R	M
DOUBLER	.07	.07
SPAR TO PIN RETENTION	.04	.04
SLEEVE	.15	.17
SPAR TO PIN TRANSITION	.03	.03
CORE	.10	.10
CLOSURES	.10	.10
TRAILING EDGE	.10	.10
S/S WEAR PLATES	.10	.10
ANTI-FRETTING	.31	.29

TABLE 21. OH-58C/A BLADE RELIABILITY - ROOT END SECTIONS

COMPONENTS	A (HAIRPIN - SPAR WRAP AROUND PIN) (NOT NOSE BLOCK)	B (NOSE WRAP AROUND PIN & INTO "C" SHAPE)	C (LAMINATED ROOT)	D (FILAMENT WOUND)
UPPER & LOWER DOUBLER (FIG'S 8, 9, 10 AND 11 ONLY NOT IN FINAL DESIGN)	• SEPARATE FROM SPAR SINGLE BOND LINE	• SEPARATE FROM SPAR SINGLE BOND LINE	• INTERLEAVED WITH SPAR MATERIAL	• WINDING BECOMES EXTENSION OF SPAR NO BOND LINES
SPAR RETENTION TO PIN	• ONLY UNI SPAR MATERIAL WRAPS - NOT NOSE BLOCK • EXTENSIVE EXPERIENCE WITH DESIGN	• ENTIRE SPAR UNI WRAPS • EXTENSIVE EXPERIENCE EXISTS	• NO UNI WRAP LAMINATED CROSSPLY DOUBLER • LITTLE EXPERIENCE	• WRAP SLIGHTLY LESS EFFICIENT • LITTLE EXPERIENCE
SLEEVE	• COMPOSITE SLEEVE • COULD DEBOND OR WEAR	• COMPOSITE SLEEVE • COULD DEBOND OR WEAR	• METAL SLEEVE COULD CRACK	• COMPOSITE SLEEVE • COULD DEBOND OR WEAR
SPAR TO PIN TRANSITION BLOCK	• COMPLEX BLOCK MAY UNBOND	• COMPLEX BLOCK - MAY UNBOND	• FLAT BLOCK - GOOD BOND INTERFACE	• SIMPLE BLOCK - LESS PROBABILITY OF DEBOND
CORE	• SAME IN ALL DESIGNS			
CLOSURES L.E. & T.E.	• SAME IN ALL DESIGNS			
TRAILING EDGE (WEDGE)	• SAME IN ALL DESIGNS			
S/S WEAR PLATES	• SAME IN ALL DESIGNS			
ANTI-FRETTING MATERIAL	• SAME IN ALL DESIGNS			

TABLE 22. OH-58C/A ROOT END MAINTAINABILITY

	A	B	C	D
DOUBLER	• Same in all cases			
SPAR RETENTION TO PIN	• Same in all cases			
SLEEVE	• Same in all cases			
SPAR-TO-PIN TRANSITION BLOCK	• Minor delams repair-able	• Probable scrap	• Minor delams repair-able	• Probable scrap
CORE	• Same in all cases			
CLOSURES	• Same in all cases			
S/S WEAR PLATES	• Same in all cases			
TRAILING EDGE	• Same in all cases			
ANTI-FRETTING MATERIAL	• Same in all cases			

LEGEND:

(A) SPAR PACK WRAP AROUND PIN

(B) NOSE TO SPAR PACK WRAP AROUND PIN

(C) PUNCH THROUGH

(D) FILAMENT WRAP AROUND PIN

TABLE 23. ROOT END PRIORITIES FOR

RELIABILITY AND MAINTAINABILITY FACTORS

	A		B		C		D	
	R	M	R	M	R	M	R	M
DOUBLER	.09	.25	.09	.25	.55	.25	.27	.25
SPAR TO PIN RETENTION	.40	.25	.40	.25	.08	.25	.13	.25
SLEEVE	.25	.25	.25	.25	.25	.25	.25	.25
SPAR TO PIN TRANSITION	.15	.2	.15	.2	.23	.4	.47	.2
CORE	.25	.25	.25	.25	.25	.25	.25	.25
CLOSURES	.25	.25	.25	.25	.25	.25	.25	.25
PROTECTIVE PLATE	.25	.25	.25	.25	.25	.25	.25	.25
TRAILING EDGE	.25	.25	.25	.25	.25	.25	.25	.25
ANTI-FRETTING	.25	.25	.25	.25	.25	.25	.25	.25

LEGEND:

(A) SPAR PACK WRAP AROUND PIN

(B) NOSE TO SPAR PACK WRAP AROUND PIN

(C) PUNCH THROUGH

(D) FILAMENT WRAP AROUND PIN

TABLE 24. ROOT END LCC DATA - INPUT

ROOT END DESIGN	NON RECURRING (MILLION)	RECURRING PER BLADE	MTBR	AVERAGE REPAIR COST
A	$3,160,000	1,122	15,000	1,200
B	3,840,000	1,173	15,000	1,200
C	3,240,000	1,020	16,875	1,000
D	3,000,000	1,020	15,625	1,200

TABLE 25. ROOT END LCC DATA - OUTPUT

ROOT END DESIGN	RECURRING	NON RECURRING	O&S	TOTAL	PRIORITY
A	$3,366,000	$3,160,000	$691,200	$7,217,200	.248
B	3,519,000	3,840,000	691,200	8,050,200	.222
C	3,060,000	3,240,000	512,000	6,812,000	.263
D	3,060,000	3,000,000	663,552	6,723,552	.267

LEGEND:

(A) SPAR PACK WRAP AROUND PIN

(B) NOSE TO SPAR PACK WRAP AROUND PIN

(C) PUNCH THROUGH

(D) FILAMENT WRAP AROUND PIN

TABLE 26. ROOT END EVALUATION SUMMARY

	R&M	LCC	BAL. TOL.	PERF.	RADAR	TOTAL
(A) SPAR PACK WRAP AROUND PIN	.048	.074	.027	.062	.038	.249
(B) NOSE TO SPAR PACK WRAP AROUND PIN	.048	.067	.027	.062	.038	.242
(C) PUNCH THROUGH	.054	.079	.019	.062	.038	.252
(D) FILAMENT WRAP AROUND PIN	.050	.080	.027	.062	.038	.257

3.3 AERODYNAMIC DESIGN

This section describes the procedure used to develop an aerodynamically improved design for the main rotor blades for the OH-58 helicopter. The primary design objective was to determine a planform, twist and airfoil contour for the blades which, when installed on the OH-58, will yield a 6 percent reduction in the engine shaft horsepower required to hover at 3200 lb gross weight at 4000 ft and 95°F. Another objective was that the resulting design should not substantially degrade the aircraft's forward flight performance.

3.3.1 Design Approach

The aerodynamic features of the current OH-58 helicopter main rotor blade are presented in Figure 16. The rotor has two blades of rectangular planform incorporating a 70° leading edge sweep over the outer 2% of the blade. Blade twist is -10.6 degrees and the airfoil (constant) is an 11.2% thick, drooped leading edge, cambered airfoil - a Bell Helicopter Company proprietary section. Rotor diameter is 35 ft 4 in. and the airfoil chord is 13 in., giving a geometric solidity of 0.039.

Because considerations of main rotor/tail rotor clearance preclude increasing the main rotor diameter, only three means for improving the rotor efficiency remain:

1. employ more efficient airfoil sections
2. alter the twist distribution
3. change the planform

These must be combined in a suitable way to yield the required increase in efficiency.

3.3.1.1 Review of Factors Affecting Hover Performance

The power absorbed by a hovering rotor is the sum of the induced power, expended in accelerating the air to produce thrust, and the profile power required to overcome the profile drag of the blades. Both the induced and the profile power are affected by blade planform, twist and airfoil section.

3.3.1.1.1 Induced Power

At normal hover thrust levels the induced power accounts for roughly 80% of the total power required. The greatest power savings is therefore to be found by minimizing this component. The blade span loading must be arranged so that the resulting downwash distribution is as uniform as possible. More precisely, the distribution of blade circulation (Γ) must be

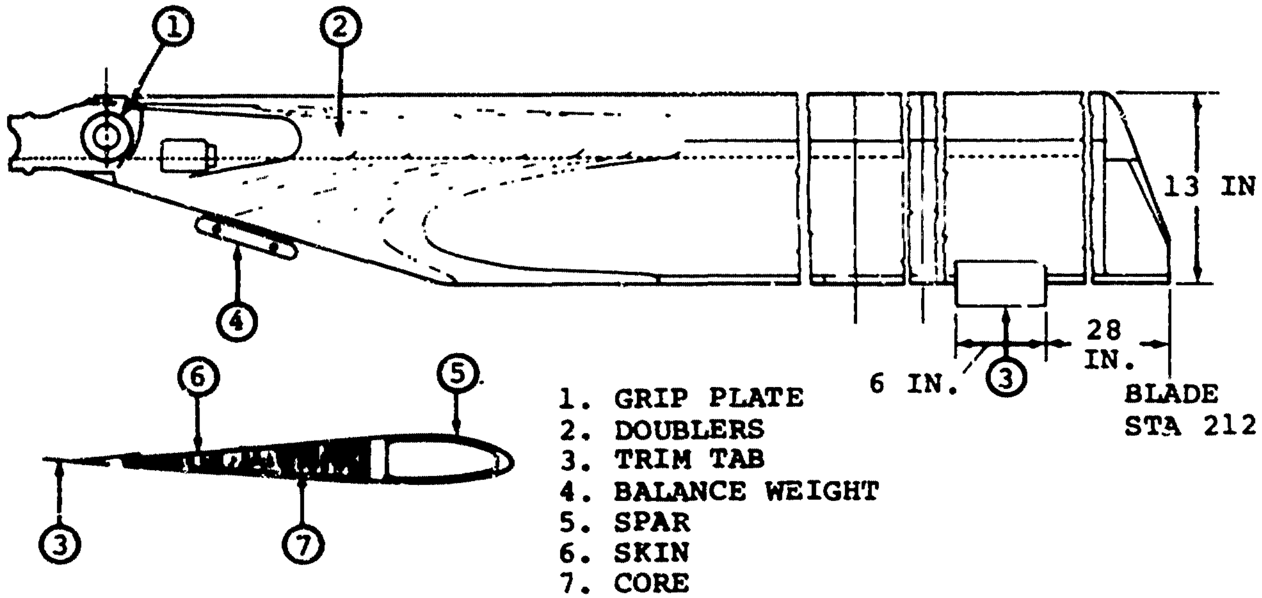

Figure 16. OH-58C/A Metal Blade

optimized because the downwash depends on the spanwise rate of change of Γ. The circulation is related to the local blade section lift coefficient, C_ℓ, and chord, c, through $\Gamma = 1/2\, C_\ell c\Omega Rx$, where Ω is the rotor rotational speed, R is the rotor radius and x is the nondimensional radial distance. Therefore, since the local C_ℓ depends on angle of attack, it is clear that the correct combination of twist and chord must be made to achieve a reduction in induced power.

For rectangular planform blades, increasing overall twist generally improves hover performance. Too much twist, however, results in unacceptable increases in rotor hub and blade loads in forward flight. The precise amount of twist that will yield an improved figure of merit without significantly affecting hub and blade loads depends on the type of rotor (articulated, hingeless or teetering) and on the blade structural properties.

Boeing Vertol has conducted a number of analytical and experimental studies on the effects of blade twist. During the development of the HLH rotor, wind tunnel tests were made on model rotors with rectangular blades and the same airfoils but with different twist distributions. It was found that while increasing overall linear twist did improve the figure of merit, no benefit in forward flight lift/drag ratio was obtained. However, when only the outer 15 percent of the blade was given an increased twist, a higher figure of merit was achieved together with an improved lift/drag ratio. The test results clearly showed that the most effective place to increase twist is the outer 10 to 15 percent of the blade.

This result may be qualitatively explained by considering the twist required to produce uniform downwash (minimum induced power) and minimum profile power. For minimum induced power the twist varies inversely with radial distance, and near the tip this variation is nearly linear. For minimum profile power the blade sections must be operated at the angle of attack for best lift-to-drag ratio. For most airfoils this angle is constant up to about M = 0.4 and then reduces rapidly as Mach number is increased. Thus the blade must be given a sharply increased washout as the high mach number (tip) region is approached.

3.3.1.1.2 <u>Profile Power</u>

The above discussion showed that by varying twist and chord, induced power can be reduced. Rotor profile power also depends strongly on the chord distribution and to a lesser extent on twist. For a blade of general planform the profile power coefficient is given by (for B blades):

$$C_{P_o} = \frac{B}{2\,\Pi\,R} \int_{xc}^{1.0} c(x)\; C_d(x)\; x^3 dx$$

Here the product of the local chord (c) and the section drag coefficient (C_d) determines the profile power. If the drag coefficient were constant (independent of C_ℓ, Reynolds number and Mach number) then the profile drag would be given by:

$$C_{P_o} = \frac{B\; C_d\; c_Q}{8\,\Pi\,R} = \sigma_Q\; C_d/8$$

where B is the number of blades

$$c_Q = 4 \int_{xc}^{1.0} c(x)\; x^3 dx$$ is the equivalent torque-weighted chord and

$$\sigma_Q = \frac{Bc_Q}{\pi R}$$ is the torque-weighted solidity.

Thus, a reduction in the blade chord near the tips reduces the value of σ_Q and hence reduces the profile power. Of course the profile power could also be reduced by cutting down on the entire blade chord. This is undesirable because a reduced overall chord increases the average lift coefficient at which the blade sections must operate to achieve a given thrust. This in turn increases the lift-dependent component of profile drag and reduces the range of available thrust before blade stall occurs. By reducing the chord only in the tip region, where the operating $C\ell$'s are low and the values of C_d relatively constant, these problems are avoided.

Profile power can also be reduced by replacing the existing airfoils with sections having lower drag at the same lift level. The sections must be chosen so as to ensure that forward flight performance is not penalized by premature drag divergence or by an inadequate $C_{\ell_{max}}$ capability throughout the Mach number range.

The above discussion has outlined three ways for improving the hover performance of the OH-58 rotor:

- Incorporate improved airfoils
- Change the aerodynamic twist
- Shape the tip planform

The following sections present in detail the basis for selecting the final design configuration.

3.3.2 Airfoil Selection

3.3.2.1 Baseline Data

As stated above, the airfoil used on the existing OH-58 helicopter is a 11.2% droop nose section. No published data exists for this section. For the purpose of establishing a common baseline for evaluation, the Government recommended that Boeing Vertol use section data for the NACA 0012 section supplied by the Government in the form of a listing for the Rotorcraft Analysis Program C-81. In order to determine approximately the performance of the actual OH-58 airfoil, Boeing Vertol obtained casts of the airfoil from an OH-58 blade and estimated the performance using the analysis of Reference 5 for Mach numbers less than 0.7, and the analysis of Reference 6 for Mach numbers greater than 0.7.

Based on the performance of both the baseline NACA 0012 data and the OH-58 cast data, the advanced airfoil sections VR-7 and VR-8, developed by Boeing-Vertol, were selected for evaluation as replacement airfoils for the OH-58 rotor. Since the NACA 0012 data was obtained for a smooth airfoil under test conditions different from those at which the VR-7 and VR-8 airfoils were tested, the following correction procedure was developed (with Government approval) in order to compare performance on a consistent basis.

The NACA 0012 data was obtained from a model with very smooth surfaces tested in a wind tunnel with a turbulence level lower than the turbulence level of the test environment of the VR series airfoils. A correction to the 0012 drag levels was therefore obtained by computing the theoretical drag with free transition and with transition fixed at 20% chord. The resulting increments in drag are shown in Figure 17 as a function of angle of attack. The computations were made using the Government-owned potential flow/boundary layer interaction analysis (Reference 5).

3.3.2.2 VR-7 and VR-8 Data

The VR-7 and VR-8 airfoils have been extensively tested (Reference 7) with chords ranging from 15 inches to 35 inches.

---

5. Stevens, W.A., Goradia, S.H., and Braden, J.A., MATHEMATICAL MODEL FOR TWO-DIMENSIONAL MULTI-COMPONENT AIRFOILS IN VISCOUS FLOW, NASA CR-1843, July 1971.
6. Bauer, F., Garabedian, P., Korn, D., and Jameson, A., SUPERCRITICAL WING SECTIONS II, Lecture Notes in Economics and Mathematical Systems, Volume 108, Springer-Verlag, New York, 1975.
7. Dadone, L., and McMullen, J., HLH/ATC ROTOR SYSTEM TWO-DIMENSIONAL AIRFOIL TEST, Boeing Vertol Company, D301-10071-1, December 1971.

13-INCH CHORD

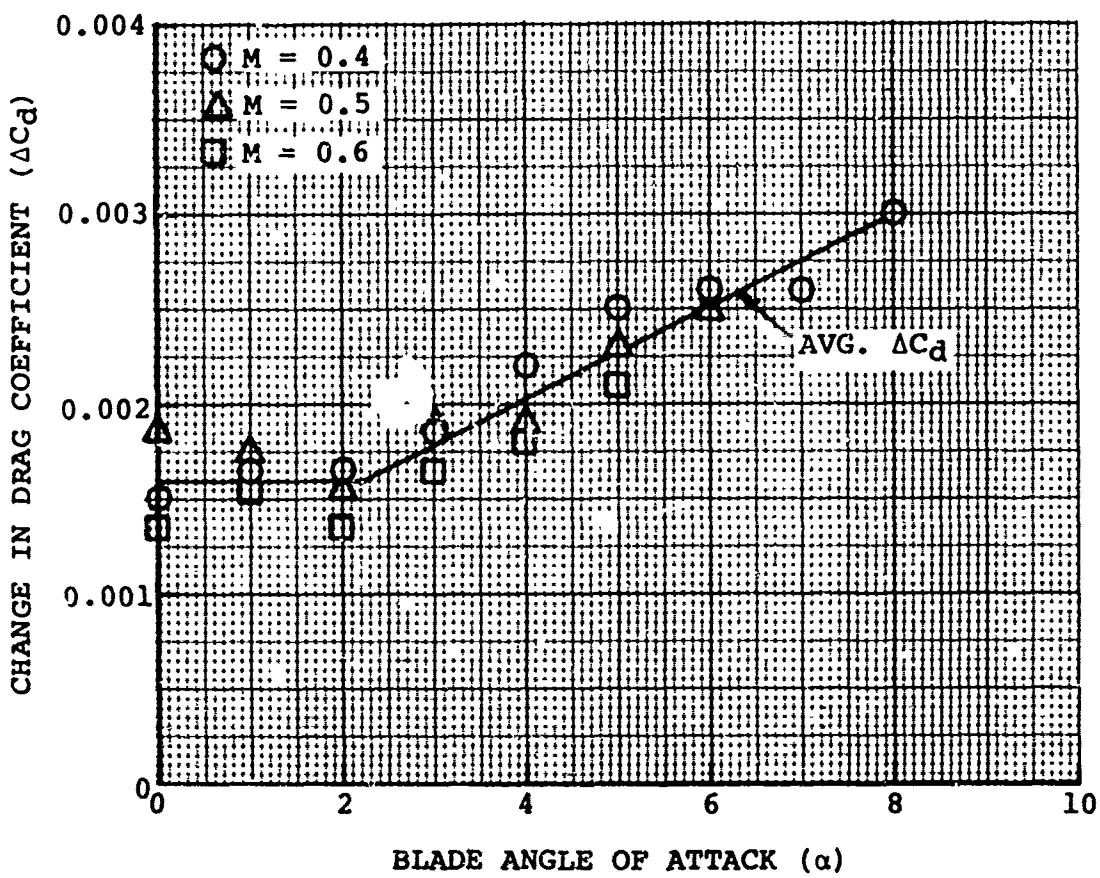

Figure 17. Drag Increments Applied to 0012 Data

Figure 18 presents lift-drag polars of the VR-7 and VR-8 obtained from this test data compared to the (corrected) reference 0012 airfoil and to the estimated performance of the OH-58 blade sections. The figure shows, at the average hover section lift coefficient of 0.6, that the selected airfoils have lower drag than the reference 0012 airfoil and much lower drag than the OH-58 section estimates. Figure 19 compares the drag divergence boundaries of the VR-7 and VR-8 against the 0012. The VR-7 has M_{DD} values lower than the NACA 0012 but, by introducing the thinner lower camber level VR-8, a distribution of airfoils can be defined with overall performance better than the NACA 0012. The plot presented in Figure 20 shows that at 90% blade radius the VR-7 airfoil should begin to transition to the VR-8 contour in order to remain below drag divergence at the conditions shown, while delaying as far outboard as possible the transition to the thinner VR-8 section. The value of section lift coefficient (0.3) is representative of lift levels occurring on the advancing blade at cruise speeds.

The maximum lift boundaries of the selected airfoils are compared to the reference airfoil in Figure 21. The VR-7 offers a substantial improvement in stall margin over the NACA 0012 at Mach numbers between 0.4 and 0.6. The VR-8 has a lower maximum lift capability at M=0.4 but, since this section will be used at the tip only, the lift capability of the sections between the tip and the 90% station (VR-7) will still be better than the reference airfoil.

Figure 22 shows the zero-lift pitching moment characteristics of the proposed and reference airfoils and those estimated from the OH-58 casts. Since the 0012 is a symmetrical airfoil its pitching moment is zero. The proposed airfoils have approximately the same level of pitching moment as the OH-58 section. Based on estimates of the pitching moment levels required by the OH-58 blade sections, a trailing edge tab angle of -3° was selected for the VR-7 airfoil, and 0° for the VR-8 section. The effect of -3° tab angle on the lift/drag polar of the VR-7 was calculated from polars at 0° tab angle by the scaling technique described in Reference 8. No tab angle changes were required for the VR-8.

3.3.3 Selection of Twist and Planform - Parametric Studies

As indicated in Paragraph 3.3.1.1, reductions in the blade chord near the tips will reduce the torque-weighted solidity and hence rotor profile power. In order to maintain a satisfactory operating $C\ell$ distribution in the tip area with reduced

8. Dadone, L.U., U.S. ARMY HELICOPTER DATCOM, VOLUME 1 - AIRFOILS, USAAMRDL CR 76-2, September 1976, AD A033425.

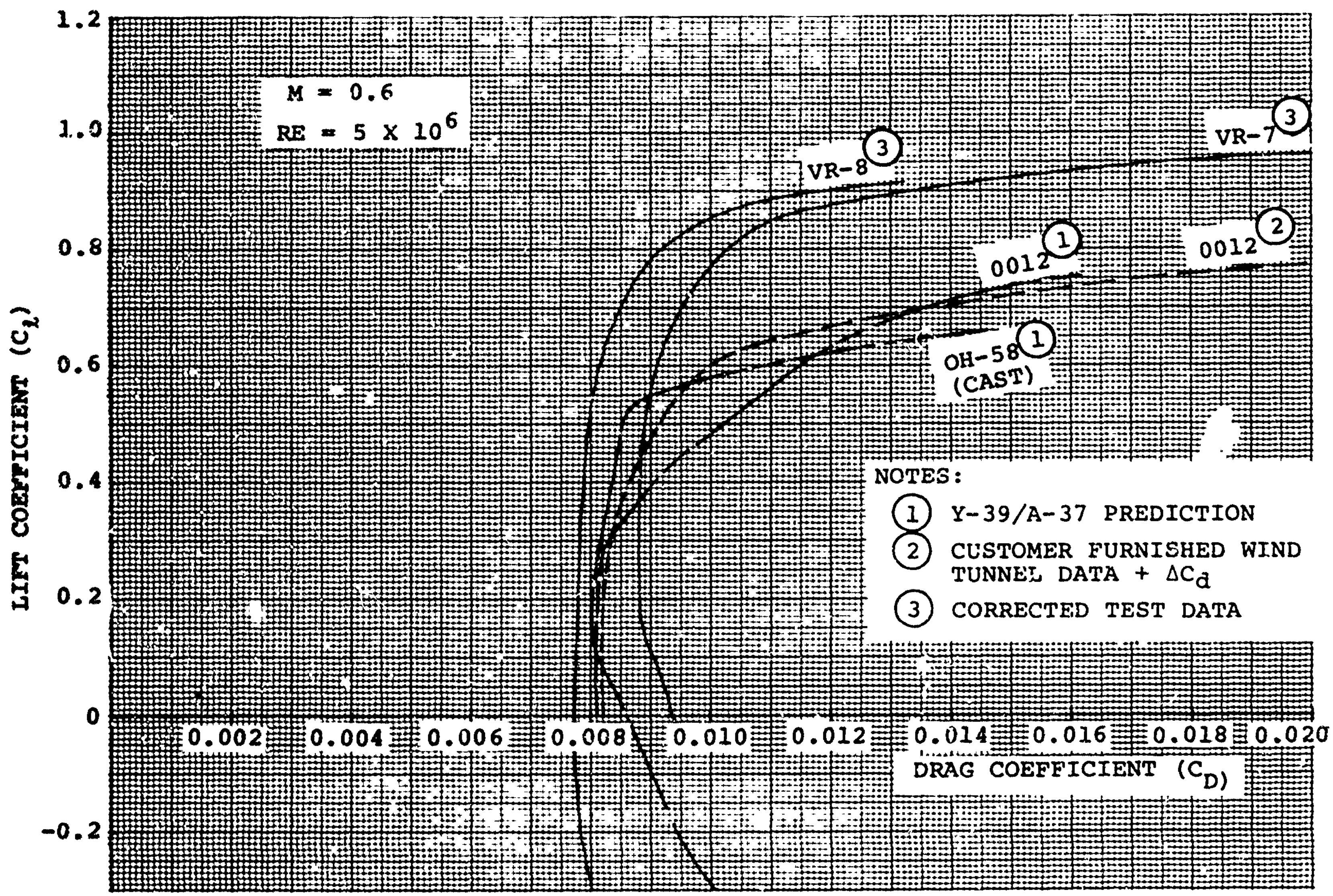

Figure 18. Airfoil Lift/Drag Polars

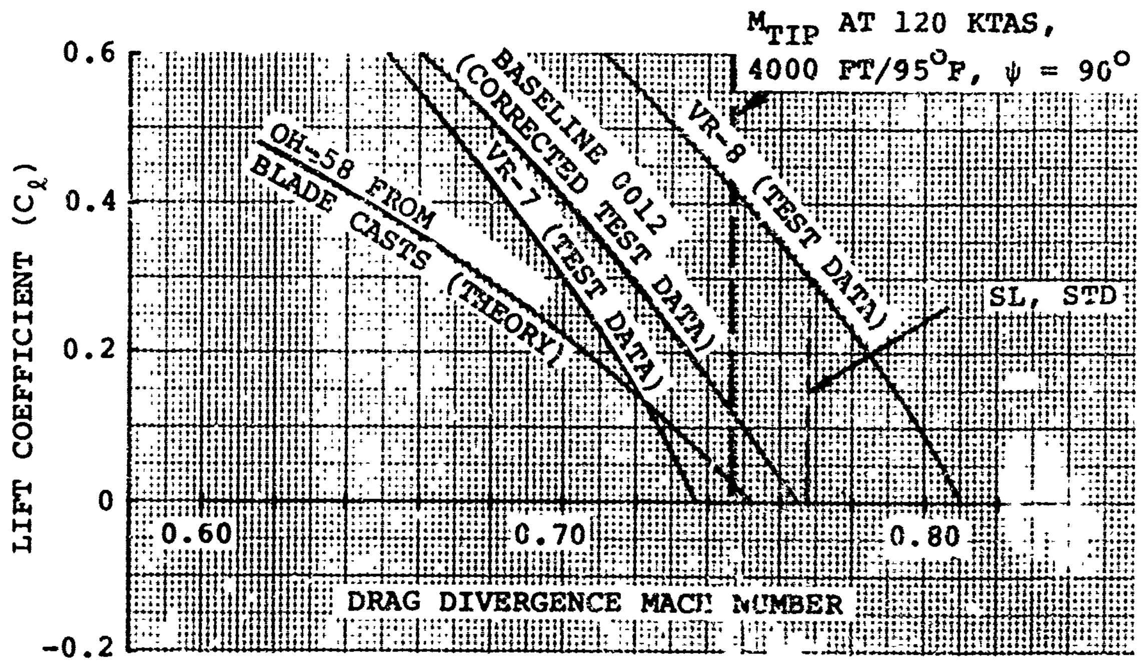

Figure 19. Drag Divergence Boundaries

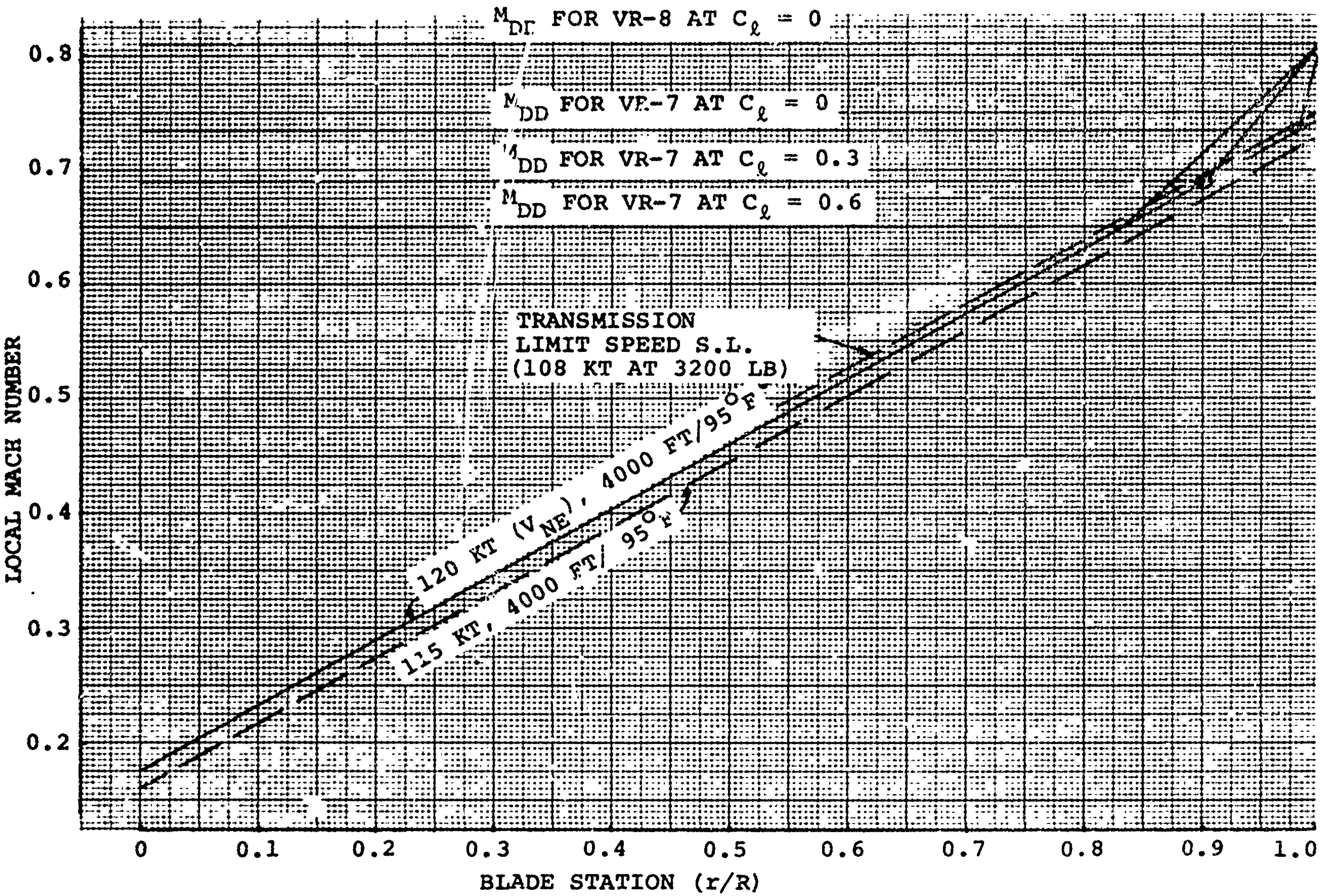

Figure 20. Selection of Point for Transition to VR-8

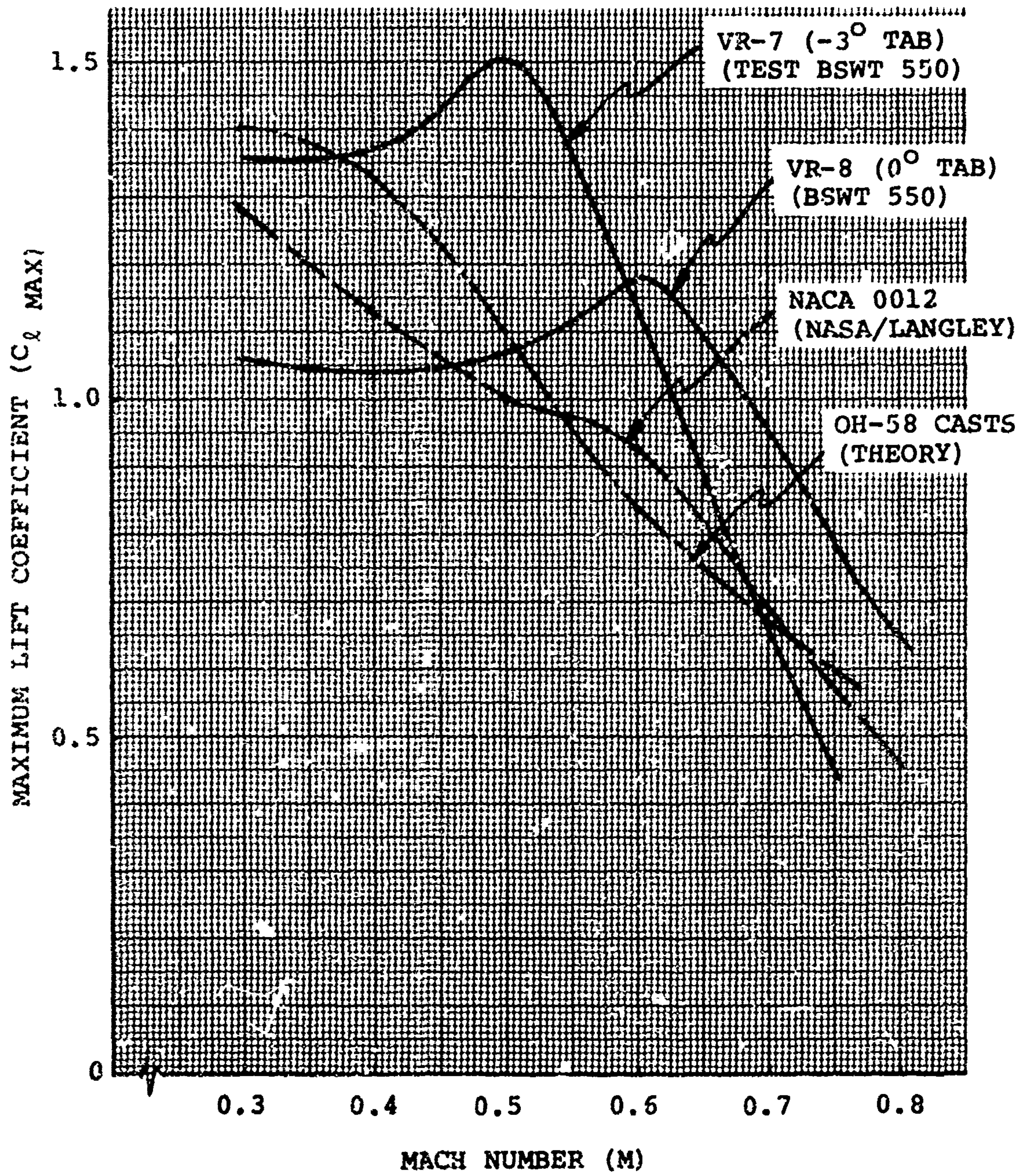

Figure 21. Comparison of Maximum Lift Boundaries

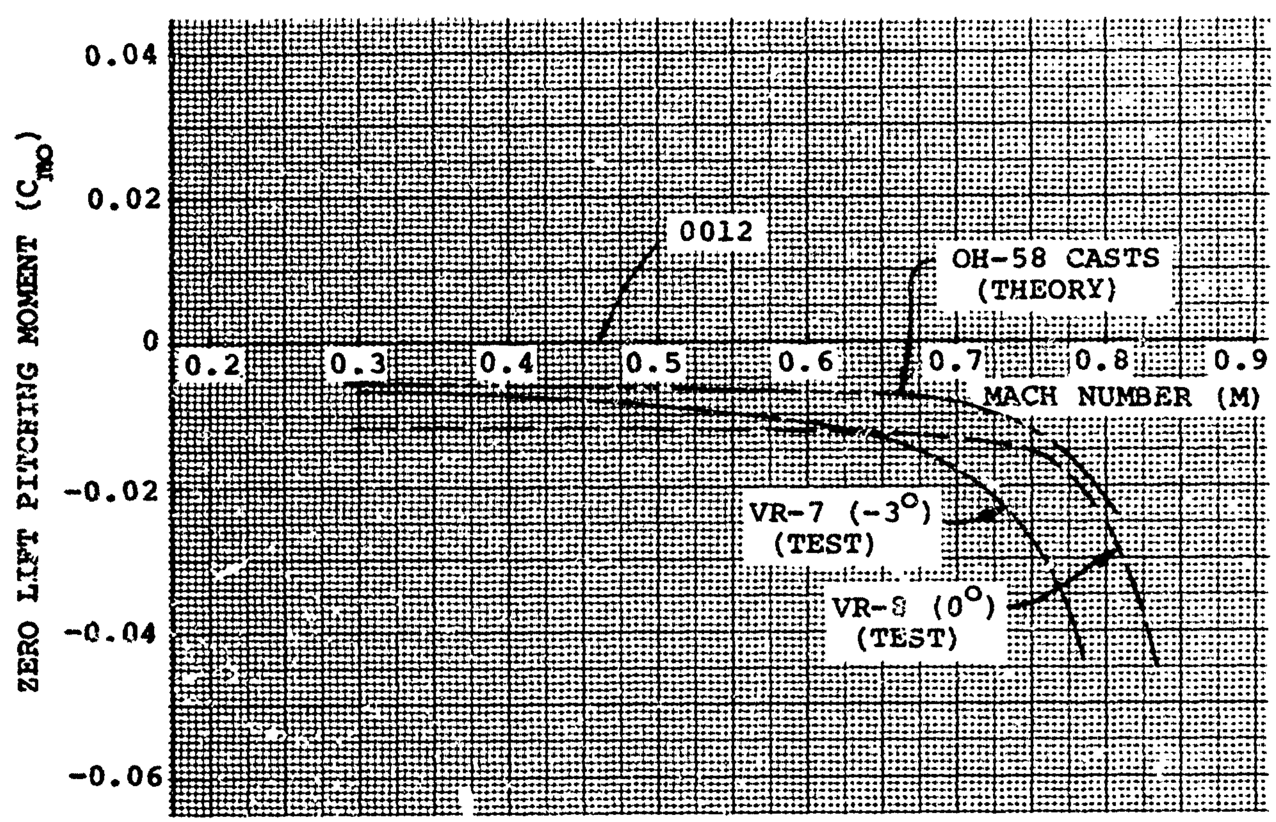

Figure 22. Comparison of Zero Lift Pitching Moment Coefficients

chord, the angle of attack must be reduced by increasing the twist (more washout) over this region. A parametric analysis was therefore made to establish the correct combination of tip washout and blade chord reduction that would yield the best performance. The parametric study covered linear tip washout from 0° to 4° starting at selected radial stations (0.75 to 0.95) in combination with chord taper (3:1) starting at radial stations between 0.7 and 1.0.

The data were computed using computer program B-92, a lifting line analysis having a prescribed wake and nonuniform inflow. The taper ratio of 3:1 was selected based on the results of Figure 23 where the percentage savings in power due to taper are shown for various taper ratios and various locations for the start of taper. The data shows that increasing taper results in increased savings. However, design and construction considerations effectively limit the allowable taper to 3:1. Larger values result in thinner tip sections, making it difficult to accommodate the necessary structure and tip weights.

The selected 3:1 taper is distributed so that the blade 1/4 chord line is straight. This tends to minimize aeroelastic effects. No advantage in terms of compressibility drag considerations is to be gained by sweeping the tip because of the low hover tip Mach number at which the OH-58 rotor operates.

The results of the parametric study are presented in Figures 24 through 26. Figure 24 shows the percentage power savings using different combinations of taper and washout, with washout starting at 75% radius. Figures 25 and 26 present the corresponding results for washout starting at 85% and 95% radius. These data were all computed assuming that the VR-7 section extended from root to tip. With the VR-8 at the tip, approximately 0.4% improvement over the plotted values is attained.

The results show that 3 degrees of additional tip washout is optimum for each radial station at which taper begins. Also shown in Figure 25 is the effect of increasing the overall linear twist. It can be seen that this is less effective than increasing the outboard twist only.

Based on these results, an initial design having 3° washout starting at 85% with 3:1 taper also starting at 85% was selected for further investigation. Analysis of the forward flight loads and power required showed that tapering from 90% rather than 85% would be more acceptable because rotor stall was delayed more with this configuration. This is discussed in Section 3.4. Tapering from 90% also eased the blade structural and manufacturing tasks.

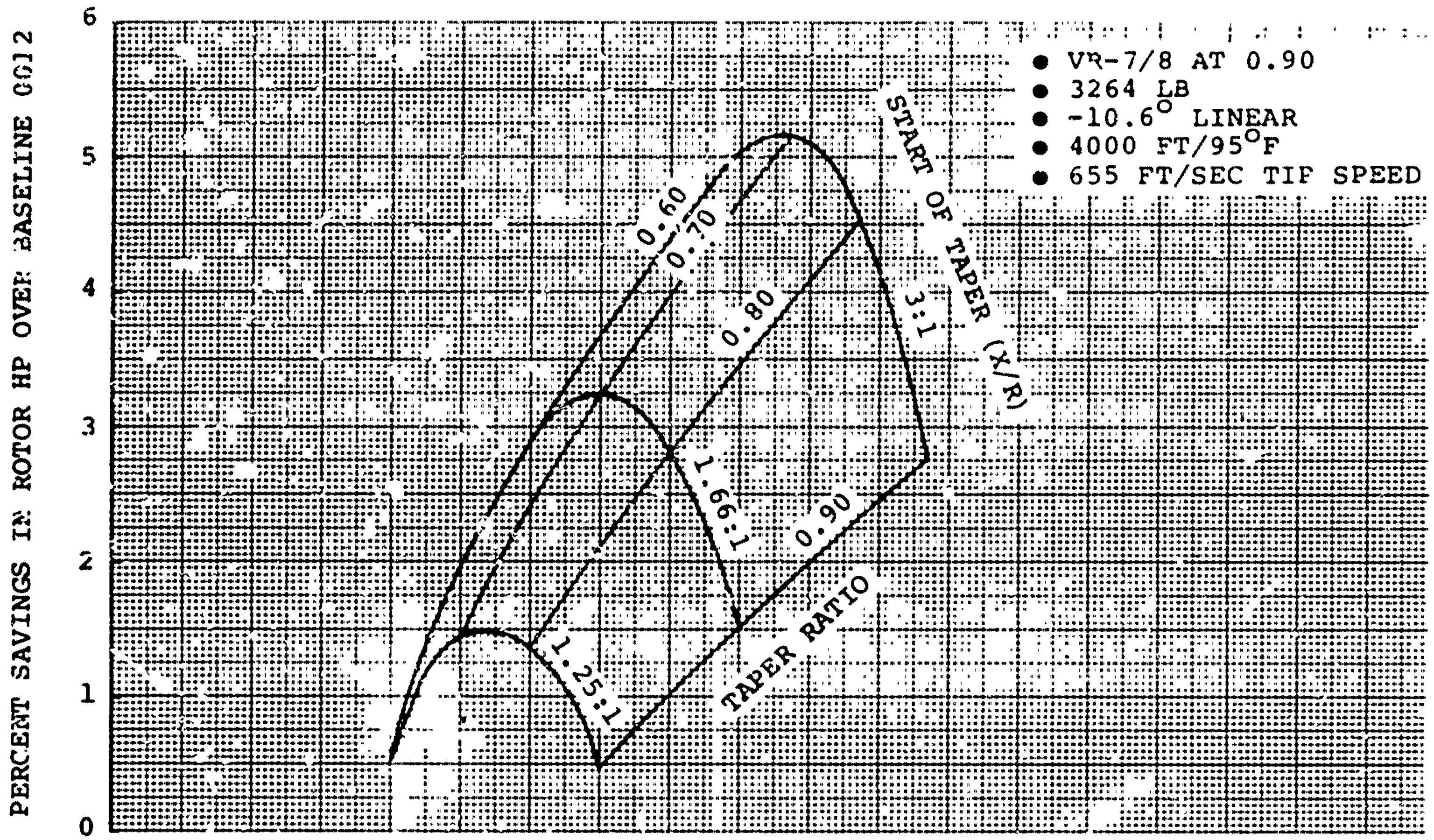

Figure 23. Influence of Taper Ratio on Hover Performance

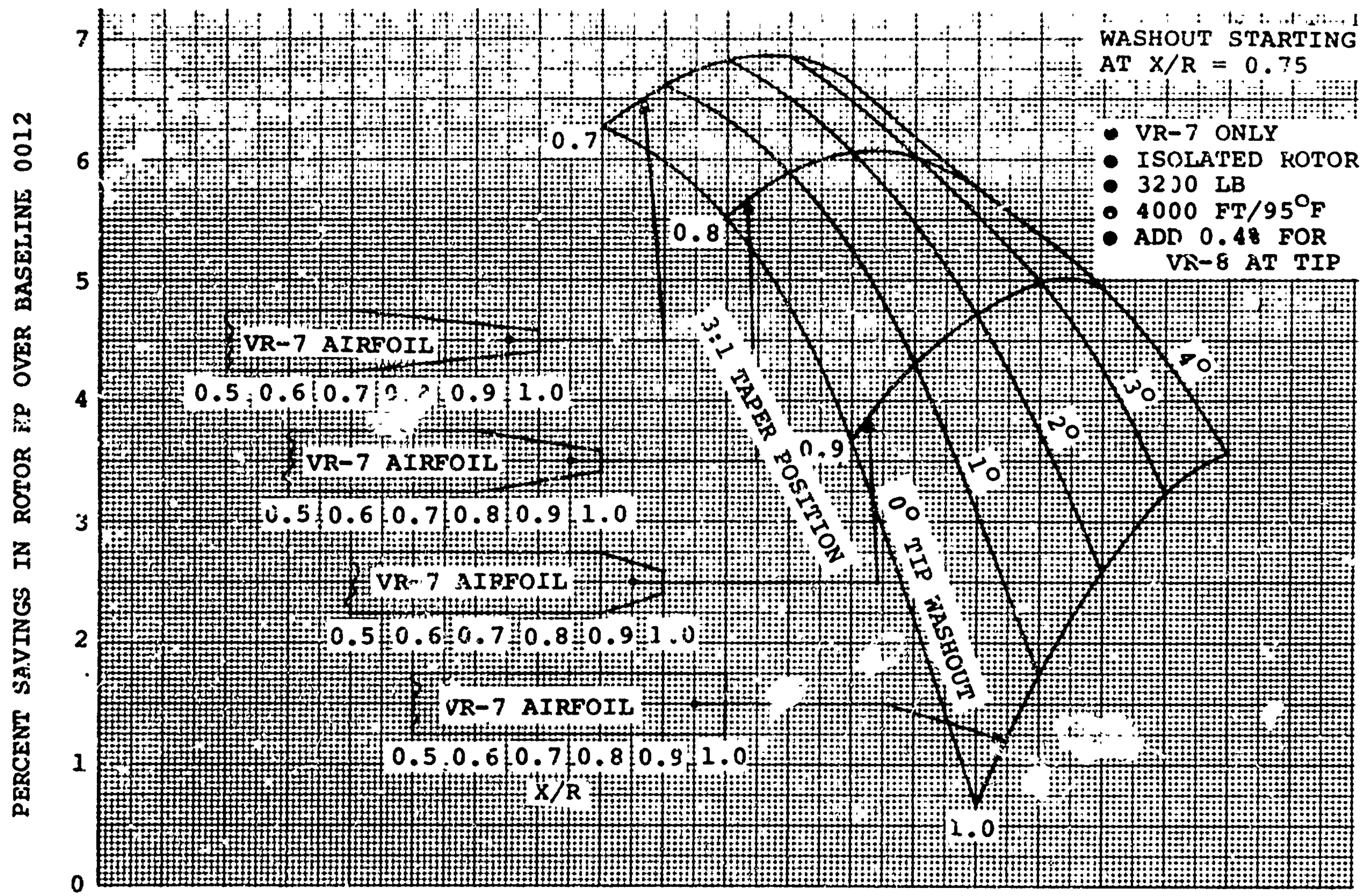

Figure 24. Effect of Taper With Tip Washout From 75% Radius

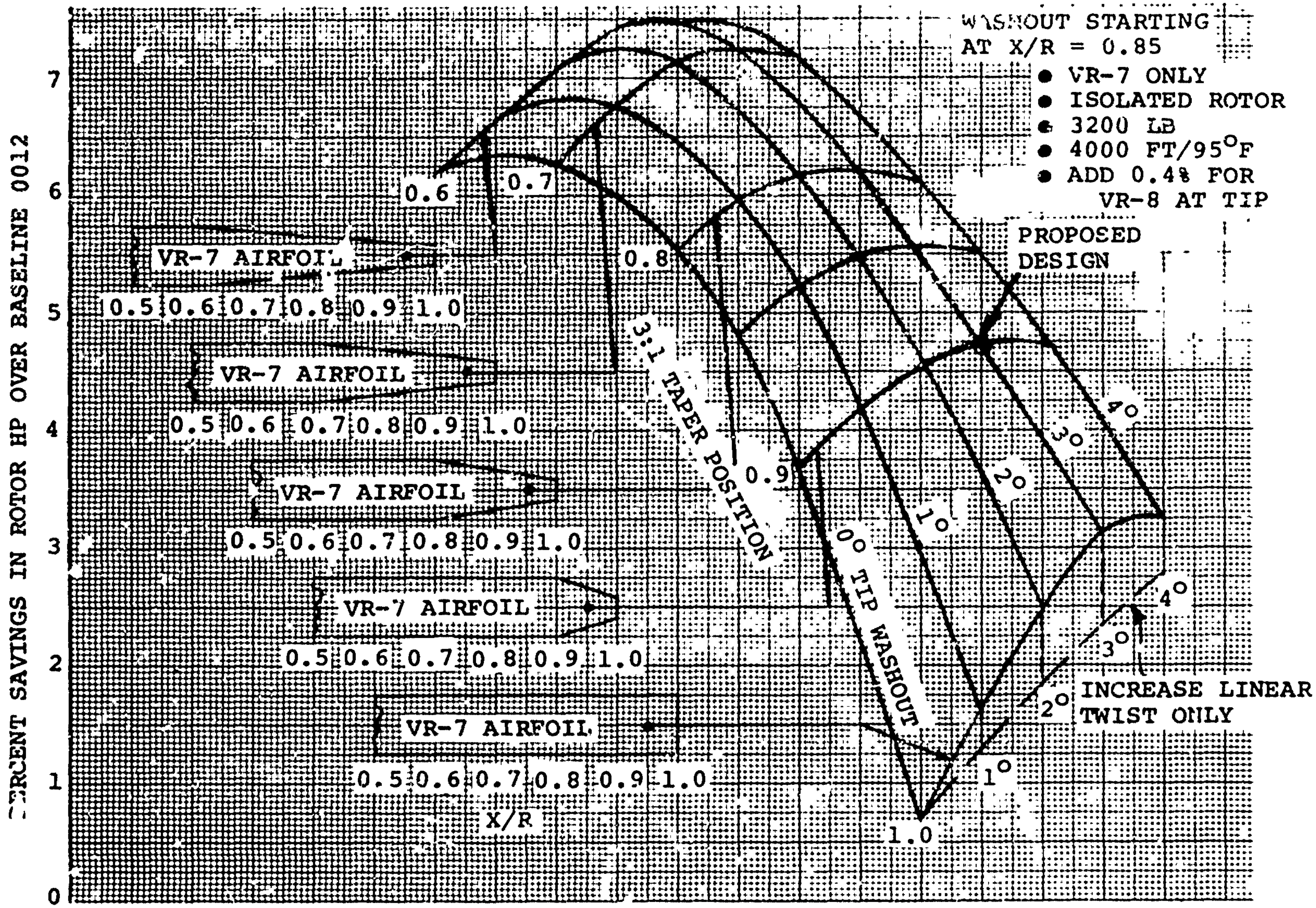

Figure 25. Effect of Taper and Tip Washout From 85% Radius

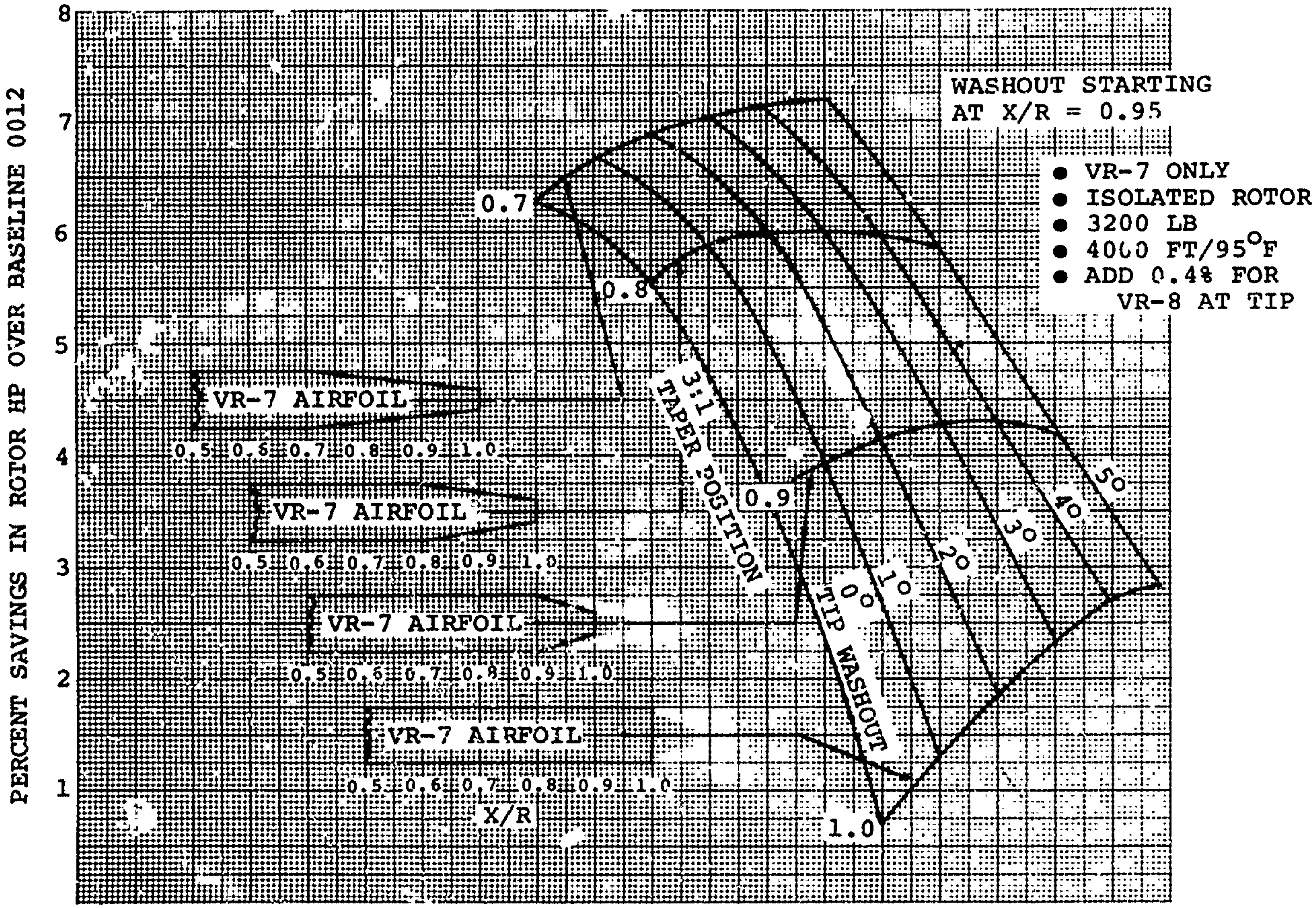

Figure 26. Effect of Taper and Tip Washout From 95% Radius

3.3.4 Source of the Hover Performance Benefit

At 3200 lb thrust and 4000 ft/95°F, the recommended design yields, for the isolated rotor, a 5.1% savings in power compared to the baseline isolated rotor with the NACA 0012 airfoil. Figure 27 shows a breakdown of the power savings. Approximately 52% of the gain is in profile power reduction and 48% in induced power. If 100% of the savings were profile power this would mean that blade area was removed without changing the blade lift distribution. However, the combination of taper and washout also alters the blade lift distribution favorably and hence savings in induced power are also realized.

The source of the improved performance is further shown by Figures 28 through 33. Figure 28 compares the angle-of-attack distributions and shows that the proposed design operates at slightly lower angles of attack than the baseline rotor. The corresponding lift and drag coefficient distributions are presented in Figures 29 and 30. A comparison of blade pitching is shown in Figure 31. The improved composite blade operates with higher lift and lower drag coefficients for the same thrust than the baseline configuration. In Figures 32, 33, and 34 the running thrust, torque and torque-to-thrust ratios are presented. The proposed design moves the loading inboard compared to the baseline rotor. This reduces the maximum velocities induced by the tip vortex, thereby improving blade-to-blade interference.

Figure 35 compares the overall hover performance of the improved rotor with the baseline rotor in terms of isolated rotor thrust coefficient and power coefficient. Noted on the figure is the estimated operating weight empty of the OH-58 (2449 pounds) and the maximum weight of 3200 pounds. The recommended blade design shows an improvement at all operating weights of interest.

3.3.5 Performance Comparison With the OH-58 Cast Data

As discussed in Paragraph 3.3.2.1, casts were taken of the airfoil sections of the OH-58 rotor blade and used to estimate their aerodynamic characteristics. Figure 36 shows the hover performance improvement estimated for the recommended design compared to the existing rotor with the Army-supplied 0012 data and to the rotor with the OH-58 cast airfoil data. The figure is in terms of total aircraft shaft horsepower and shows that a larger performance increase is realized (6.1% vs. 5.1%) based on the measured airfoil characteristics since the OH-58 cast airfoil demonstrate higher drag levels than the baseline 0012 section.

3.3.6 Forward Flight Performance and Rotor Limits

Figure 37 presents OH-58 forward flight power required at a

	ROTOR POWER REQ. AT 4000 FT/95°F WEIGHT = 3200	RHP SAVINGS
BASELINE ROTOR	231.5	6.0 PROFILE
		11.6
		5.6 INDUCED
PROPOSED DESIGN	219.9	

Figure 27. Breakdown of Hover Power Savings/Isolated Rotor

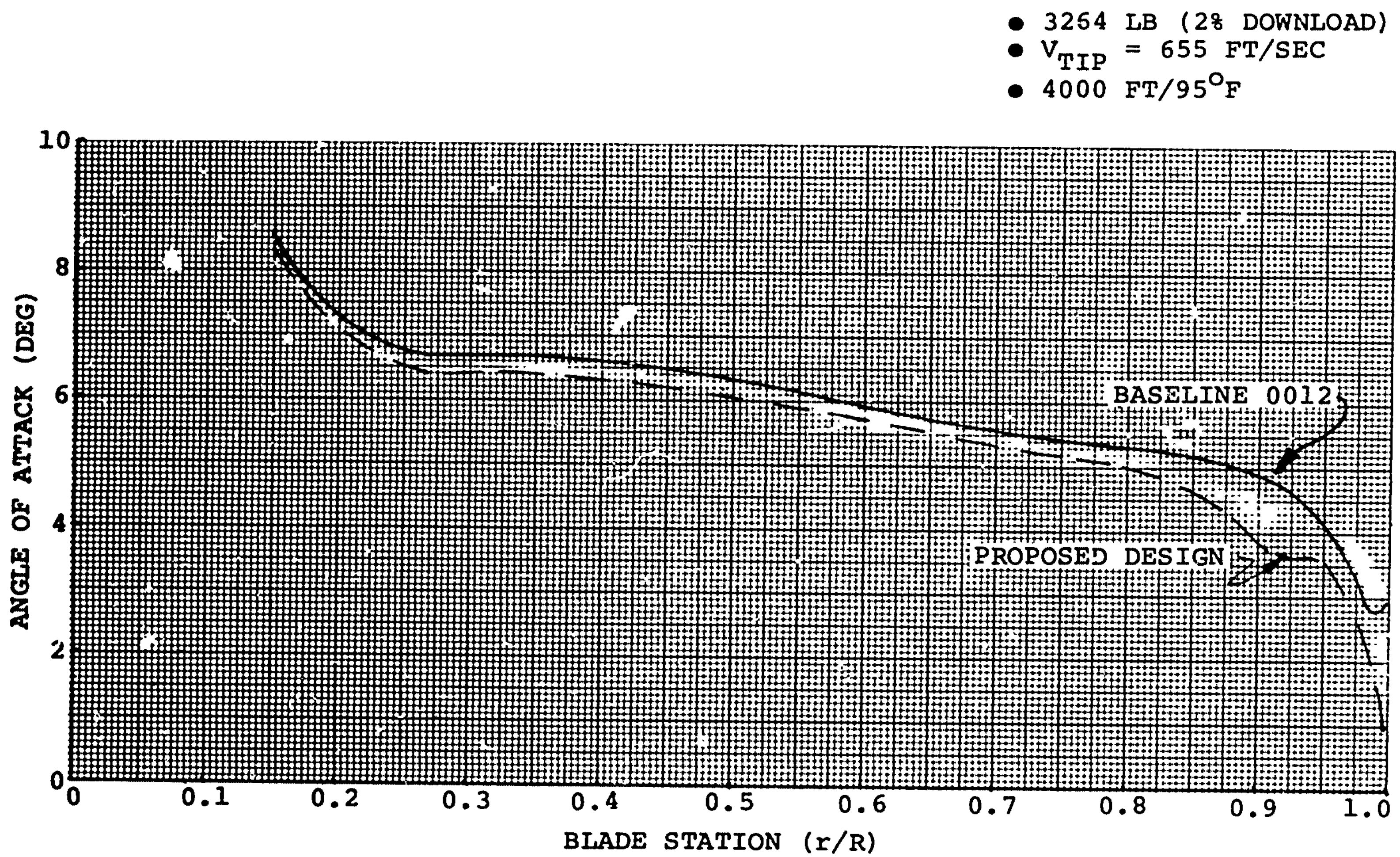

Figure 28. Angle of Attack Comparison

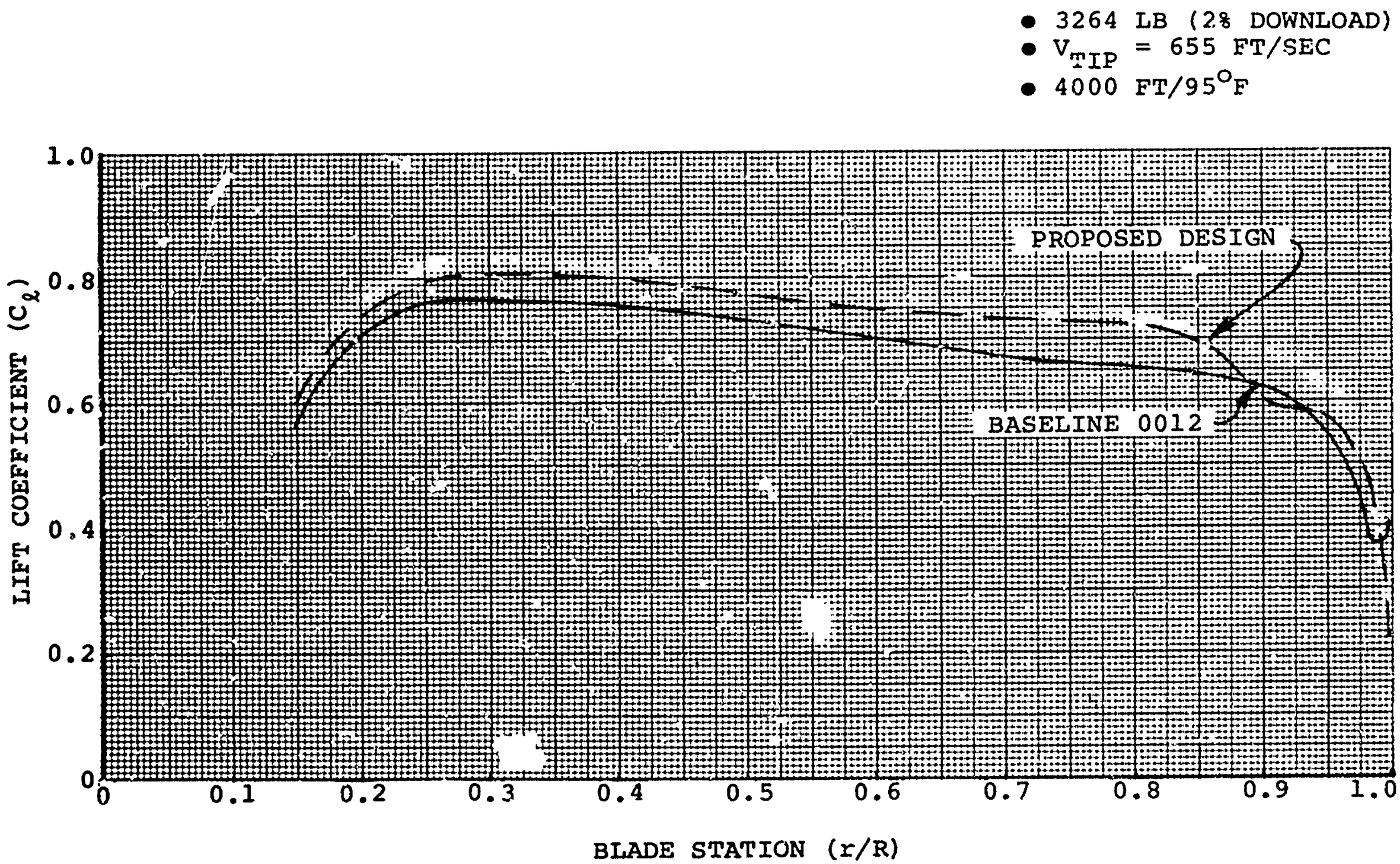

Figure 29. Lift Coefficient Comparison

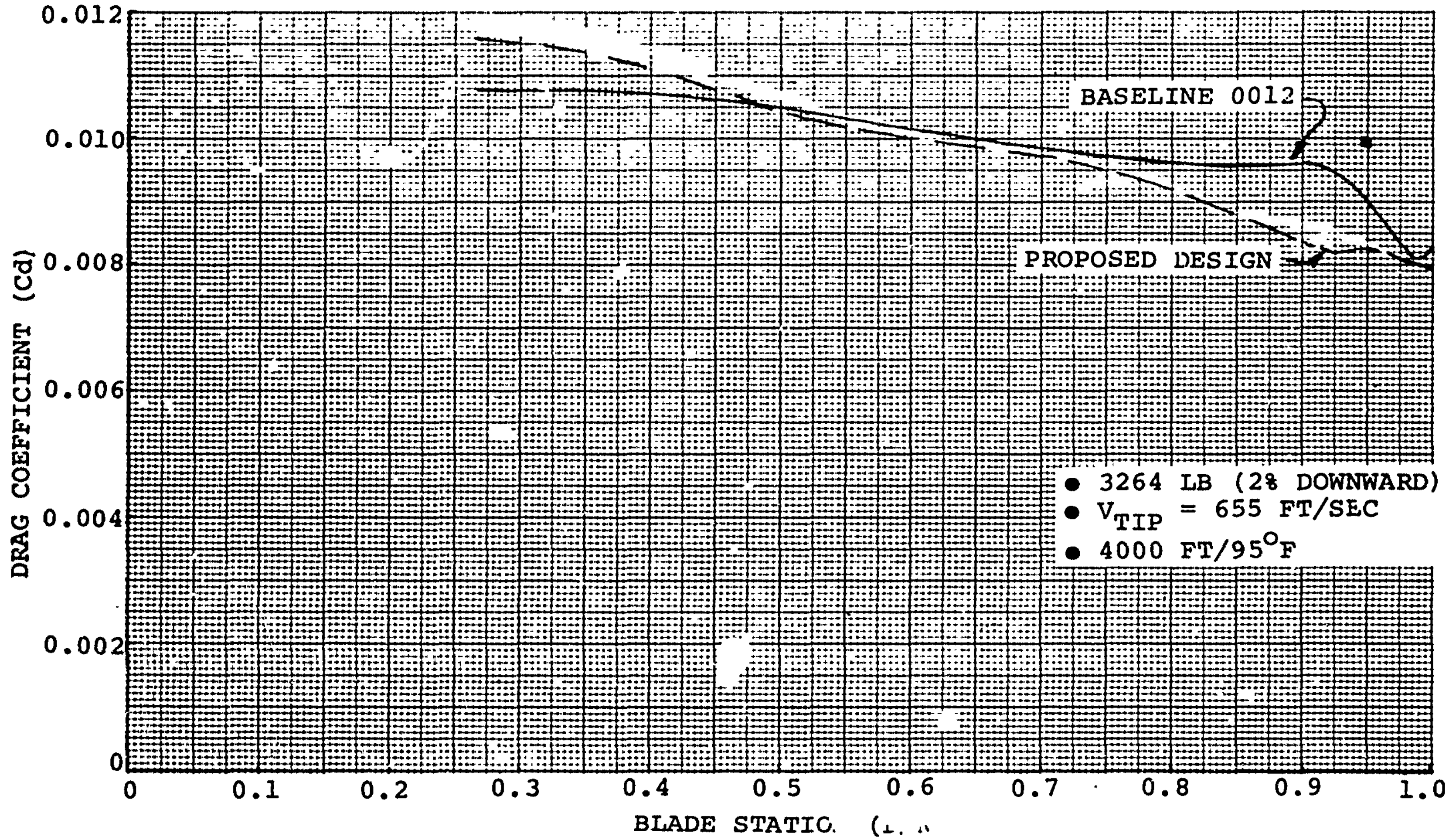

Figure 30. Drag Coefficient Comparison

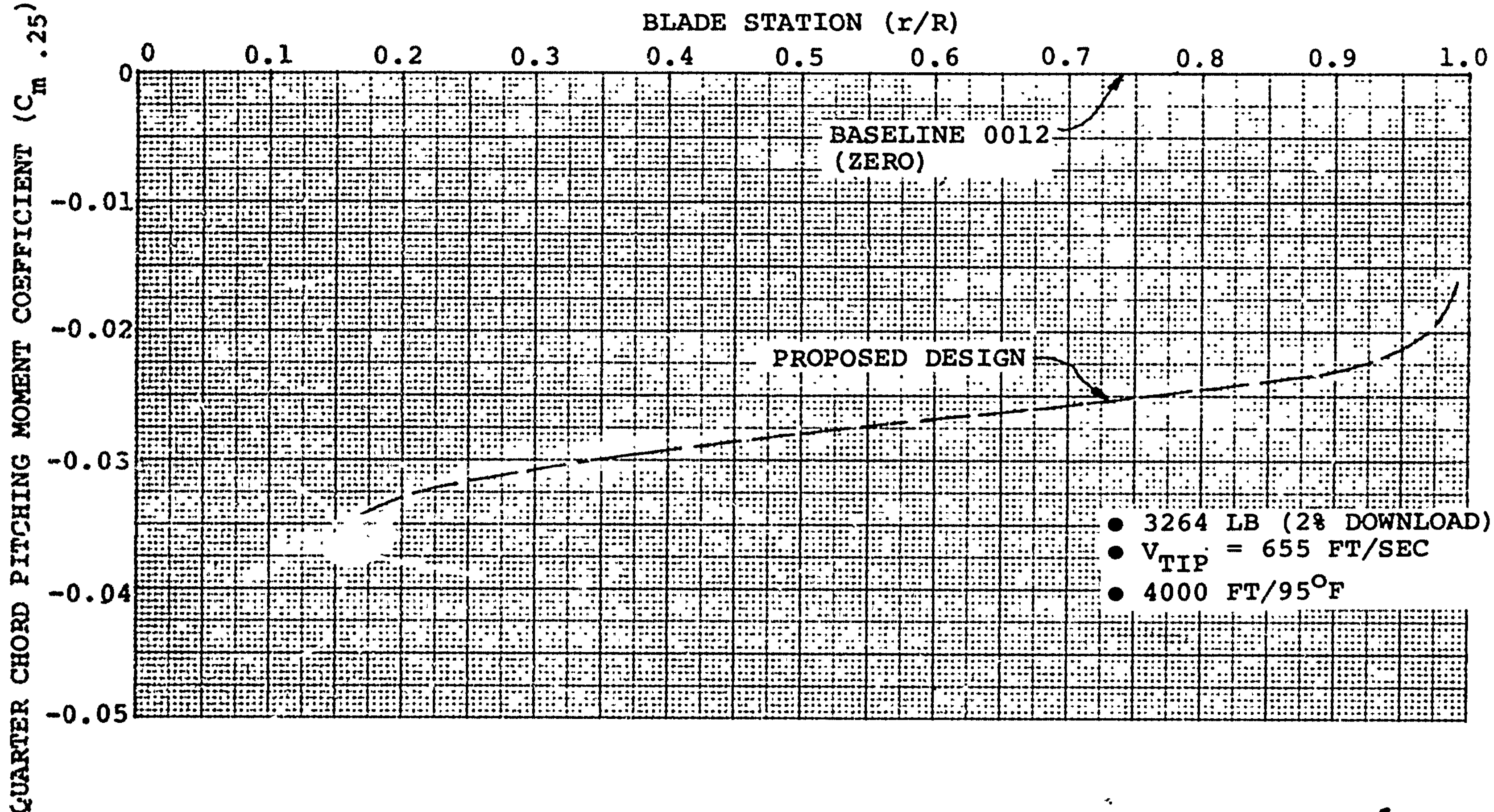

Figure 31. Pitching Moment Comparison

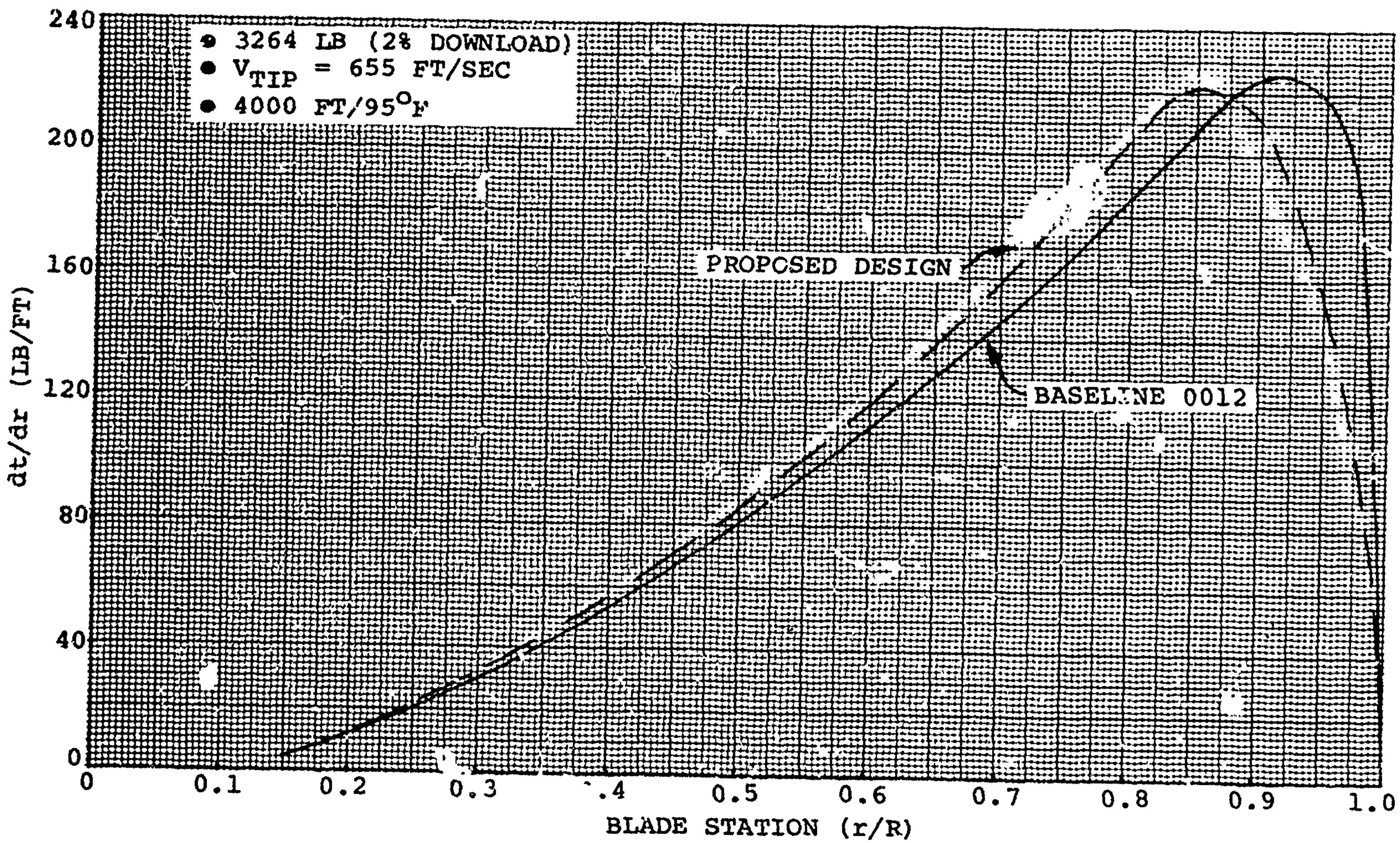

Figure 32. Running Thrust Loading Comparison

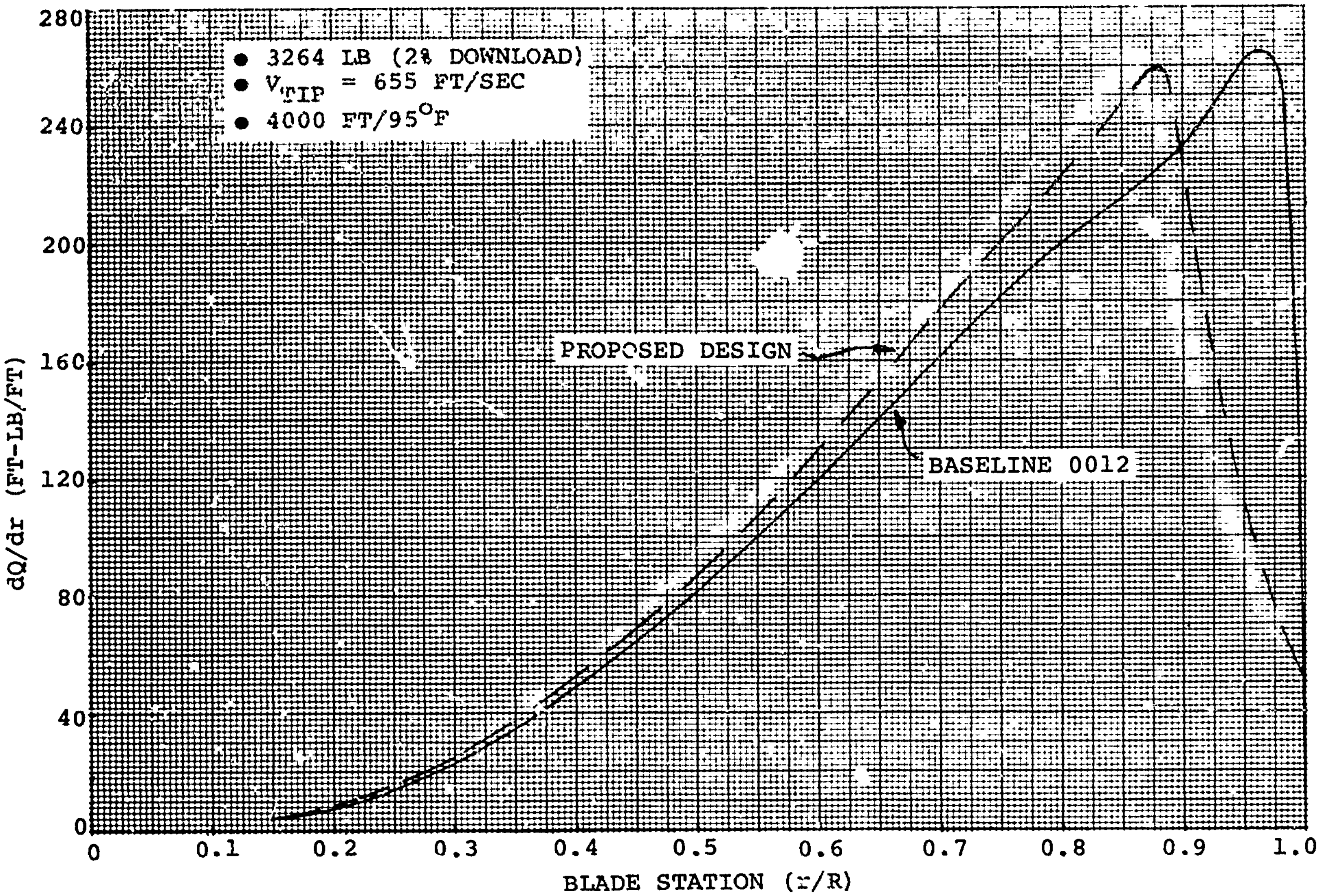

Figure 33. Running Torque Loading Comparison

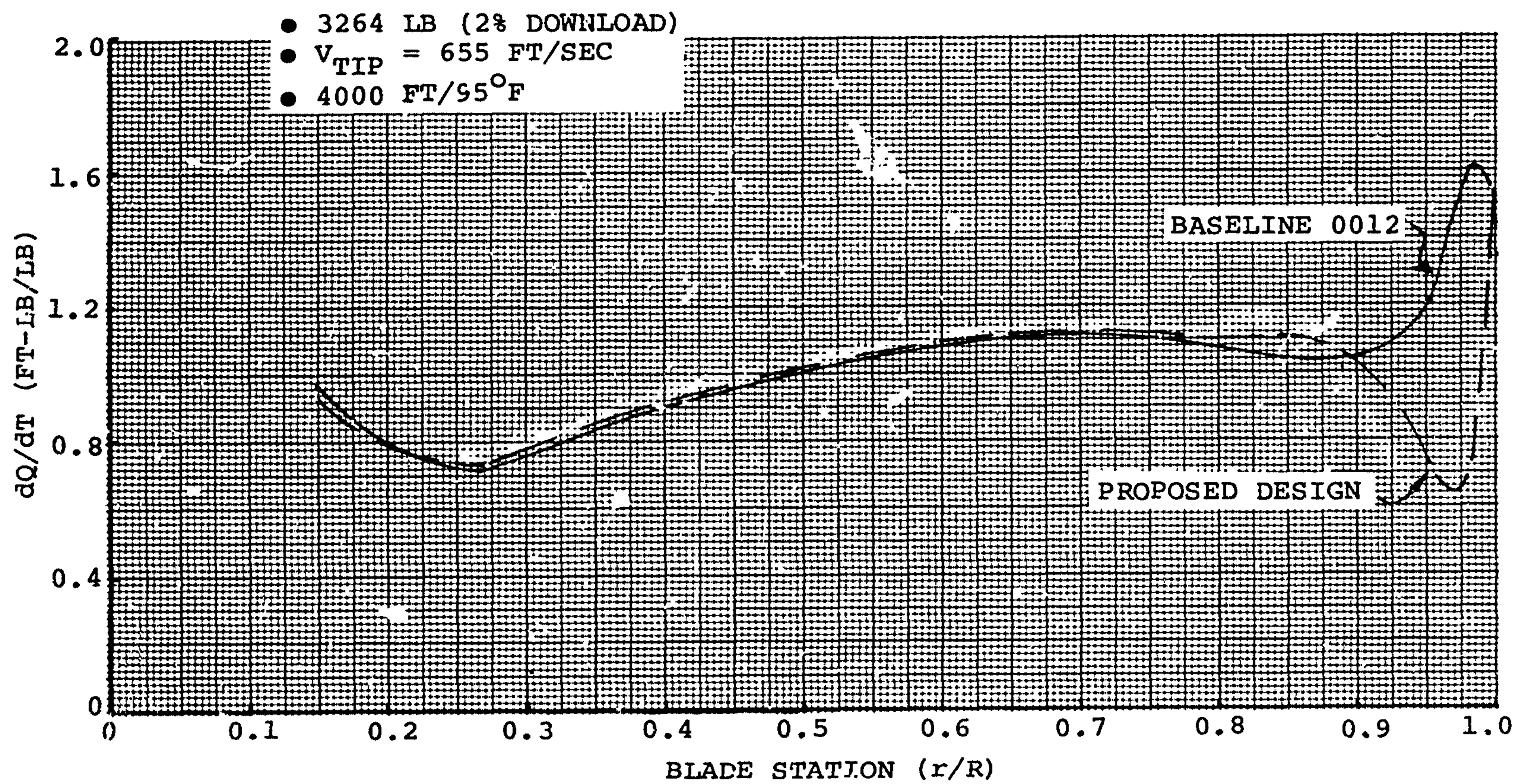

Figure 34. Ratio of Torque Loading to Thrust Loading

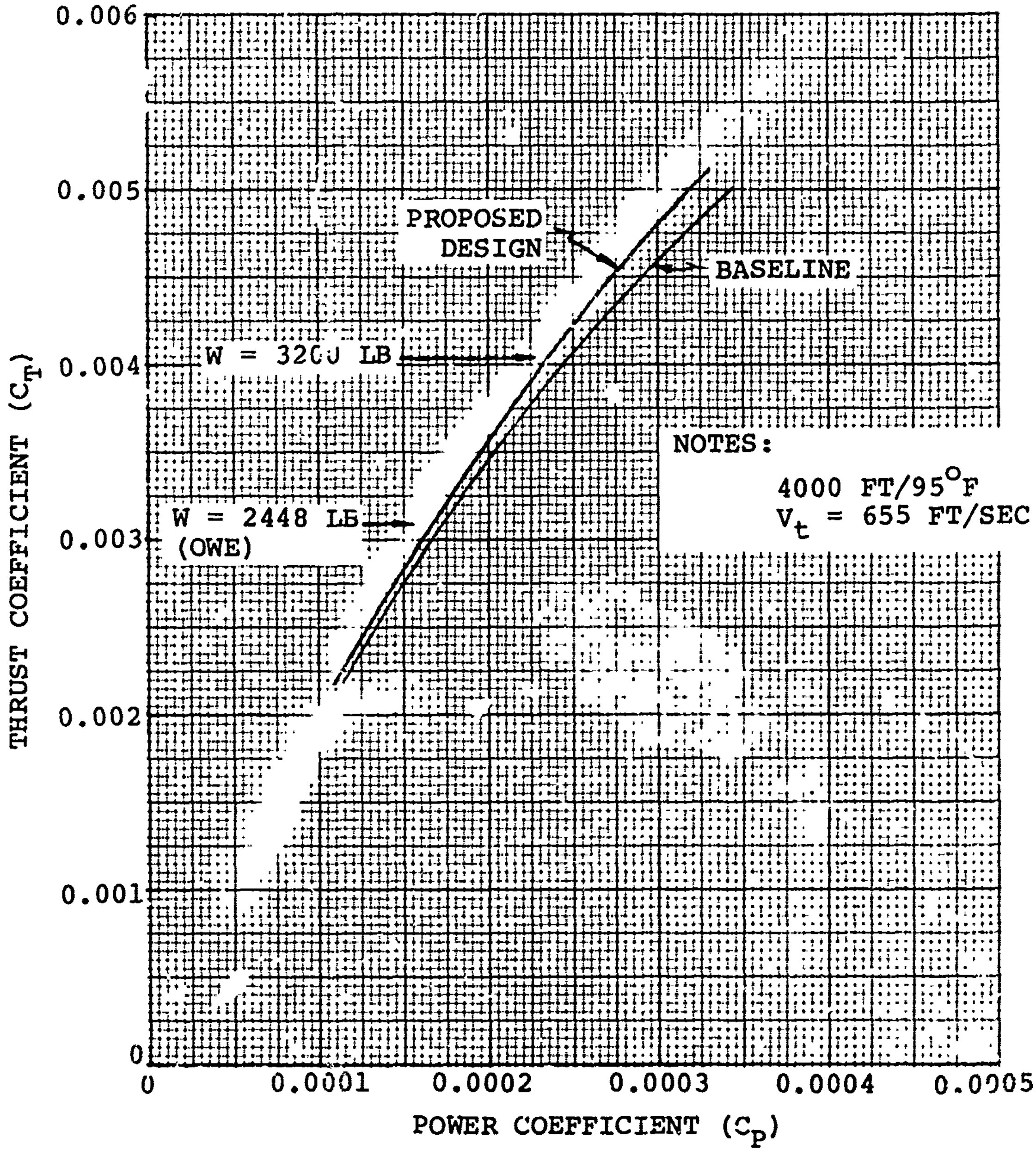

Figure 35. Isolated Rotor Hover Capability

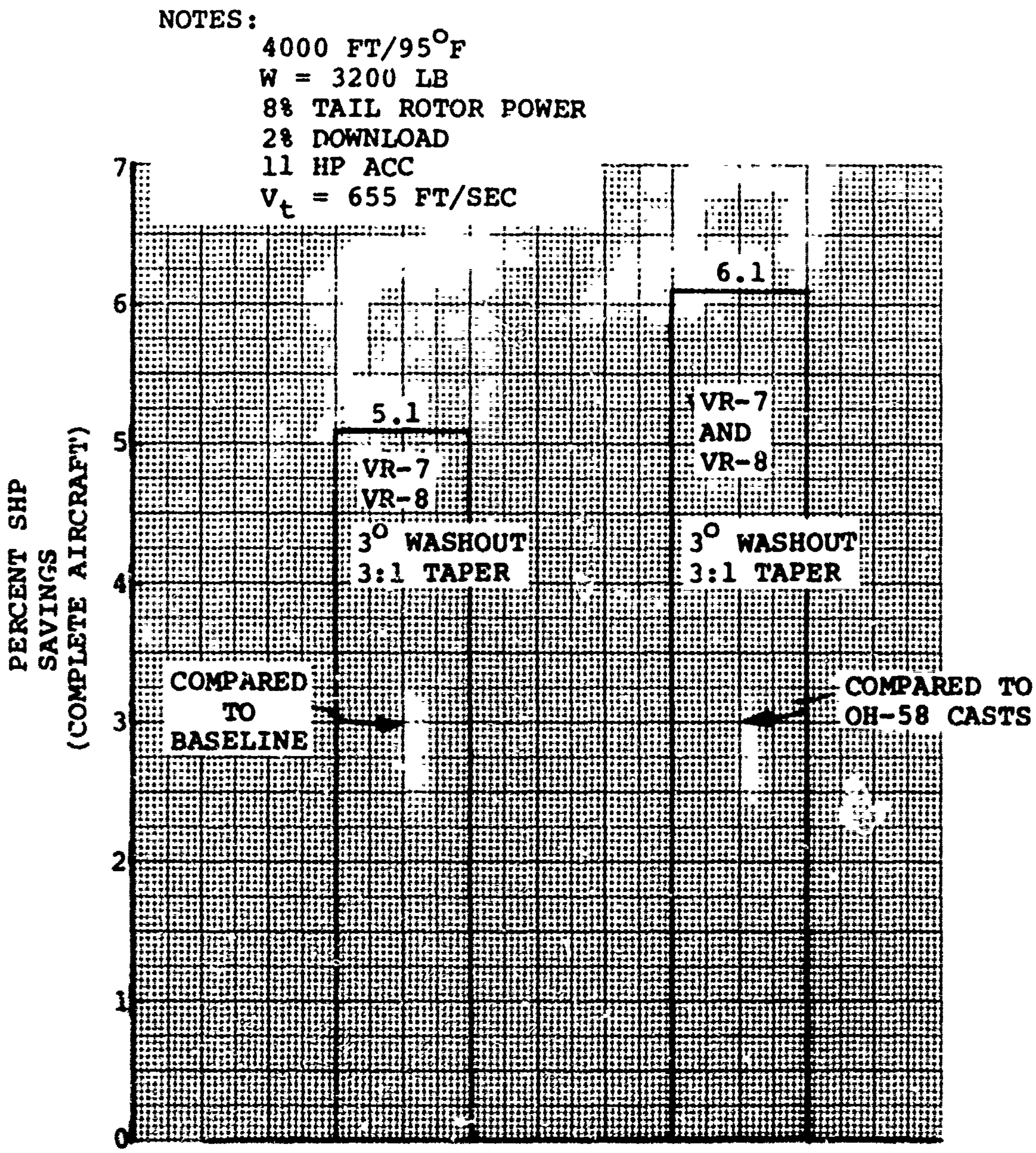

Figure 36. Effect of OH-58 Cast Data on Power Savings

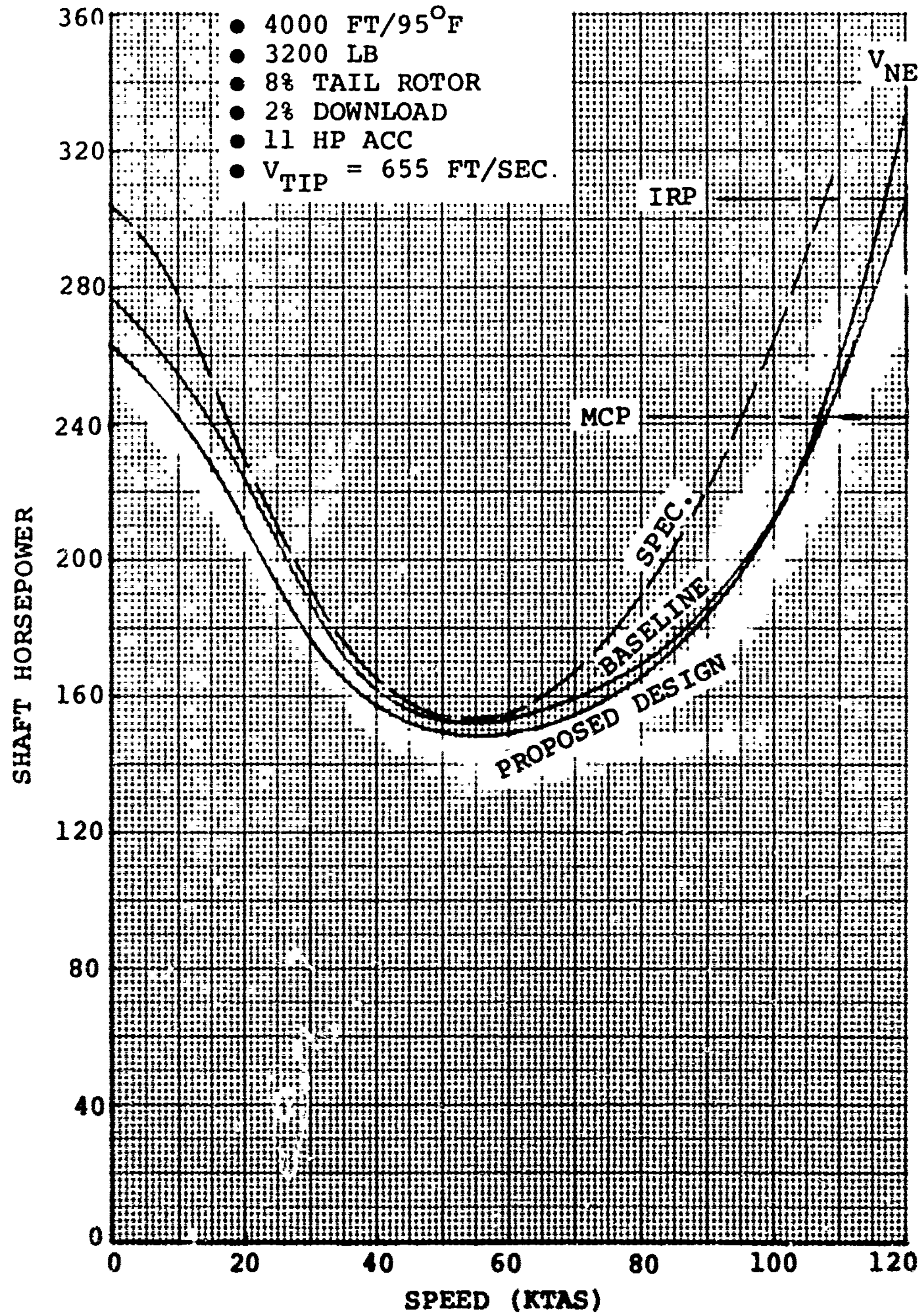

Figure 37. Power Required Comparison

gross weight of 3200 pounds at 4000 ft/95°F. The data reflects tail rotor and accessory power required. The tail rotor power and trim requirements were obtained from the C-81 program using the Government-supplied data on the OH-58 fuselage and tail rotor. The main rotor power was estimated from the non-uniform downwash teetering rotor performance program (B-14). The recommended design shows a small power improvement over the baseline rotor up to the maximum continuous power speed. Also shown is the power required for the existing OH-58 as given in the aircraft specification document (BHC Report No. 206-947-203). Some of the differences between the power levels given in the specification and the calculated values may be attributable to differences between fuselage drag levels and also rotor aerodynamic data used in the present calculations and those used in the preparation of the specification document.

Estimated single-rotor helicopter limits are shown in Figure 38. The Bell teetering rotor limits were obtained from various sources. The limits shown are not hard boundaries but are indicative of the rotor lift levels at which stall can be expected. Shown on the figure are the operating values of C_T/σ_T for the baseline rotor and for the improved rotor design at a gross weight of 3200 pounds. The recommended rotor, because of its lower thrust-weighted solidity (σ_T = 0.039 for the baseline and 0.0354 for the recommended design), meets the stall inception boundaries at a slightly lower airspeed than the baseline rotor. However, the recommended design will not substantially reduce the forward flight performance of the OH-58.

3.4 TIP SECTION

The design of the tip of the blade, outboard of 90% radius was driven by the desired increase in hover performance. The blade has a 3.1 taper at 90% radius. A 3° washout is added to the basic 10.6° linear twist schedule starting at 85% radius. The airfoil remains a VR-7 to 90% radius transitioning to a VR-8 airfoil at the blade tip.

The impact of outboard taper and twist on hub loads and vibration is shown in Table 27. Moving the start of the taper location inboard increases hub arm loads (M_{CH} and M_B), while twist washout is predicted as having an alleviating effect. The load effects of both these changes are attributed to a change in airloading resulting in a change in the trailing vortices. These in turn impact the self induced nonuniform downwash field entered by succeeding blades. As shown in Table 27 neither change appears to have a significant effect on hub vibrations as indicated by hub loads in the fixed system. It has been calculated that as much as a 10% increase in vibratory hub loads can be absorbed by the critical hub

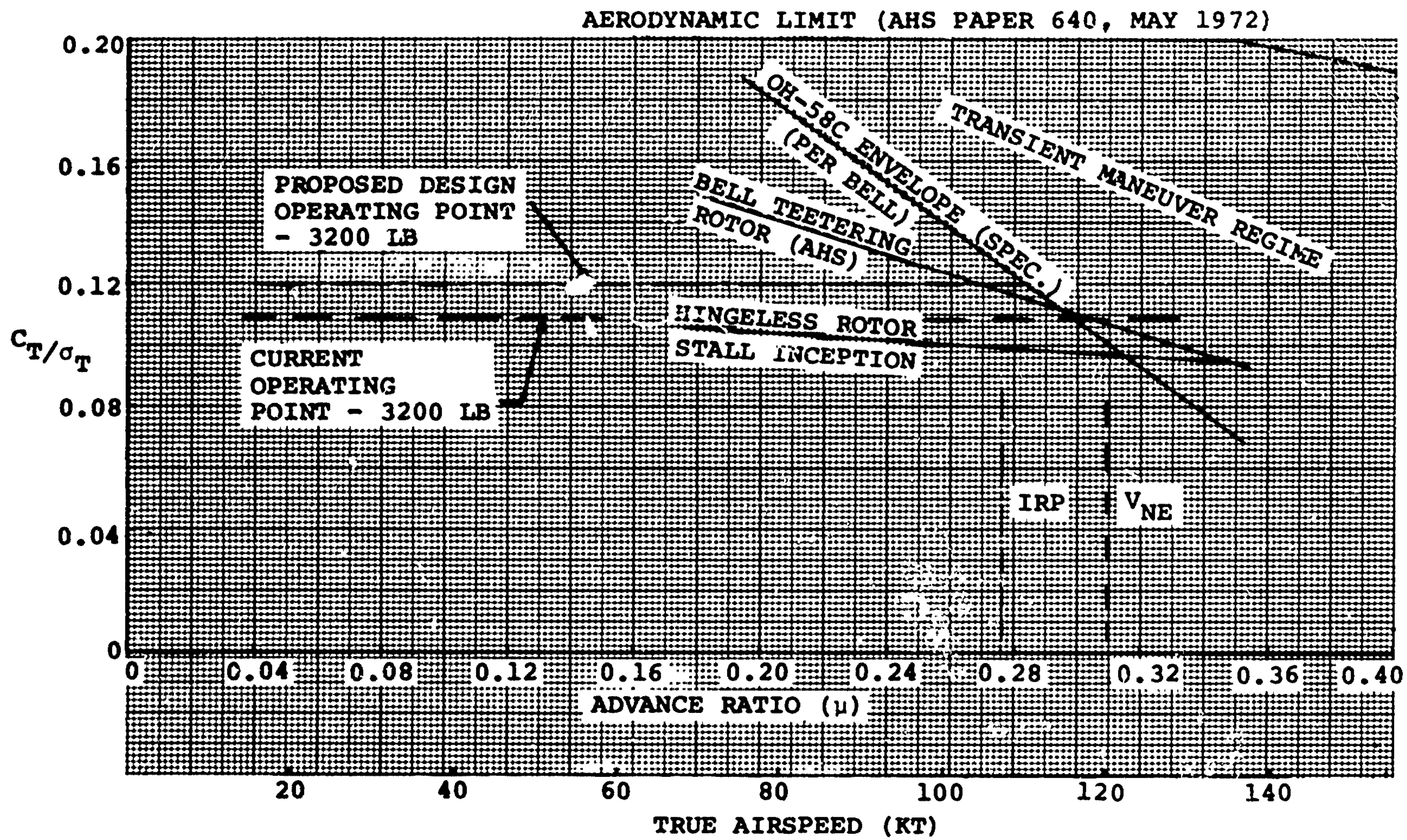

Figure 38. Single Rotor Helicopter-Rotor Limits

TABLE 27. EFFECT OF TIP TREATMENT ON BLADE AND HUB LOADS

	BASELINE		2° TWIST .90R		3° TWIST .90R		3° TWIST .85R	
	ST'DY	ALT	ST'DY	ALT	ST'DY	ALT	ST'DY	ALT
M_{CH} (in.-lb)	23517	94949	23572	90559	23603	88221	23636	86689
M_F (in.-lb)	8674	9333	8250	9065	8037	8923	8045	8609
P_{LL} (lb)	122	154	123	137	124	131	125	127
HUB								
Fx (lb)	-23.6	1780	-15.9	1702	-11.4	1659	-6.3	1631
Fy (lb)	41.3	1805	41.0	1729	40.8	1687	40.6	1660
Fz (lb)	3562	268	3543	270	3533	270	3284	270
Mz (in.-lb)	47040	2155	47145	2121	47206	2094	47273	2107
TWIST(1)	-.74	.43	-.89	.21	-.97	.10	-.93	.04

	3-1 TAPER .85R		3-1 TAPER .90R		3-1 TAPER & 3° TWIST .90R	
	ST'DY	ALT.	ST'DY	ALT.	ST'DY	ALT.
M_{CH} (in.-lb)	23218	129,590	23360	115163	23162	109,380
M_F (in.-lb)	8425	10,531	8445	9702	7937	9299
P_{LL} (lb)	72	180	94	135	98	135
HUB						
HUB						
Fx (lb)	-36.1	2454	-29.1	2175	-19.9	2070
Fy (lb)	30.9	2494	34	2210	33.9	2107
Fz (lb)	3554	182	3553	214	3530	215
Mz (in.-lb)	46303	1932	46720	1977	46325	1948
TWIST(1)	-.48	.67	-.61	.126	-.85	.25

L02
GW=3200 LB
A/S=113 KT
ALT=4000 FT
TEMP=95°F

(1) Blade tip with respect to 4.5% radius.

grip without degrading the calculated retirement life to below 5000 hours. Consequently, the proposed outboard tip configuration is acceptable.

The loads of Table 27 are predicated on avoiding stall flutter. Figure 39 shows the effect of the inboard start of blade taper on power required (nondimensionalized to power required with a taper) as predicted by the C-60 Program. Two curves are presented, one blade having the torsional stiffness of the existing OH-58 C/A blade and a second with the softer torsional stiffness of the replacement blade. The sharp break in the trends is indicative of the onset of stall flutter resulting from the higher blade lift coefficient as a consequence of the reduction in blade tip area. The softer blade has better stall flutter characteristics, which is consistent with our wind tunnel experience. Stall flutter is avoided by restricting the taper area to outboard of 90% radius with the torsionally softer blade.

Although a 10% increase in rotor inertia is desired, any increase in blade centrifugal force will degrade the fatigue life of the tie bar assembly currently set at 2400 hours. A substantial reduction in airfoil section weight is not feasible. Consequently, weight cannot be redistributed to the tip to achieve increased inertia with no increase in centrifugal force. A review of the fatigue life calculation of the critical component of the tie bar assembly shows that a 5% increase in centrifugal force (7% inertia increase) will reduce the life from the current 2400 hours to 2000 hours. Although it was decided not to degrade the component life of the tie bar, this could be reversed depending on how much the inertia increase is desired.

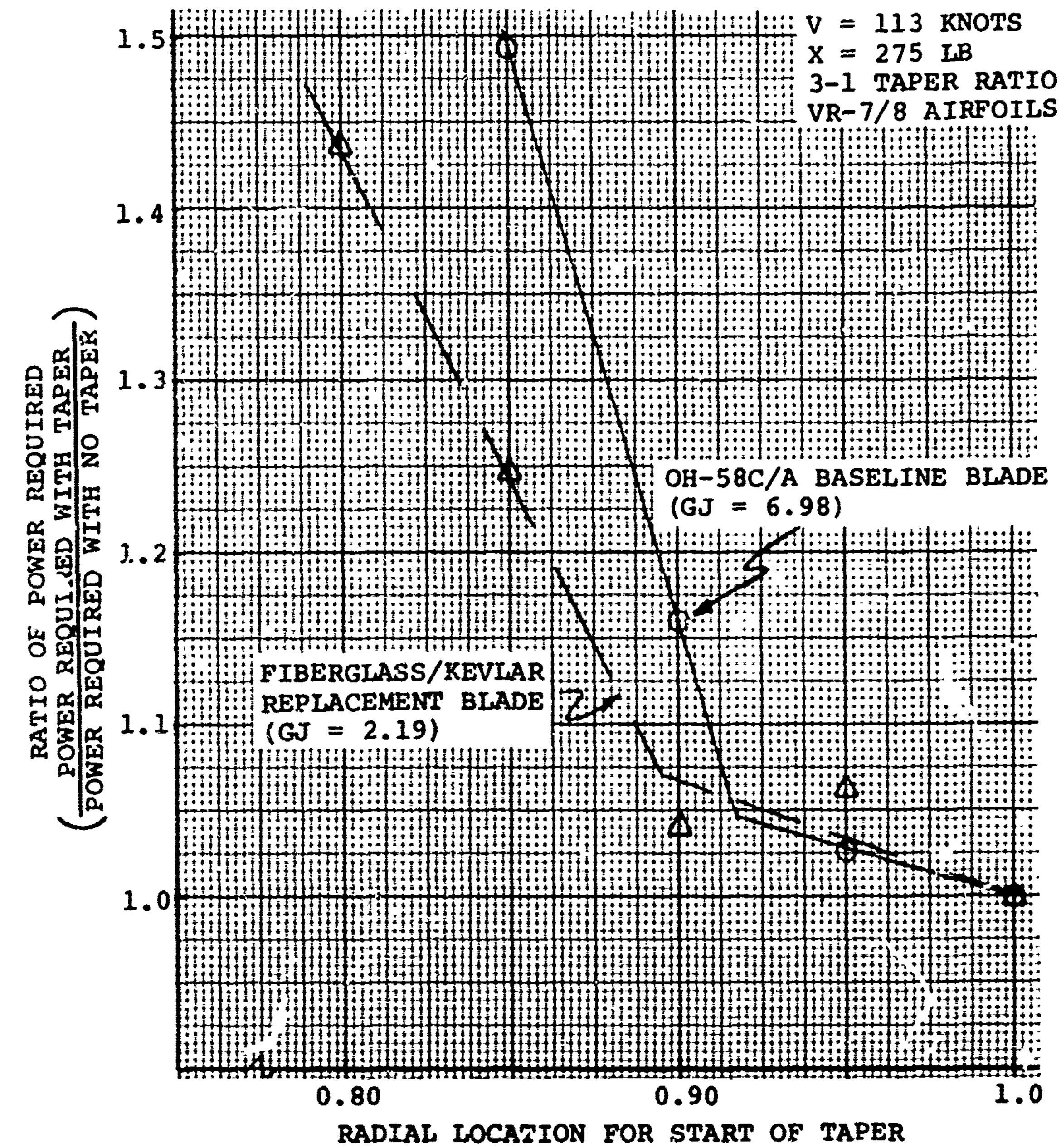

Figure 39. OH-58 C/A Stall Flutter Inception vs. Taper Location

4.0 DETAILS OF FINAL BLADE DESIGN

4.1 MANUFACTURING PLAN

The design of the OH-58 Composite Rotor Blade has been reviewed by Tool Design and Manufacturing Technology for feasibility of fabrication and the identification of a related tooling string.

Based on Boeing Vertol's past experience, the OH-58 rotor blade fabrication will consist of two major cure cycles: (1) the spar assembly, and (2) the final assembly which includes the cured spar, the uncured fairing skins, the machined core, and the uncured trailing-edge wedge. The two-cure process permits a thorough inspection of the spar, less complex tooling, and less risk of major rejections, than a single-cure process approach. It is noted that there are no hard-to-hard surface bonds in the two-cure process.

The design of the rotor blade components is conducive to the use of pre-impregnated tapes, rather than pre-impregnated roving, or the "wet" filament winding process. Pre-impregnated tapes permit accurate and repeatable orientation of unifibers, with excellent control of the resin-to-glass ratio. It is planned to utilize 1-inch-wide tapes which will be positioned by the automated layup machine.

All cross-ply material will be purchased as wide goods and cut to the desired shapes. This approach is more cost effective than laying up cross ply components with a tape layup machine when the N/C programming and handling problems are considered.

Filament winding of the spar outer torsion wrap would require manufacturing development. There are problems related to holding the spar straps and fillers in their proper position on an extremely flexible mandrel during the winding process and there could be a significant problem in fitting a filament-wound spar assembly into the curing mold. Filament winding the outer torsion wrap over the preassembled uncured spar strap and filler assembly would result in a variable periphery of the outer layer of filaments due to geometric differences in the spar strap and filler assemblies. Deviations from the exact periphery of the outermost winding relative to the curing mold would result in buckled fibers or a bridging effect. Neither of these conditions would be acceptable in a rotor blade spar.

A Nomex core was selected over a foam core. In addition to the weight penalty associated with a foam core, Boeing Vertol's experience indicates that a machined Nomex core presents less problems in producing a satisfactory bond to the skin. The honeycomb core will be machined to net size prior to bonding.

The fabrication process for the blade utilizes automated tape layup for components which are made up of unidirectional fibers. The nose block, layed up of unidirectional fibers, will be coined to produce a geometry compatible with engineering requirements and the molding process. In some instances, multiple widths may be layed up to reduce layup time, followed by a slitting operation to produce the final width.

The root end of the blade will be fabricated by assembly of previously layed up components. Upper and lower spar halves will be assembled on a layup mandrel. These subassemblies will consist of the spar straps, which will fit around a root end pin, the leading and trailing edge compacted members, droop stop, and various fillers. The upper and lower spar assemblies will be positioned on an inflatable mandrel which contains the inner torsion wrap. The premolded chopped fiber filler blocks and the extended leading and trailing edges will be fitted. The outer torsion wraps including the tapered fairing at the root end will be positioned. This assembly will be installed in the spar bonding tool for curing. The root end hole will be molded to net size utilizing an expandable pin.

Cross ply components such as inner and outer spar torsion wraps, and the fairing skins will be fabricated from purchased cross ply material which will be cut to shape via steel rule dies and the clicker press.

To permit bag removal following the blade cure, the outboard 9 inches of the blade will be separately formed, cured, and permanently bonded to the main spar section. The tip section will be precured in matched metal molds. The nickel erosion caps will be bonded to the tip cover during the cure cycle. The filler will be foamed in place after cure. Trimming and drilling will be accomplished after cure and foaming to coordinate with the matching section of the blade.

The curing of the assemblies will be accomplished in matched steel molds to provide the optimum conditions for long dependable service, and repeatability in the rotor blade geometry. These molds, with airfoil contours, will be machined to engineering dimensions by numerical control. Subassembly or component tools, will be made of suitable material to meet shop requirements for repeatability, ease of handling, and minimum maintenance. The main bonding tools will be heated, cooled, and pressurized in platen presses which use oil for heating and water for cooling. Thin film plastic bags will be used to apply pressure to the spar area.

All cure cycles will be accomplished in accordance with Boeing documents for composite structures. The 250°F cure resin system utilized in this blade will be brought from room temperature to 250°F at a controlled rate and held for 120 minutes. The platens will be force cooled until the cured assembly reaches a temperature of 150°F. At that point the molds may be opened and the assembly removed. The cure cycle will be recorded and retained for each rotor blade.

Other final fabrication steps include filament winding of the inboard chordwise reaction plates, boring at the vertical pin location and bonding installation of the fiberglass sleeve, bonding of the Estane boot and trim tab, installation of the teeter weight canister, the studs to retain the sweep balance weights, and wear plates and painting. The use of non-product materials, such as peel ply, will be discouraged. Their use will have to be justified from both technical and economic viewpoints.

A general flow chart and sketches of the tooling is shown as Figure 40.

4.2 RELIABILITY AND MAINTAINABILITY

Table 28 represents our best estimate of the OH-58 C/A blade's unscheduled maintenance reliability. The rates on the table are based on inherent failures only. In order to predict the total MTBF for all failures, inherent plus externally caused, the results of previous blade studies were utilized. These studies, made for the UTTAS and the CH-47 fiberglass blade programs, showed that approximately 30% of all blade removals are for inherent causes. Due to the similarity of the OH-58 C/A fiberglass blade and the similarities of mission environments of the OH-58 C/A and UTTAS aircraft, it was estimated that 30% of the OH-58 C/A blade failures would also be inherent and the remaining 70% would be due to external causes such as maintenance damage, excessive FOD, erroneous removal during troubleshooting minor accidents and incidents, etc.

The detail rates were derived by comparing the physical characteristics of the OH-58 C/A blade with those of existing Boeing-Vertol blades having similar physical characteristics and with which we have had considerable flight and ground test experience, including:

a. CH-46F Metal spar production blades.

b. UH-61A Fiberglass spar blade (8,000 blade flight hours, 6,000 blade ground test hours)

c. CH-47 B/C Metal spar production blade.

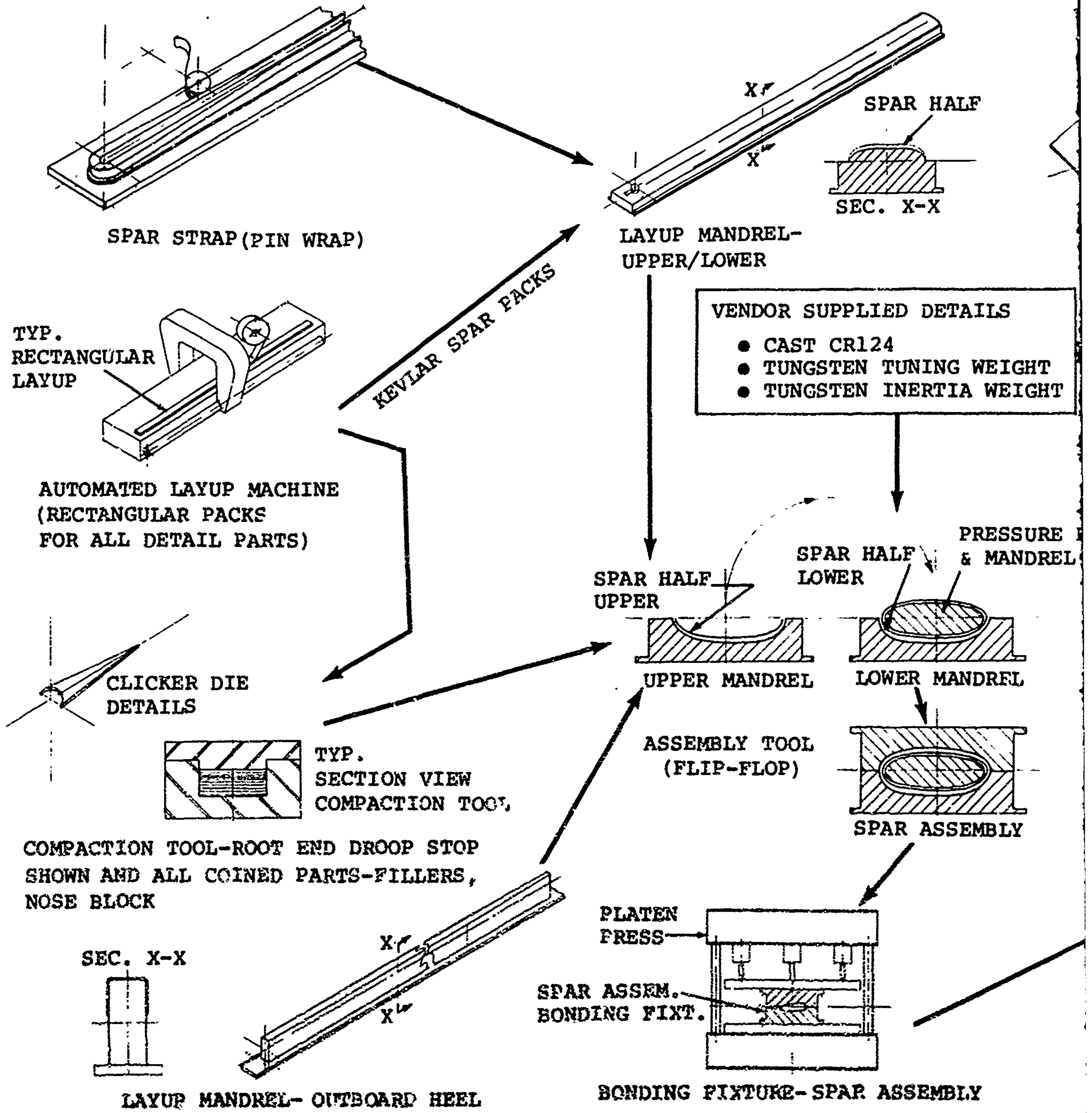

Figure 40. Manufacturing Plan Flow Chart

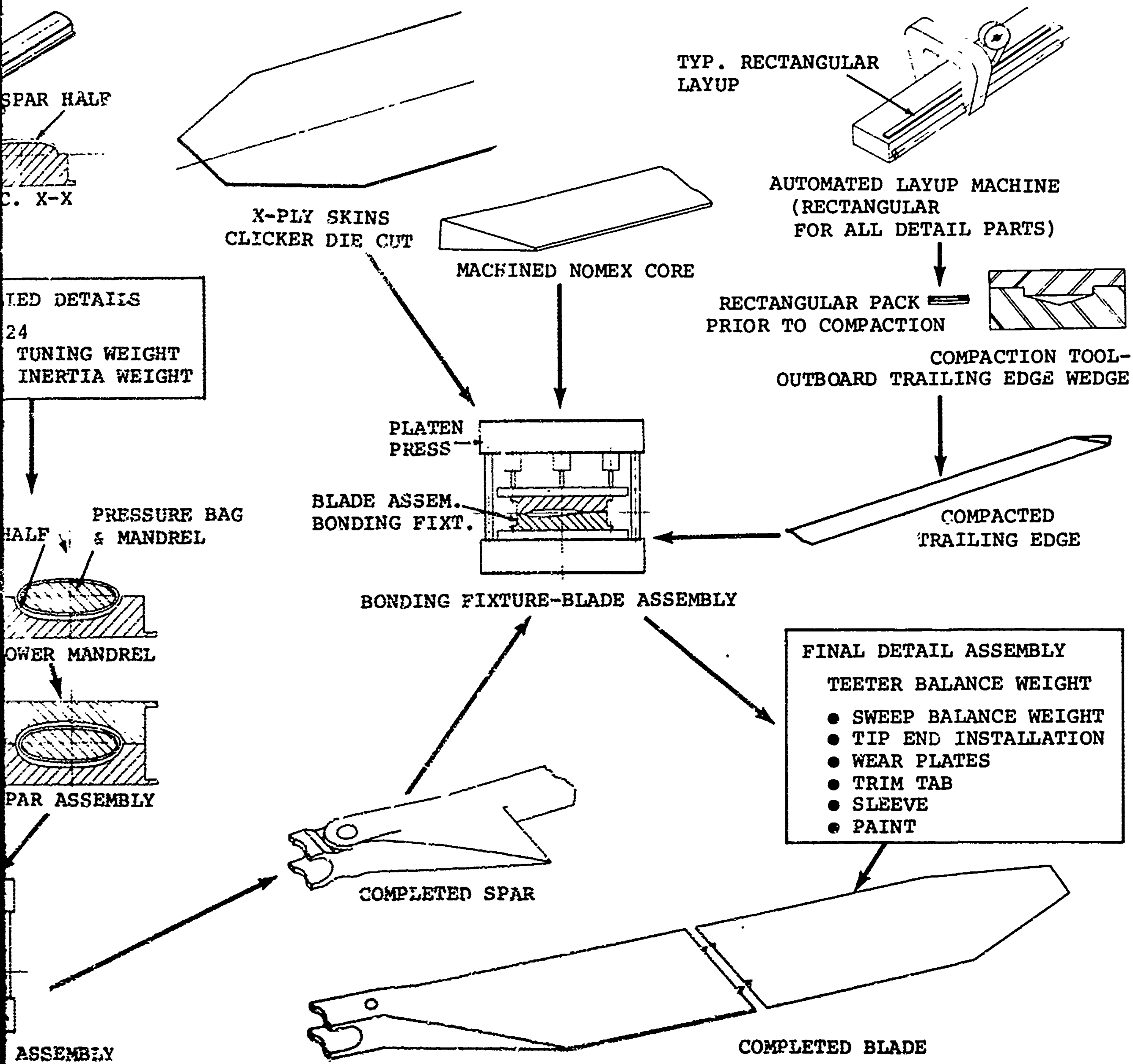

SPAR HALF
C. X-X
X-PLY SKINS
CLICKER DIE CUT
MACHINED NOMEX CORE
TYP. RECTANGULAR
LAYUP
AUTOMATED LAYUP MACHINE
(RECTANGULAR
FOR ALL DETAIL PARTS)
RECTANGULAR PACK
PRIOR TO COMPACTION
COMPACTION TOOL-
OUTBOARD TRAILING EDGE WEDGE
IED DETAILS
24
TUNING WEIGHT
INERTIA WEIGHT
PLATEN
PRESS
BLADE ASSEM.
BONDING FIXT.
COMPACTED
TRAILING EDGE
HALF
PRESSURE BAG
& MANDREL
BONDING FIXTURE-BLADE ASSEMBLY
OWER MANDREL
FINAL DETAIL ASSEMBLY
TEETER BALANCE WEIGHT
● SWEEP BALANCE WEIGHT
● TIP END INSTALLATION
● WEAR PLATES
● TRIM TAB
● SLEEVE
● PAINT
PAR ASSEMBLY
COMPLETED SPAR
ASSEMBLY
COMPLETED BLADE

2

TABLE 28. OH-58 C/A FIBERGLASS BLADE UNSCHEDULED MAINTENANCE RELIABILITY FREQUENCY (ALL RATES PER THOUSAND BLADE HOURS - INHERENT FAILURES ONLY)

	DATA BASE	TOTAL MALF.	AVUM	AVIM	DEPOT	REMARKS
1. Root End						
Sleeves	D/E	.01120	------	.01008	.00112	May Wear or Distort.
Pads (S.S. Wear Plates)	D	.00560	------	.00504	.00056	May Wear, Fret or Debond.
Lag Bearing Plate	Est.	.00560	------	.00504	.00056	
Debond & Delam. of Root	D/D/E	.01200	.00400	.00400	.00400	Delam & Debond Should Be Similar to UH-61A & CH-46 F G.
2. Spar						
Debond & Delam. of Spar	B/E	.02100	.00300	.01600	.00200	Debond & Delam. Should Be Similar to UH-61A & CH-46 F G.
Inertia & Tuning Weights	B/D/E	.00181	.00065	.00070	.00046	Securely Mounted.
Estane Erosion/Deicing Cap	Kaman/Goodrich & Ft.Rucker Tests	.06000	.03500	.00250	.00250	Vibration would be the First Likely Indication of Failure.
3. Aft Fairing						
Fiberglass Skins	A/B/C/D/E	.07540	.04971	.01101	.01468	Basically Similar to CH-46 & CH-47
Nomex Honeycomb Core	A/B/C/D/E	.01085	.00163	.00705	.00217	Same as UH-61A. Eliminates Corrosion and Reduces Unbonding.
4. Trailing Edge						
Trailing Edge Joint	A/B/D	.00370	.00185	------	.00185	Similar to UH-61A & CH-46 F G Blades.
Trim Tab	A/B	.04230	.02115	------	.02115	Similar to UH-61A & CH-46 F G Blades
5. Tip End						
Tip Cover & Nose Cap	A/B/C	.01632	.00544	.00544	.00544	Simple Bonded on Cover & Nose.
Tip Fitting Structures	A/B/C	.00500	.00250	.00125	.00125	Simple Structures.
6. Hardware & Balance Weights	A/B/C	.025[illegible]	.02500	-------	-------	Minimum Amount of Hardware.
Entire Blade Rate (Inherent)		.27578	.1499.	.06811	[illegible]	
MTBF (Inherent)		3,626 Hours	6,670 Hours	14,682 Hours	17,319 Hours	
MTBF (Total Failures)		1,100 Hours	2,000 Hours	4,400 Hours	5,200 Hours	
MTBR (All Levels)		2,400 Hours				

LEGEND: DATA BASE
A - CH-46E
B - UH-61A
C - CH-47 B/C
D - CH-46 Fiberglass
E - HLH Fiberglass

d. CH-46E Fiberglass spar blade (6,000 blade flight hours).

e. HLH Fiberglass spar blade (1,000 blade ground test hours).

The following describes the Reliability and Maintainability characteristics of the OH-58 C/A blade as outlined in Table 28.

4.2.1 Root End

The root end of the blade carries the centrifugal force loads and most of the flap moment through the single-blade retaining pin. This pin also reacts chordwise moments together with the inboard clamp connection to the hub. Therefore, the composite sleeve around the root pin is subjected to a variety of steady and alternating loads. The inherent MTBF projections for the composite sleeve and the wraparound root material that go with it have been developed as a result of extensive ground and flight experience with HLH and CH-46 fiberglass blade roots. There is the possibility of eventual wear and/or distortion of the sleeve or of damage resulting from improper removal or installation. The sleeve can be readily replaced by drilling out the damaged sleeve and bonding in a new one.

The stainless steel wear plates at the top and bottom of the root section protect the fiberglass from abrasion. They could fret, wear, debond, or be damaged by improper removal or replacement of the blade or pin. These plates are readily replaceable with simple tools.

The lag bearing plates are subject to some rubbing and wear. Such occurrences should be rare but, if they occur, they can be corrected by tightening the screw adjustment or by replacing the plates.

It is possible that minor debonding or delamination could occur at the root. Based on experience with several composite blades, it is anticipated that most debond/delamination type failures can be handled on the aircraft or at the AVIM level.

4.2.2 Spar

Debonding and/or delamination of the spar has been rare in Boeing Vertol composite blades. Visual examination will show any significant delamination on the exterior which can generally be repaired on the aircraft. It is our experience that internal bonds or delaminations are unlikely to occur on this type of blade. Such failures would be slow to propagate and would eventually show as surface delamination prior to loss of load carrying capacity.

Blades in which the spar is damaged by foreign objects or small caliber ballistic hits will probably not require structural repair to restore their original strength. It is anticipated that such damage will be treated only to prevent damage propagation, to provide proper aerodynamic characteristics, and to seal out the elements. This spar is designed primarily to meet stiffness requirements and can lose some of its strength locally without causing life limitation, although this would have to be proved by structural testing of damaged blades. Such spar repairs would be made on the aircraft or at AVIM level.

The tungsten inertia weight at the blade tip and the tuning weight near midspan will be made in short segments to prevent their picking up excessive loads and breaking. This may also be desirable with the CR-124 radar absorber material. The inertia weight at the tip is failsafe because it is retained in an area of the spar which is decreasing in cross section as it goes outboard and would therefore be retained by the wedging action. The inboard tuning weight will be retained by a mechanical dam at its outboard end.

Regarding the nose cap, tests conducted by Kaman/Goodrich and Fort Rucker indicate that Estane is superior to most metals with respect to sand erosion but inferior in rain erosion. However, Estane only deteriorates rapidly in extremely heavy rain which would be likely to prevent flight for other reasons. It is suggested that an R&D program should be conducted on the Estane to assure the achievement of the minimum 1200 hour life required.

The only truly proven method of rotor deicing is the electrothermal system. The Estane/pneumatic system should be a part of the recommended R&D program. This deicing system can fail as a consequence of air leaks. Loss of suction during non-deicing operation could cause a loss of aerodynamic performance by degrading the airfoil shape at the nose. Also, during deicing operations, a leak in one of the spanwise air passages could cause that passage to become inoperative and decrease the effectiveness of the entire blanket. Leaks could generally be repaired by applying a urethane putty while the blade is on the aircraft. Complete removal and replacement of Estane nose cover would be made at the AVIM level.

4.2.3 Aft Fairing

Fiberglass skins have proved to be generally superior to metal. Fiberglass skins, removed from CH-47 blades after several years of operation and exposure in Viet Nam, were tested for ultimate and fatigue strength. They were found to have virtually the same strength as when new. Although delamination and debonding from the honeycomb, spar or trailing edge could occur, most of these could be repaired on the aircraft.

The Nomex honeycomb is an especially appropriate material for this blade. It does not corrode as aluminum can. It bonds well to fiberglass skin without the possibility of damaging the skin during manufacturing. Its moisture absorption rate is minimal, and any absorption that does occur is mostly from the edges that are sealed by bonds. Inherent failures of Nomex honeycomb are extremely unlikely. Additionally, tests have shown that the impact resistance of fiberglass skin, together with Nomex honeycomb, is far superior to that of aluminum skin with aluminum honeycomb.

Damage to the aft section will generally be externally caused and may affect only the fiberglass skin or both the skin and the nomex honeycomb. Repair development programs conducted by Boeing for the CH-46 Fiberglass Blade Program and by other companies have shown that this type of construction is particularly suited to quick and easy field repairs, which may be made without removal from the aircraft.

Damage to the skin only can be repaired by routing the damaged layer of skin from the honeycomb. The router is set for the depth of the skin and the size of the hole is determined by a metal template taped or otherwise fastened to the blade (Figure 41). This provides a clean area of honeycomb onto which a skin patch (which could come in standard sizes, Figure 42) can be bonded with EA 9309.3 adhesive or equivalent. In order to properly and quickly cure the bond a clamp device (Figure 43) has been developed which inflates to apply even, controlled pressure to the patch and is electrically heated to reduce the cure time. The edges of the patch are then faired in by carefully sanding around the edges. Curing could also be accomplished by vacuum bagging to apply pressure and allowing more time for an ambient temperature cure.

In the event of small holes, including through holes such as bullet holes (Figure 44), it is only necessary to repair the skin (not the honeycomb). Again, the patches are faired in by carefully sanding around the edges.

Where both skin and core damage exist over larger areas, but not totally through the blade, the same routing technique is used as previously described for the skin. In this case, however, the router is set to a depth sufficient to remove all the damaged honeycomb (Figure 45). A section of skin material, the diameter of the hole, is then bonded on both sides and placed on top of the remaining honeycomb. After that, a standard plug (Figure 46) is inserted with bond between the blade skin and the plug skin and around the honeycomb. This repair is cured in a manner similar to the skin repair.

Figure 41. Routing the Skin

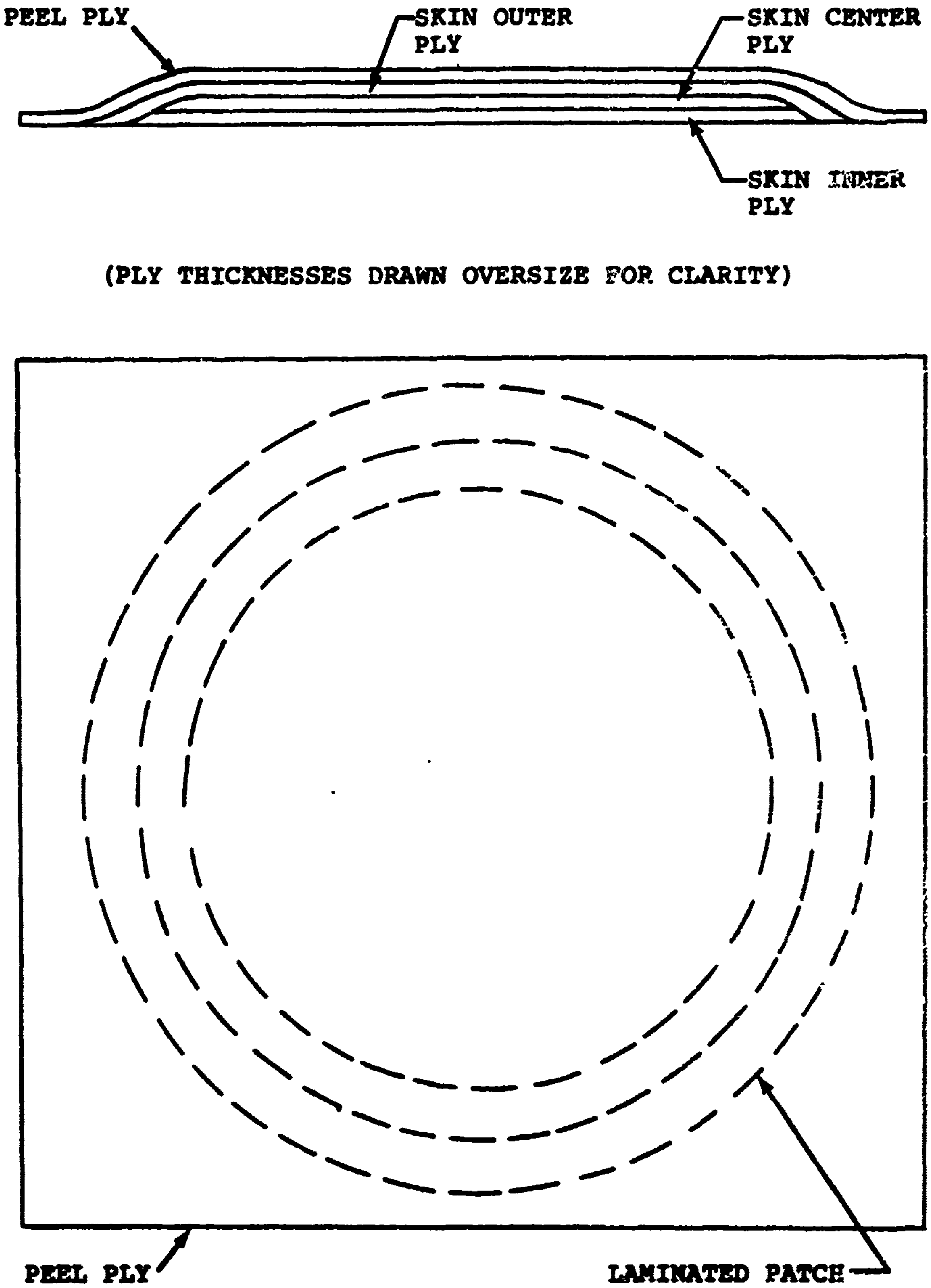

Figure 42. Typical Skin Patch Construction

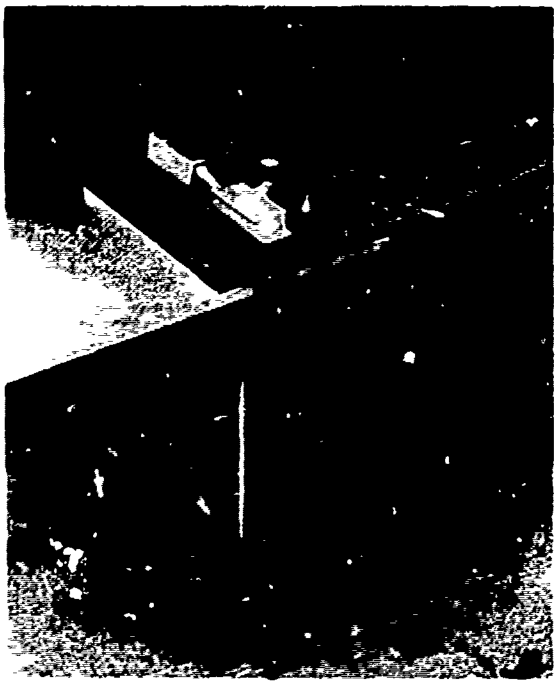

PRESSURE/HEAT PACK IN PLACE

PRESSURE/HEAT PACK SECURED

Figure 43. Application of the Pressure/Heat Pack

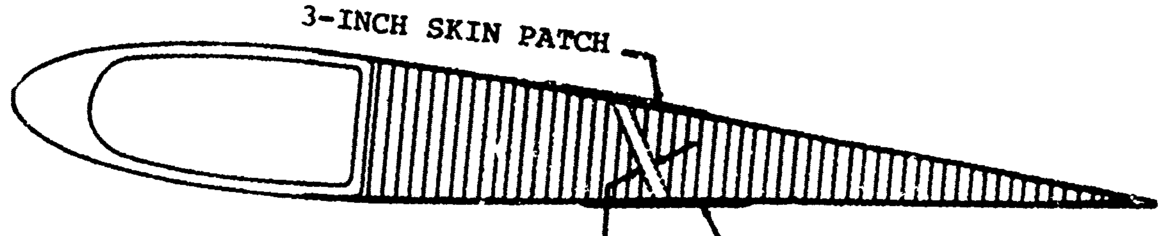

Figure 44. Typical Double Skin Patch Repair.

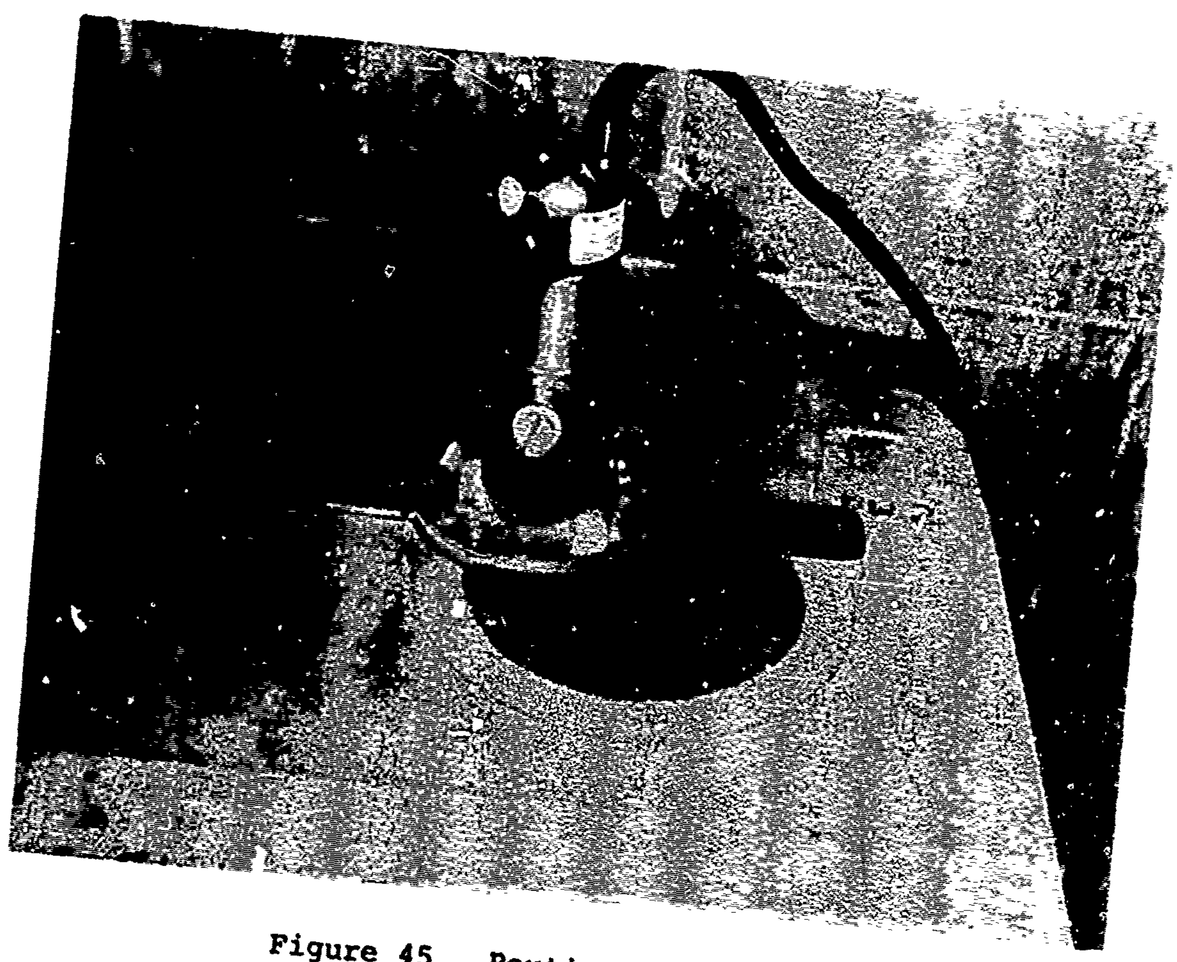
Figure 45. Routing of the Core

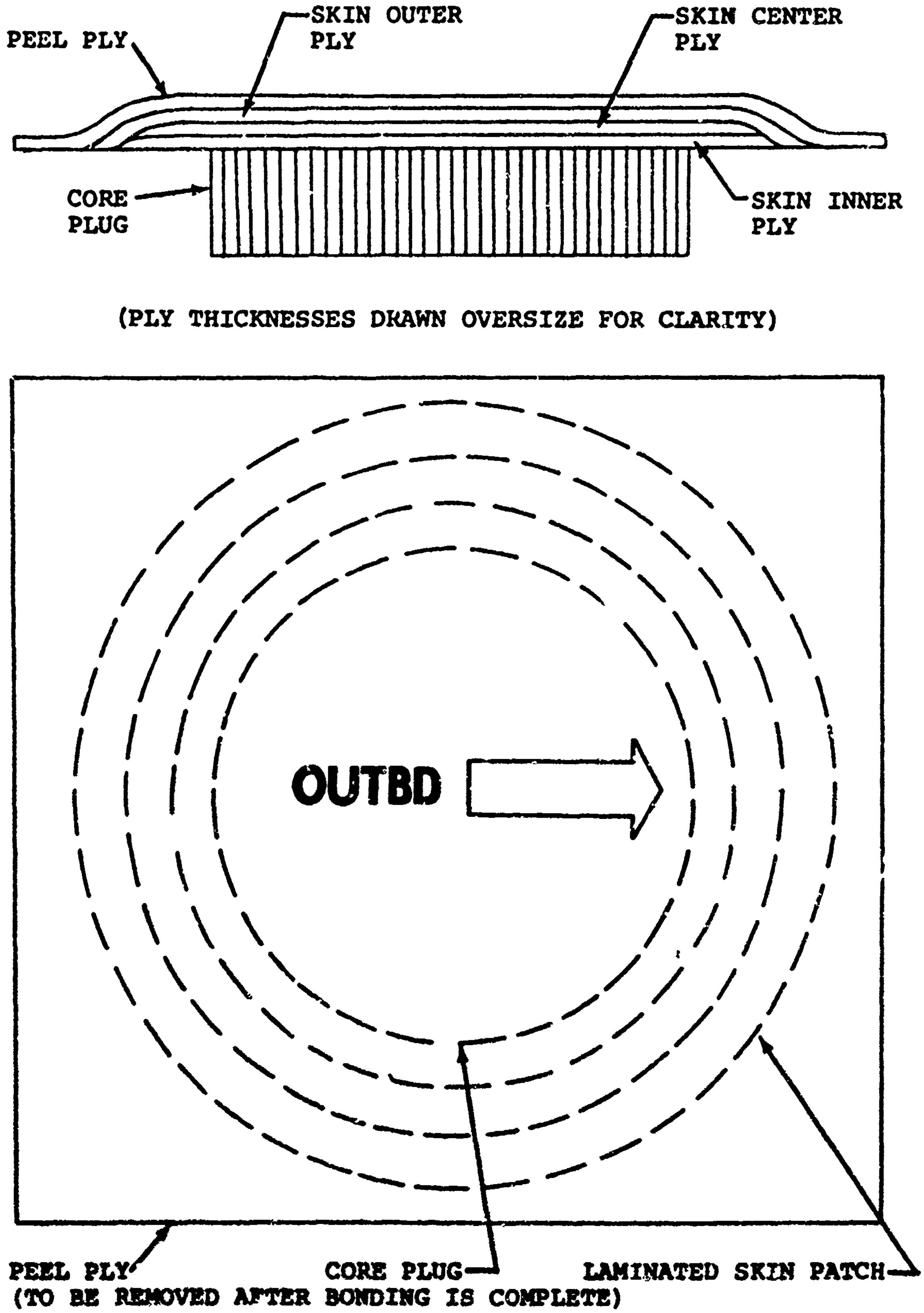

Figure 46. Typical Plug Patch Construction

Where damage areas exist that are both large and deep, a repair is made as shown in Figure 47. Either the upper or lower side may be routed out first (in Figure 47 the upper was done first). A bonded piece of skin is placed on the honeycomb and a plug patch installed as described above. After this has cured, the damaged area is routed out from the bottom and the process repeated.

4.2.4 Trailing Edge

Inherent failures of trailing-edge joints can result from debonding or delaminating. These are low-frequency failures that can generally be repaired on the aircraft. The trailing edge is also subject to damage from handling and F.O.D., which can usually be handled at the AVUM or AVIM level.

The trim tabs could fail by cracking or debonding. Minor cracks can be stop drilled and/or smoothed out. Major cracks require replacement of the tabs. All of this work can be done on the aircraft. Figure 48 shows a simple clamping method to apply pressure for repairing the bond or replacing a trim tab. The OH-58 C/A tabs will be adjustable in the field to improve tracking in forward flight.

4.2.5 Tip End

The teeter balance weights have a low inherent failure rate. They are installed at the factory and are only adjusted in the field if a blade is repaired such that its weight changes. They are contained by a rigid metal carnister which is, in turn, mounted in the blade spar in a slurry of chopped fiber/epoxy material. In the unlikely event that the canister comes loose, it could be rebonded in the same hole. Other failures could be caused by cracking of the metal cover or loosening of the retaining screws. Both of these are readily detectable at preflight inspection.

The tip fitting structure is separately made and bonded onto the blade. It is comprised of fiberglass skin filled with chopped fiber material in the nose and foam in the aft section. Its most likely failure modes would be debonding of the trailing edge or debonding where it is joined to the main section of the blade. Both of these are readily detectable during routine inspection and repairable on the aircraft or at the AVIM level.

The tip cover is the small, flanged nickel cover over the extreme tip. The corner is securely bonded to the fiberglass skin and the chopped fiber and foam filler material. Its inherent failure modes could be debonding or cracking. It is also susceptible to erosion and foreign objective damage. The tip cover would be repairable or replaceable on the aircraft.

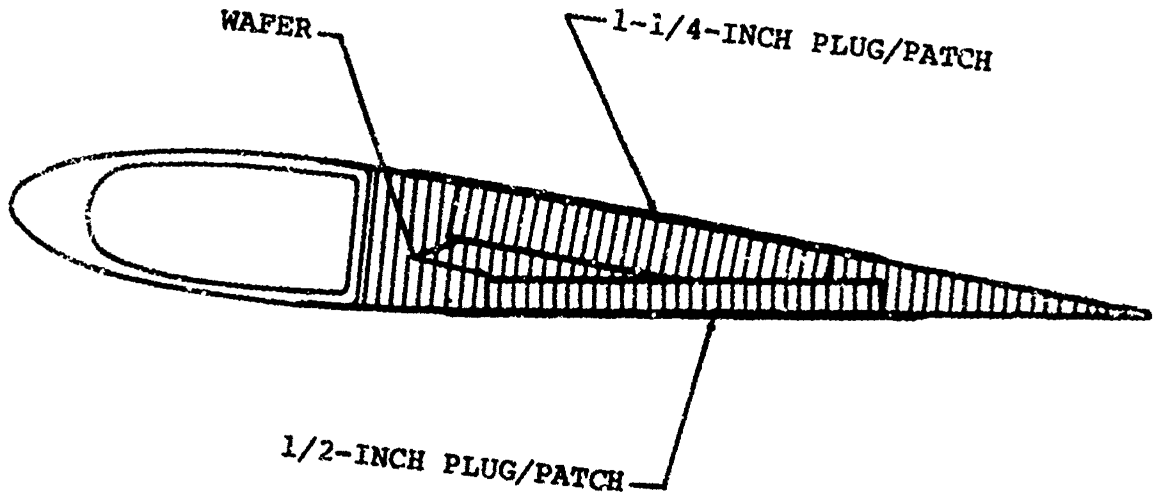

Figure 47. Typical Double Plug Patch Repair.

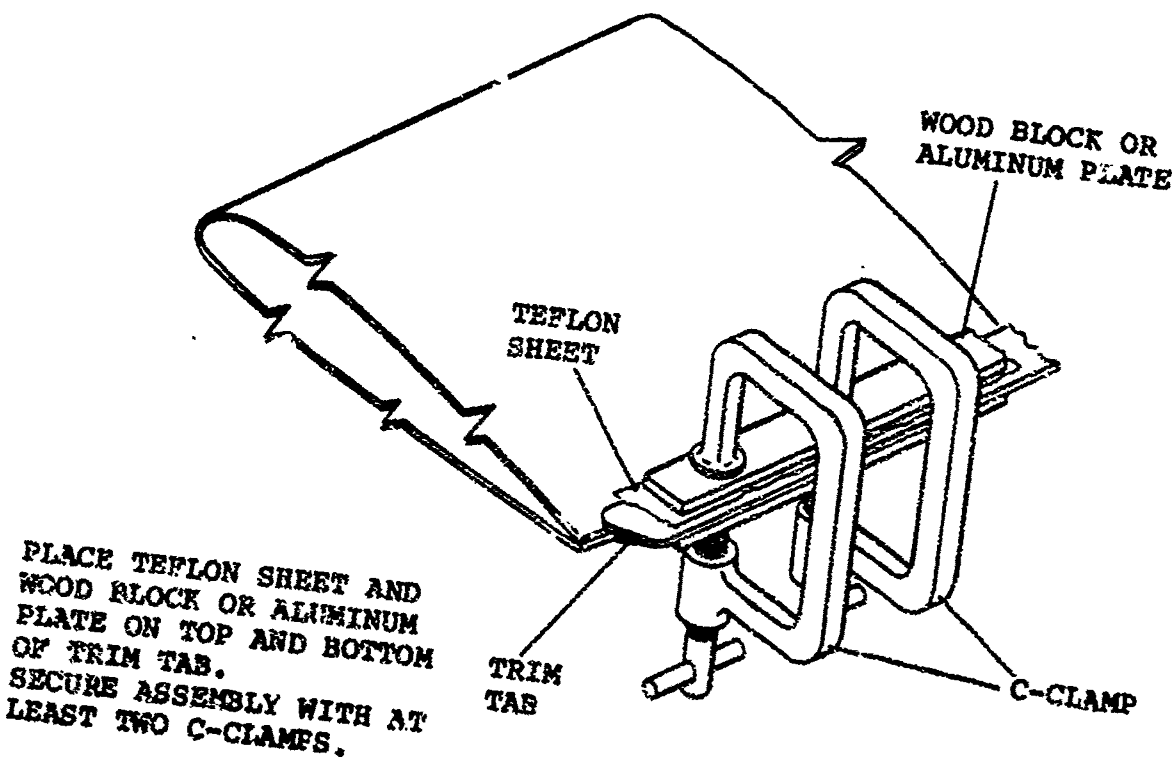

Figure 48. Trim Tab Repair

The nickel erosion nose cap on the tip section could debond or crack and is also susceptible to erosion and foreign object damage. This nose cap will be replaceable either at organizational or intermediate repair levels.

4.2.6 Hardware and Balance Weights

This blade has a minimum of both hardware and balance weights. The outboard teeter balance weight assembly has already been described. Additional weights for chordwise sweep balance are located at the aft end of the root transition area. These are retained by three studs bonded into the trailing edge. This provides fail safety in that any two of the three studs could carry the loads. Any loosening of these studs would be readily detectable in routine inspection.

4.3 LIFE-CYCLE COST

This section of the report presents the direct operating costs over the life cycle for the OH-58 fleet operating with the present metal blade, and with the proposed composite blade. Included in the analysis are the investment nonrecurring costs and investment recurring costs for the composite blade. Several alternative operating scenarios are shown to examine the effects of different composite blade incorporation policies, different life cycles, various predicted blade scrap rates, and various aircraft utilizations. The results show that in all cases tested, incorporation of composite blades on the OH-58 fleet is cost-effective.

4.3.1 The PIPE Model

The technique chosen for performance of the cost analysis was the Product Improvement Program Evaluation (PIPE) Model. This model was developed for the Army, and is documented in Reference 9. The method compares a baseline component configuration with an alternate, by simulating the operation of a fleet of aircraft over the life cycle, first with the baseline configuration installed, then with the alternate. Total failures at various levels of repair are computed and their repair costs calculated. Generally, the improved fleet with the alternate configuration installed costs less to operate and maintain over the life cycle, and this cost saving is then compared with the investment cost required to develop and procure the improved parts. All costs shown

---

9. Blewitt, S. J., PRODUCT IMPROVEMENT PROGRAM EVALUATION US AAMRDL-TR-77-17, U.S. Army Air Mobility Research and Development Laboratory, Ft. Eustis, Virginia, June 1977, ADA042134.

below are in constant 1976 dollars.

4.3.2 Baseline Definition

The baseline configuration is defined as the OH-58 fleet equipped with the current metal rotor blades. Table 29 shows the model input parameters for the baseline. Some of these inputs such as number of components and study duration are common to the alternate as well. The 15-year study duration includes a 5-year period of engineering, manufacture and substantiation and will be further explained in Section 4.3.3. The number of aircraft, utilization, MTBF at Aviation Unit Maintenance (AVUM), and MTBR to depot were stipulated parameters. The depot repair cost was calculated as 70% of $1080 (the historical average repair cost), plus 30% of $3740 (the estimated replacement cost for a scrapped blade). This accounts for the fact that 70% of the blades are repairable at depot and 30% are scrapped, resulting in an average cost of $1878. The remaining inputs were supplied by the Government or estimated by Boeing Vertol.

TABLE 29. BASELINE INPUT PARAMETERS

Study Duration	15 years
Number of Aircraft	2432
Utilization (Flight Hours/Aircraft/Month)	13
Mean Time Between Failures (MTBF) - AVUM	380 hours
Mean Time Between Removal (MTBR) to Depot	475 hours
Percent Repaired at Depot	70%
Percent Scrapped at Depot	30%
AVUM Maintenance Manhours (MMH) to Repair	.5 hour
Depot Repair Cost	$1878
Component Weight	95 lb
AVUM Labor Rate	$ 15 per hour
Blade Replacement Cost	$3740

4.3.3 Alternate 1. Definition

Table 30 shows those input parameters for the composite blade that differ from the baseline configuration, plus other inputs required to define the configuration and its operating scenario. All inputs were estimated based on R&M analysis, and experience with the YUH-61A and H-46 glass blades (reference section 4.2).

TABLE 30. ALTERNATE 1. INPUT PARAMETERS

MTBF - AVUM	1100 hours
MTBR to AVIM (Intermediate Maintenance)	4400 hours
MTBR to Depot	5200 hours
Percent Repaired	90%
Percent Scrapped	10%
Intermediate Repair Cost	$ 130
Depot Repair Cost	$1240
Component Weight	91 lb
Incorporation Rate (Blades per Month)	100
Investment Nonrecurring	$ 5.0 M
Investment Recurring (4864 Blades)	$16.5 M
Blade Replacement Cost	$3400

Figure 49 shows the schedule and major milestones that comprise the 15-year study duration, starting on January 1, 1978 and ending December 31, 1992. The analysis was based on the stipulated 10 years of operation with the composite blade through the end of 1992. The schedule is consistent with this requirement, with the 10-year period beginning at the mid-point of the blade incorporation.

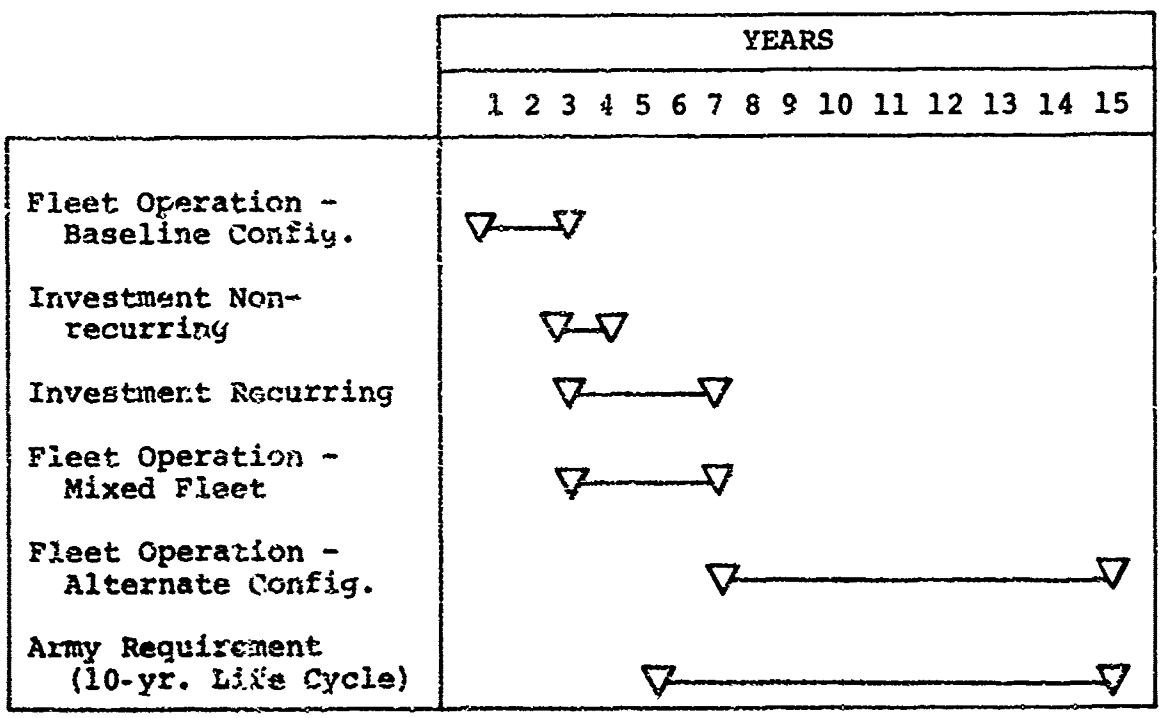

Figure 49. Alternate 1 Schedule.

4.3.4 Results

The first run compared 15 years of operation of the fleet with metal blades, versus installation and operation of the fleet with composite blades according to the schedule shown in Figure 49. The results are shown in Table 31.

TABLE 31. BASELINE VERSUS ALTERNATE 1 - 15 YEARS

	Baseline	Alternate 1.
Operations and Maintenance (O&M) Cost	$45.8 M	$17.6 M
O&M Savings		28.2 M
Investment Cost		
Nonrecurring		5.0 M
Recurring		16.5 M
Total Investment Cost		21.5 M
Total Cost (O&M + Investment)	$45.8 M	39.1 M
Net Savings		$ 6.7 M

Examination of the schedule in Figure 49 shows that the fleet with composite blades fully installed only operates for eight years before the study period ends. Analysis of computer output from the PIPE Model showed that for each additional year of operation after full installation of the composite blades, cost savings increased by about $2.8 million. This is the annual cost difference between operating the fleet with metal blades, and operating with composite blades. Based on this, the study duration was extended to 20 years and 25 years, with net cost savings of $20.9 million and $35.1 million, respectively. These are referred to as alternates 1A and 1B. The effect of changing the life cycle is graphically illustrated in Figure 50. The cumulative cash flow for the baseline and alternate configurations is shown in Figure 51. As can be seen, the break-even point occurs in the twelfth year after initial investment is begun.

Sometimes in the course of a product improvement trade study, it is more cost-effective to incorporate the improved part as the older parts are scrapped, rather than on a more rapid basis. In the run discussed above, glass blades were installed at the rate of 100 per month. In the following cases, composite blades were installed as the metal blades were scrapped. This method of incorporation results in composite blades being incorporated at an ever decreasing rate, since each year there are fewer metal blades which fail and are scrapped. For example, using the 15-year study

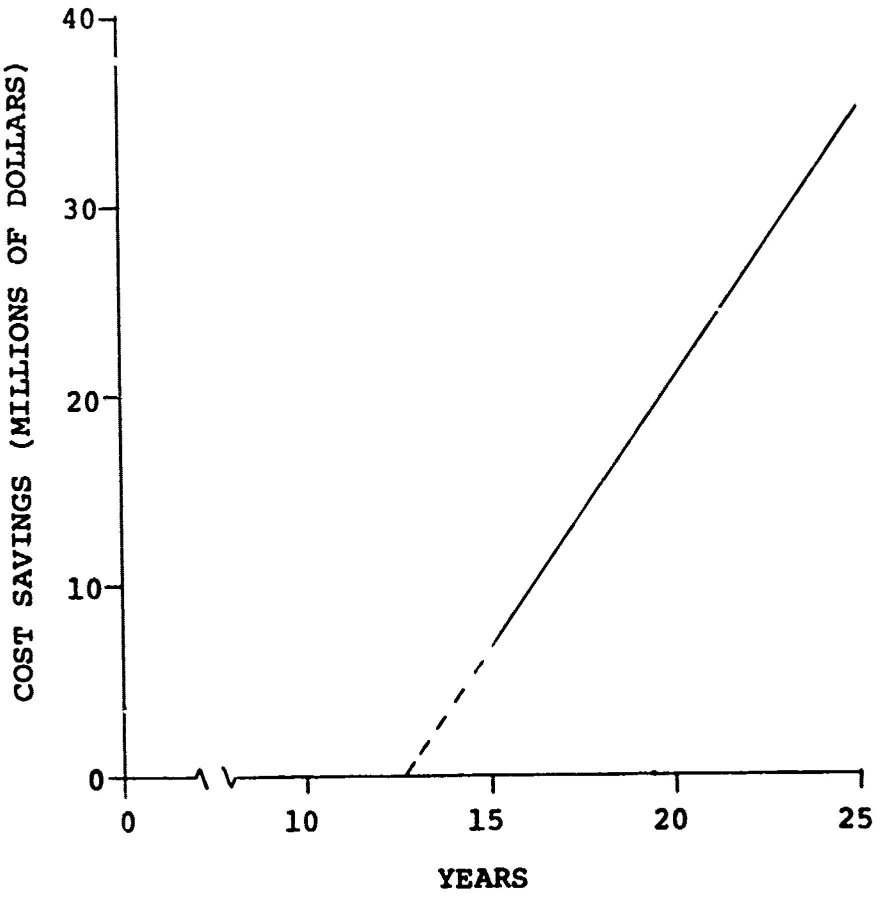

Figure 50. The Effect on Cost Savings of Varying the Life Cycle

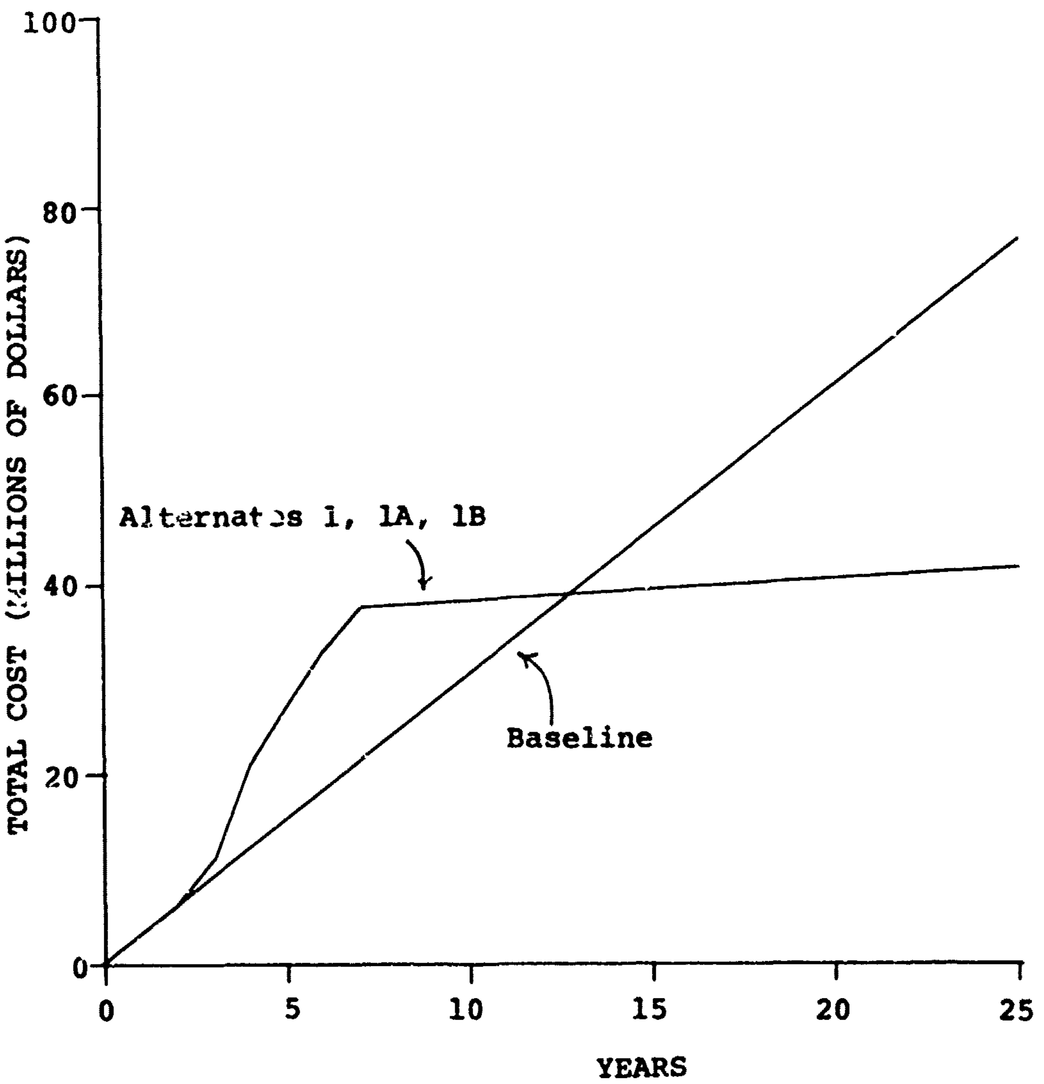

Figure 51. Total Costs for Varying Life Cycles
(Scheduled Incorporation)

duration, in the first year of incorporation, 480 metal blades are scrapped and replaced by composite blades, and in the last year of operation 180 metal blades are scrapped and replaced by composite blades. Two cases were run to examine the effect of changing the incorporation policy. The first (labeled alternate 2), considers attrition replacement in a 15-year study duration; the second, alternate 2A, uses a 20-year study duration. In both cases, incorporation of composite blades begins in year 4, as previously shown in Figure 49. The results are shown in Table 32. Under the baseline column, values represent a 15- and 20-year study duration. The difference in investment recurring between alternate 2 and alternate 2A is found in the fact that in the 15-year study period, only 3456 composite blades are needed to replace scrapped metal blades, while in the 20-year study period, 4044 are needed. In neither case do all 4864 blades get replaced. Comparison of alternates 1 and 2 reveals a nearly identical cost saving. However, as the study duration is extended the cost savings diverge. This is due to the fact that once the entire fleet of metal blades is replaced, annual costs are constant. Since the entire fleet is not replaced in the alternate 2 cases, costs are still decreasing but are not as low as alternate 1; Figures 52 and 53 illustrate this point.

TABLE 32. BASELINE VERSUS ALTERNATES 2 AND 2A

	Baseline	Alternate 2	Alternate 2A
O&M Cost	\$45.8M/\$61.0M	\$22.6M	\$25.4M
O&M Savings		23.2M	35.6M
Investment Cost			
Nonrecurring		5.0M	5.0M
Recurring		11.7M	13.7M
Total Investment Cost		16.7M	18.7M
Total Cost (O&M & Investment)	\$45.8M/\$61.0M	39.3M	44.1M
Net Savings		\$ 6.5M	\$16.9M

An additional advantage of rapid, scheduled incorporation, in alternates 1, 1A and 1B, is not quantified here. This is the benefit of not operating for as long a period with a mixed fleet of metal and composite blades. Having a mixed fleet requires maintaining two items in the logistics system. It also carries the risk of not having the right blade configuration when and where it is needed.

Figure 50 showed how the cost savings could increase due to increases in the study duration or life cycle. Similarly, cost savings are shown to increase as utilization increases. Two utilizations other than the 13 hours per aircraft per month

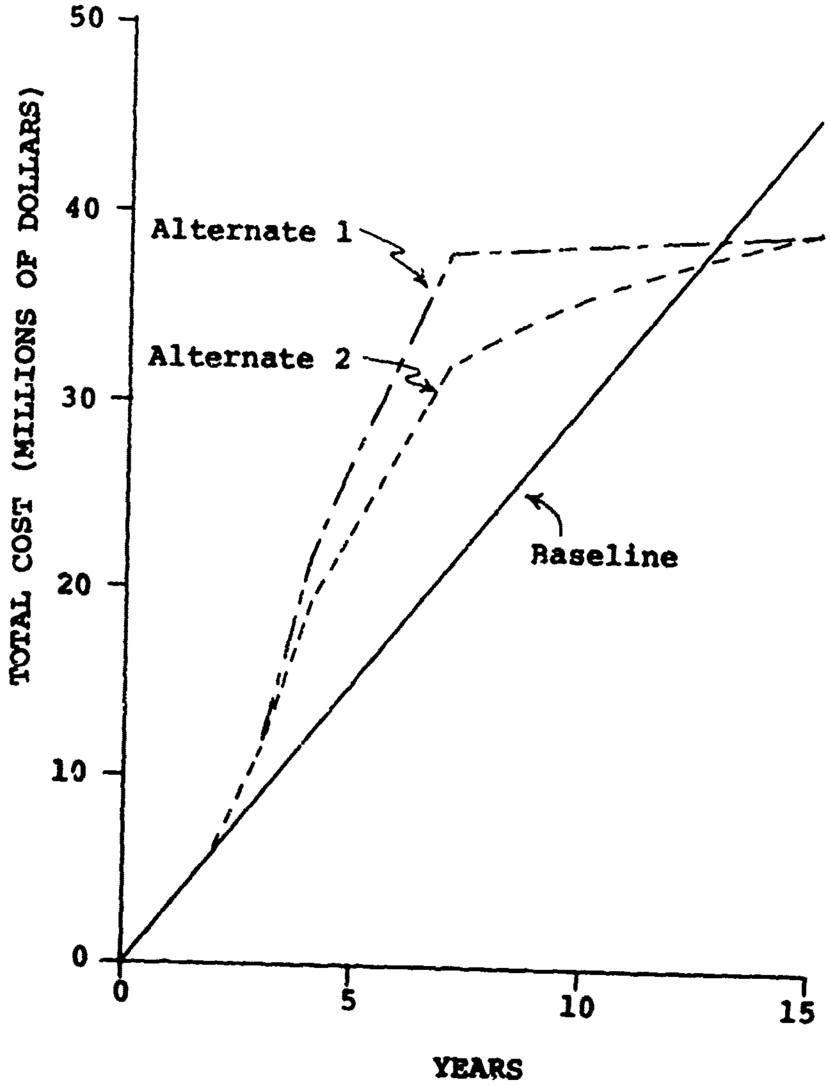

Figure 52. Total Costs for Two Incorporation Policies (15 Years)

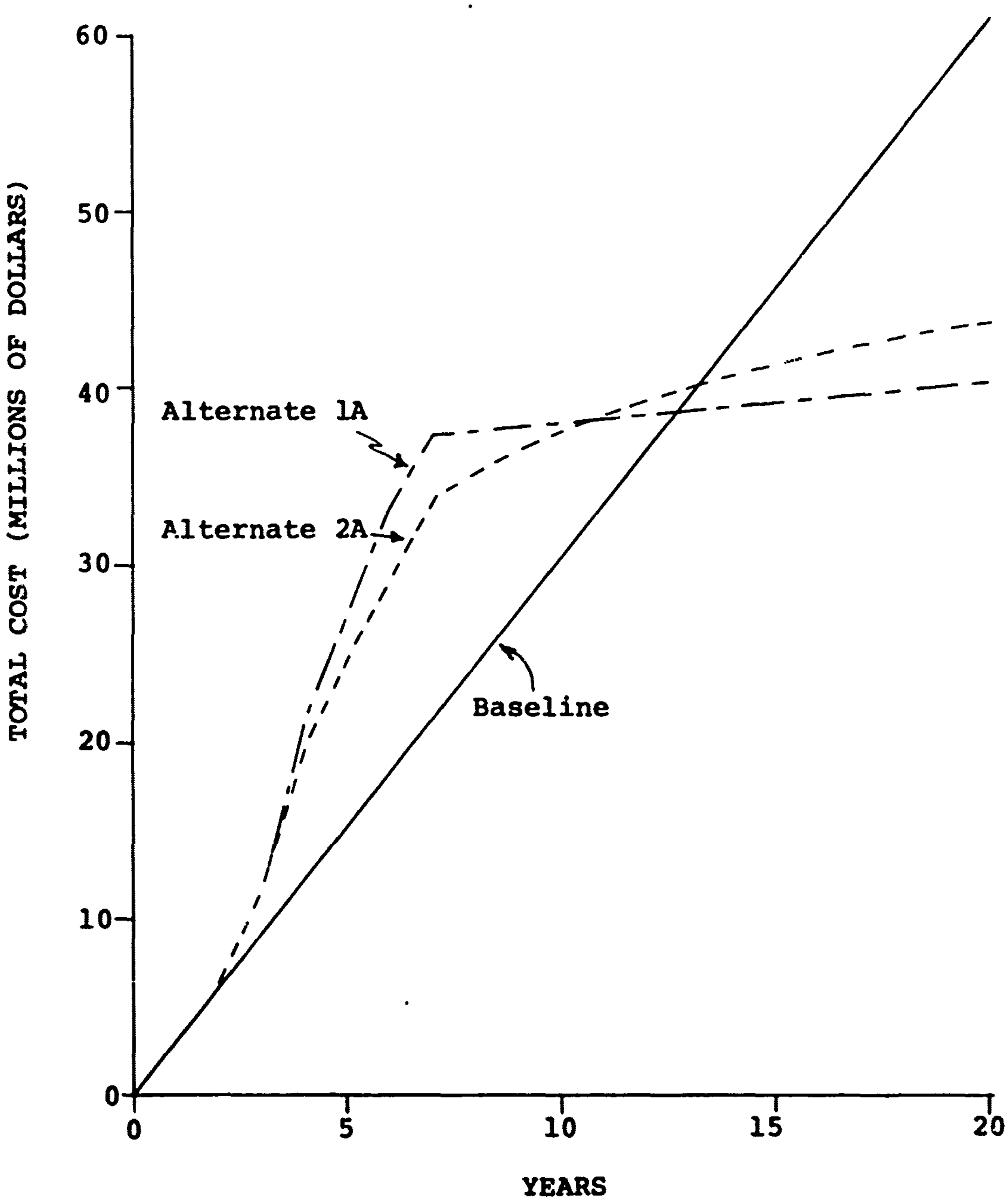

Figure 53. Total Costs for Two Incorporation Policies (20 Years)

were chosen for analysis. Using the same input parameters as alternate 1, utilization was changed to 20 hours and then 50 hours per aircraft per month. These are referred to as alternates 3 and 3A. At 20 hours, cost savings increased from $6.7 million (alternate 1) to $21.9 million. At 50 hours utilization, cost savings were projected to be $87.0 million. This is illustrated in Figure 54.

Finally, since the most expensive maintenance event is always the scrapping of a part (requires purchase of new part), the sensitivity of scrappage rate at depot was investigated (alternate 4). In the baseline case, it was stated that 30% of all metal blades removed and sent to depot were scrapped. In alternate 1 it was estimated that only 10% of those composite blades sent to depot would be scrapped. Alternate 4 took the "worst-case" approach that there would be no improvement in the scrap rate, and that 30% of the composite blades sent to depot would be scrapped. Using the 20-year study duration, cost savings were only reduced from $20.9 million (alternate 1A) to $19.2 million.

4.3.5 Summary

Table 33 lists all of the alternates discussed above, ranked in order of cost savings from lowest to highest. It is noted that this study has been conducted at the target blade recurring

TABLE 33. COST SAVINGS OF ALL ALTERNATIVES

Alternative	Cost Savings ($3400/Blade)	Cost Savings ($6000/Blade)
2. 15 years, incorporation by attrition	$ 6.5M	$-2.8M
1. 15 years, scheduled incorporation (100/mo.)	$ 6.7M	$-6.4M
2.A. same as 2, but 20 years	$16.9M	$ 6.1M
4. 20 years, scheduled incorporation, 30% scrap rate	$19.2M	$ 1.5M
1.A. same as 1, but 20 years	$20.9M	$ 7.6M
3. same as 1, but 20 hours utilization	$21.9M	$ 8.6M
1.B. same as 1, but 25 years	$35.1M	$21.6M
3.A. same as 1, but 50 hours utilization	$87.0M	$72.8M

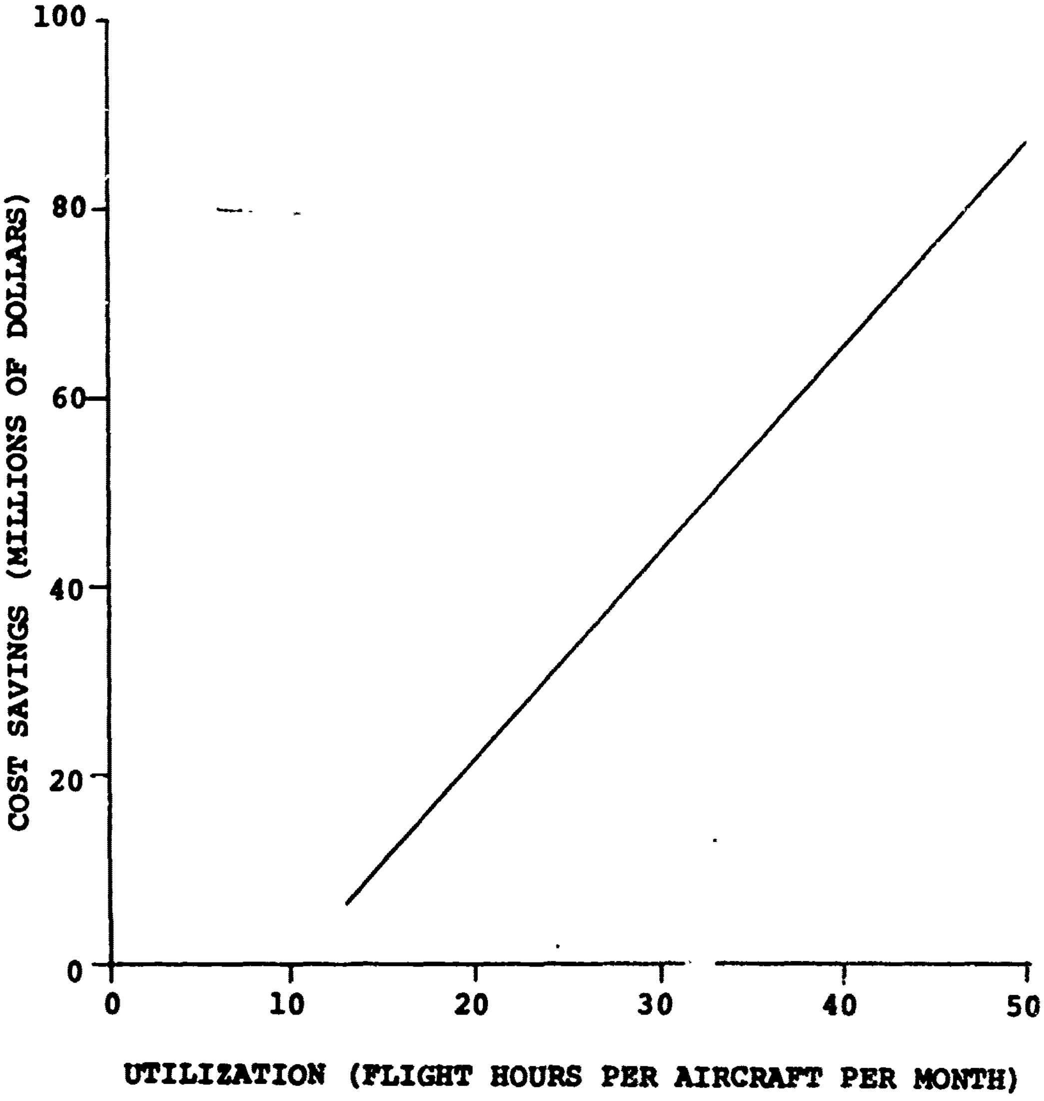

Figure 54. The Effect on Cost Savings of Varying Utilization

cost of $3400/blade. If, as believed, this target is unrealistic, all listed savings would be reduced. Additional values have been provided in Table 33, based on a recurring cost of $6000/blade to show sensitivity to this variable.

One factor that was not considered in the analysis was the quantity of OH-58 spare metal blades now in the supply system. In the PIPE models, each time a metal blade was scrapped, the cost of a new metal blade was charged to O&M costs, except in the cases where it was replaced by a glass blade. The effect of accounting for the metal blades in the supply system would be to reduce O&M costs for both the baseline and the alternates, but more heavily for the baseline, since more metal blades are scrapped in the baseline case.

Based on the sensitivity analyses performed, it is recommended that the composite blade be evaluated in the light of a longer life cycle, that is, through 1997 (alternate 1.A.) rather than 1992 (alternate 1), alternate 1.B. with utilization through 2002 may be unrealistically long. The choice of a longer life cycle can be supported by the low utilization predicted and the high blade fatigue lift. In alternate 1.A., the average blade still would have less than 2700 hours on it.

These recommendations are based on blade costs only. The life cycle costs of the other helicopter systems would have to be evaluated in conjunction with this information.

4.4 SURVIVABILITY

This section includes a discussion and analysis of radar reflectivity, ballistic tolerance, the environmental subsystems, and obstacle strike. Within the environmental subsystems are lightning, erosion and ice protection.

4.4.1 Radar Reflectivity

Radar reflectivity information is presented in Appendix B, which is classified and under separate cover.

4.4.2 Ballistic Tolerance

The selected design was evaluated for survival against the three required threats based on the following criteria:

1. The blade must remain attached to the aircraft and not separate at the hit point.
2. It must retain adequate fatigue strength to continue operation for the contractually specified time.
3. It must not go unstable.
4. It must not go excessively out of track.

Generally the first consideration has been found to be the dominant one. Numerous blade and coupon fatigue tests have demonstrated that, in general, damaged fiberglass composite structures which have sufficient residual strength to sustain the required loads will have a long fatigue life. A Vertol test of a fiberglass blade spar which had lost more than half its original AE showed no visible signs of damage propagation after the equivalent fatigue of 6 hours of flight and 8 minutes of maneuvering loads. Calculations indicated that similar results would be obtained if losses were up to 70% or 80% of the original strength.

Numerous analyses of a variety of blade/hub arrangements indicate that a blade that has sufficient residual strength to prevent separation will also retain enough stiffness to prevent instability. This has been confirmed by wind tunnel tests in which a blade was progressively weakened at several chord and spanwise locations until it barely had the strength to stay on. It demonstrated no signs of instability.

During these same analyses and wind tunnel tests, out of track was measured and determined to be well within acceptable limits. On flight aircraft, blades have been purposely set as much as 6 inches out of track without prohibitive vibration.

Based on the above, it was concluded that the main consideration would be "whether the blade would remain attached to the aircraft and not separate at the hit point".

4.4.2.1 Residual Strength

The ability of the blade to stay on after ballistic damage is related to the residual strength of the composite material and its layup in the spar. In general, the layup most important to blade retention is spanwise unidirectional. Damage tests (References 10 and 11) of both fiberglass and high modulus materials indicate that the loss of strength in a unidirectional layup is closely proportional to the area lost. In the case of high modulus materials laid up as crossply, loss of strength with damage increases considerably faster than the loss of area. Therefore, the residual strengths of only the glass and high modulus unidirectional material were counted on for blade retention in the vulnerability evaluation.

---

10. DESIGN DATA FOR COMPOSITE STRUCTURE SAFE LIFE PREDICTION, Boeing Vertol Company, AFML-TR-73-223.

11. EVALUATION OF BALLISTIC DAMAGE RESISTANCE AND FAILURE MECHANISMS OF COMPOSITE MATERIALS, AVCO Corporation, AFML-TR-72-79.

In order to make the ballistic survival evaluation, scale drawings were made on transparencies of 7.62 mm, 12.7 mm, and 23 mm, API rounds. These were superimposed on the drawings of the root and outboard section to simulate a wide variety of hit positions and angles.

It became apparent that the blade was invulnerable to 7.62 mm projectiles in either the straight or tumbled attitudes. It was also evident that 12.7 mm in the untumbled attitude is not a survivability threat. The 12.7 mm in the tumbled position required a minimal degree of judgement. Its length dimension is such that if it is side-hit on the nose of the blade it could go completely through the spar. However, tests have shown that such a hit would not have the energy to go through and would tend to divert to a different direction before doing catastrophic damage. Therefore, the blade was judged to be invulnerable to any hits by 7.62 mm or 12.7 mm.

In order to determine the vulnerability to 23 mm API, the damaged blade was stress analyzed on a "worst hit" basis. After examining the span of the airfoil section, Station 53 (.25R) was selected as the point at which a hit would leave the residual material most highly stressed. The sections further inboard have large positive structural margins in order to provide the required stiffness. The calculations of Figure 56 show that, at Station 53, a section so damaged would have sufficient residual strength to permit blade retention for unlimited life at cruise speed and to sustain an instantaneous maneuver load up to 2.5 g's. Inboard of Station 53, a 23 mm API hit is survivable at any point and direction of entry. This conclusion is based on experience with hits on similar materials and masses. While a 23 mm API round would penetrate deeply, and in most cases go through, the blade would not be lost. Thus, the conclusion is that, from a strength standpoint, the blade is invulnerable to all of the required threats. Hits on specific locations such as the various balance and inertia weights could cause severe vibrations but are not believed to be catastrophic.

A dynamic analysis was conducted to determine blade stability after sustaining the same damage to Station 53 noted above.

4.4.2.2 Dynamic Response

The three areas of concern for the effects of ballistic damage on rotor dynamics are:

1. Possible reduction in the aeroelastic stability margins
2. The potential for vibration caused by blade out-of-track
3. Excessive in-plane vibration resulting from the tip weight loss

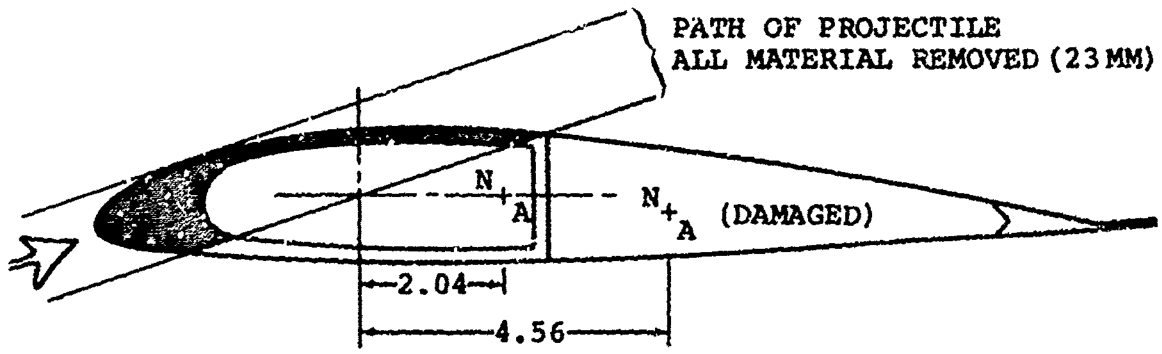

CONSIDER HIT AT BLADE STA 53 (.25R). JUST BEFORE SPAR MATERIAL BUILDUP FOR INCREASED STIFFNESS AT ROOT, BUT WITH PARTIAL TRAILING EDGE BUILDUP.

SECTION PROPERTIES

	EI_F	EI_{CH}	AE
UNDAMAGED	4.32	336	18.86
DAMAGED	0.744	160	10.59

LOADS

THE FLAPWISE BENDING LOADS ARE DETERMINED BY THE LOADED SPANWISE SHAPE OF THE BLADE, WHERE THE LOCAL CURVATURE IS THE BENDING RADIUS. THEREFORE THE BM_F OF THE DAMAGED BLADE IS 17.2% OF THE UNDAMAGED BLADE.

$$\left[\frac{0.744}{4.32} = 0.172\right] \qquad \frac{1}{R} = \frac{M_F}{EI_F}$$

THE CHORDWISE AND AXIAL LOADS ARE NOT SO AFFECTED. THE CHORDWISE MOMENT IS AFFECTED BY THE LOCAL SHIFT OF THE NEUTRAL AXIS, (STEADY ONLY) STA 53

CONDITION	M_F IN.-LB	M_C IN.-LB	C_F LB
UNDAMAGED			
STATIC NO. 1	-7000	133,000	47700
NO. 3	15000	97,000	26100
FATIGUE	960 ± 2580	67,000 ± 17900	35380
DAMAGED			
STATIC NO. 1	-1204	253,200	47700
NO. 3	2580	162,800	26100
FATIGUE	165 ± 444	156,200 ± 17900	35380

REF SECT. 5.7

Figure 56. 23 mm API Damage Tolerance Structural Analysis

DETERMINE STRESSES AT PT A (SEE SKETCH) (KEVLAR 0^o)

$X = -6.1$
$Z = -0.6$

$$+\varepsilon_t = \frac{M_F(-Z)}{EI_p} + \frac{M_C(-X)}{EI_{CH}} + \frac{CF}{AE}$$

STRAINS μ IN./IN.

CONDITION	M_F	M_C	C_F	TOTAL
STATIC NO. 1	-971	9353	4504	13,186
NO. 3	2080	6206	2465	10,751
FATIGUE	133 ± 358	5955 ± 682	3340	9428 ± 1040

KEVLAR 0^o
STATIC

STATIC STRAIN ALLOWABLE = 14,500 μ IN./IN. (SECT 5.7)
STATIC CASE (2.5 G) MAX STRAIN = 13,186 μ IN./IN.
(REQUIREMENT IS 1G)

$$MS = \frac{14500}{13186} - 1 = +0.10$$

FATIGUE

USE 75% OF NORMAL FATIGUE DESIGN LOADS AND CONSERVATIVELY, MEAN-3σ ALLOWABLES AT 10^8 CYCLES

$\varepsilon_t = 0.75\ (9428 \pm 1040) = 7070 \pm 780$ μ IN./IN.

ALT ALLOWABLE AT 10^8 CYCLES WITH A STEADY OF 7070 is 1650 μ IN./IN. (SECT 5.7)

$$M.S. = \frac{1650}{780} - 1 = +1.12$$

(REQUIREMENT IS 30 MINUTES OR 30 (354) = 10,620 CYCLES)

Figure 56. 23 mm API Damage Tolerance Structural Analysis (Continued)

As discussed in detail in the Dynamic Analysis Section on aeromechanical stability, the stability of the rotor is a function essentially of the flap and chord natural frequencies, except when considering classical flutter and stall flutter. The change in flap and chord frequencies of the composite rotor blade due to a 23 API hit at Station 53 inches (the most critical station structurally) is less than one-half of one percent, so that the rotor stability is not adversely affected. The only remaining stability issues are blade classical flutter and stall flutter. Based on a comparison of C-60 aeroelastic analysis computer programs for the damaged and undamaged blades, the damaged blade is free of classical flutter and the onset of stall flutter is not noticeably affected by the change in torsional dynamic characteristics due to ballistic damage. This is reflected in the comparison of the rates of convergence and changes in angle of attack with successive iterations, as shown in Figure 57.

The issue of vibration induced by blade out-of-track is addressed in Figures 58 and 59. The data is predicted by the C-60 rotor aeroelasticity computer program for comparable cases with undamaged and damaged blades. In Figure 58 the blade root dynamic moments and shears for the damaged and undamaged blades are compared. The loads are nondimensionalized by assuming the undamaged blade moments and shears equal unity. It can be seen that the vibratory moments and in-plane shears all show less than a 5-percent change due to the effects of a damaged blade. The vertical shear increased by 12 percent, so this was investigated further, especially in light of the fact that this is a major source of airframe vibration in two-bladed teetering rotors. Figure 59 shows the fixed system hub vertical forces for both the undamaged and damaged composite rotor blades. It is significant that the two-per-rev shaking force actually decreases by 4 percent while the steady increases by 2 percent and 4 per rev by 7 percent. Since the magnitude of the 2 per rev is generally ten times the 4 per rev amplitudes, it can be concluded that the hub vibrations will see little or no increase due to ballistic damage.

Referring back to Figure 58, it should be noted that there is minimal change to tip deflection flapwise; another indication that there will be no out-of-track problems. Finally, the vibratory pitch angle of the damaged blade is 12 percent higher than the undamaged composite blade. This amount does not result in any significant increase in blade stall, as observed by comparing the pitch link load waveforms. Thus, the damage to one blade as specified earlier will not result in adverse stability or vibration levels that will make aircraft control impossible.

The tip weights and their canister are located at Station 201.34 and nominally weigh 1.3 pounds. The canister presents

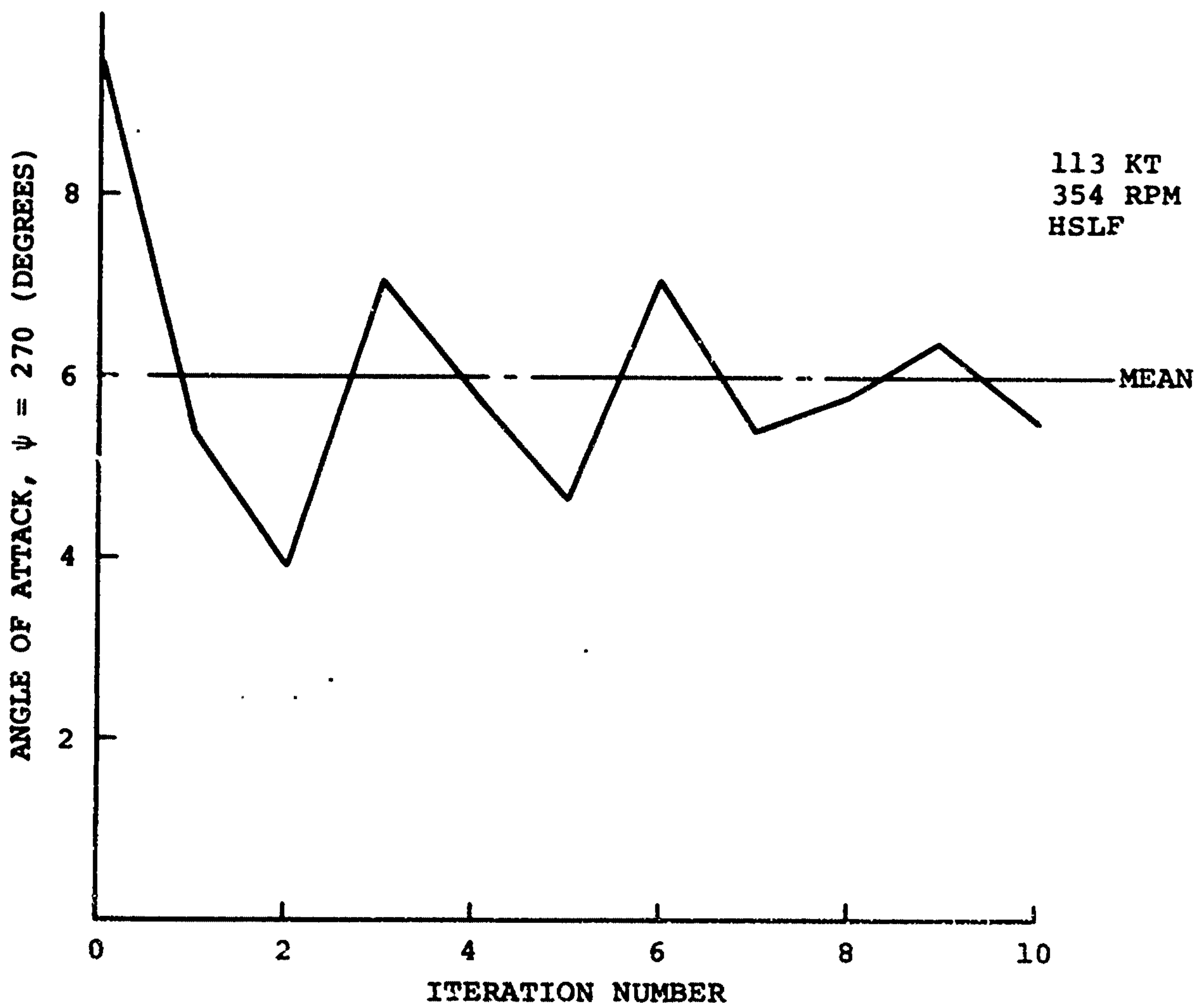

Figure 57. Convergence of Angle of Attack for a Ballistically Damaged OH-58C/A Blade

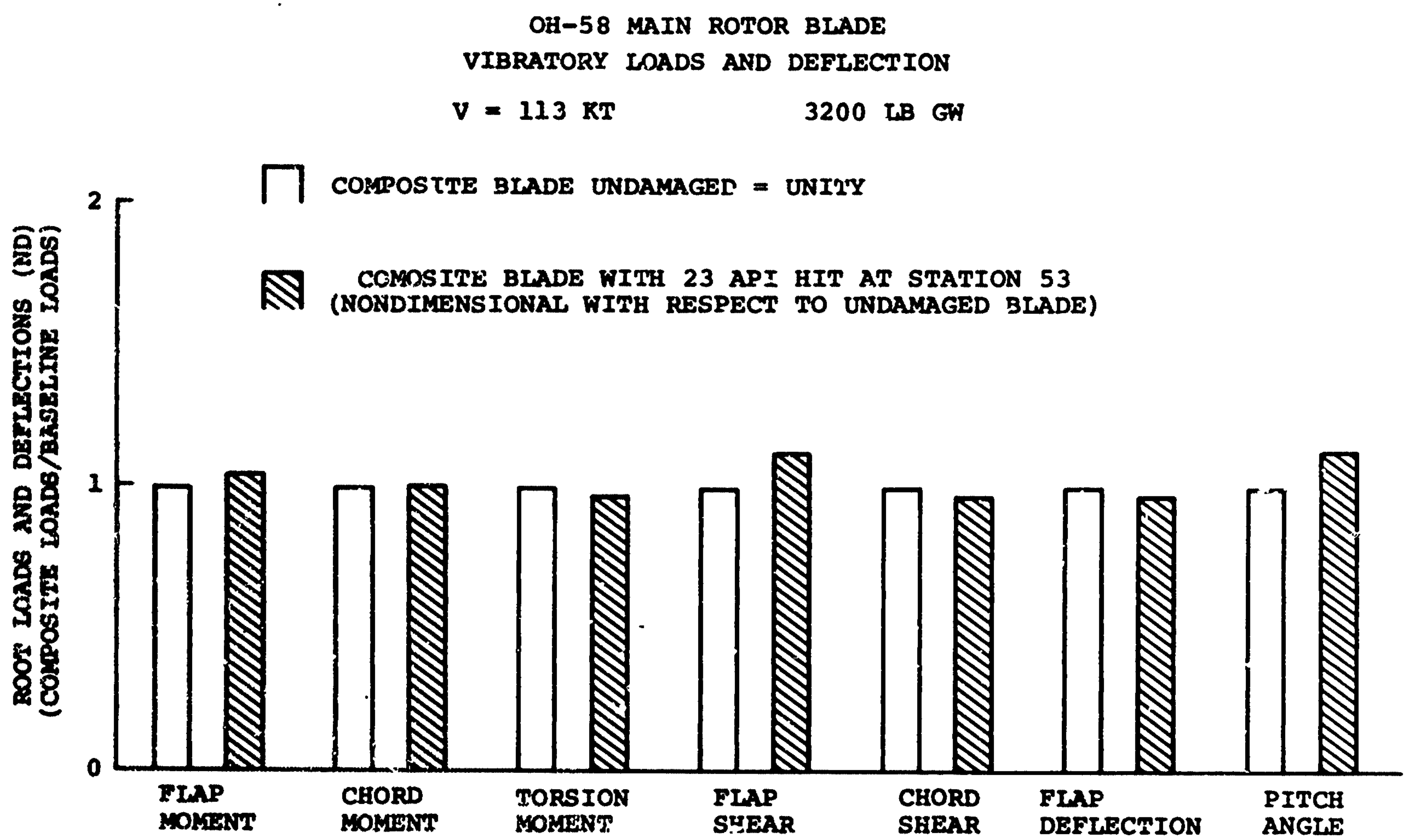

Figure 58. Effect of Damage on Root Loads

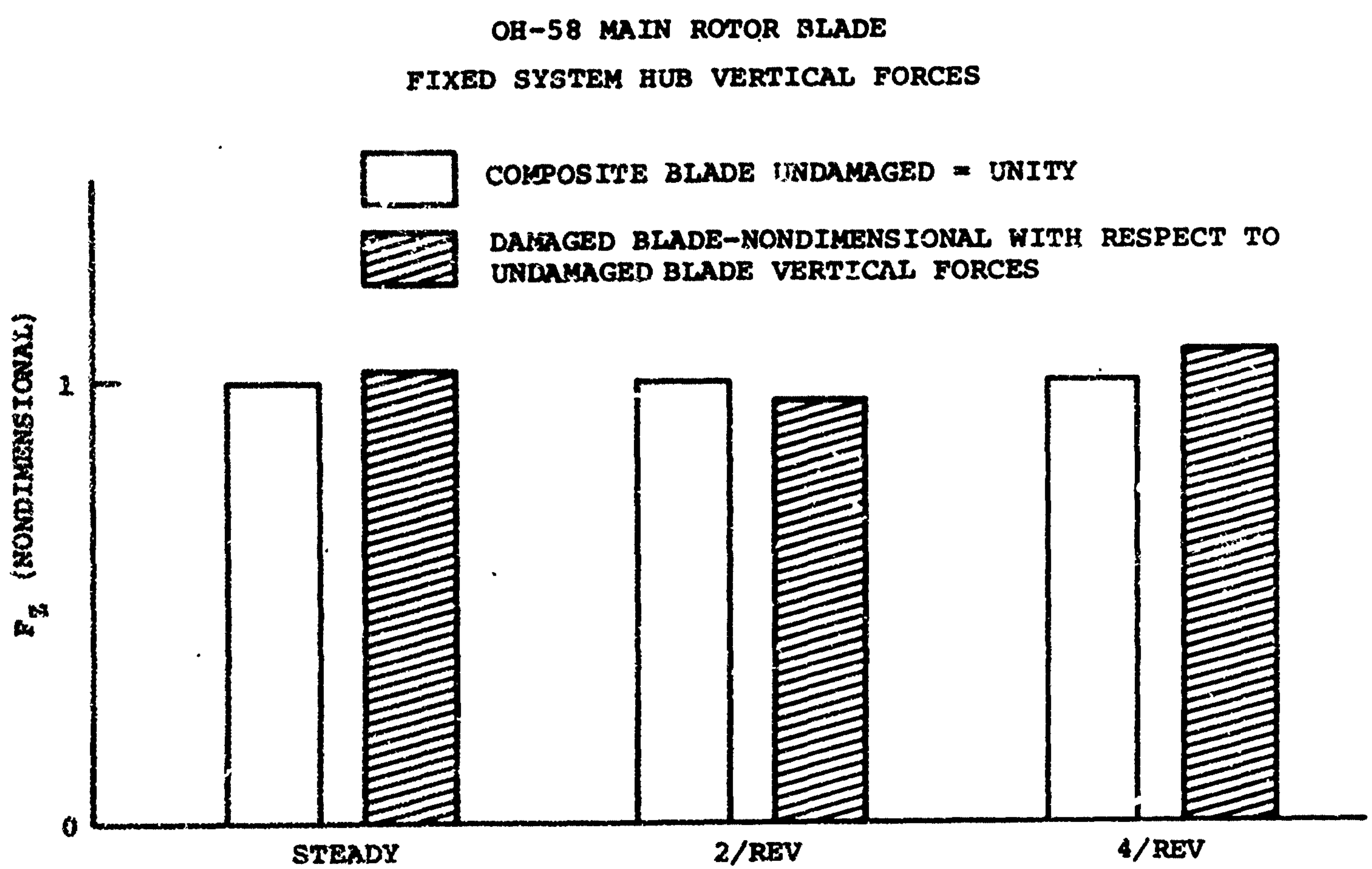

Figure 59. Effect of Damage on Fixed Hub Vertical Forces

a small target, especially at low blade angles. However, the loss of the tip weights due to a ballistic impact would cause an unbalance force of approximately 900 pounds which offers a strong possibility of causing sufficient impairment of pilot control to prevent a safe landing.

4.4.3 Environmental Subsystems

The environmental subsystems include lightning, erosion and ice protection. The Boeing Vertol OH-58C/A composite replacement blade includes each of these subsystems.

4.4.3.1 Lightning Protection

The outboard 18 inches of blade will be covered by a wire mesh. This will create a lightning screen in the blade area most susceptible to lightning strike because of static electricity buildup and the presence of metal components at the tip. The screen is attached to a .16-inch-diameter (20,000 circular mills) copper wire to permit grounding of a 200,000 amp lightning strike without catastrophic failure.

Other metallic parts such as the inertia weights, mid-span tuning weights and sweep balance weights shall also be connected to the copper grounding wire. However, in the case of the inertia and tuning weights, a noncatastrophic amount of burning through nonmetallic material would occur, if the charge penetrates to the subsurface weights.

Some degree of damage would also be expected in the event of a blade passing through an ionized air mass, one through which lightning had just passed. The charge may attract to the copper wire within the nose resulting in damage to the material forward of the wire. Such damage would be non-catastrophic; although the blade would probably be unrepairable.

4.4.3.2 Erosion Protection

The erosion protection system is designed to protect the blade leading edge from excessive wear under adverse environments such as sand, dust and rain. The system consists of a .075-inch-thick Estane boot bonded in a recess of the leading edge. The boot would extend spanwise from 13% radius to within 9 inches of the tip (96% radius). The outboard 9 inches of blade would utilize an electroformed nickel leading edge. The tip cover is also of nickel.

The Estane boot in the flat is 5.5 inches wide with a chordwise coverage, from the leading edge, of 1.53 and 3.33 inches on the upper and lower surfaces of the airfoil respectively. The boot is field replaceable, and replacement will not affect the R&M properties of the basic blade.

The Estane boot does not extend to the blade tip since the airfoil at the tip is very small and thin and the .075 inch thick Estane would be a large percentage of the tip leading edge cross section. Any erosion would have a large adverse aerodynamic effect on such a thin airfoil.

Erosion is disproportionately severe at the tip and although Estane is the best of the nonmetallic materials from an erosion standpoint, its resistance to rain erosion is inferior when compared with metals. Using a nickel leading edge for the outmost 9 inches will increase the boot life. It is anticipated that the Estane leading edge will meet the 1200 flight hour requirement; provided the aircraft is used in reasonable rain conditions, up to 1/2 inch/hour. Use of the aircraft in heavy rainfall conditions would be likely to cause more frequent replacement of the Estane boot.

4.4.3.3 Ice Protection

The requirement to minimize the radar cross section eliminates the standard helicopter electrical deicing system because of the metal heating elements. The only other method of ice protection used on production helicopters (by the user) is the chemical (alcohol) system. This system is heavy when the weight of the alcohol is included. It has not been possible to efficiently use the alcohol because of non-uniform dispersion and it is basically an anti-icing system so that the alcohol is used continuously. Therefore, the pneumatic boot deicing system is proposed since it has been used successfully for many years on fixed-wing aircraft. It has the following advantages:

- Nonmetallic blade boot
- Low weight
- Low electrical power required
- Low pneumatic power
- Simple/low cost
- Noncritical cycle (no runback if cycle is off optimum)

It has the disadvantage that it has not been developed for helicopter rotors, and, therefore, potential problems have not been resolved. Consequently, a development program would be required.

Each blade has a .075-inch-thick Estane boot which would be divided into .50-inch-wide spanwise flat tubes. (While chord-wise tubes have less drag when inflated, a spanwise feeder tube is required which compromises the design, and fixed-wing experience has shown the chordwise tube to be less effective in shedding ice.) A single supply tube would connect each boot at its root with the hub, then pass through the rotor shaft to the stationary supply system by way of a rotary gland. Pressure is supplied during the deicing cycle and a vacuum is provided during the dwell cycle. The pressure and air volume per cycle are 22 psi and .2 cubic foot respectively.

When the boot is not being inflated for deicing, a vacuum is maintained in the tubes to keep the boot tubes' outer wall against the blade to preserve the airfoil contour. This vacuum pressure must offset the low surface pressure which provides most of the blade lift on the upper surface and which tends to raise the tubes' outer wall. The vacuum at the hub must be a lower pressure than required at the blade tip to allow for the pressure increase as a result of the centrifugal forces on the column of air in the blade boot. In forward flight, minimum pressure is required when the blade has an azimuthal position of 350° to 10° (Ref.0° forward). At this azimuth, the vacuum needs to be approximately 5 psi absolute.

In fixed-wing turbine-powered aircraft, bleed air controlled by a regulator is used to provide the inflation pressure, and the vacuum is provided by bleed air powering an ejector. For a helicopter the same system could be used, except that the ejector would be replaced by a positive displacement vacuum pump to obtain the lower pressures with reduced power consumption. When bleed air is used, the positive pressure is limited to the pressure available at flight idle, which would occur during descent. This is approximately 22 psi gage with the OH-58 engine. The cycle can be controlled manually or automatically with an icing rate instrument.

The boot would extend spanwise from 13% radius to within 9.0 inches of the tip (96%R). A metal leading edge without an active deicing system is utilized for the outmost 9.0 inches. Based on data from limited hovering tests of helicopters in icing conditions, the blade from 96% to 100% radius would not collect ice at ambient temperatures above 9.2°F. At lower temperatures, if the ice at the tip reached an average thickness of .25 inch on the total impinged area, the weight of the ice would be .18 pound, which with unequal shedding would produce an unbalance force of 133 pounds until the opposite blade shed. 133 pounds of unbalance would result in an unpleasant, but not unacceptable pilot environment of approximately ±0.04 g's.

4.4.4 Blade Obstacle Strike

The requirement for the OH-58 C/A blade is to permit strikes of 1-inch-diameter pine branches or .25-inch-diameter non-shielded copper wire without catastrophic blade damage.

Vertol's historical data shows that 55% of blade strikes occur at the outboard 10% of the blade. This is the portion that tapers on our design. Boeing Vertol has conducted an extensive whirling arm impact test program to determine the ability of a variety of blade types and sizes to survive hits on tree branches. Figure 60 shows a schematic of the test equipment used and Table 34 itemizes the blades tested. The blades were whirled at their actual flight tip speeds. Then maple dowels of various diameters, supported at each end were injected into the blade tips. One of these blades, the BO-105 tail rotor, most closely simulates the size and construction of the OH-58 C/A fiberglass blade near its tip. This blade was driven through a 1-inch-diameter maple dowel without sustaining any visible damage. A 1-inch-diameter maple dowel is considered to be roughly equivalent to a 2-inch-diameter pine branch. Based on these tests, the blade easily meets the requirement. It should be considered, however, that tree branches are not supported rigidly at both ends and may be struck at a variety of angles. Still, the probability of this blade's surviving any hit of a 1-inch-diameter pine branch must be considered very high. Assessing the blade's ability to survive a strike on a .25-diameter-copper wire is less subject to quantitative evaluation. Most wires are strung rather loosely in a nearly horizontal plane, which is also the plane of the rotor. This means that a sliding swipe of the wire is more likely than a perpendicular chop. The effect of this may be to not cut the wire but to divert it over the rotor, into the rotor mast or into other parts of the aircraft. However, assuming that the wire is somewhat off the rotor plane, a high probability exists that the wire will be cut and the blade will not be seriously damaged.

Vertol did a study of 136 wire strikes of Army helicopters that occurred between July 1967 and November 1973. Of these 136 strikes, 18 were on the main rotor. Seven of these 18 were crashes, and eleven were other types of mishaps. Of the seven crashes, all were with high tension lines. None of the crashes were due to hits on communications lines. One of the incidents was of an OH-23D whose rotor hit a 1/4-inch-diameter copper wire. This resulted in a precautionary landing with no noted damage. The whirling arm tests of wooden dowel hits consistently showed less damage to fiberglass blades than to equivalent metal blades. Thus, it appears logical to assume that the OH-58 C/A would also

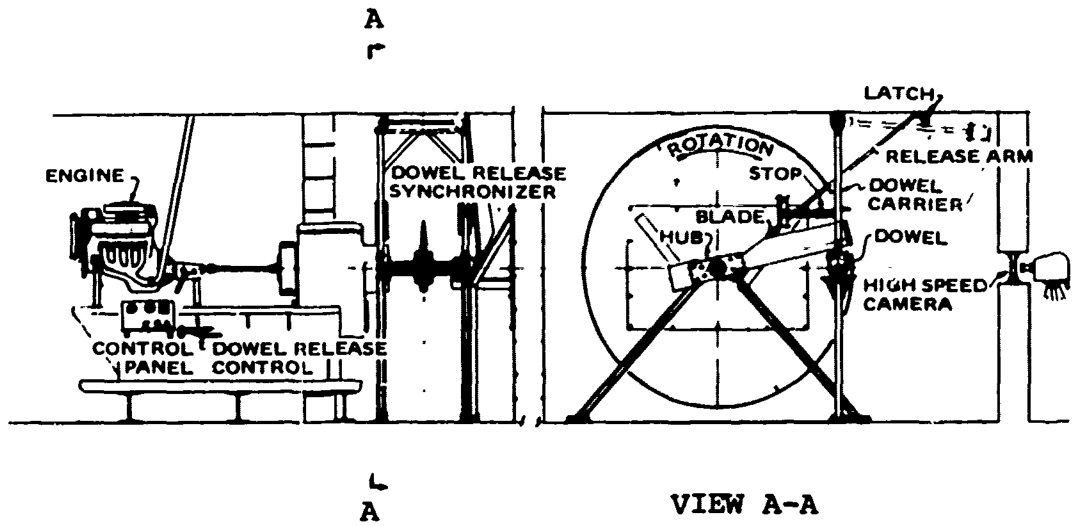

Figure 60. Schematic of Impact Test Fixture

Table 34. Whirling Arm Impact Test Summary

Tail Rotor Blades	Main Blades
<u>Existing Tail Blades</u>	18-in. Chord (Outboard Section)
H-13 Aluminum	CH-46A Steel Spar
H-19 Aluminum	UTTAS Fiberglass/Steel Nose
H-34 Aluminum	UTTAS Fiberglass/Glass Nose
UH-1A Aluminum	UTTAS Fiberglass/Titanium Nose
UH-1D Aluminum	Mixed Modulus/Steel Nose
BO-105 (4 Types)	
<u>Vertol Tail Blades</u>	3.367-in. Chord (Entire Blade)
UTTAS Fiberglass C-Spar, Metal Nose	UTTAS Fiberglass/Steel Nose
UTTAS Fiberglass C-Spar Glass Nose	UTTAS Fiberglass/Glass Nose
UTTAS Fiberglass Compartmented	UTTAS Fiberglass/Steel Nose, Scaled Weight
UTTAS on Flex-Strap Hub	Mixed Modulus/Steel Nose
	Comparison Blades
	Gyrodyne Fiberglass Blade Section
	DC-3 Propeller (Forged Aluminum)

	Tail Rotor	Main Rotor
Blade Types	15	13
Blade Specimens	28	13
Tests	81	41
Total Tests	22	

survive a wire hit better than an equivalent metal blade and that a direct hit on a .25-inch-diameter copper wire would not result in a catastrophic blade failure.

4.5 DYNAMIC ANALYSIS

4.5.1 Physical Properties

The spanwise distributions of running weight, flapwise, chordwise, and torsional stiffness; chordwise center of gravity and neutral axis locations; pitch inertia and shear center location are presented in Figures 61 through 68. These physical properties are shown for the proposed composite blade design and are compared to the existing OH-58 metal rotor blade. As seen in the figures, the objective of matching the current weight per inch, flap and chord stiffnesses, and center-of-gravity location was achieved satisfactorily. The flap stiffness shows some reduction, but it will be shown that this did not impact the flap natural frequencies. The effect of the aft shift in neutral axis on loads and the effects of the reduced torsional stiffness on frequencies and stability will be discussed in subsequent sections.

4.5.2 Natural Frequencies and Mode Shapes

The fully coupled natural frequencies of the composite OH-58 main rotor blade predicted by the Y-71 frequency analysis computer program are shown in Figures 69 and 70. There are two basic types of modal deflections given in the frequency diagrams. The collective mode for a two-bladed teetering rotor may be characterized as a hingeless rotor flapwise and an articulated rotor in the chord direction. The resulting frequencies are shown in Figure 69. The cyclic mode, whose frequencies are seen in Figure 70, is characteristic of an articulated rotor in both flap and chord, with a negative chordwise translational spring emperically defined on the OH-58 as representative of the shaft flexibility and an infinite chordwise rotational spring. The frequencies of the current metal OH-58 rotor blade at 354 RPM are also indicated in the figures. In all cases the flapwise natural frequencies of the composite blade and the existing metal blade agree to within 3 percent. The chordwise frequencies of the composite blade are predicted to be 6 to 8 percent higher than those of the metal blade. However, experience at Boeing Vertol has shown that coupling with the drive system will reduce the predicted frequencies slightly and place them very close to the current design.

The torsional frequencies are considerably lower due to a large reduction in torsional stiffness. The fundamentally coupled torsional frequency has been changed from 6.4 per rev at 354 RPM to 3.8 per rev for the composite design. This is placed away from any potential adverse coupling in the normal operating

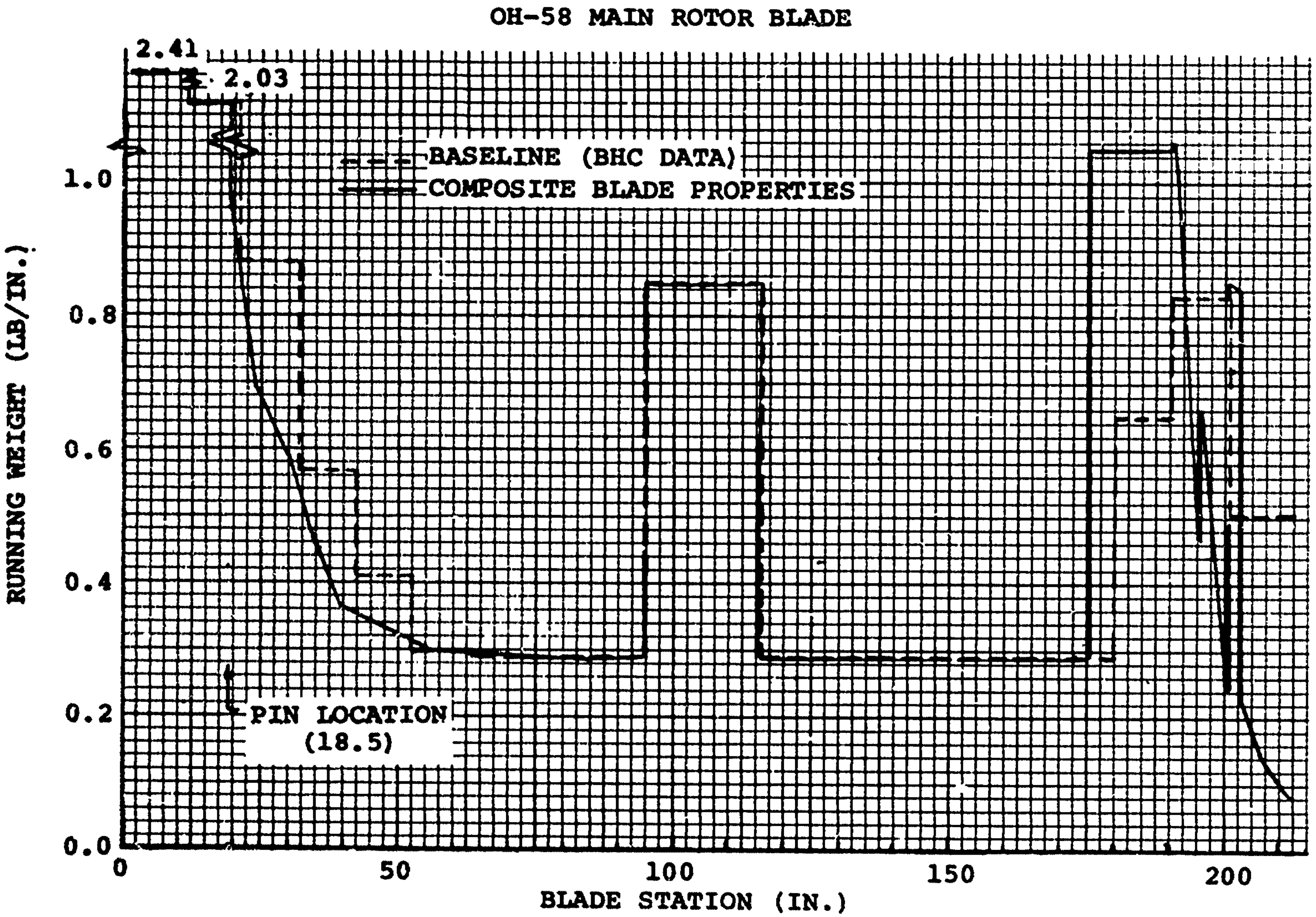

Figure 61. Spanwise Distribution of Running Weight

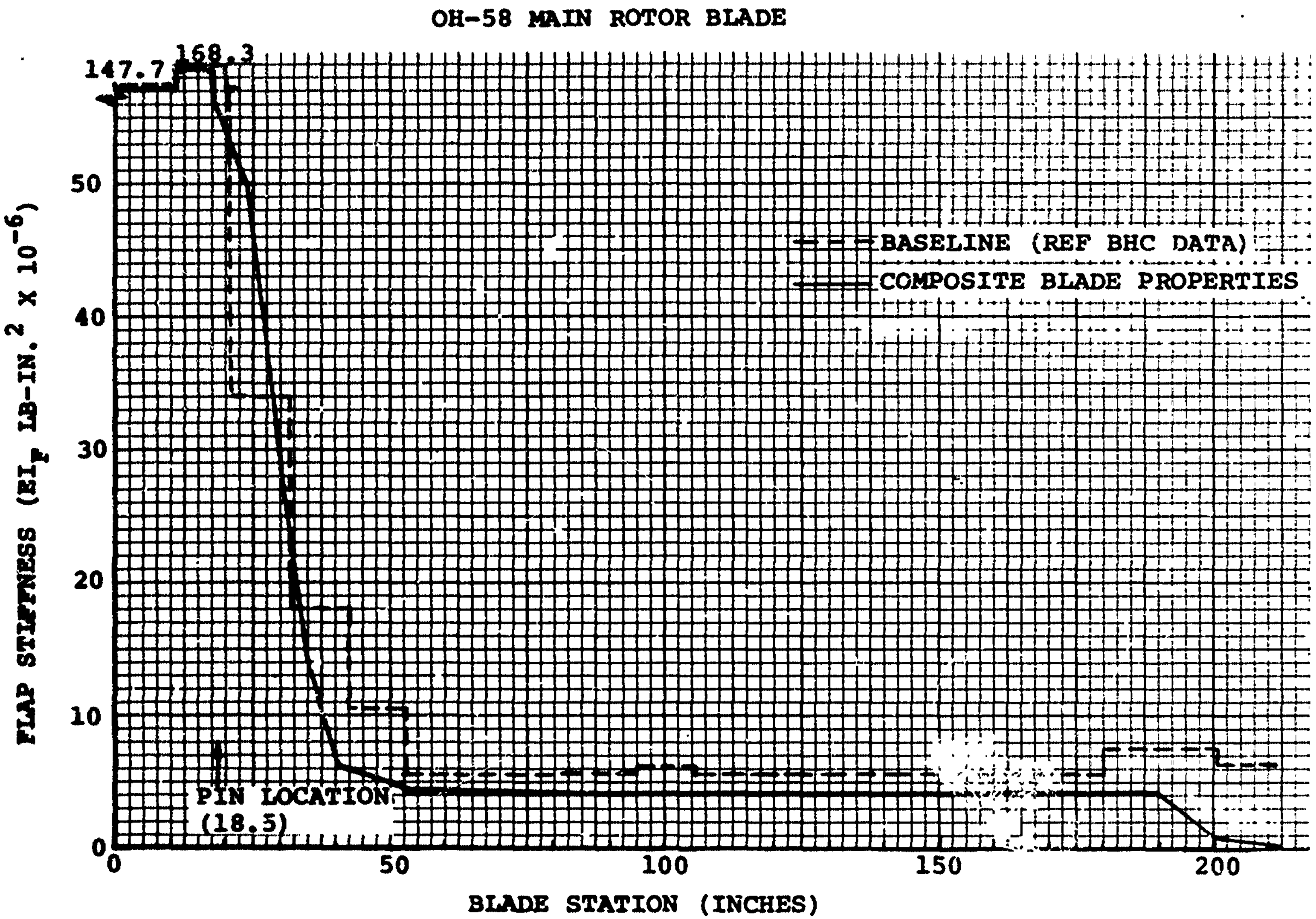

Figure 62. Spanwise Distribution of Flapwise Stiffness

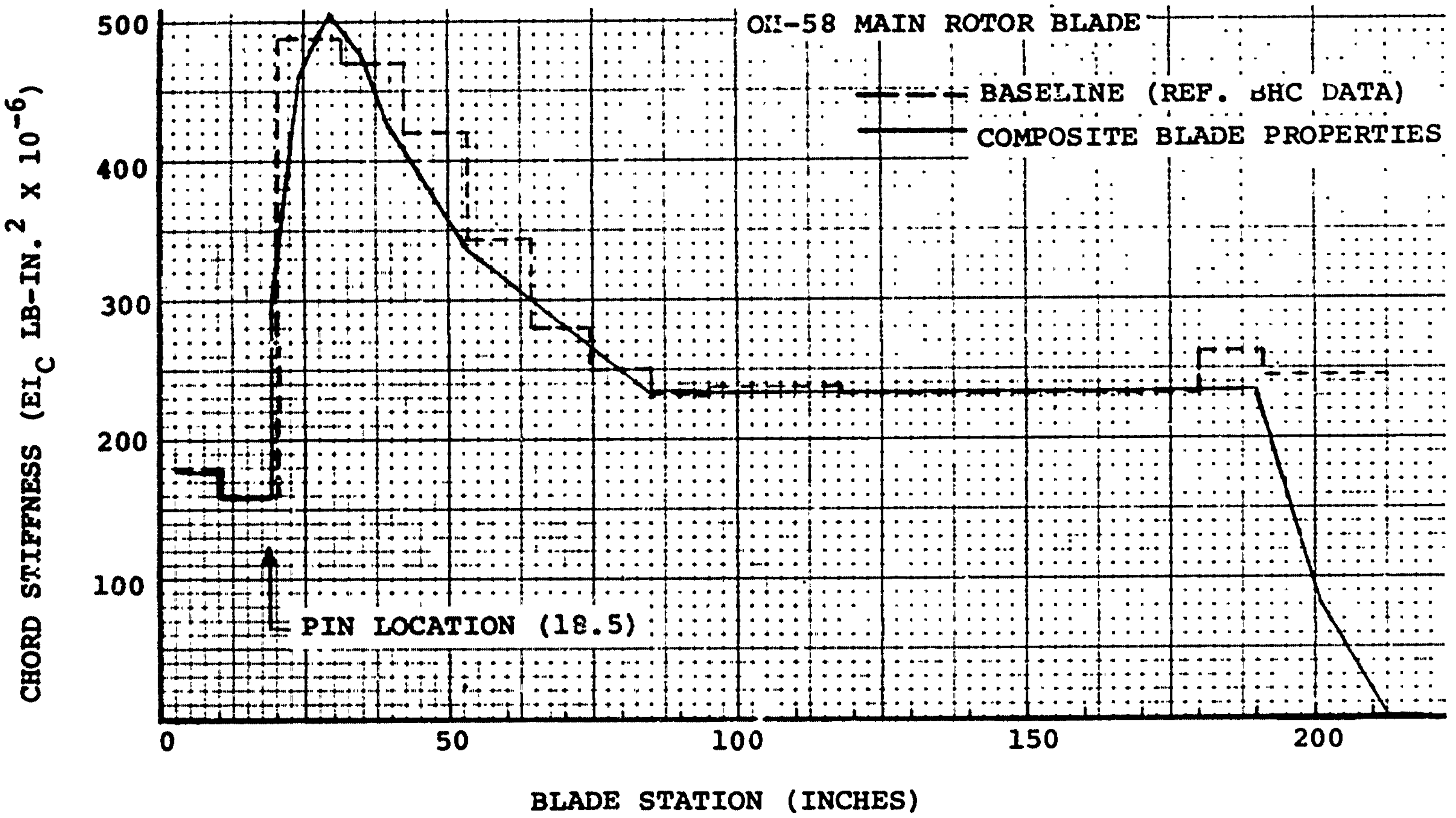

Figure 63. Spanwi- Distribution of Chordwise Stiffness

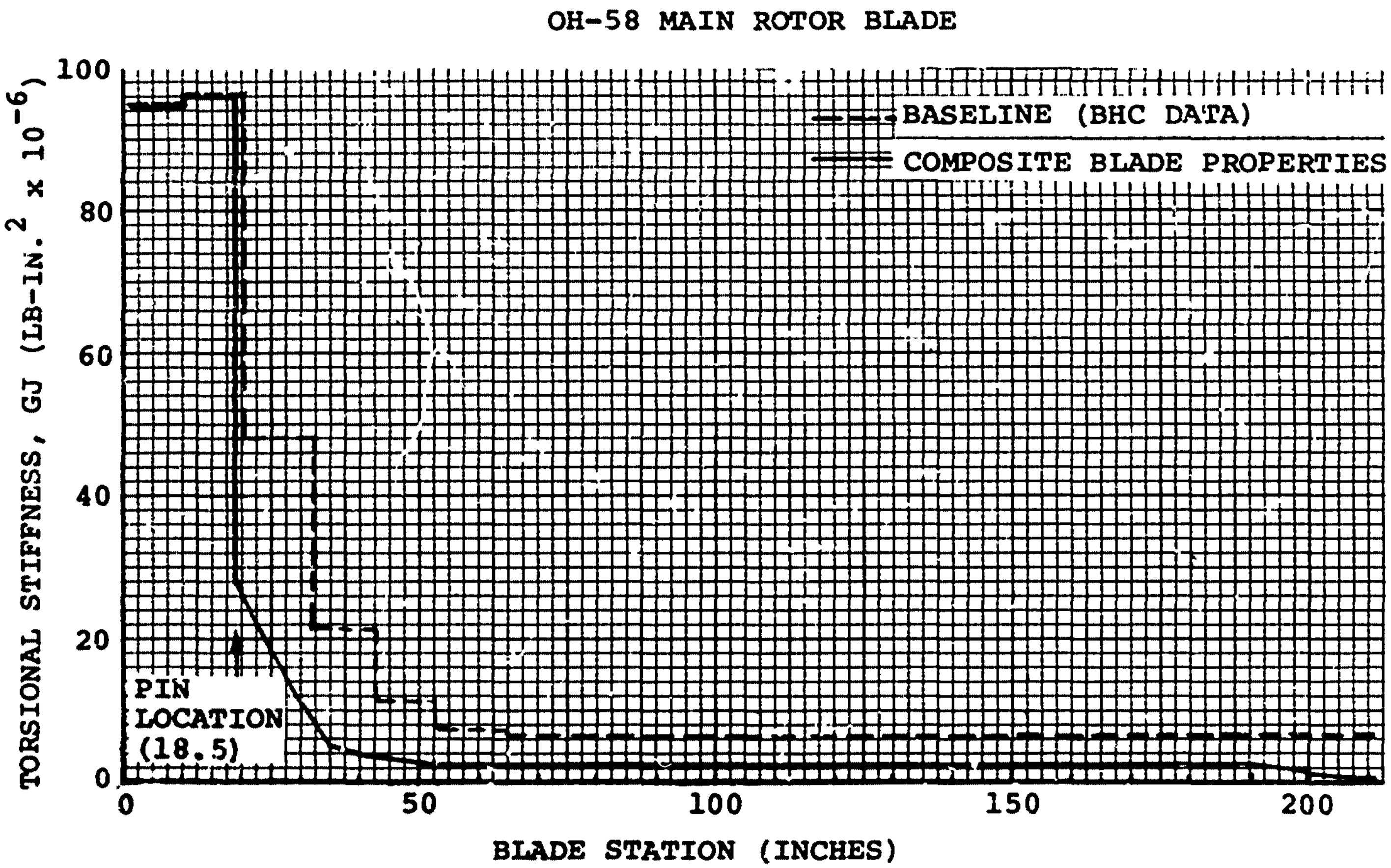

Figure 64. Spanwise Distribution of Torsional Stiffness

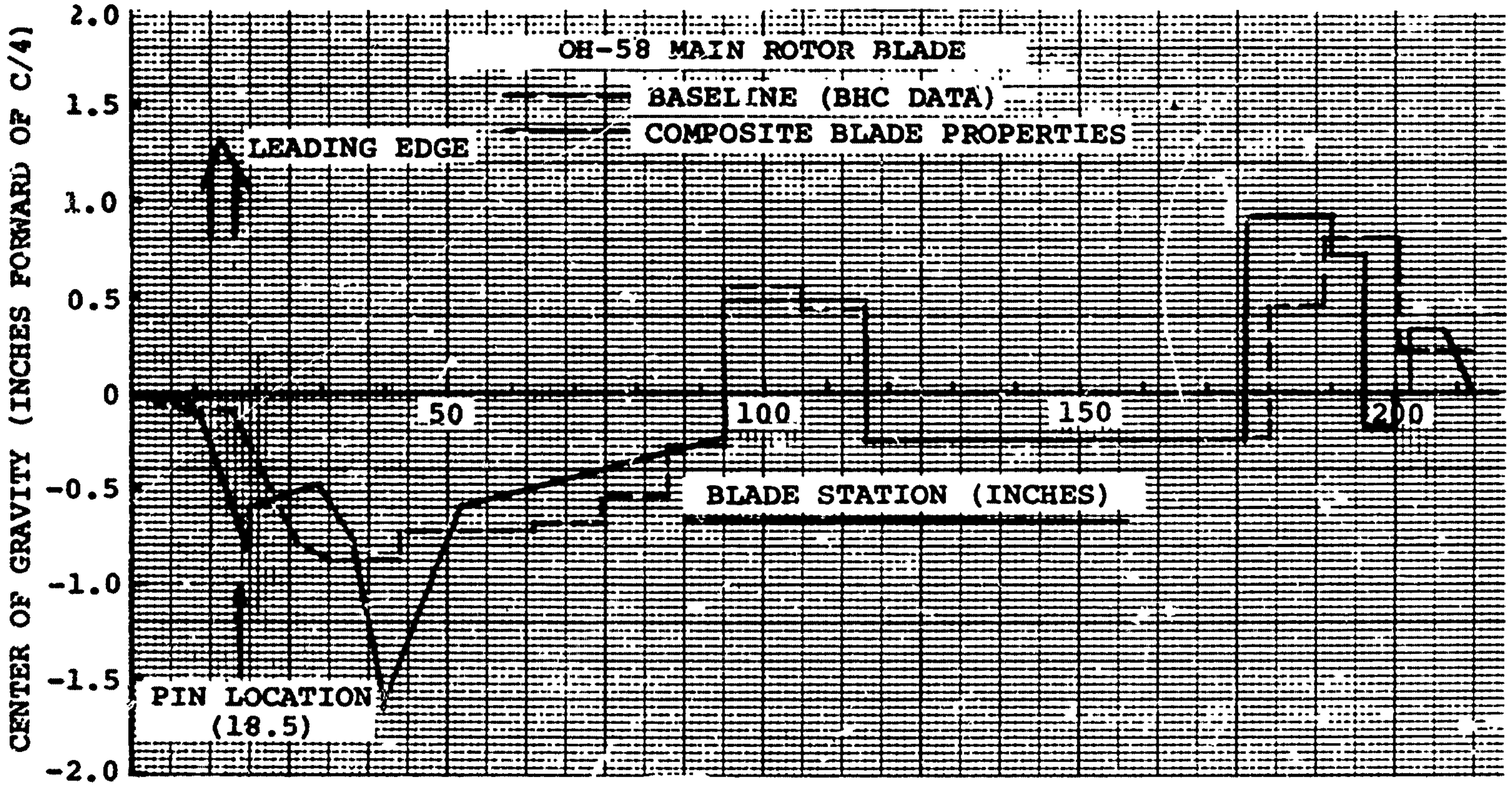

Figure 65. Spanwise Distribution of C.G. Location

OH-58 MAIN ROTOR BLADE

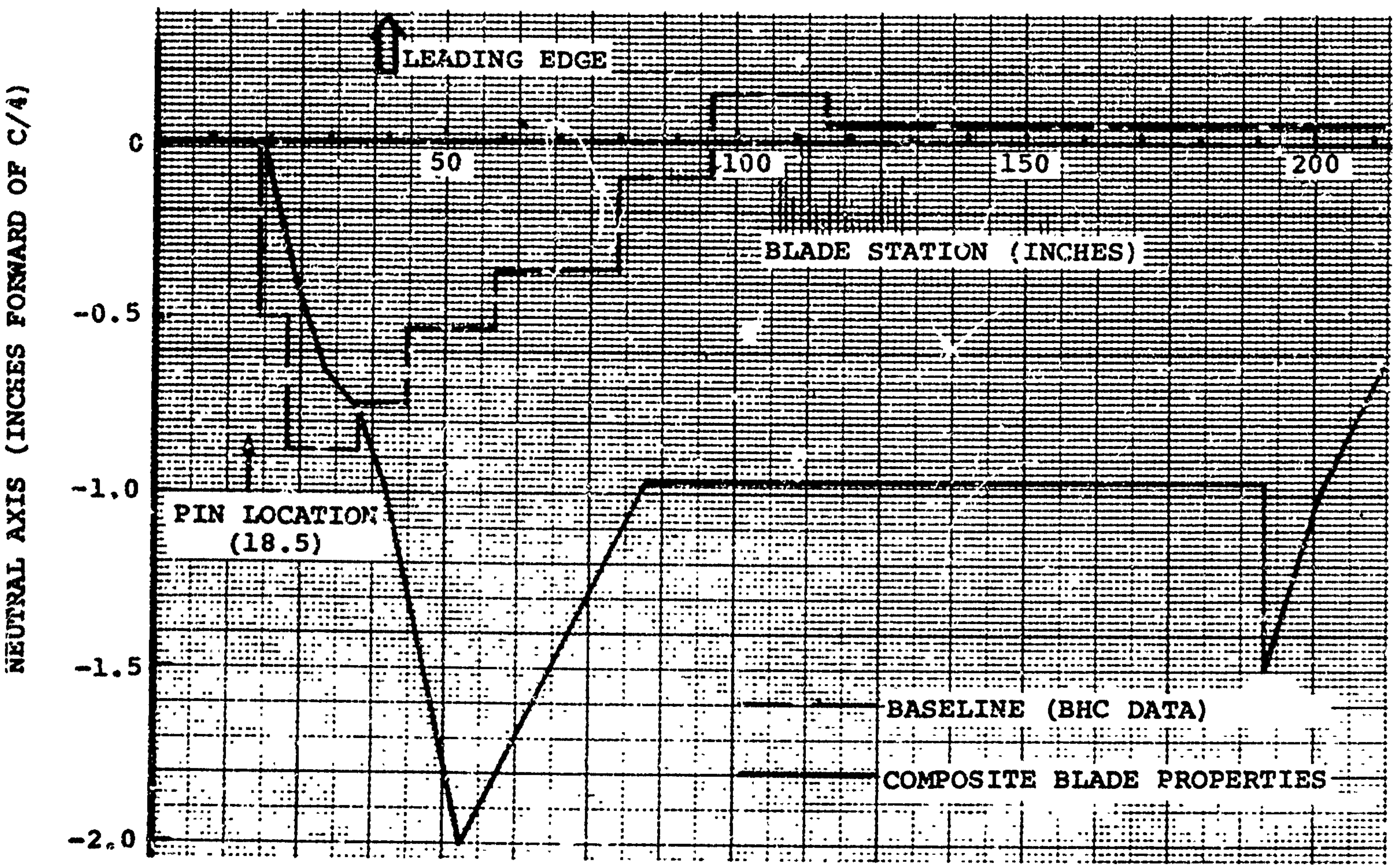

Figure G6. Spanwise Distribution of Neutral Axis

OH-58 MAIN ROTOR BLADE

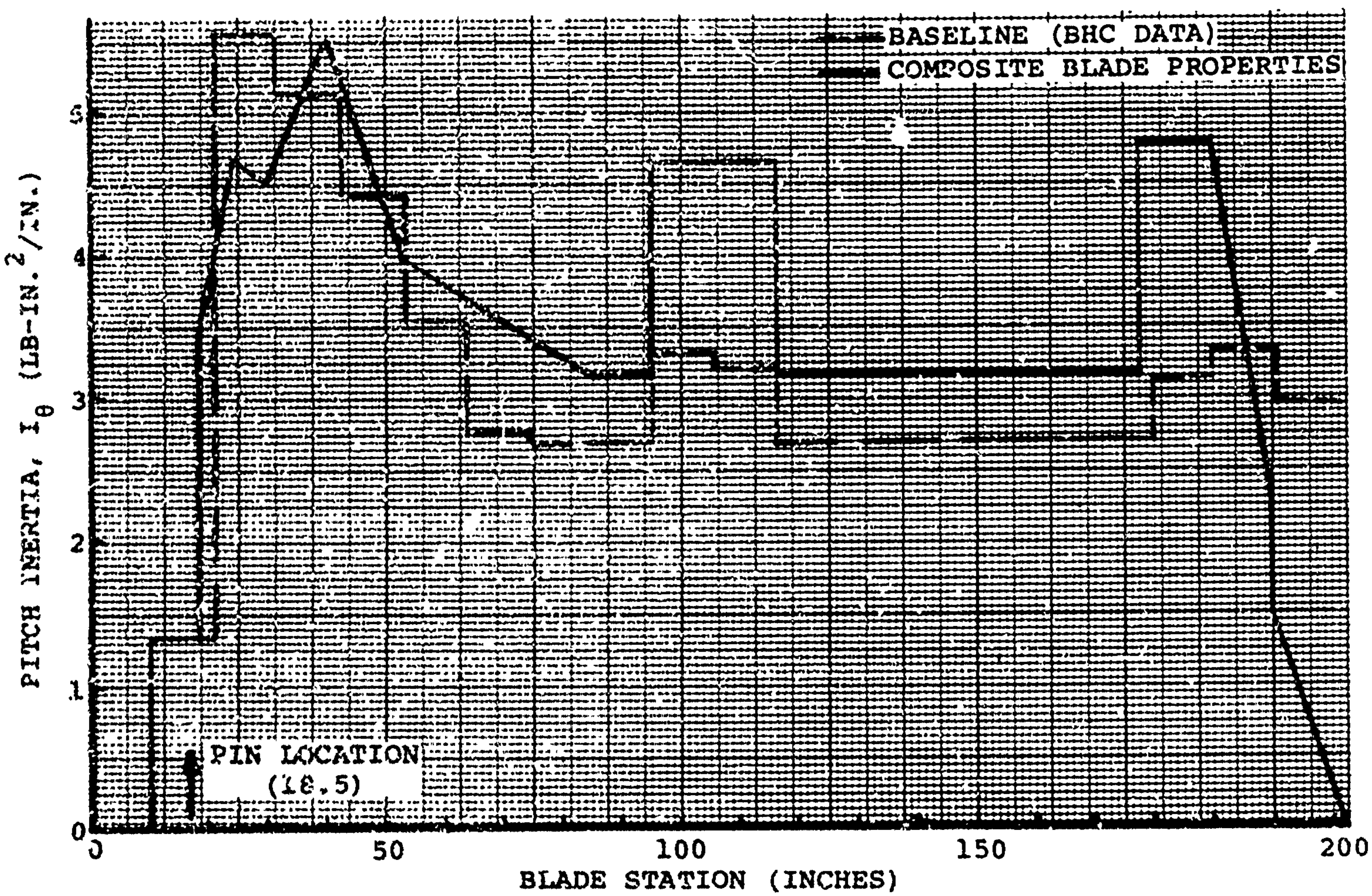

Figure 67. Spanwise Distribution of Pitch Inertia

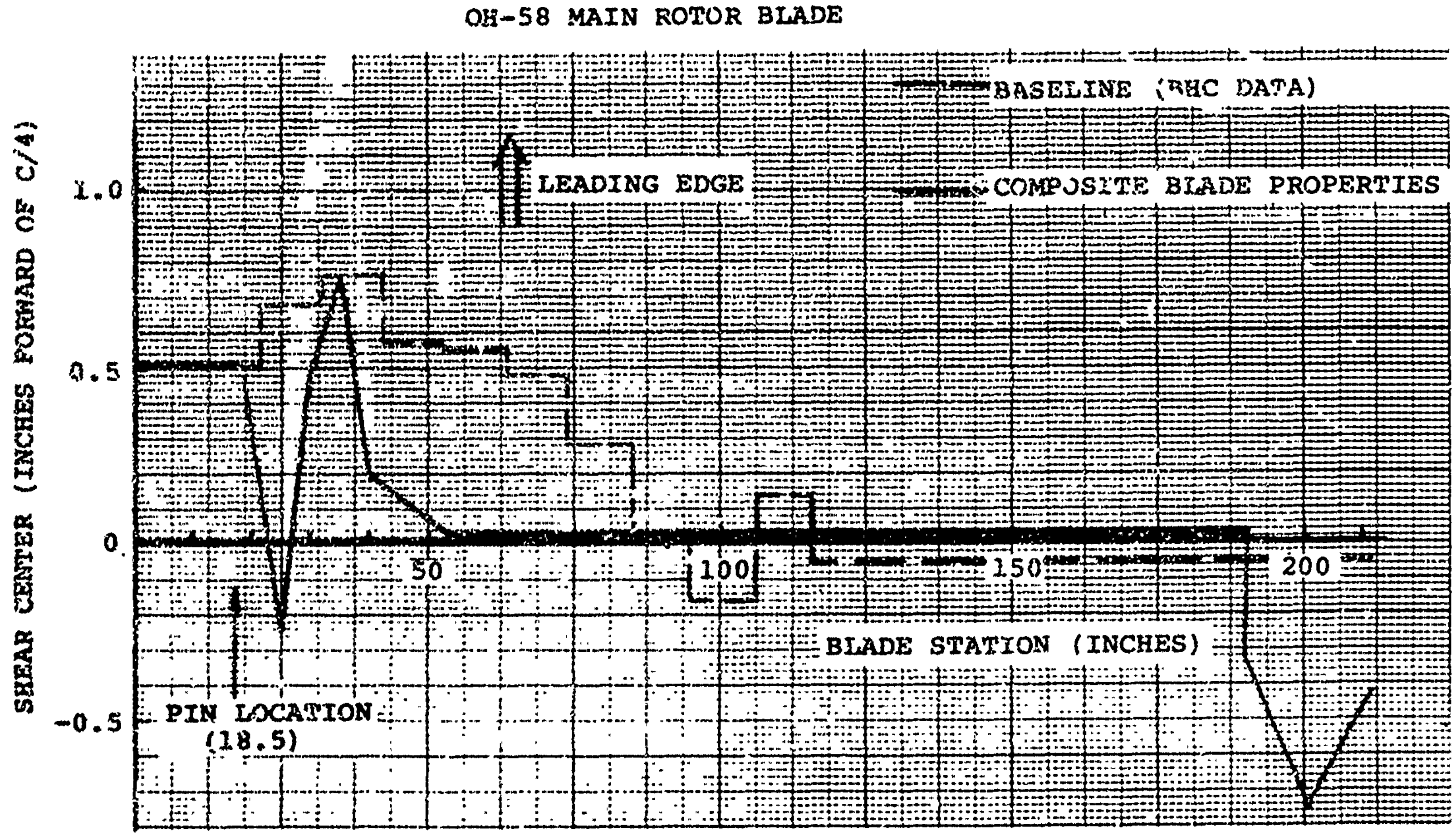

Figure 68. Spanwise Distribution of Shear Center

OH-58 MAIN ROTOR BLADE

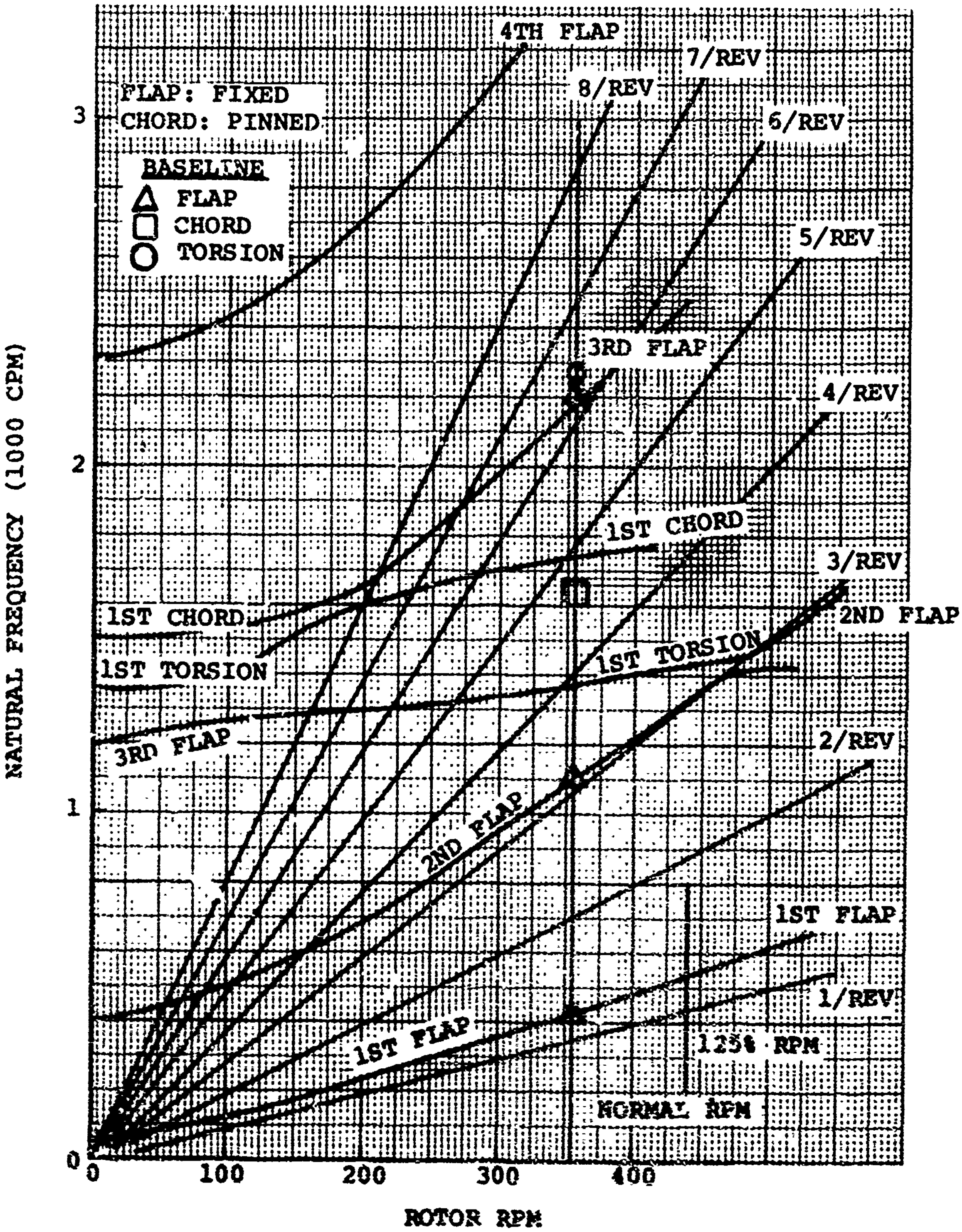

Figure 69. Collective Mode Frequencies

OH-58 MAIN ROTOR BLADE

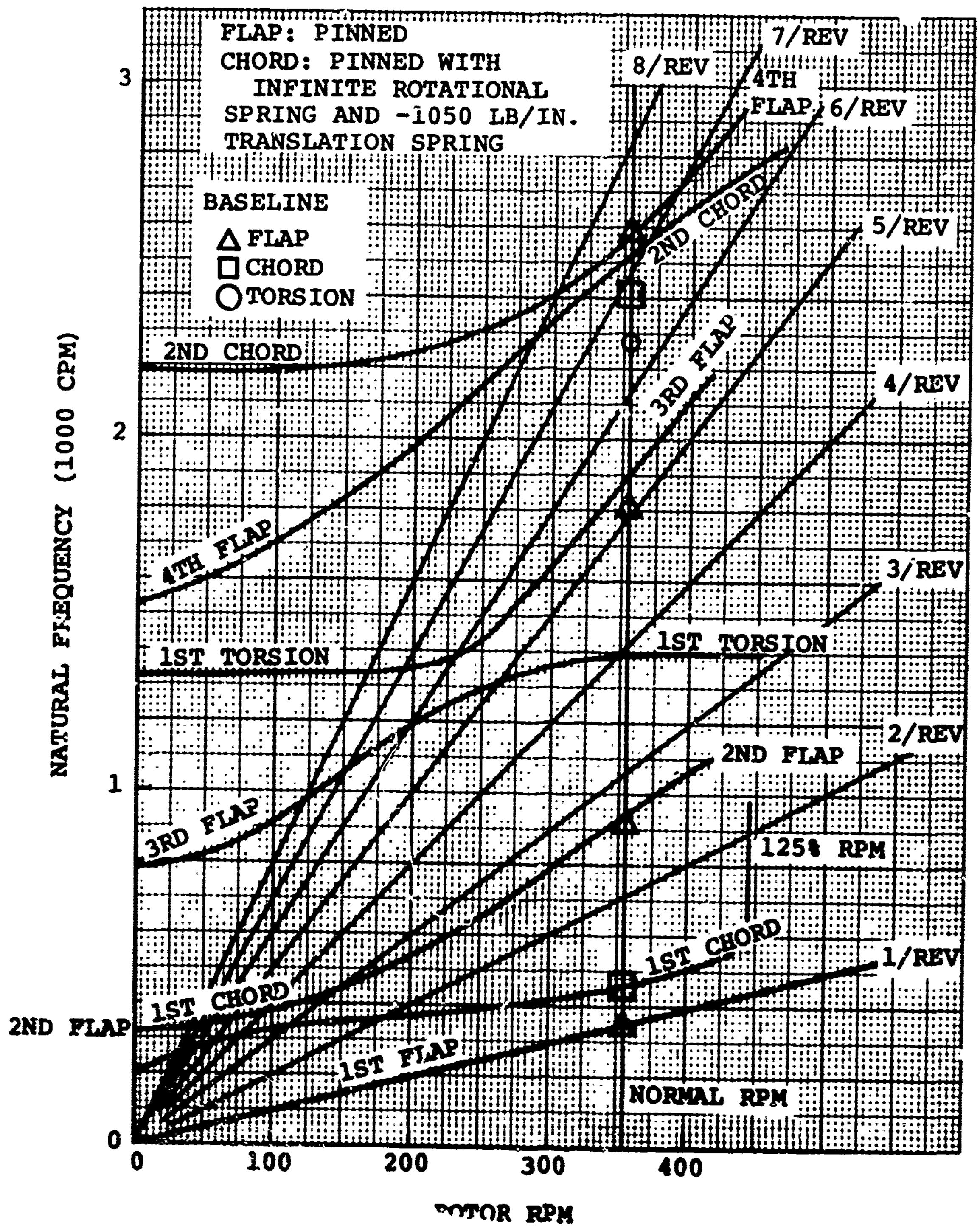

Figure 70. Cyclic Mode Frequencies

range and is close to the first torsional frequency of other Boeing Vertol aircraft: 3.7 per rev for the YUH-61A and 3.5 per rev for the BO-105, a fact which is directly applicable since both 2-bladed and 4-bladed rotors are subject to 4/rev vibratory hub loads as a major contributor to fuselage vibration. It will be seen that this drop in torsional frequency has no detrimental effect on control loads or stability.

The fully coupled mode shapes for the first three-flap, two-chord and first-torsion natural frequencies are presented in Figure 71 for the collective mode and in Figure 72 for the cyclic mode. These mode shapes are nondimensionalized to a 1-inch tip deflection in the flap direction.

4.5.3 Rotor Loads and Control Loads

The spanwise distributions of high-speed level flight loads for flap, chord and torsional moments as predicted by computer program L-02 are presented in Figures 73 through 75. It can be seen that the composite blade provides beneficial reductions in flap bending moments due to reduced flap stiffness and negligible change in dynamic chord loads. The steady chord moments show a marked increase in loads at 25 percent radius for the composite blade. This is due to a significant aft movement of the neutral axis location. However, it is shown in the structural analysis section that this did not impair fatigue life or structural integrity. The increase in steady chord moments does not affect blade dynamic response.

The predicted level flight control loads as indicated by pitch link loads do not differ significantly from the measured flight loads of the baseline OH-58 main rotor.

4.5.4 Hub Loads and Vibration

The vertical and in-plane fixed system hub loads for the composite blade design and the baseline metal blade are shown in Figure 76. These high-speed level flight hub forces are a measure of the effect on airframe vibration of the composite rotor blade. The major contributors to airframe vibrations will be the two and four per rev components of hub forces in the fixed system. It is evident from the figure that there are small increases in the in-plane vibratory loads. However, the principal contributor to hub vibration is the 2/rev vertical force, which is unchanged. Consequently, it is concluded that the net result of the change in fixed system hub forces due to the change in blade physical properties is that there will be little or no change in the fuselage vibration characteristics.

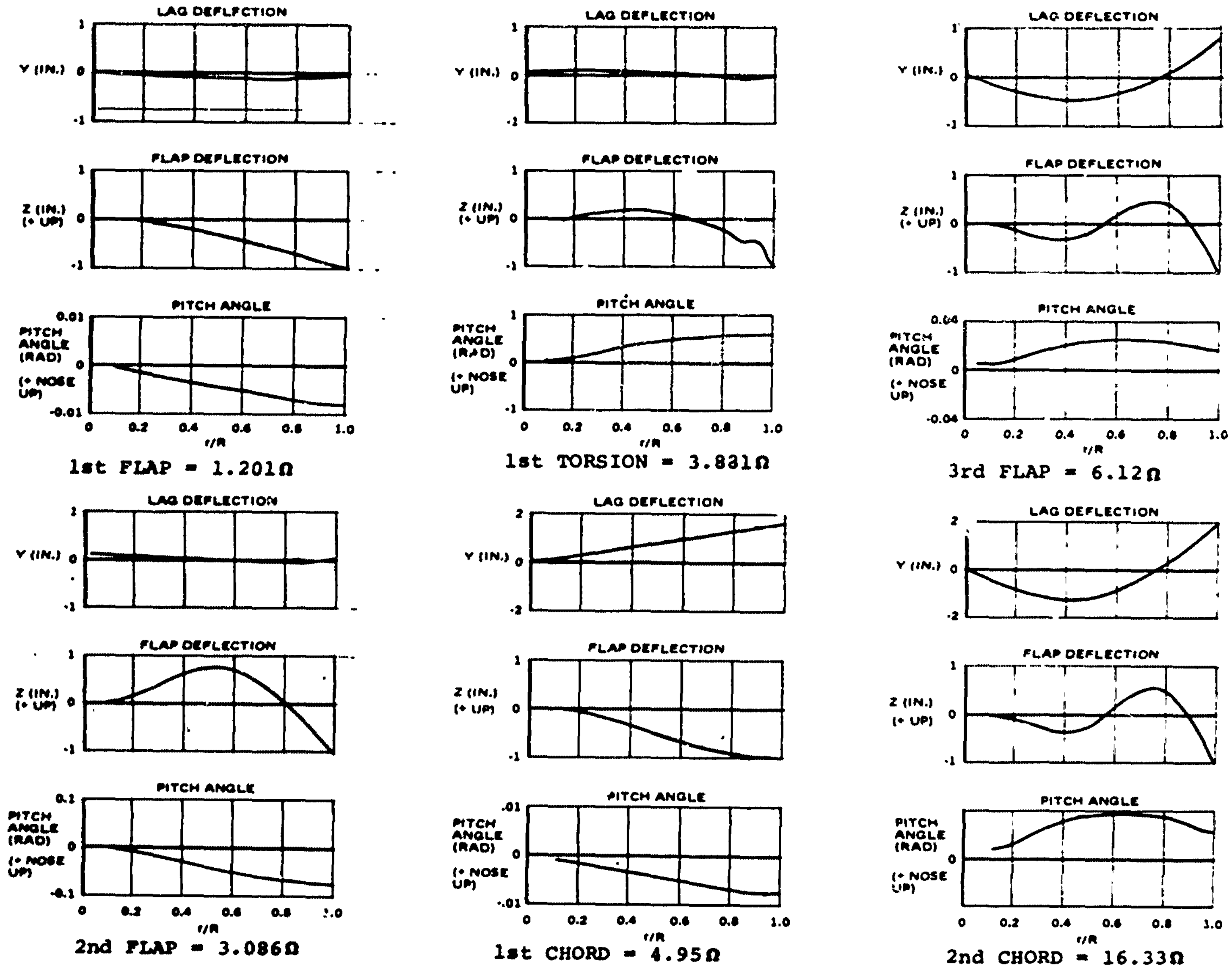

Figure 71. OH-58 Main Rotor Blade Collective Mode Shapes at 354 rpm

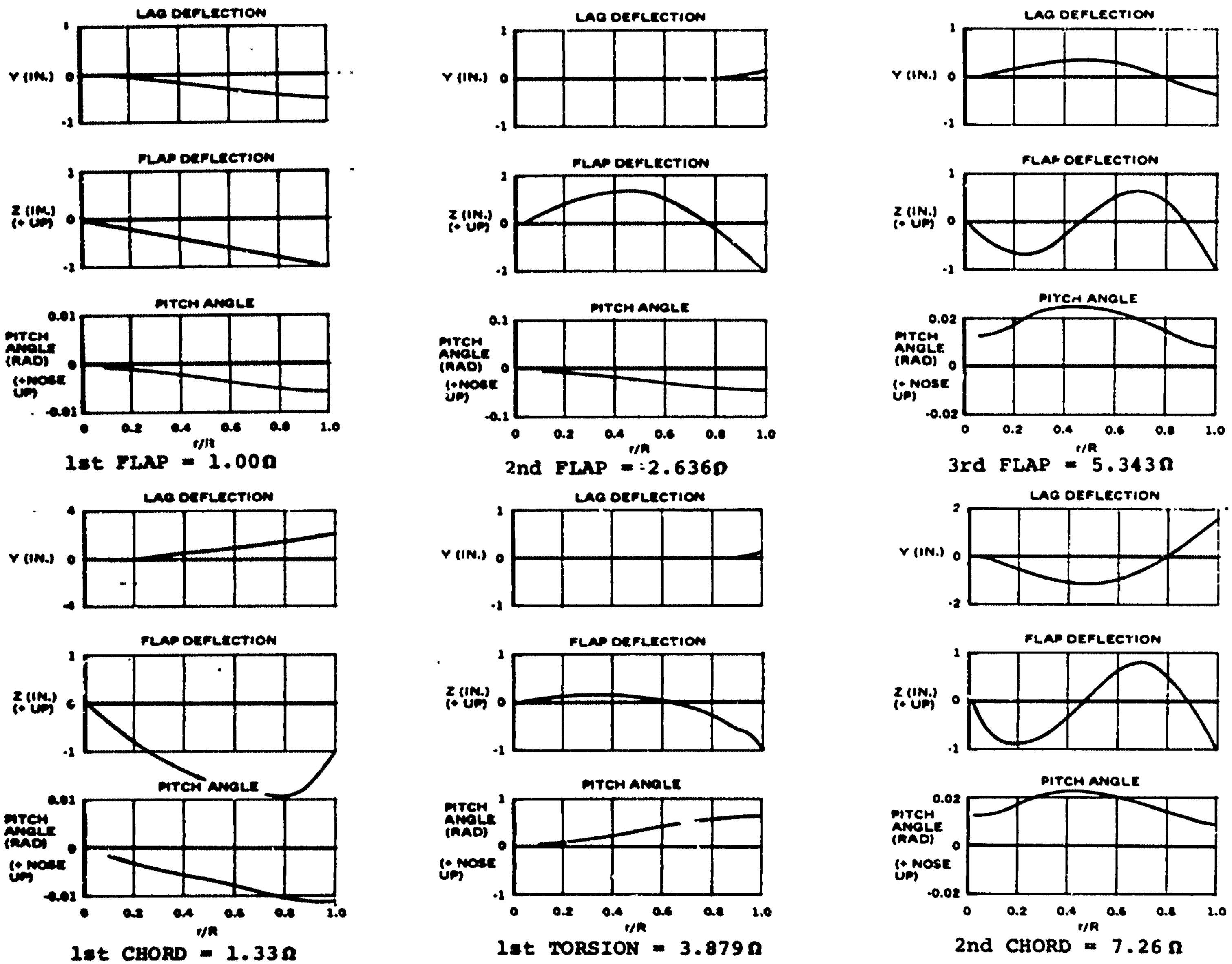

Figure 72. OH-58 Main Rotor Blade Cyclic Mode Shape at 354 rpm

L-02

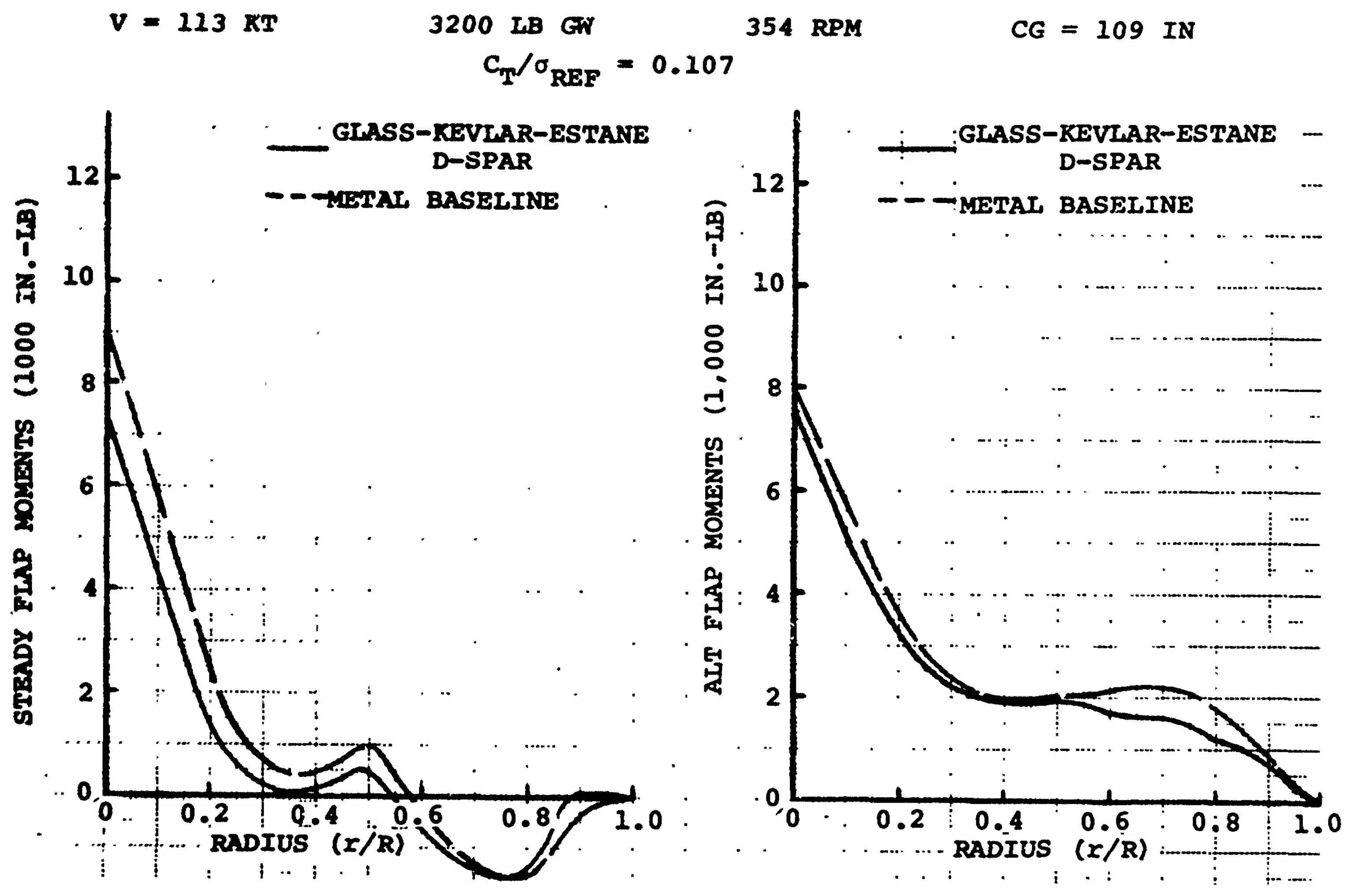

Figure 73. OH-58 Rotor Flap Bending Moments

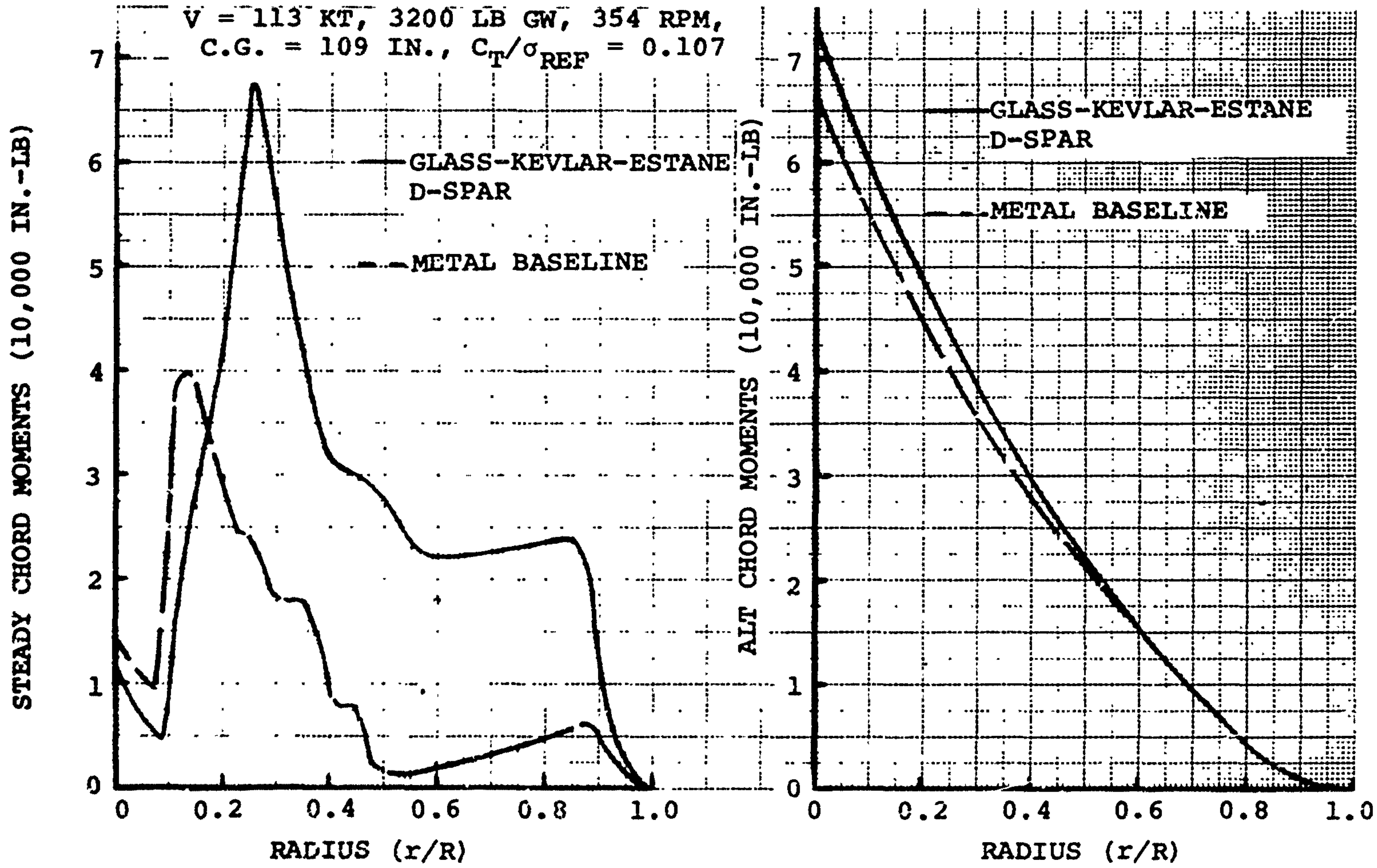

Figure 74. OH-58 Rotor Chord Bending Moments

V = 113 KT, 3200 LB GW, 354 RPM, C.G. = 109 IN., C_T/σ_{REF} = 0.107

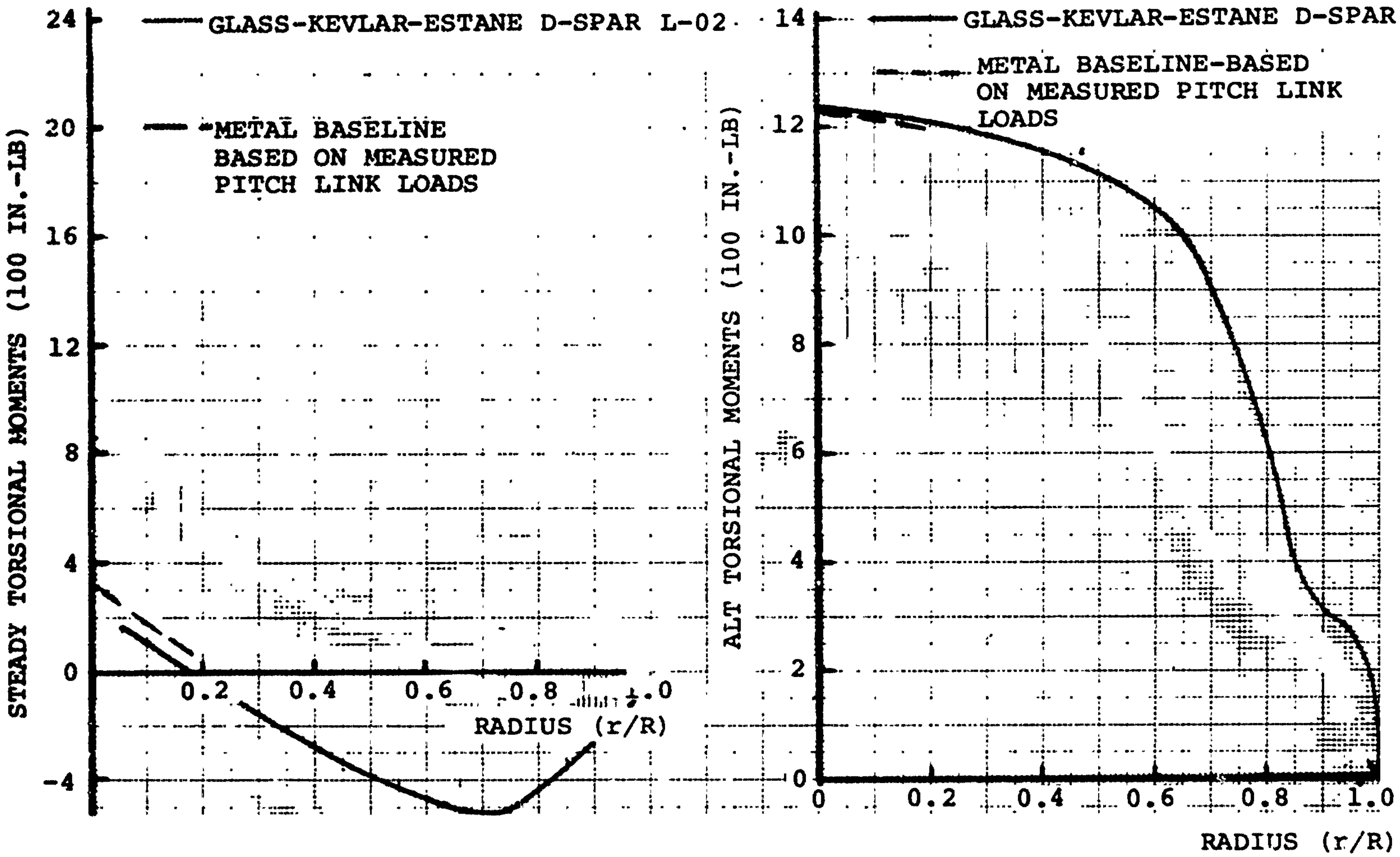

Figure 75. OH-58 Rotor Torsional Moments

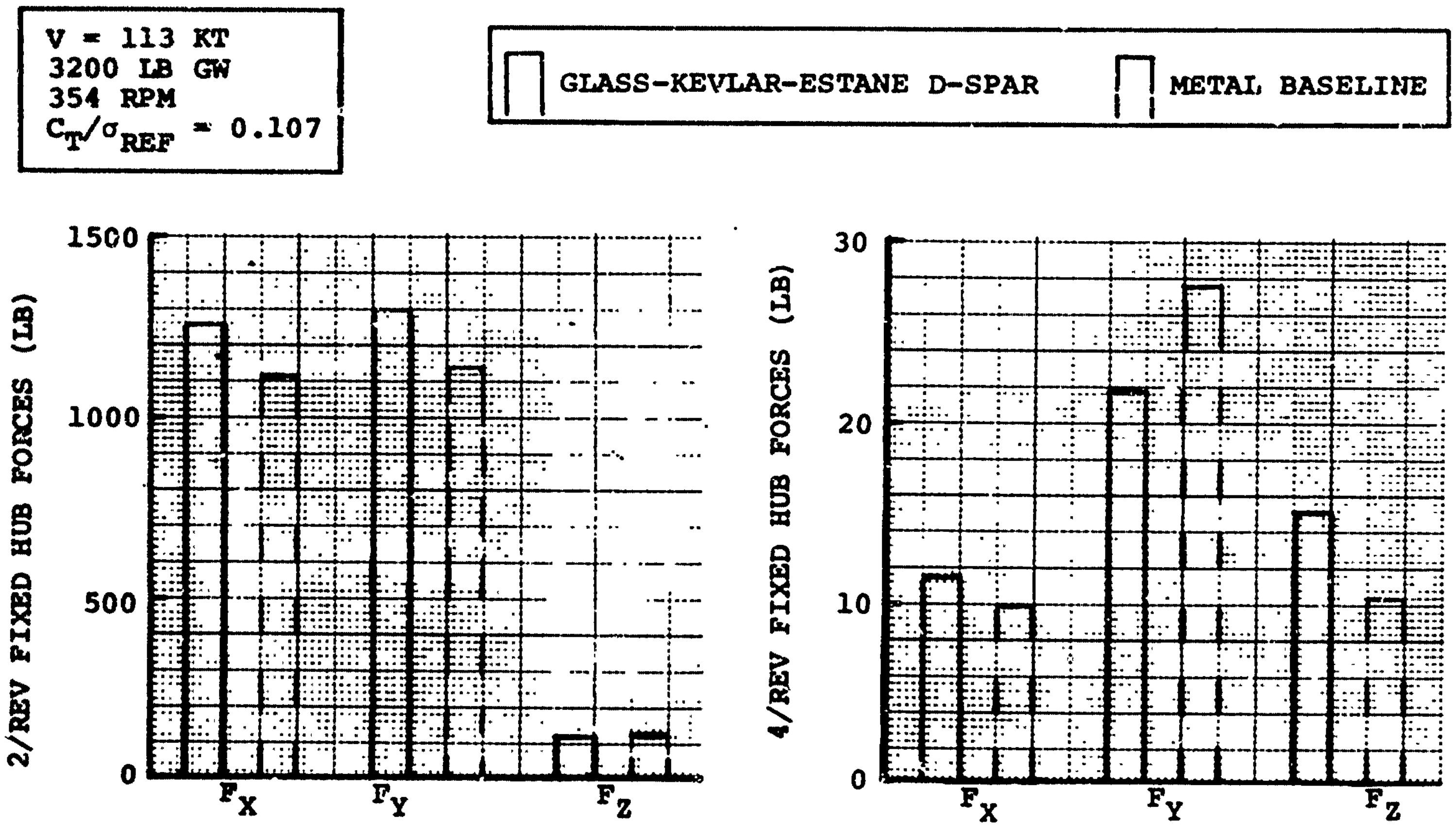

Figure 76. OH-58 Vibration as Measured by Hub Loads

4.5.5 Aeromechanical Stability

The stability of the proposed composite rotor blade configuration consists of two aspects. These are the air resonance stability analysis and classical flutter analysis. The assurance of aeroelastic stability is based on the comparison of the dynamic characteristics of the composite blade to the dynamic characteristics of the existing OH-58 metal blade, which is known to be stable. A classical flutter analysis was performed using the L-01 computer program.

As described previously, the proposed composite blade has essentially the same flap and chord bending dynamic characteristics as the existing OH-58 metal rotor blades. Only the torsional natural frequency is significantly different. However, it has been shown that this has little influence on aeromechanical stability other than flutter. This fact was demonstrated experimentally on a Froude scaled model of YUH-61A in the Boeing Vertol wind tunnel, as documented in Reference 1. The rotor blade fundamental torsional natural frequency was lowered from 4.8 per rev to 4.0 per rev at normal operating rotor speed with no perceivable change in air resonance stability in either hover or forward flight.

Since the torsional dynamic characteristics are not important in aeroelastic stability, and since the flap and chord dynamic responses are essentially the same as the current OH-58 main rotor blades, the stability of the proposed composite rotor configuration will be equivalent to the existing OH-58 rotor system. This is true because there will be no modifications to the OH-58 control system, drive system or airframe. It can be concluded, therefore, that there will be no degradation in the stability margins of the OH-58 main rotor system due to the composite rotor blade design.

A classical flutter analysis was performed using the L-01 computer program to insure that the rotor was free from flutter up to and including 509 RPM (1.15 x $N_{D.L.}$). Throughout the range of flight conditions investigated, the rotor indicated no evidence of the onset of flutter. The critical damping ratio for the fully coupled bending modes was 3 percent or greater in all cases, indicating satisfactory margins for stability.

4.6 AIRCRAFT PERFORMANCE

This subsection presents estimates of the hover and forward performance of the OH-58 helicopter with the improved composite main rotor blades installed. In the absence of complete data on the aircraft, the performance was calculated by first estimating the performance of the existing OH-58 using the

Government-supplied 0012 data and assuming the following losses:

(1)	Transmission Efficiency	97%
(2)	Download in Hover	2% of GW
(3)	Accessory Horsepower Loss	11 HP

The tail rotor power losses were obtained from the forward flight trim and performance analysis program Y-92 and C-81. Both programs predicted essentially the same fraction of main rotor power absorbed. The fraction varies between 8% in hover to 1.5% at high speed. The next step was to collapse the published performance data for the existing OH-58. It was found that the data collapsed on an SHP/σ vs GW/σ basis, where σ is the relative density. This shows the absence of substantial Mach number effects on the performance.

To provide a consistent basis of comparison with the published performance level presented in the OH-58 detail specification, the analysis utilized to predict the performance of the OH-58 with the proposed system was used to predict the basic OH-58 performance. At each value of GW/σ and airspeed the ratio of calculated SHP/σ to published SHP/σ was computed. These ratios, or correction factors, were then applied to the values of required power calculated for the OH-58 with the improved blades installed.

4.6.1 Hover and Vertical Climb Performance

The hover performance for the OH-58 with improved composite blades is presented in Figure 77 in the form of a plot of weight coefficient, C_W, against power coefficient, C_P. Also shown is the data for the existing aircraft.

The variation of hover ceiling with gross weight for the OH-58 with the improved composite blades is compared to that of the existing aircraf in Figure 78. The improved blades are estimated to increase the ceiling by approximately 1000 feet at all gross weights.

The vertical rate of climb performance, for different gross weights and altitudes at S.L. standard temperature and 95°F is presented in Figures 79 and 80, respectively. Rate of climb is most improved at the high gross weights where the power reductions were sought.

4.6.2 Forward Flight Performance

Estimated performance for the improved OH-58 is presented (in nondimensional form) in Figure 81. The aircraft performance in terms of shaft horsepower versus true airspeed is presented in Figures 82, 84, 86, 88, and 90. The corresponding performance plots for the existing OH-58 were taken from the BHC specification document and are reproduced here for comparison as Figures 83, 85, 87, 89, and 91.

Maximum rate of climb performance at intermediate power setting for standard day and 95°F is presented in Figures 92 and 93. Maximum endurance performance is shown in Figure 94. Figure 95 presents the estimated autorotation characteristics with the improved composite rotor on the aircraft and compares it with those of the existing OH-58. The mission profiles for 2000 ft/95°F and 4000 ft/95°F are shown in Figures 96 and 97 respectively.

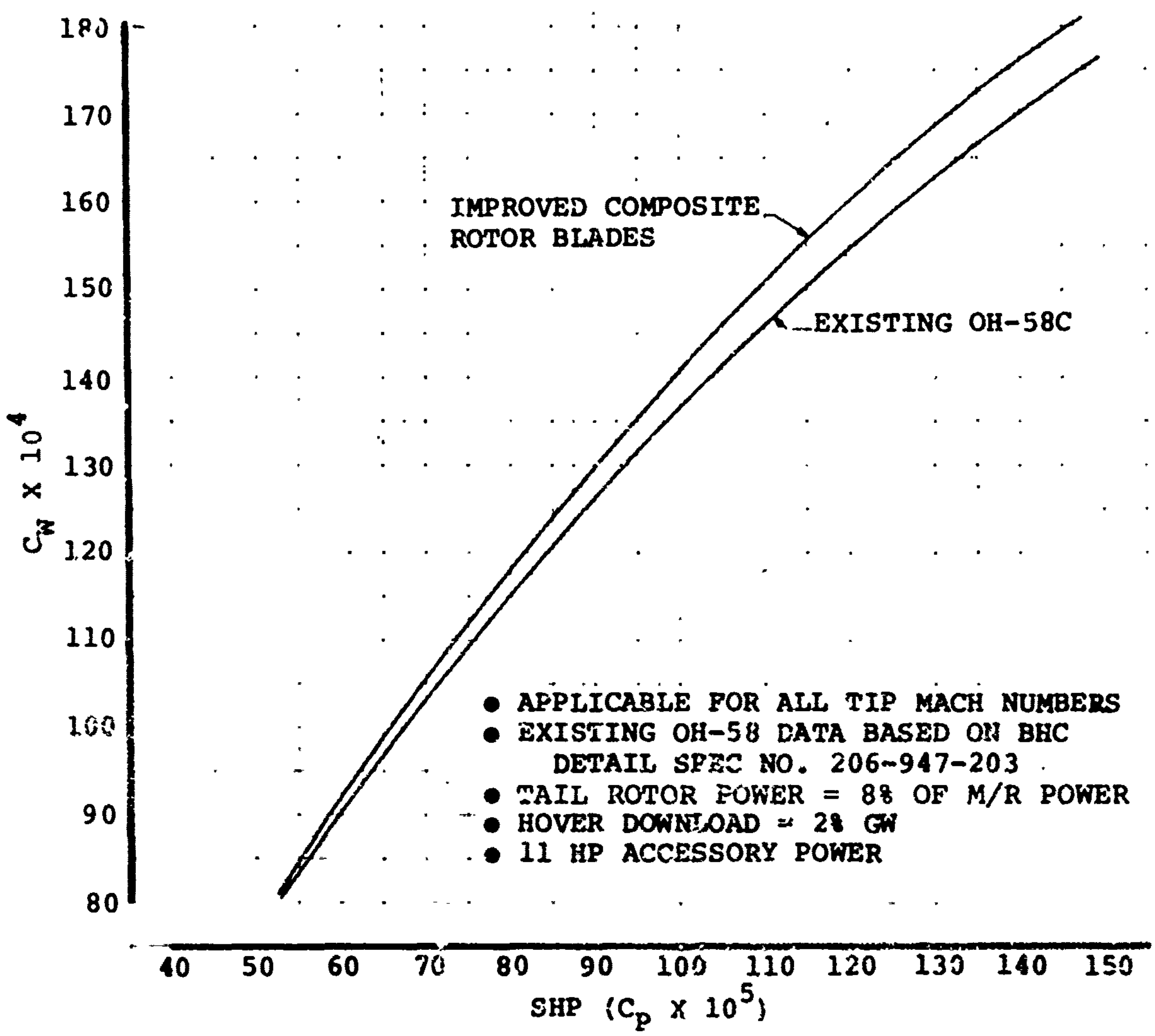

Figure 77. Nondimensional Hover Power Required Out of Ground Effect

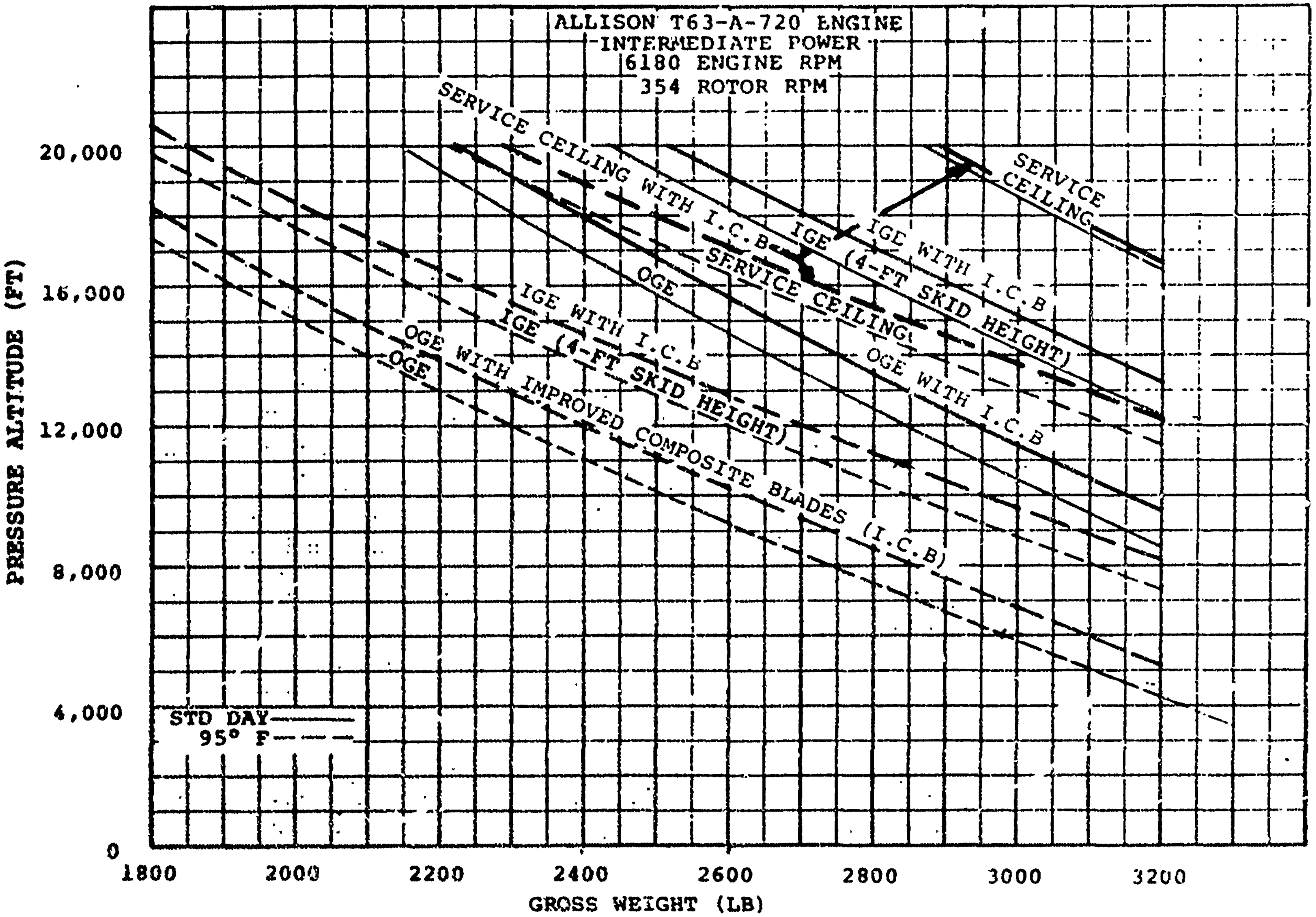

Figure 78. Ceilings

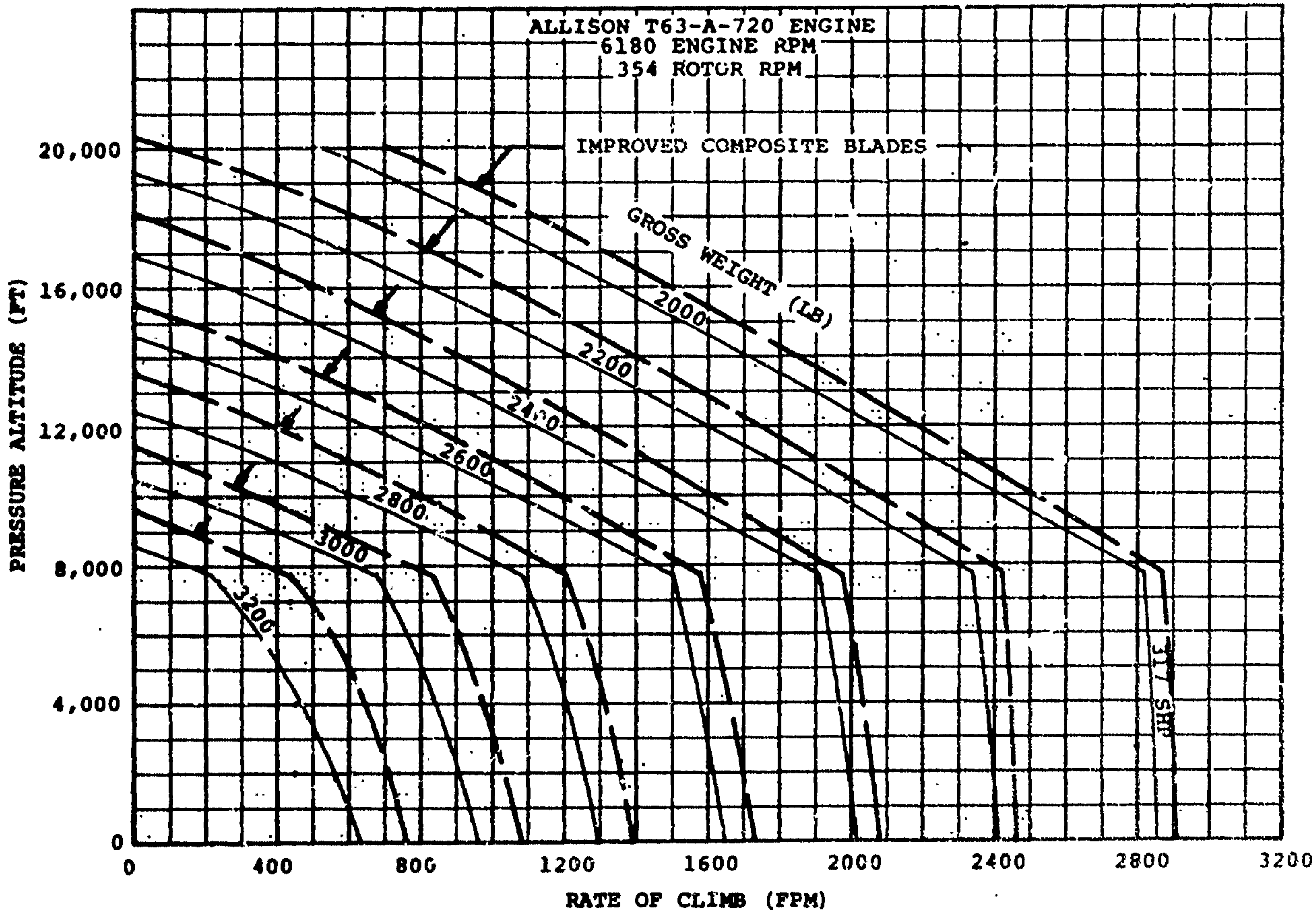

Figure 79. Vertical Rate of Climb, Standard Day

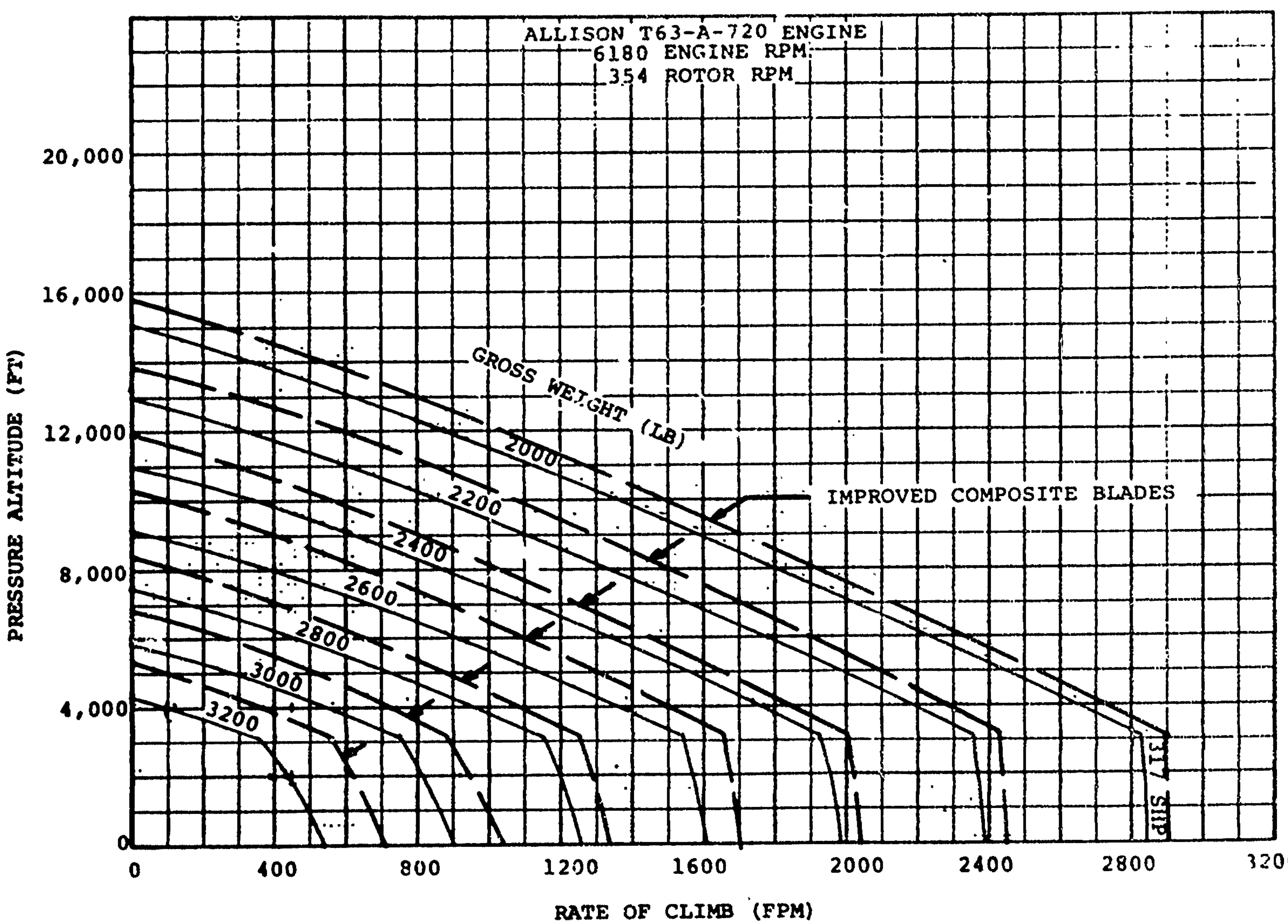

Figure 80. Vertical Rate of Climb, 95°F

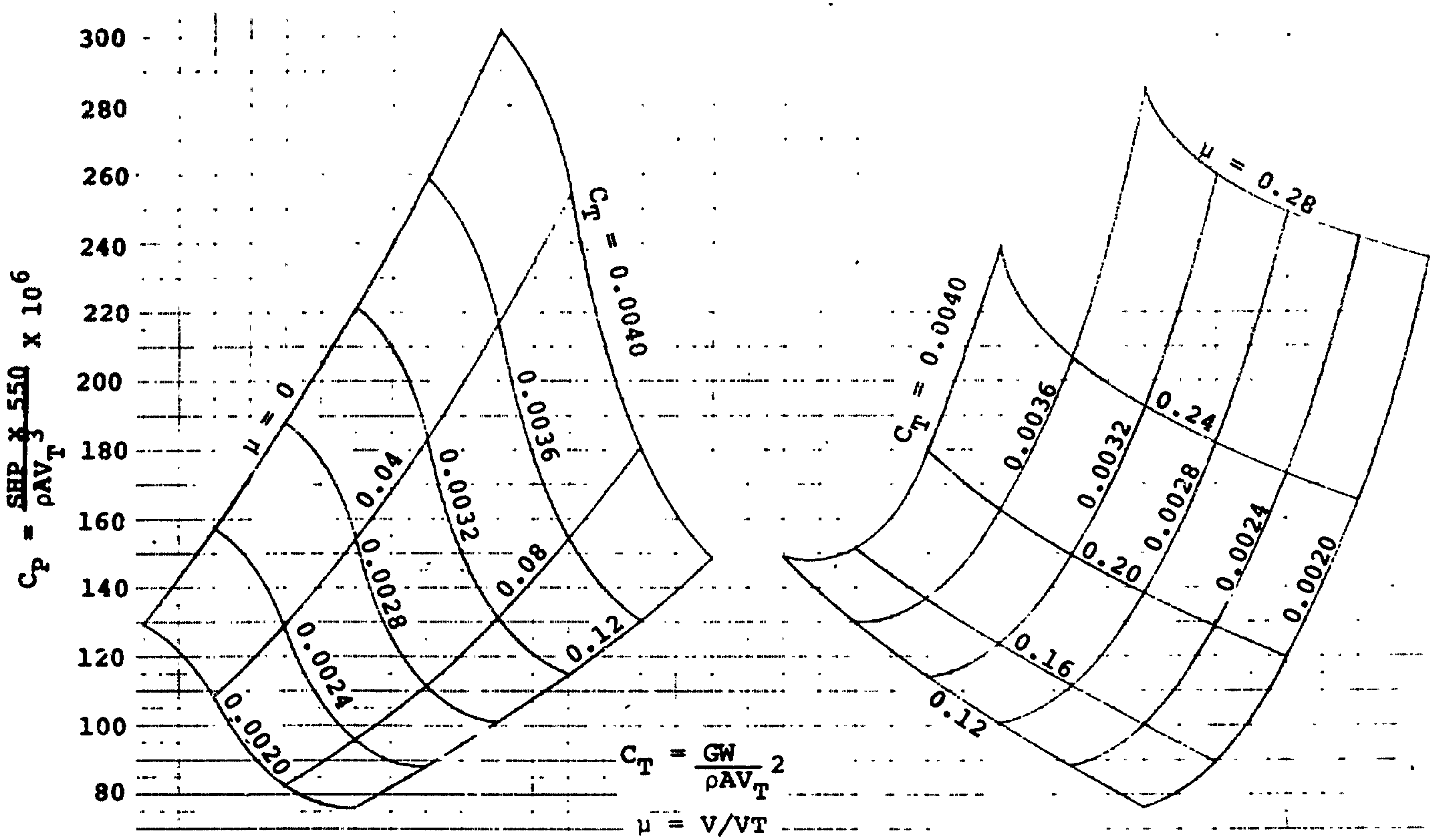

Figure 81. OH-58C/A Nondimensionalized Power Required Improved Composite Blades

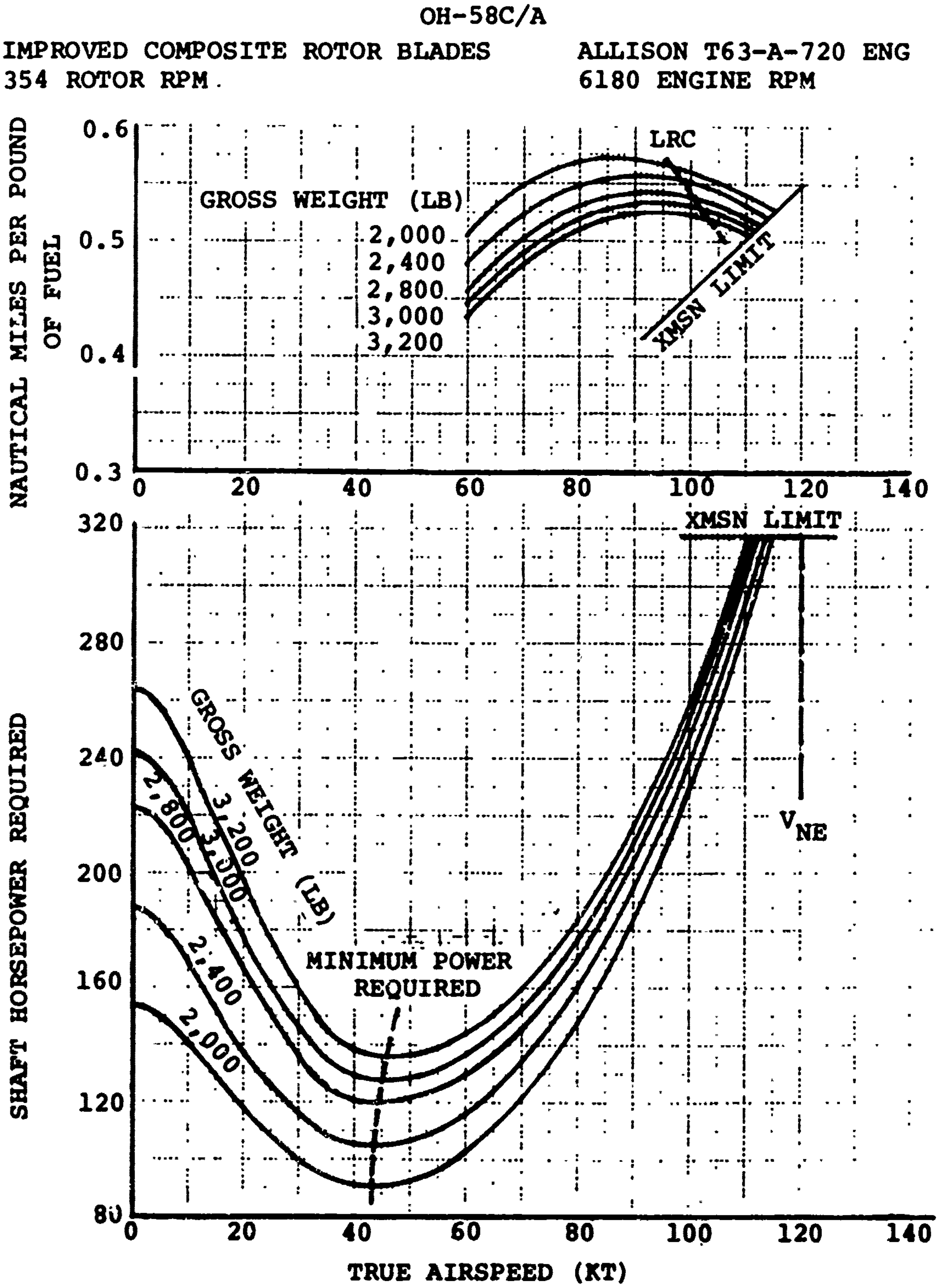

Figure 82. Level Flight Performance, Sea-Level, Standard Day Composite Blades

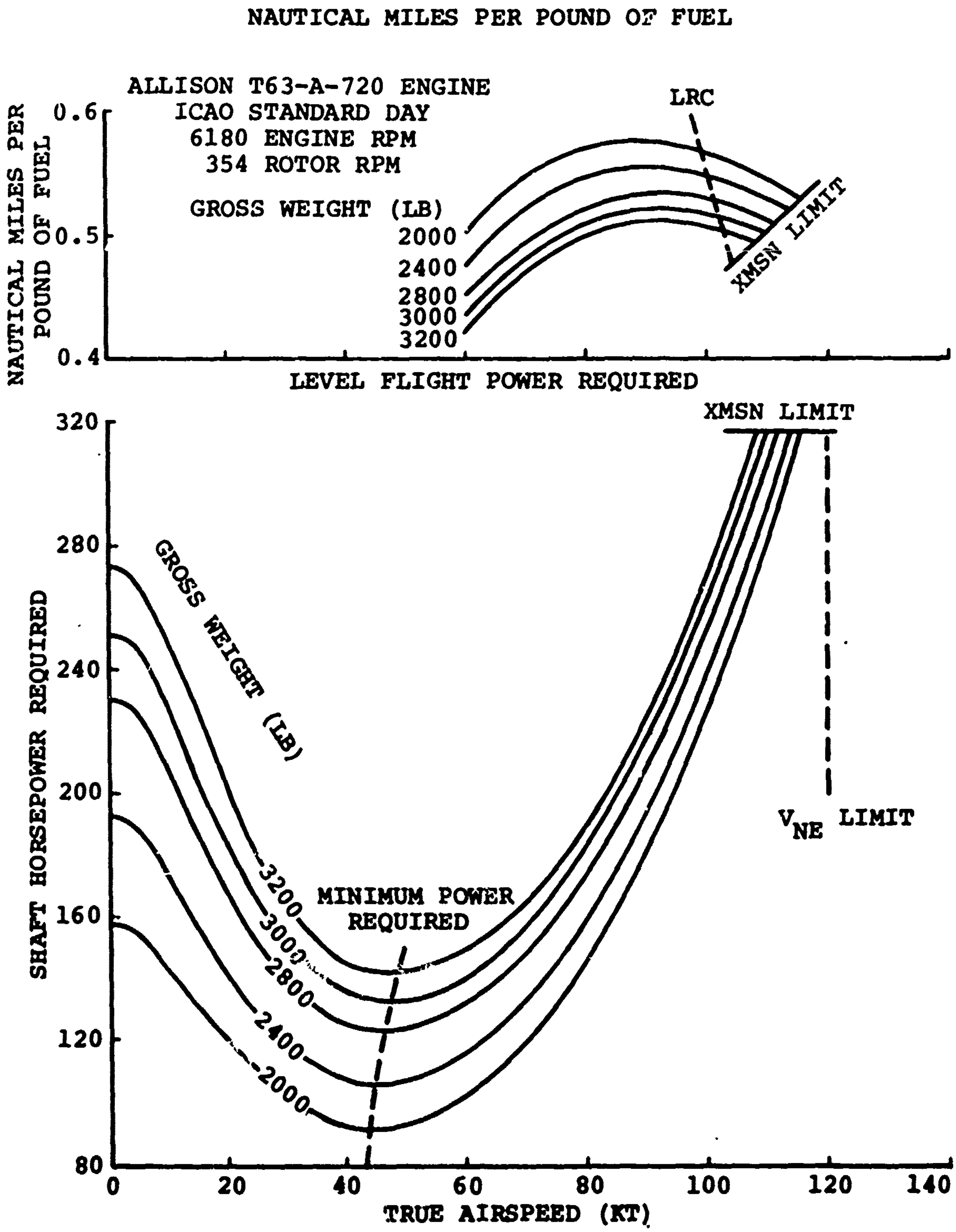

Figure 83. Level Flight Performance, Sea Level, Standard Day-Baseline

OH-58C/A LEVEL FLIGHT PERFORMANCE

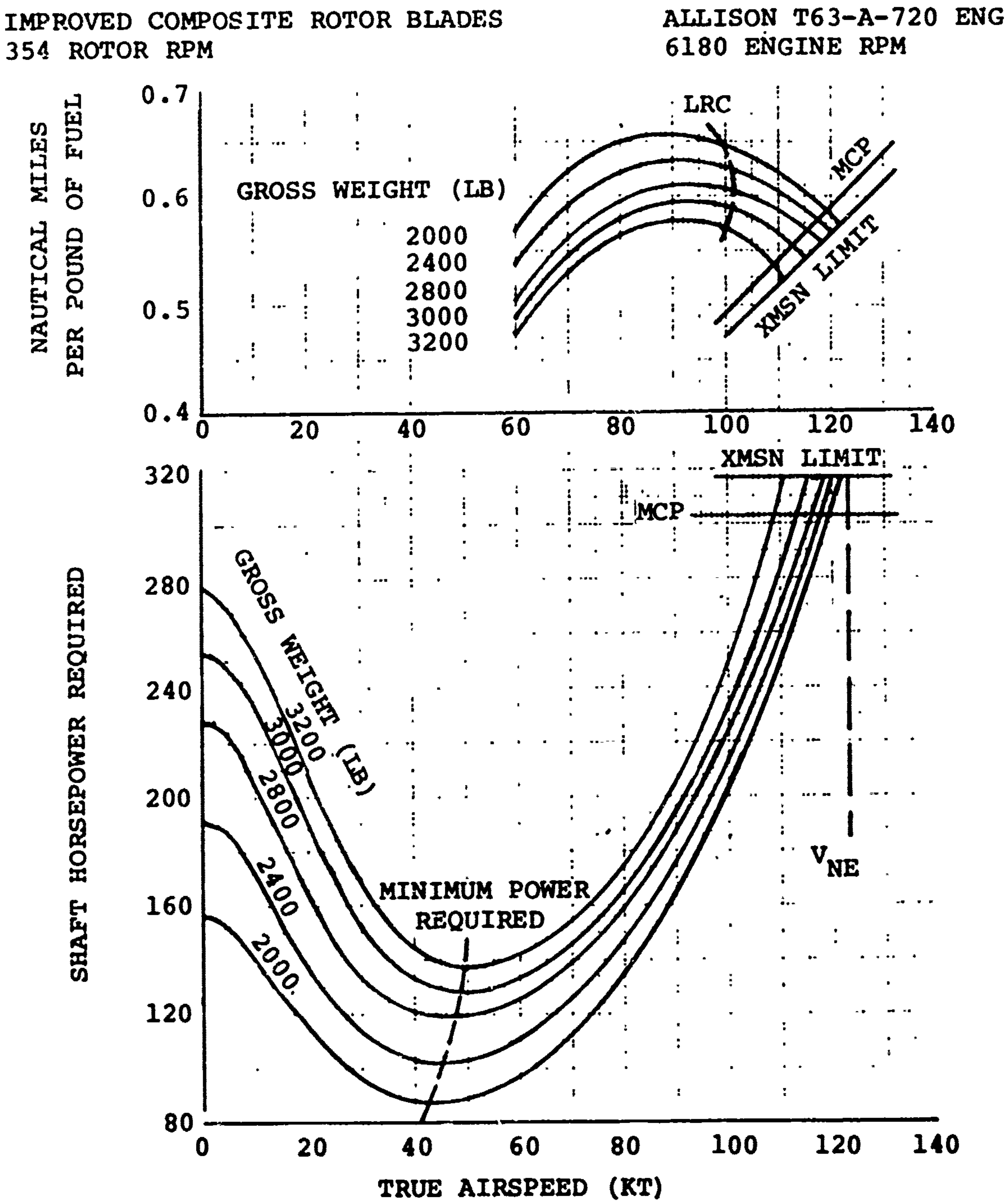

Figure 84. Level Flight Performance, 5000 Ft, Standard Day Composite Blades

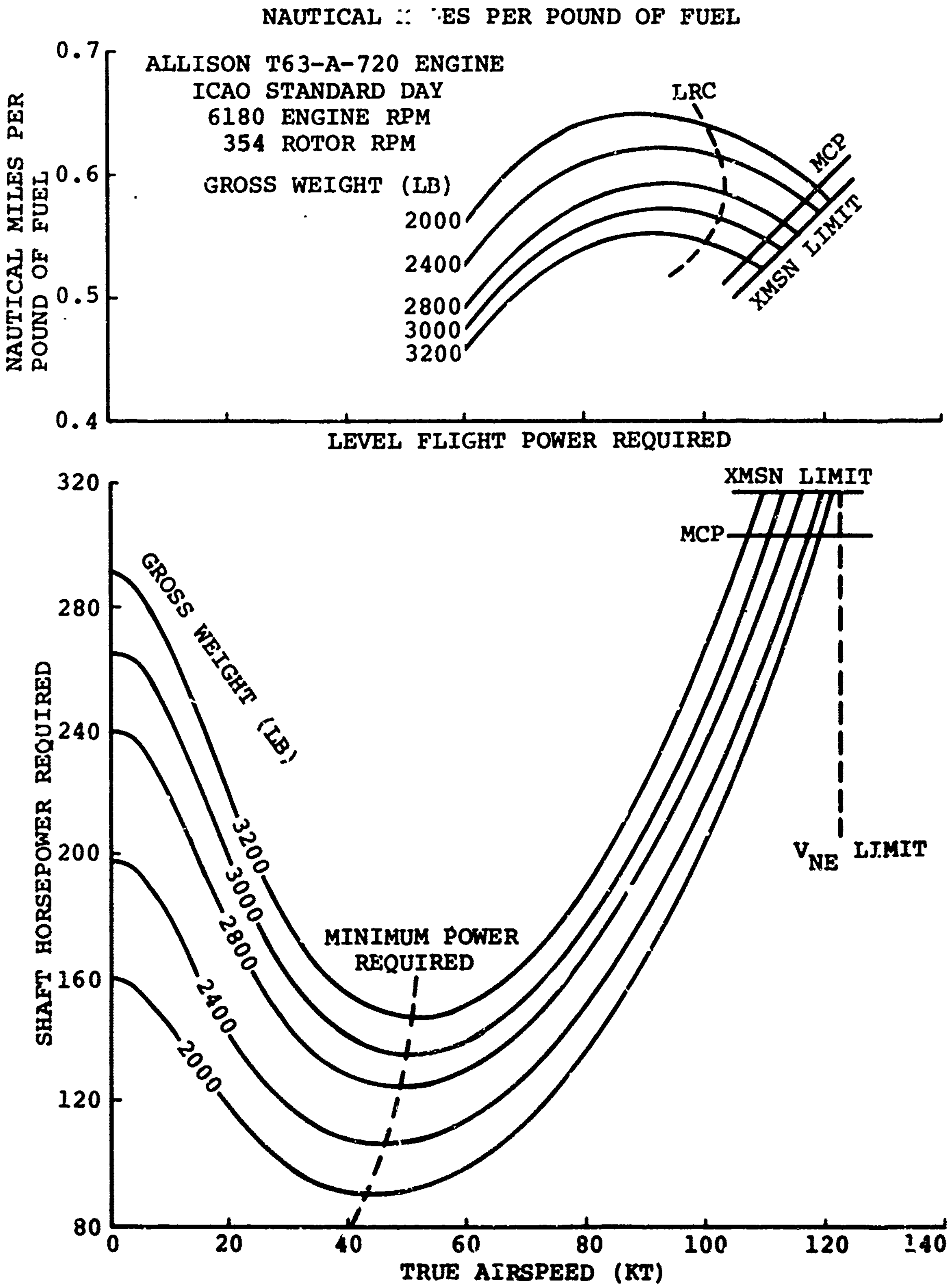

Figure 85. Level Flight Performance, 5000 Feet Standard Day - Baseline

OH-58C/A
LEVEL FLIGHT PERFORMANCE

IMPROVED COMPOSITE ROTOR BLADES
354 ROTOR RPM

ALLISON T63-A-720 ENG
6180 ENGINE RPM

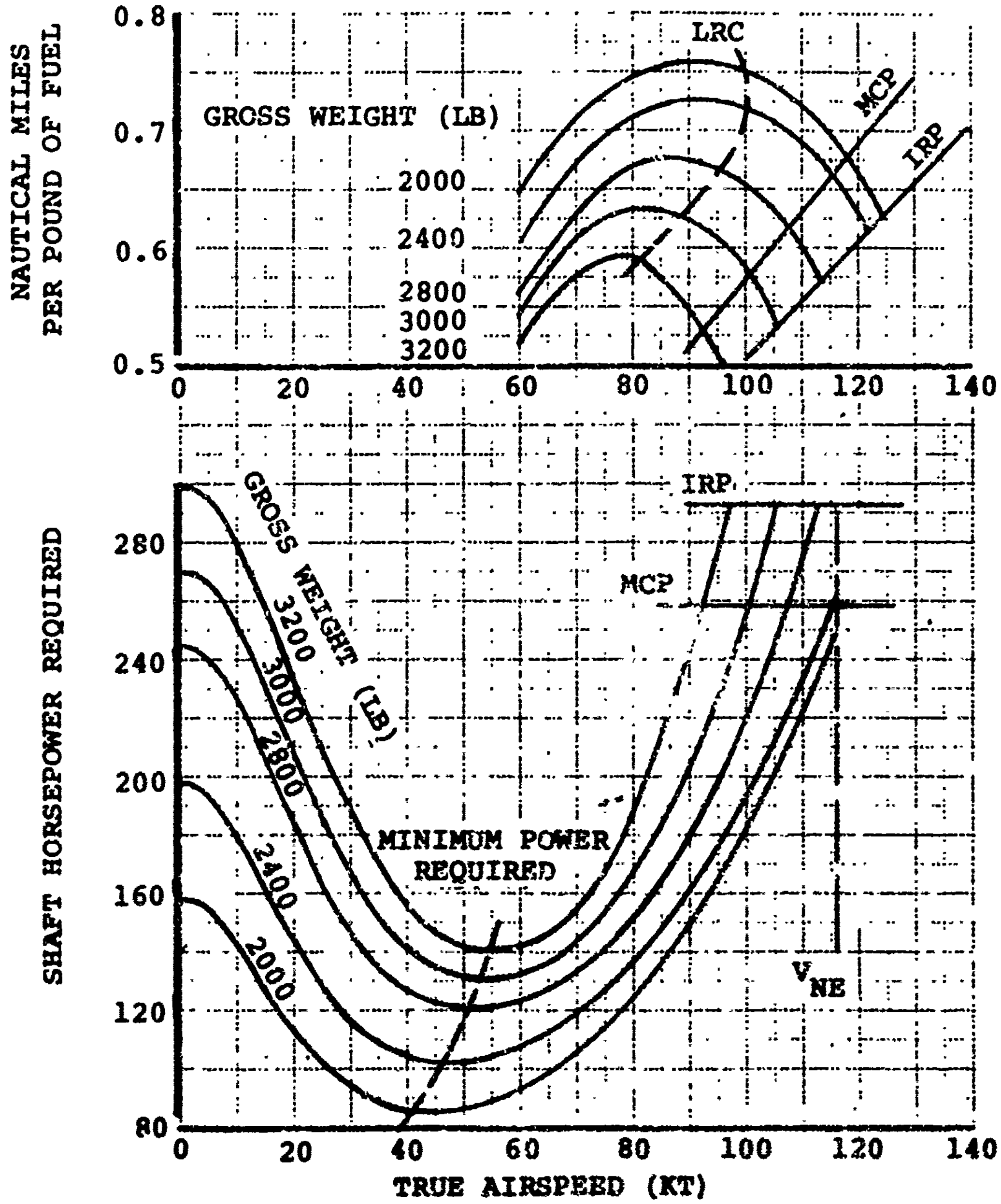

Figure . Level Flight Performance, 10000 Ft, Standard Day Composite Blades

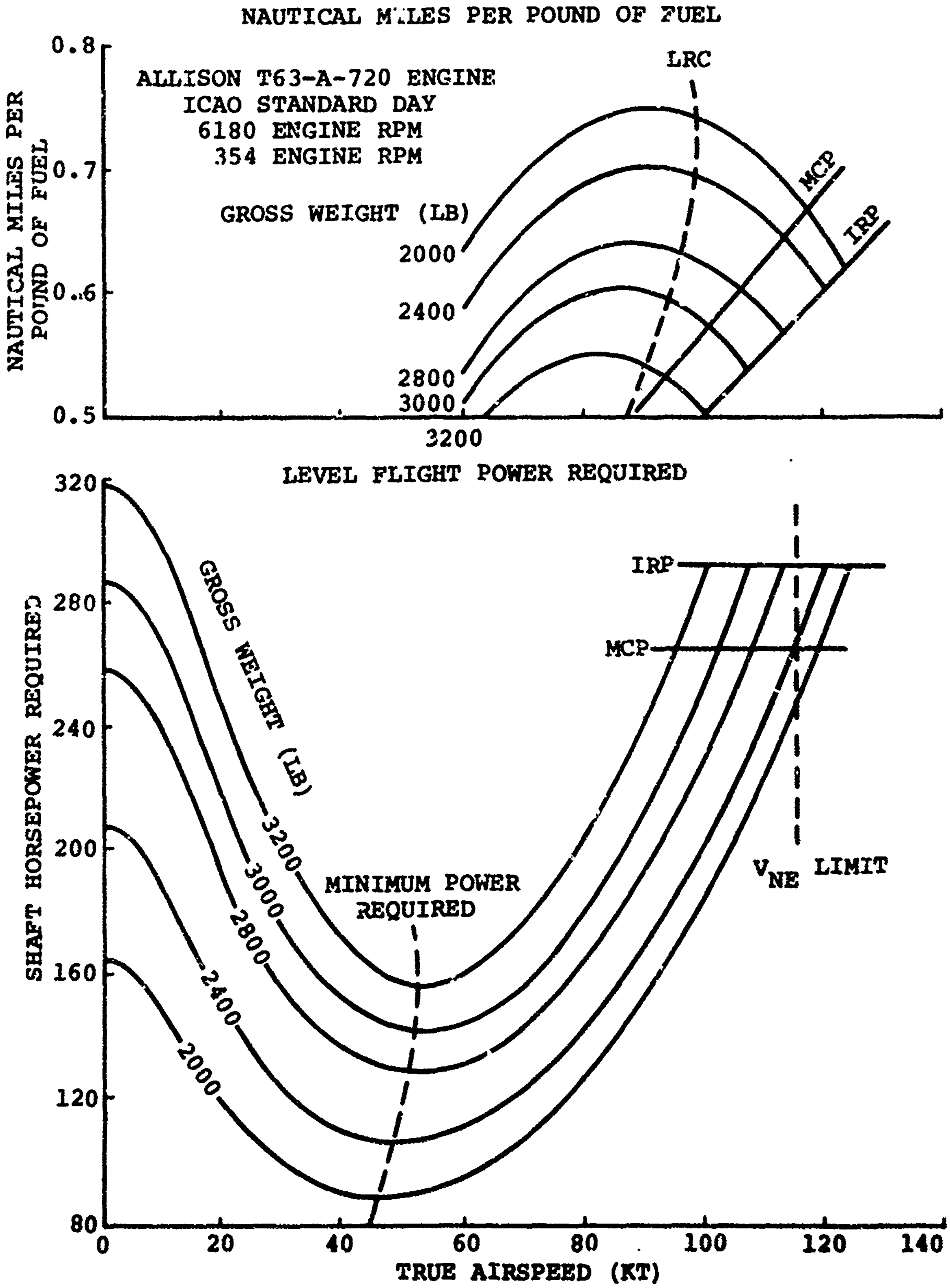

Figure 87. Level Flight Performance 10,000 Feet Standard Day-Baseline

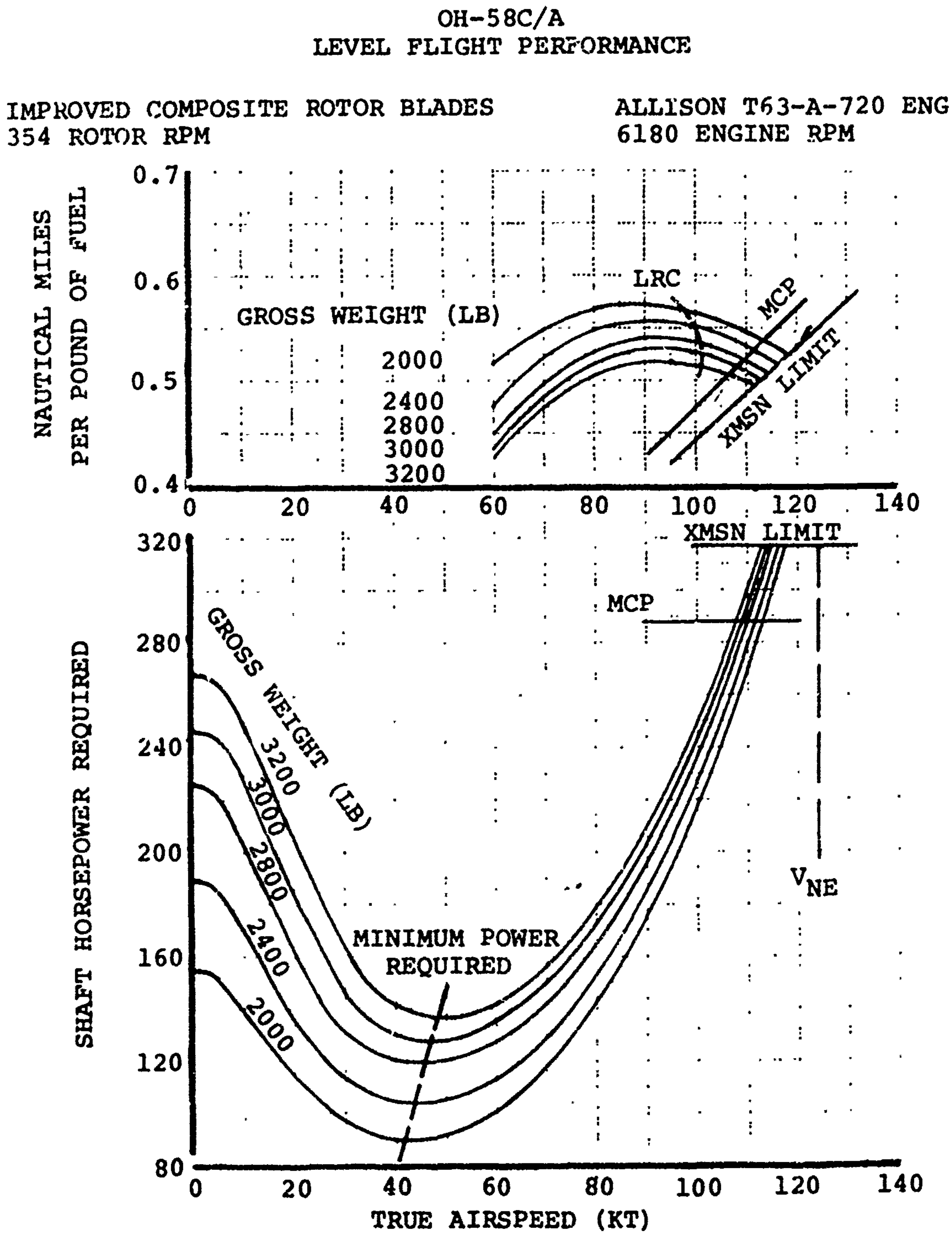

Figure 88. Level Flight Performance, Sea Level, 95°F, Composite Blades

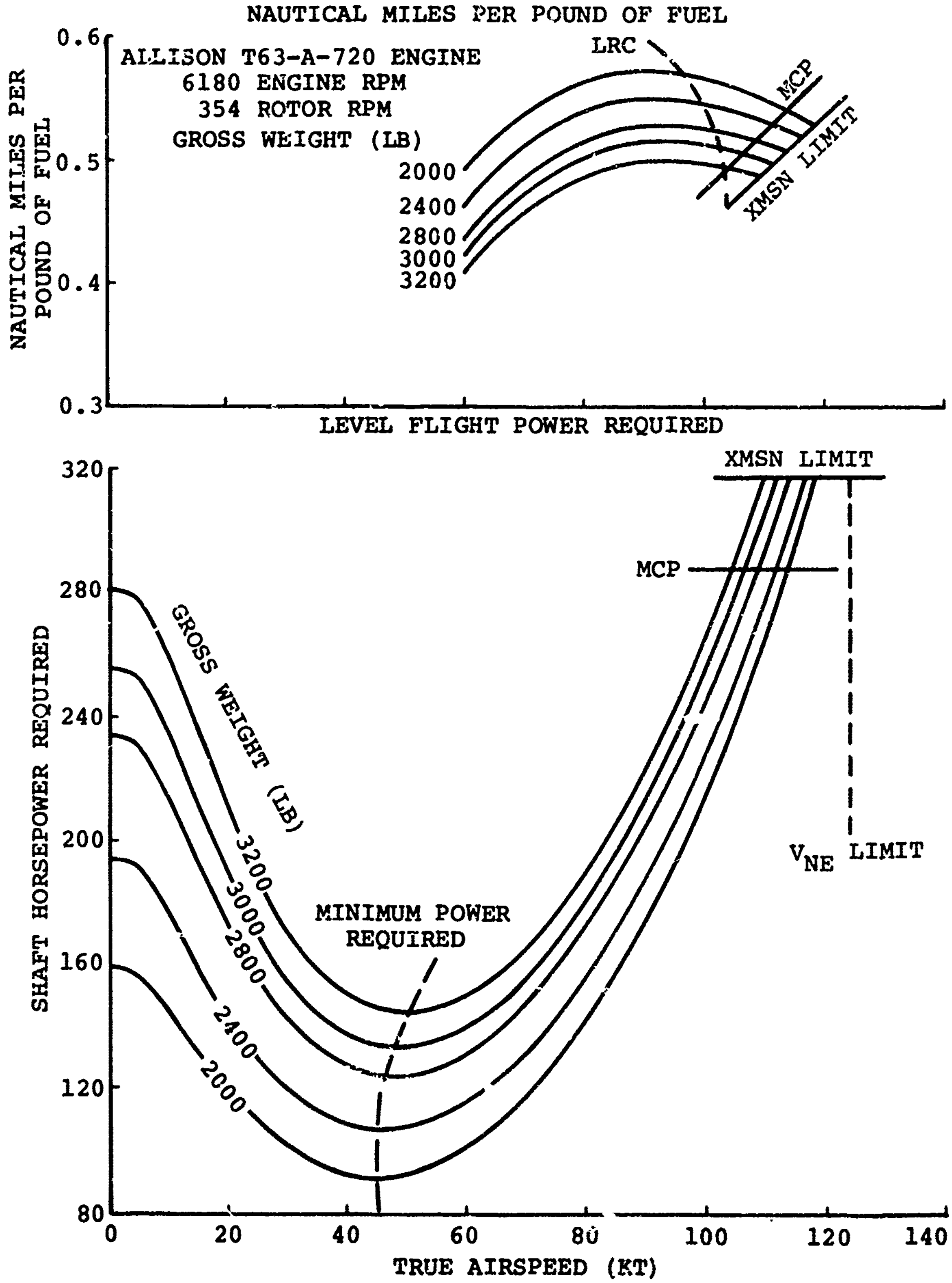

Figure 89. Level Flight Performance, Sea Level, 95°F, Baseline

OH-58C/A
LEVEL FLIGHT PERFORMANCE

IMPROVED COMPOSITE ROTOR BLADES
354 ROTOR RPM

ALLISON T63-A-720 ENG
6180 ENGINE RPM

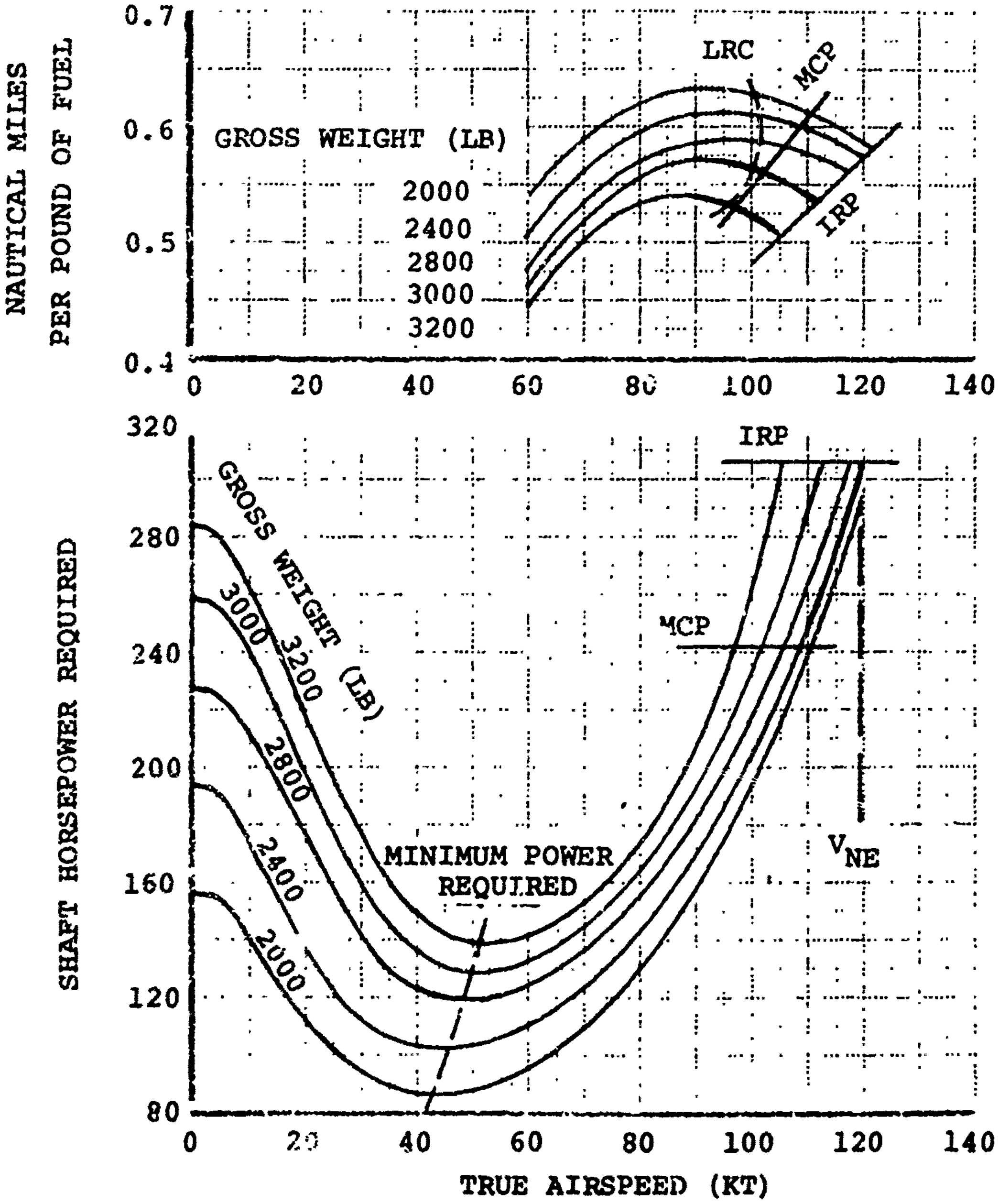

Figure 90. Level Flight Performance, 4000 Ft, 95°F, Composite Blades

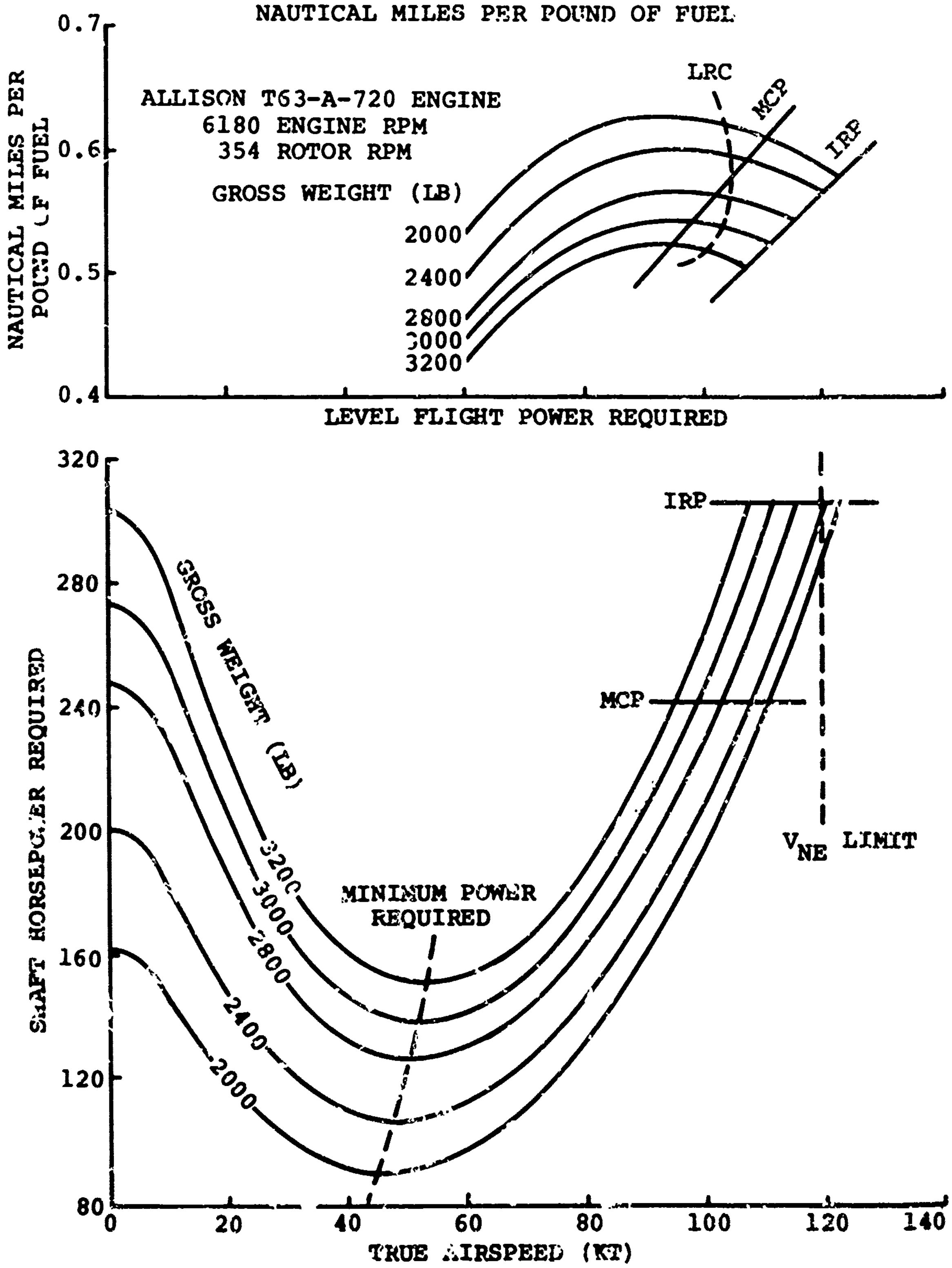

Figure 91. Level Flight Performance, 4000 Feet, 95°F, Baseline

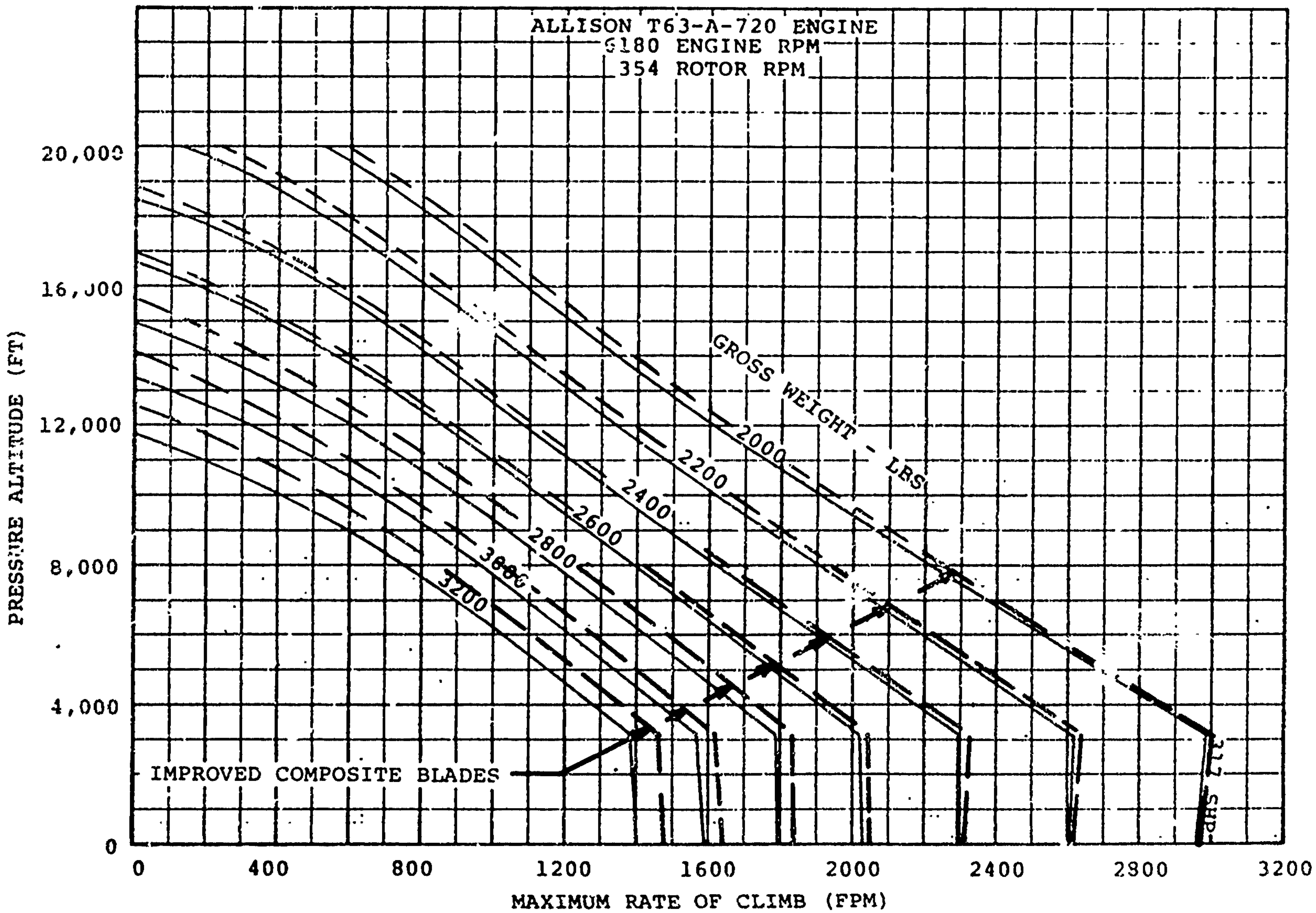

Figure 92. Maximum Rate of Climb, Intermediate power, Standard Day

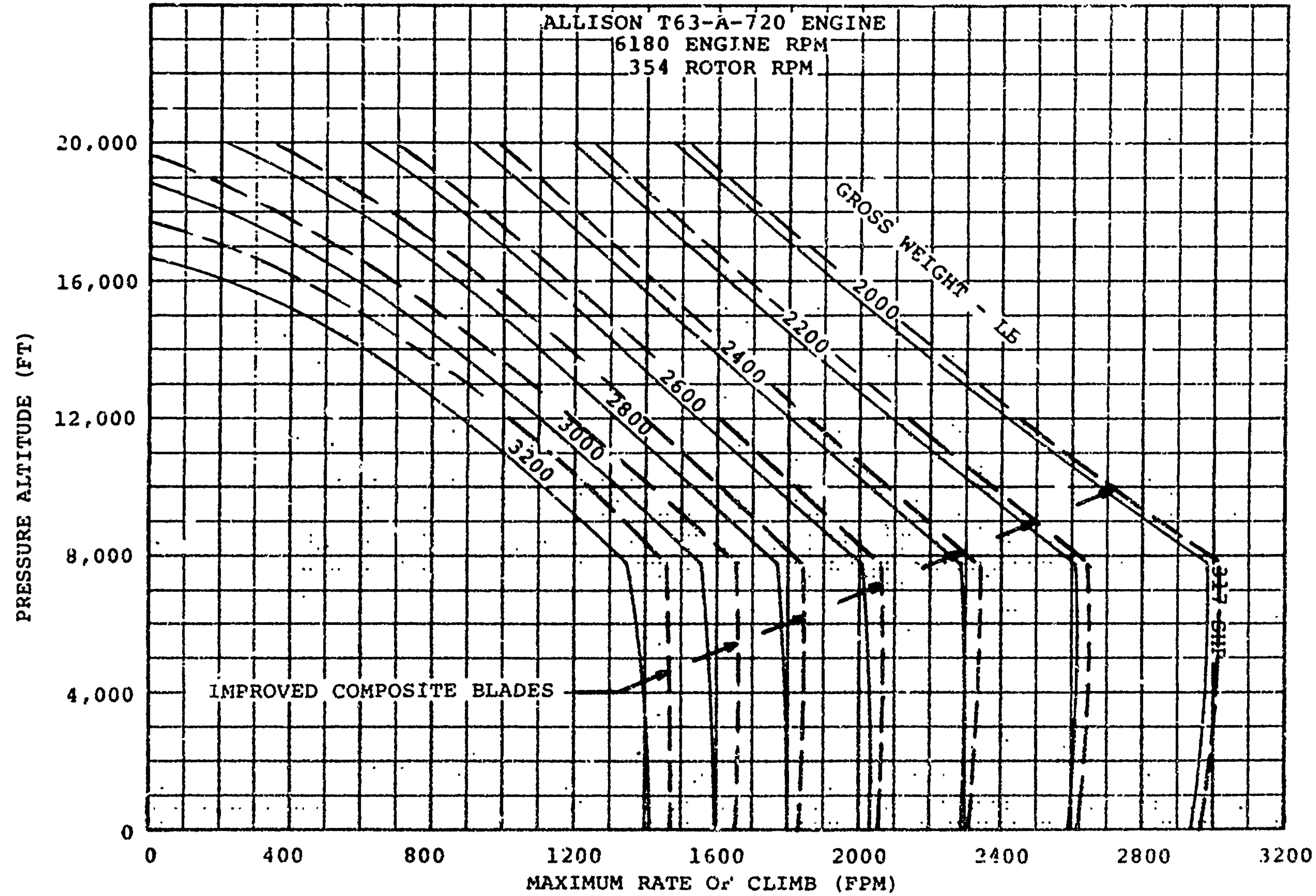

Figure 93. Maximum Rate of Climb, Intermediate Power, 95°F

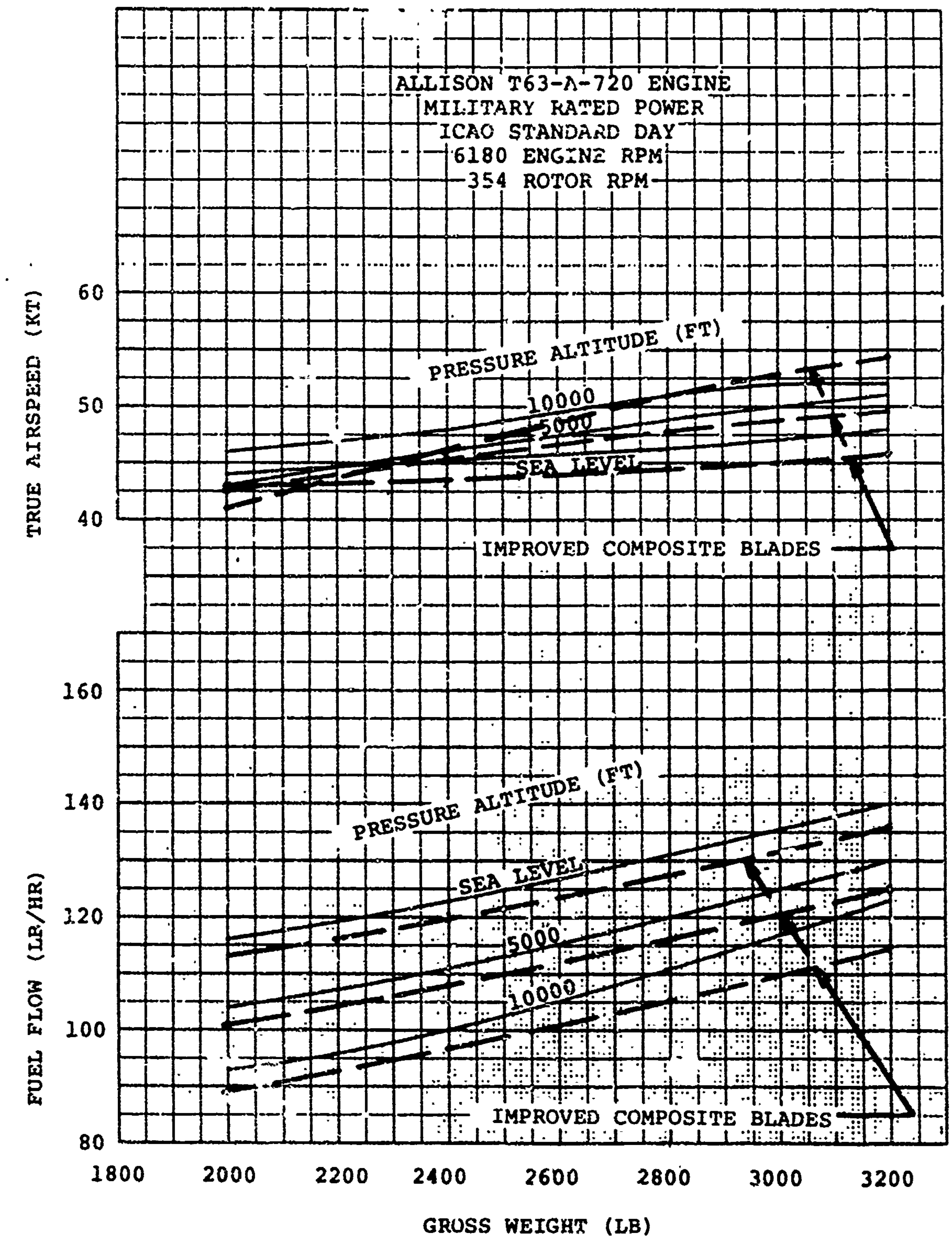

Figure 94. Maximum Endurance Performance

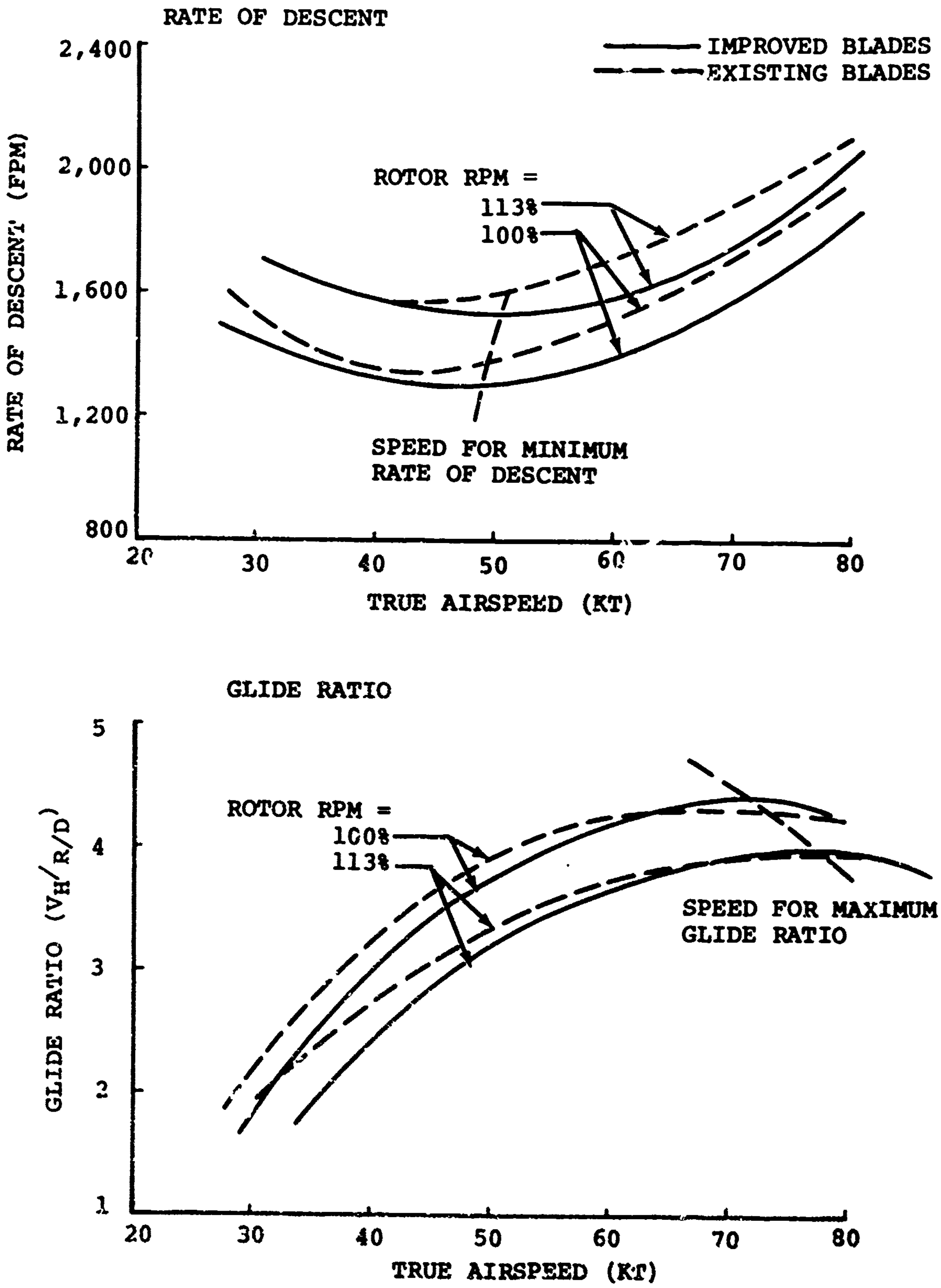

Figure 95. OH-58C/A Autorotational Descent Performance Improved Composite Blades

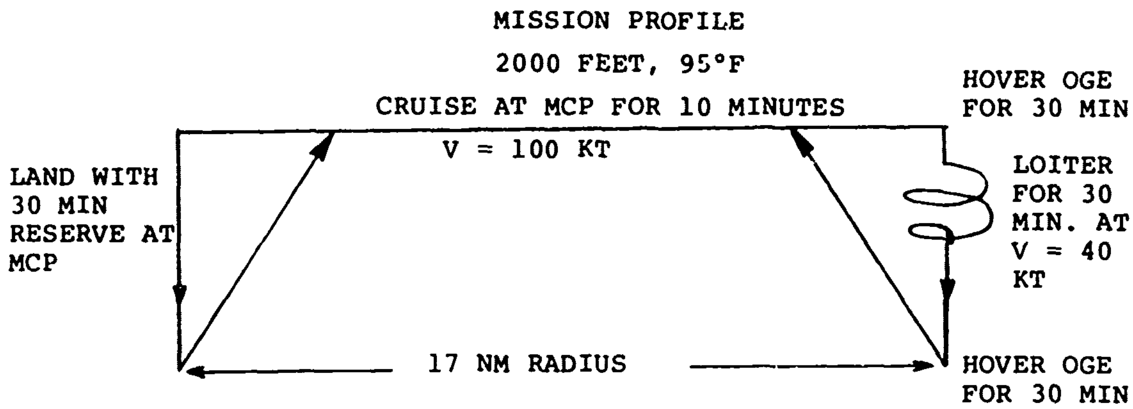

MISSION SEGMENT	FUEL USED (LB)
8 Minutes at Ground Idle	14
Cruise out at MCP for 10 Min	33
Hover for 30 Min at OGE	100
Loiter for 30 Min at V = 40 KT	67
Hover for 30 Min at OGE	100
Cruise in at MCP for 10 Min	33
Land with 30 Min Reserve at MCP	98
TOTAL FUEL FOR MISSION	445

NOTES:

1. Takeoff gross weight = 3200 lb
2. Usable fuel = 457 lb
3. All mission segments calculated at 3200 lb

Figure 96. Mission Profile, 2000 Feet, 95°F

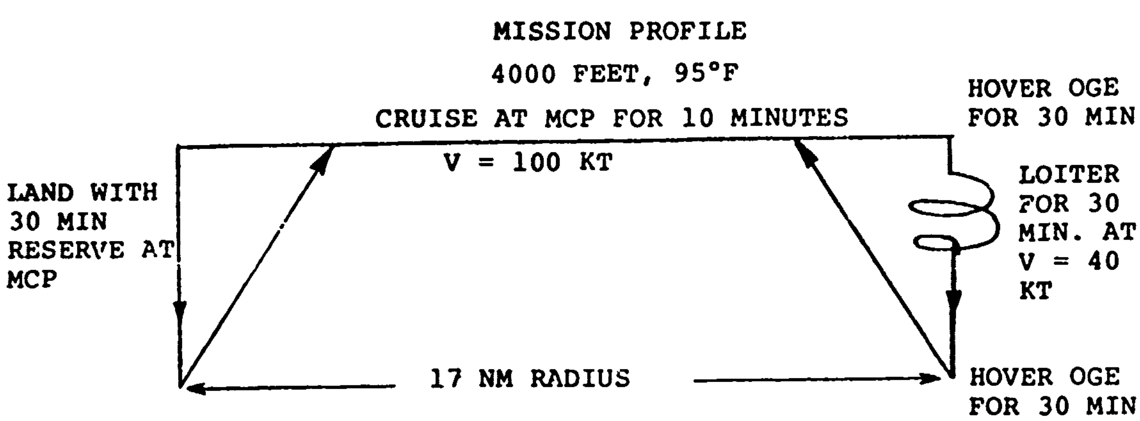

MISSION SEGMENT	FUEL USED LB
5 Minutes at Ground Idle	14
Cruise out at MCP for 10 Min	30
Hover for 30 Min at OGE	102
Loiter for 30 Min at V = 40 KT	66
Hover for 30 Min at OGE	102
Cruise in at MCP for 10 Min	30
Land with 30 Min Reserve at MCP	91
TOTAL FUEL FOR MISSION	435

NOTES:

1. Takeoff gross weight = 3200 lb
2. Usable fuel = 457 lb
3. All mission segments calculated at 3200 lb

Figure 97. Mission Profile, 4000 Feet, 95°F

4.7 STRUCTURAL ANALYSIS

4.7.1 Summary

A preliminary design analysis has been performed on a composite main rotor blade in sufficient detail to confirm the feasibility of the design concept. Fatigue and limit design load conditions have been generated from the prescribed flight profile and the known critical conditions of MIL-S-8698. A fatigue design factor of 1.25 on high-speed level flight loads was determined from the mission profile and material fatigue characteristics, to assure a minimum of 3600 hours life. Based on the large margins of safety for fatigue, as shown in Table 35, an unlimited life is anticipated. Fail-safety is achieved by virtue of the "soft" failure modes of the material used in the blade and redundant mass retention methods.

TABLE 35. SUMMARY OF MARGINS OF SAFETY

LOCATION	MODE	MARGINS OF SAFETY
Blade Retention		
Station 18.5	Chord moment; ultimate compression	+ .11
Station 14.3	Chord moment; ultimate compression	+ .08
Station 14.3	Chord shear; fatigue	+ .52
Station 18.5	Pin wrap, C.F. and flap bending;	
	ultimate tension	+ .58
	fatigue	+ .96
Basic Blade		
Station 53	Combined bending and C.F.;	
	ultimate tension	+ .96
	ultimate compression	0
Station 60	Combined bending and C.F.; fatigue	+1.10
Station 170 Aft Fairing	Core; shear fatigue	+ .79
Station 180 Upper Surface	Transverse flexure; fatigue	+1.80

4.7.2 Criteria

The structural design criteria for the composite main rotor blades are the following:

Design limit load factor of +2.5 g and -0.5 g shall be applied at a helicopter gross weight of 3200 pounds. Ultimate strength requirement shall be in accordance with the maneuver requirements of MIL-S-8698, "Structural Design Requirements, Helicopter". This shall include flight loading conditions, such as maneuvers, turns, and autorotation, and miscellaneous loading conditions, such as rotor starting and static droop.

A minimum fatigue life of 3600 operating flight hours based on the fatigue loading spectrum shown in Table 36, F ght Profile. The flight profile is that specified in Reference , modified as noted on the table.

The material properties to be used are those shown Table 37 and Figures 98, 99, and 100. These properties are ed on test data and are mean -3σ values except where noted as "estimated".

4.7.3 Loads

The basis for the loads used herein is the measured flight data of References 13 and 14. These are modified by gross weight factors and by the effects of the differences in physical properties and the configuration between the baseline and the composite blade found in Section 4.5, Dynamic Analysis. Boeing Vertol computer program L-02 is used to calculate the loads for both the baseline and the composite blades.

4.7.3.1 Limit Design Loads

The limit design loads are developed in the same manner as those in Reference 14, Part II. The chord moments are the sum of those induced by airload and centrifugal force. The

---

12. PROPOSAL FOR A TRADE STUDY AND PRELIMINARY DESIGN OF AN ADVANCED COMPOSITE ROTOR BLADE FOR THE OH-58C/A HELICOPTER, Boeing Vertol Company, D210-11287-1, in response to RFQ DAAJ02-77-Q-0143.
13. MODEL 206A-1 CERTIFICATION FLIGHT LOAD SURVEY (6 Volumes), Bell Helicopter Company, 206-194-062, August 1969.
14. LOAD DETERMINATION AND STRUCTURAL ANALYSIS OF THE 206-011-001-3 MAIN ROTOR HUB AND BLADE ASSEMBLY FOR THE 206A-1 HELICOPTER Rev. C, Bell Helicopter Company, 206-099-107, October 1977.

TABLE 36. FLIGHT PROFILE

	% Total Time				Occurrences in 3600 Hr (4)											
Airspeed (% V_H) or Condition	Level (1) Flight & Moderate Maneuvers > 0.8 < 1.2	Control (2)(3) Reversals			Maneuvers Peak Load Factor - g's at c.g.											
		Long.	Lat	Dir	0.0	0.2	0.4	0.6	0.8	1.2	1.3	1.4	1.5	1.75	2.0	2.5
0 % V_H	1.71	.0098	.0098	.0098												
10	2.72							18	1782	60989	31504	18464	4144	95	4	
20	2.33						9	52	10740	26217	32504	16699	19130	1192	18	
30	3.06					7	39	294	20124	27315	15701	17131	23306	2371	180	18
50	3.60				20	7	37	410	5827	13374	7974	5729	6264	693	256	36
70	7.23					7	39	257	3297	7097	3546	3478	4010	526	171	18
80	14.24						37	77	1326	7947	3830	2088	927	216	67	18
90	17.47						5	40	387	6480	1062	540	351	63	27	
100	8.74	.0498	.0498	.0498				8	127	464	247	117	122	18	4	
110	2.80								27	104	67	32	36	4		
Sideward Flt	0.54				Total Occurrences - Man. 20	21	166	1156	43637	149982	96435	64278	58290	5178	727	90
Rearward Flt	0.30															
Ground	0.55															
Autorotation	----	.0098	.0098	.0098												
Time/Man. (4) (Sec)	----				2.0	2.3	2.8	3.5	4.7	12.2	11.7	11.1	10.1	6.1	4.0	1.7
Total Time at Man. (Hr)	----				0.012	0.013	0.129	1.12	57.0	508.3	313.4	198.2	161.9	8.77	0.81	0.043
% Time	65.29		.208(2)		34.71											

(1) YUH-61A V_H Distribution.

(2) In addition to 3600 Hr

(3) Same % as OH-58A Spectrum (Reference 15).

(4) From exceedance Table in Reference 12.

(5) Ground-Air-Ground (GAG) cycles shall be 2/hr from 0 to normal rotor RPM and 6/hr from 0 to MIL Power Torque, at normal RPM. (7200 & 21600 cycles).

15. FATIGUE LIFE SUBSTANTIATION FOR THE DYNAMIC COMPONENTS OF THE MODEL 206A-1 HELICOPTER Rev. H, Bell Helicopter Company, 206-099-114.

TABLE 37. MATERIAL PROPERTIES - DESIGN ALLOWABLES

Material	E_T PSI x 10^{-6}	G PSI x 10^{-6}	Strain: Static ε_{TU} μ(in./in/)	Strain: Static ε_{SU} μ(in./in/)	Strain: Static ε_{CU} μ(in./in.)	Strain: Fatigue R=0.1 ε_{ET} μ(in./in.)	Strain: Fatigue R=0.1 ε_{ES} μ(in./in.)
Kevlar 49-0°	11.0	0.3	14,500	26,600	2,730	±2,730(1)	±2,750(1)
S-Glass							
0° & (0/±45)	6.3	0.52	24,300	26,420	15,100	±2,300	±2,740
±45°	1.78	1.76	83,000	26,420	83,000	±1,380	±2,740
			(23,100 PSI)		(23,500 PSI)		

(1) Estimated (insufficient data for a mean - 3σ, statistical allowable)

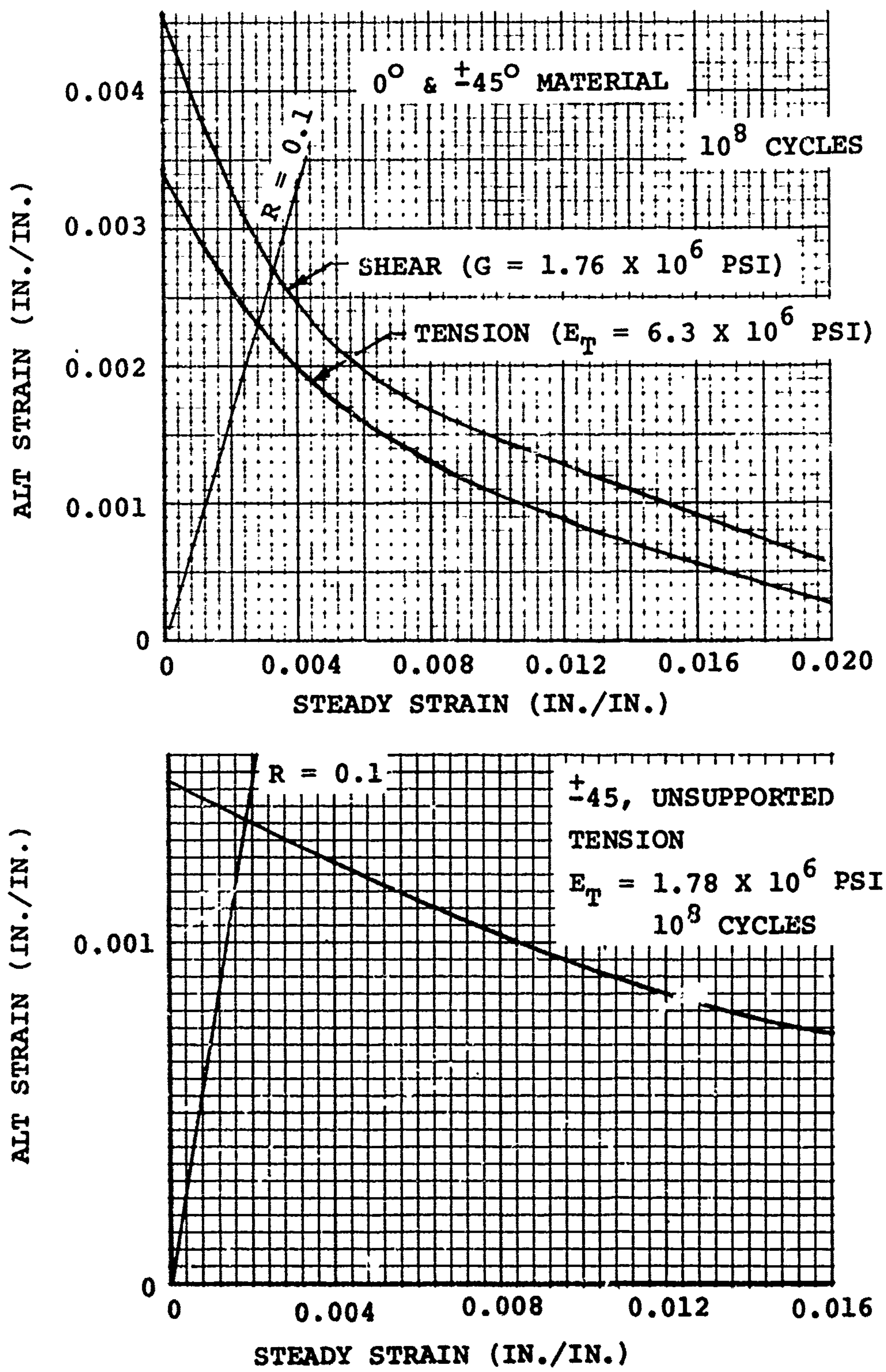

Figure 98. S-Glass, Goodman Diagrams, 0° & $\pm 45^{\circ}$

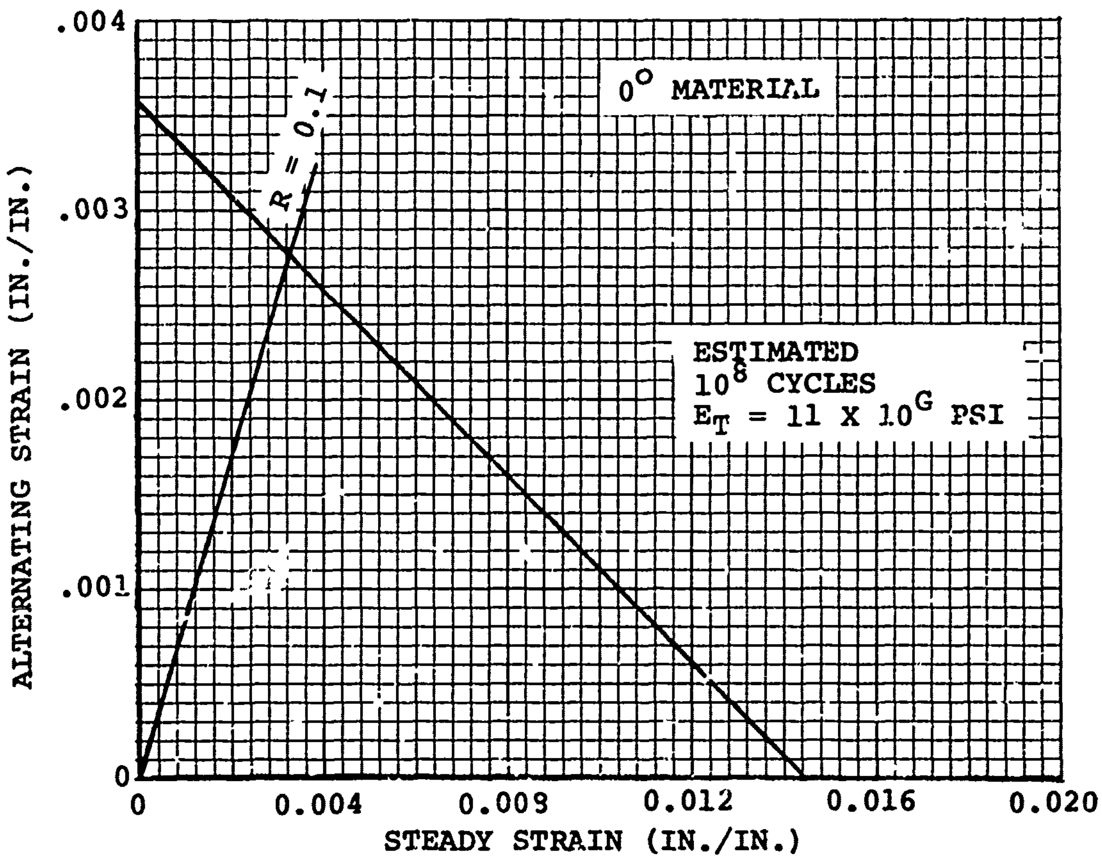

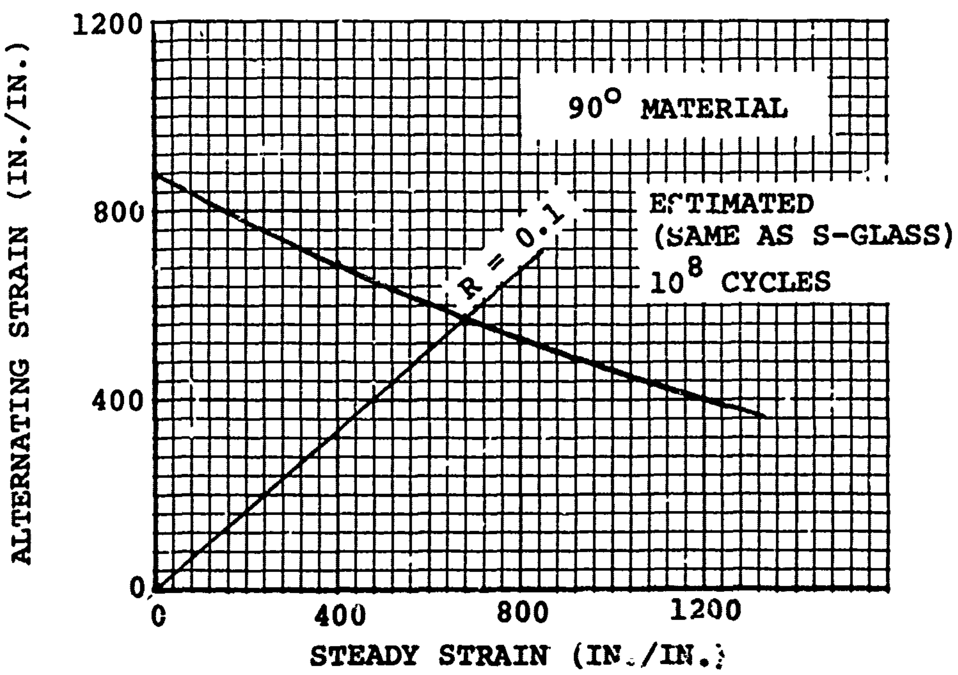

Figure 99. Kevlar 49, Goodman Diagrams, 0° & 90°

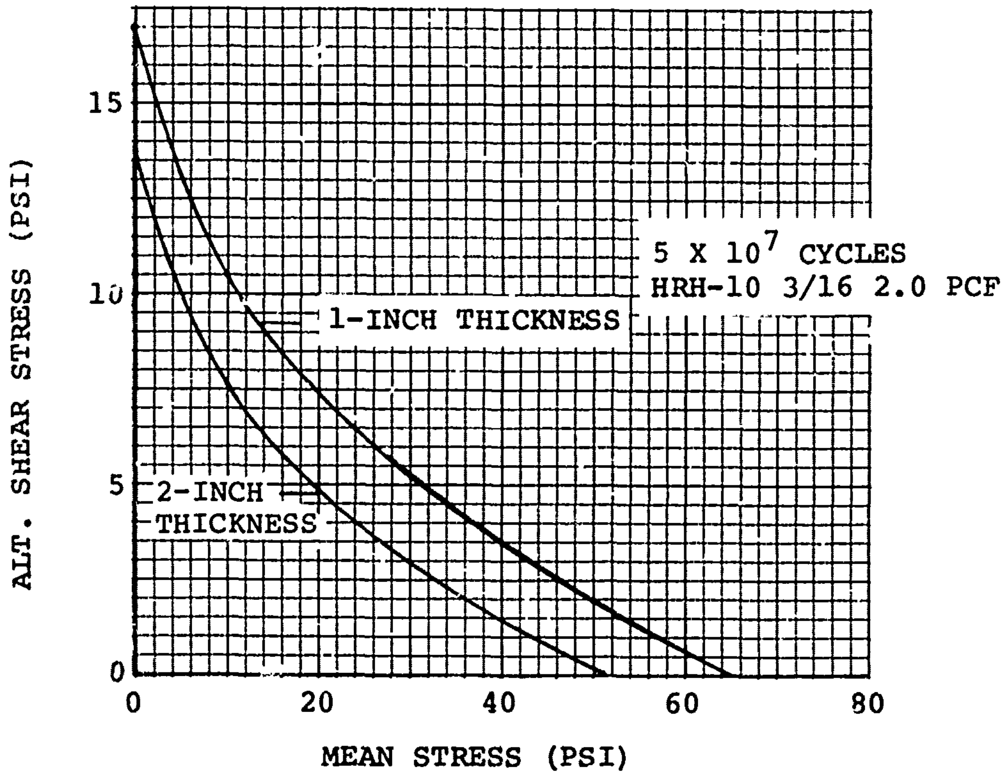

Figure 100. Nomex Honeycomb Goodman Diagram, Shear

composite blade design load uses the airload from Reference 14 and the centrifugal force induced moments from Boeing Vertol Computer Program L-02. The composite blade has a further aft c.g. than does the baseline blade resulting in larger centrifugal force induced moments. The flap or beam moments have been calculated using program L-02 are less than that of Reference 14. Therefore the latter are conservatively used in the structural substantiation analysis. Limit load plots are shown in Figures 101 through 103 for the following load conditions:

Condition	M_{CO}* (In.-Lb)	RPM	Nz (Vert.)
1	+79,500	411	-0.5
2	-53,000	411	-0.5
3	+79,500	304	+2.5
4	-53,000	304	+2.5

*M_{CO} (max) = 53,000 (1/2 + 1) = 79,500 in.-lb

M_{CO} (min) = 53,000 (0 - 1) = -53,000 in.-lb

Additionally, a 4.0-g ultimate ground flapping and a rotor start condition are also examined.

4.7.3.2 Fatigue Design Loads

The fatigue loads used for the flight profile of Table 36 are those measured flight test data of Reference 13, modified by gross weight, airspeed, load factor and configuration differences between the baseline and composite blades. Station 60 is used to examine the fatigue load spectrum for life versus endurance limit trends and is considered to be representative of both the root end and a mid-span basic blade section. The design fatigue factors for this station will be used as typical.

The analysis subsequently performed with these loads is to substantiate feasibility of design and to substantiate weights. Torsional stresses are typically of low magnitude and have been neglected in this preliminary design phase.

Flap and chord bending moment loads vary with airspeed as is shown in Figures 104 and 106. The more critical c.g. is used 100% of the time. It is assumed that the blade loads vary linearly with gross weight. The measured loads of Reference 13 are for a 3000-lb gross weight aircraft and the composite blade aircraft gross weight is 3200 lb (Figures 108 and 109). Therefore, a factor of 1.067 (3200/3000) is applied to the measured loads. An assumption is made that blade bending loads grow linearly with load factor (Nz). This is conservative throughout the airspeed range required, as is seen in Figures 105 and 107.

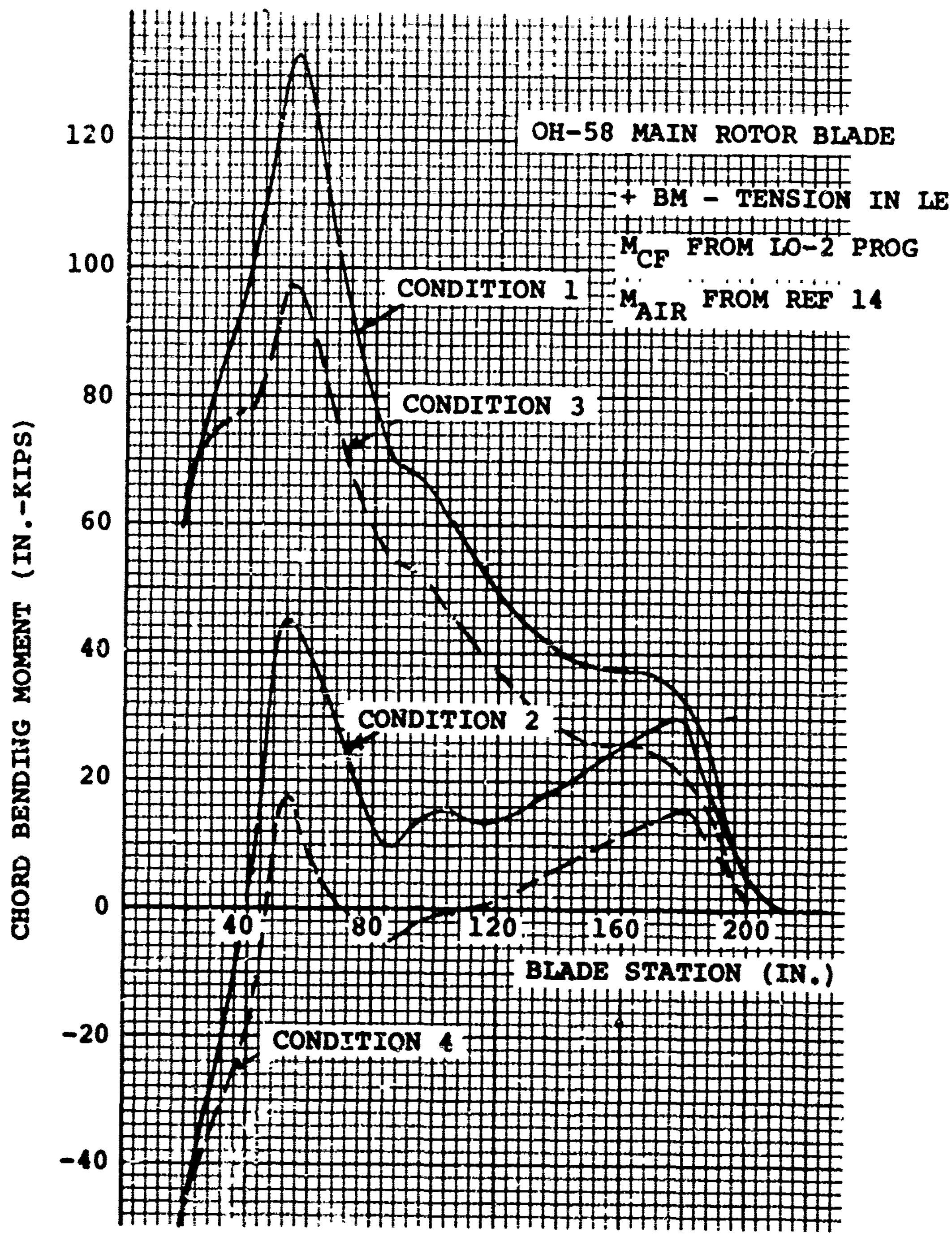

Figure 101. Static Chord Moment

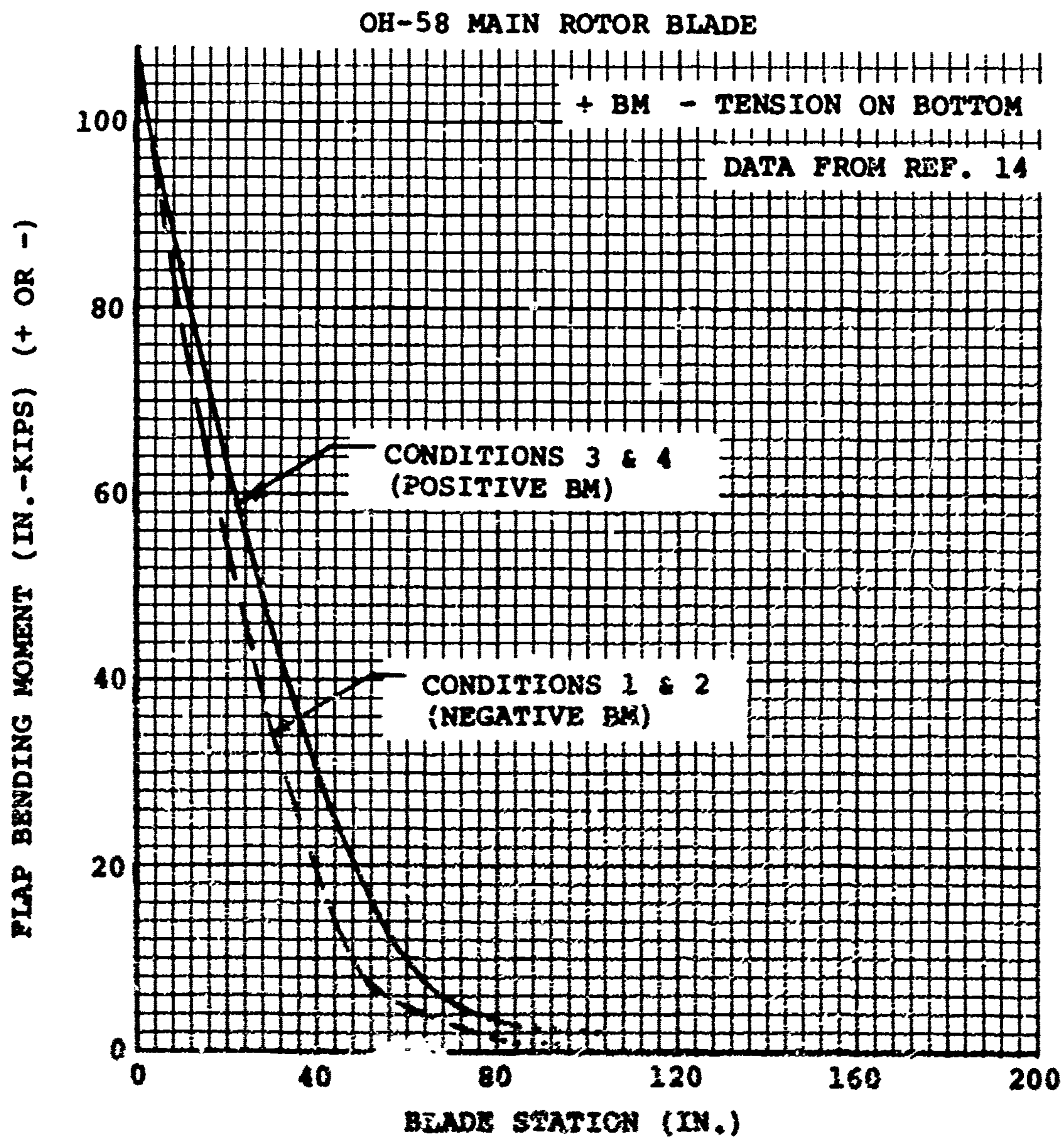

Figure 102. Static Flap Moment

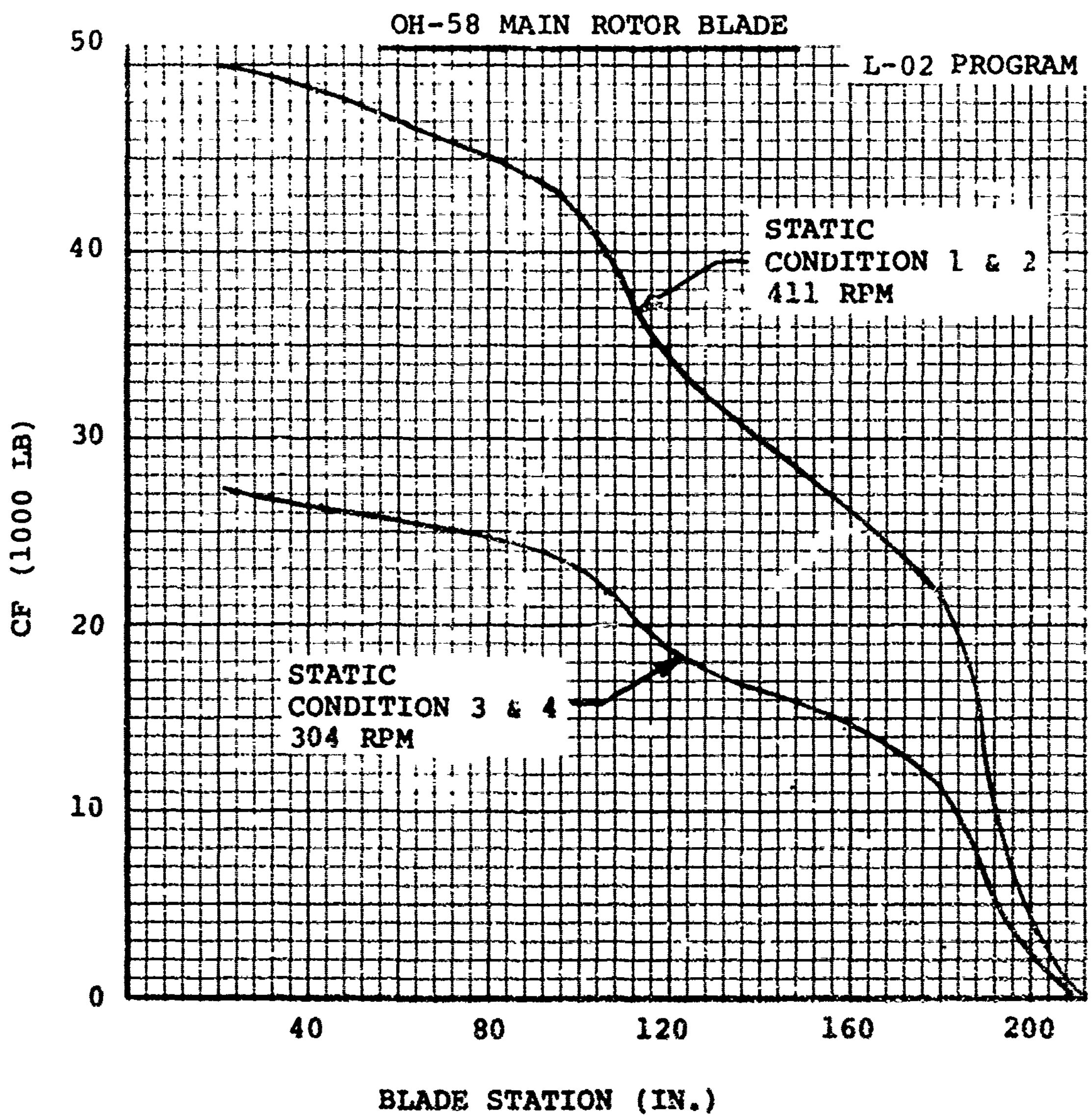

Figure 103. Spanwise Distribution of Centrifugal Force, 304 & 411 rpm

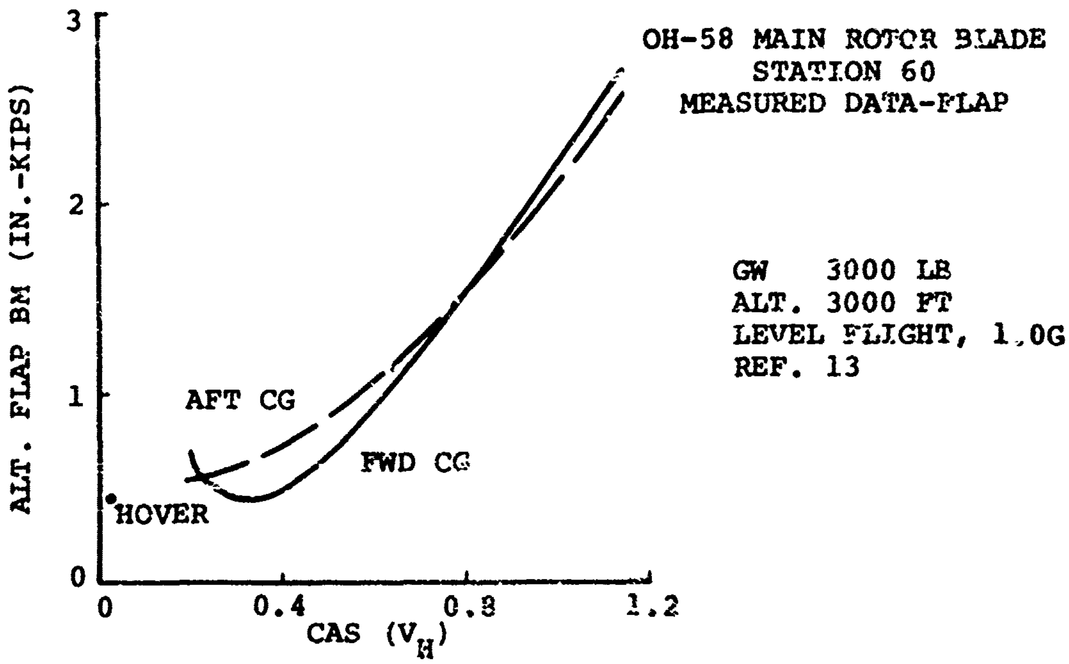

Figure 104. Alternating Flap Bending Moment Vs. Airspeed

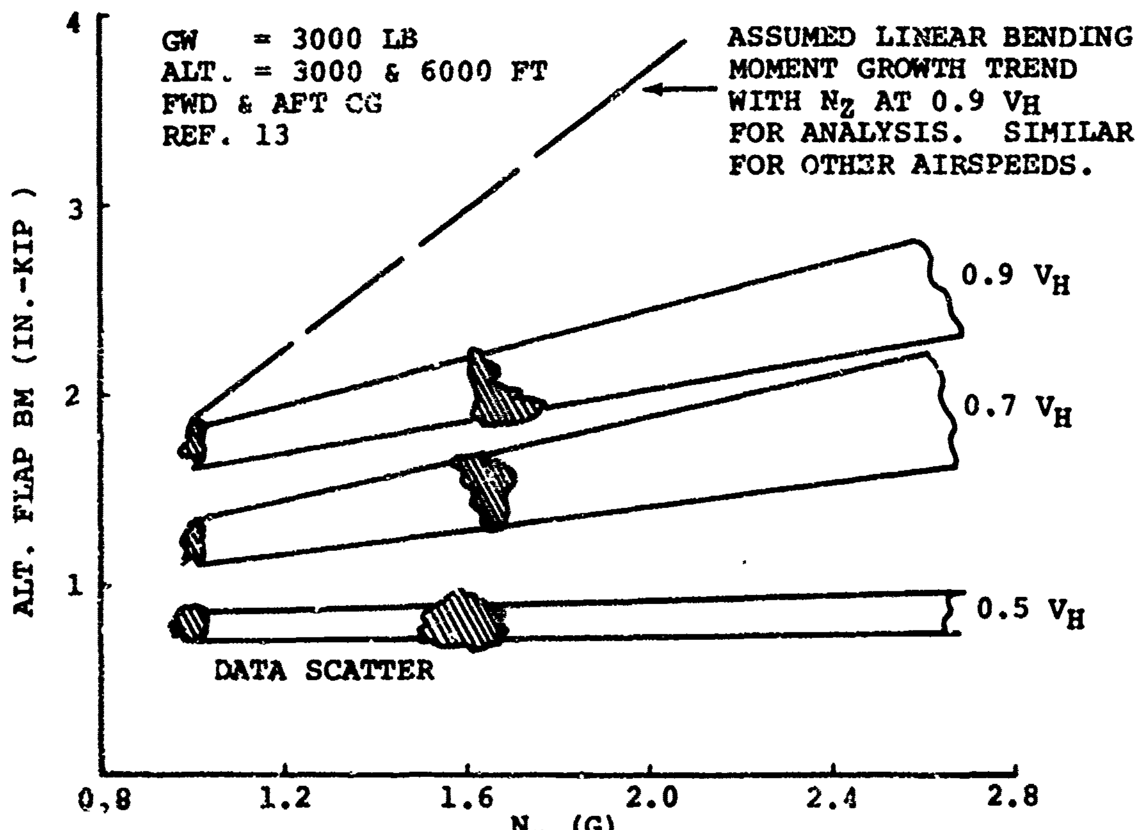

Figure 105. Alternating Flap Bending Moment Vs. Maneuver Load Factor

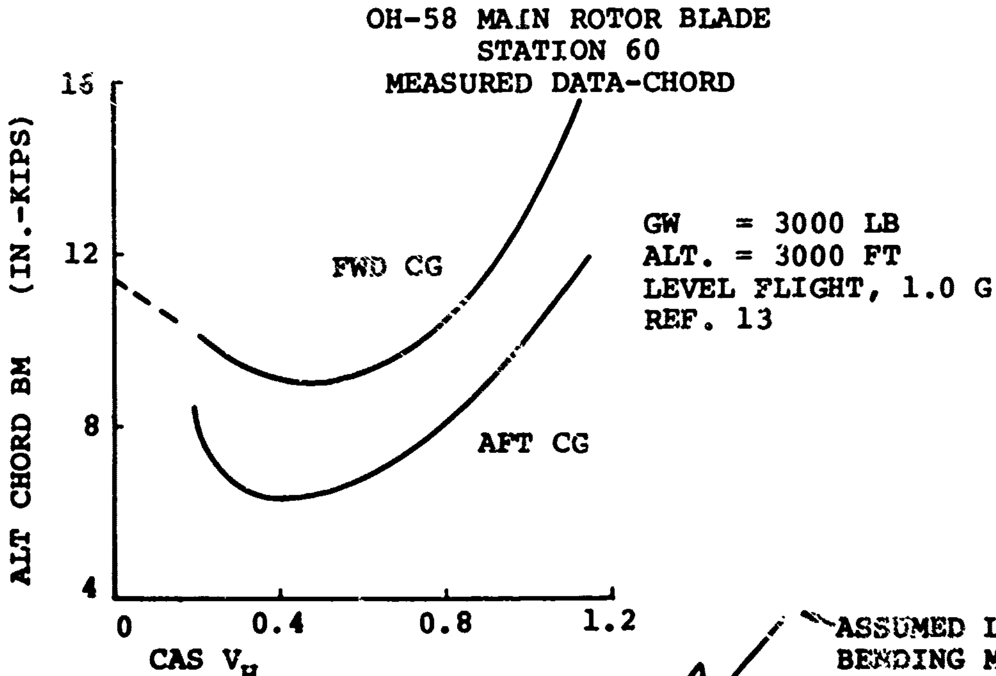

Figure 106. Alternting Chord Moment Vs Airspeed

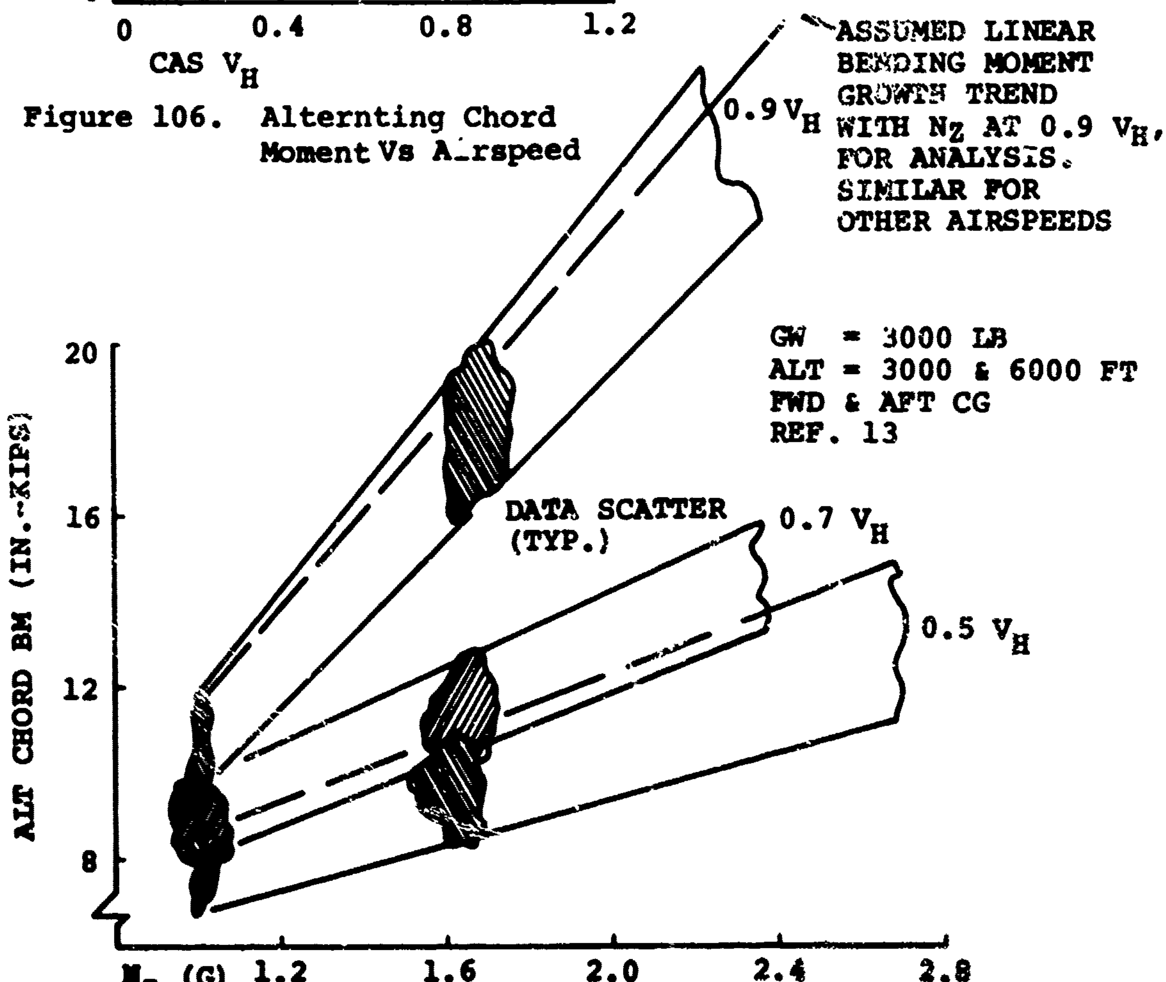

Figure 107. Alternating Chord Moment Vs Maneuver Load Factor

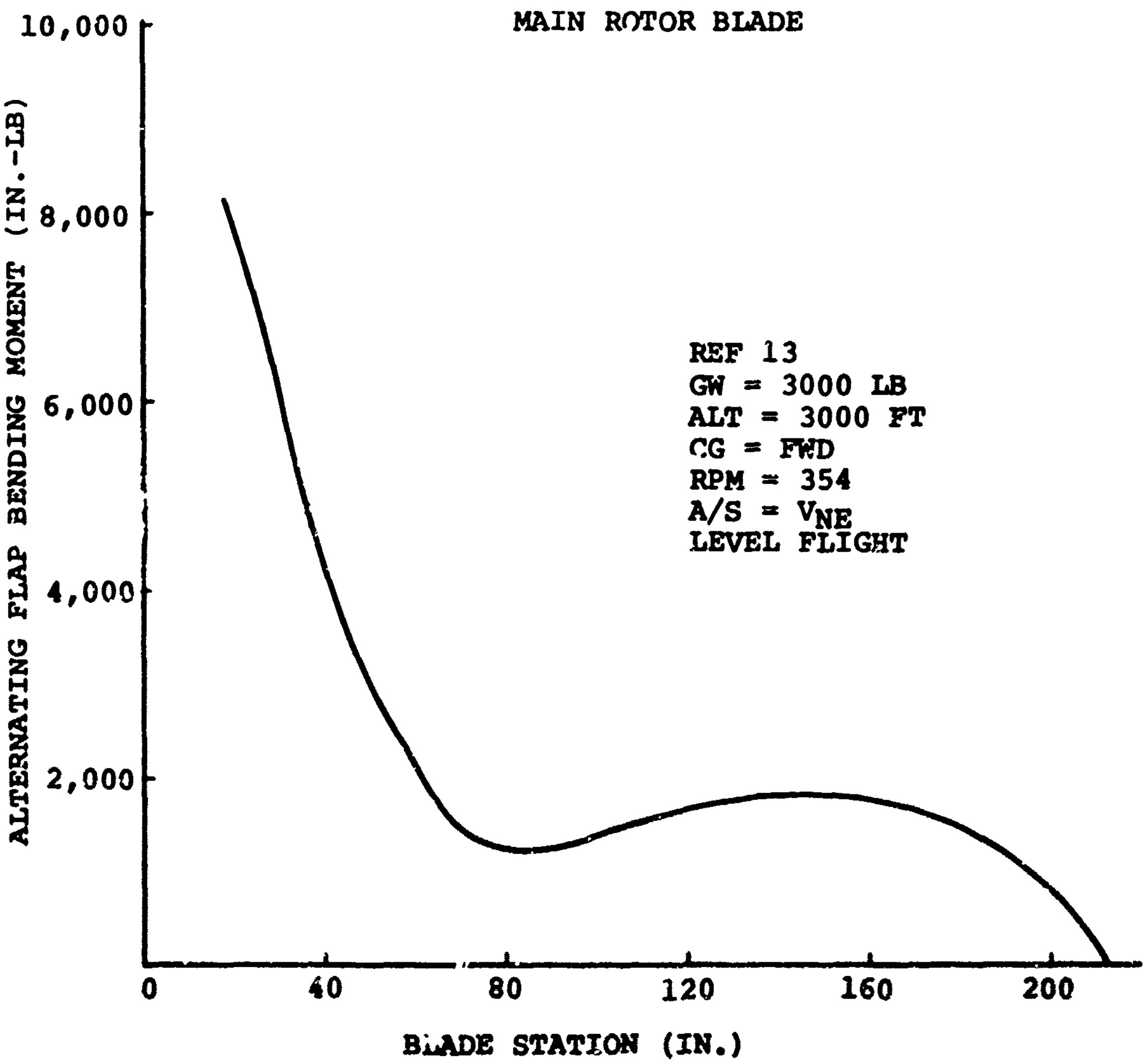

Figure 108. Measured Alternating Flapwise Bending Moment Model 206A-1

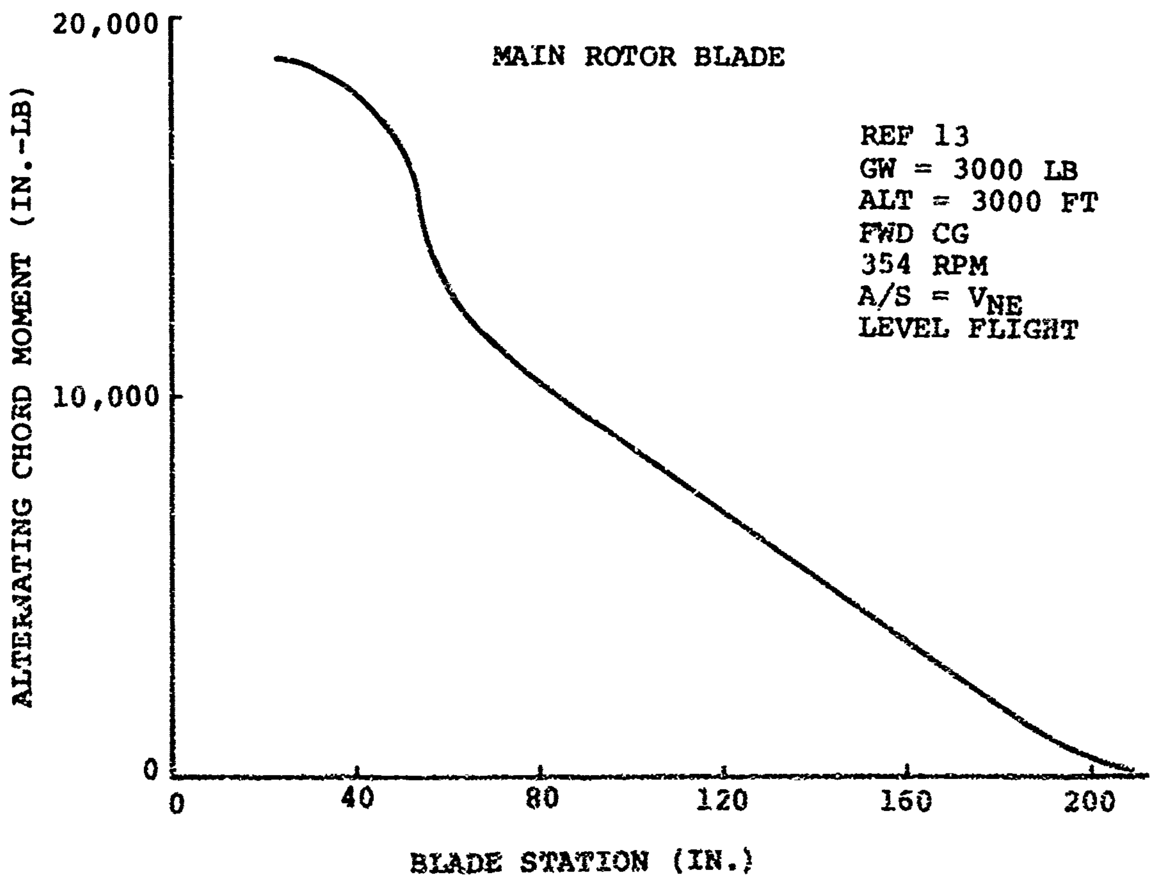

Figure 109. Measured Alternating Chordwise Bending Moment Model 206A-1

The composite blade and the baseline blade differ in physical properties which also affect loads. The difference is displayed in Figures 110 and 111. At Station 60 the flap bending factor k_f, for the composite blade is 2300/2580 or .89 and the chord moment factor, k_c, is 39400/36700 or 1.07.

The design fatigue loads therefore are calculated as follows:

$$\text{Design Loads} = (\text{OH-58 Load at airspeed}) \times \frac{3200}{3000} \times N_2 \times k_{f,c}$$

Load data for load factors less than 1.0 g were not available for the OH-58 blade. Intuitively it seemed reasonable to expect similar loading for equal increments of positive and negative load factor. To gain confidence in this hypothesis a review of YUH-61A measured flight blade loads data (Reference 16) was conducted. At all air speeds and altitudes, both flap and chord bending data consistantly displayed the same or higher incremental alternating loads per increment of positive load factor, then for an equal increment of negative load factor.

Therefore for those conditions where $Nz \leq 0.8$, the loads shall be the same as those for $Nz = 2.0 - Nz$ (e.g. for a flight condition of $Nz = 0.2$ g's, the loads for $Nz = 1.8$ g's will be used).

The design loads for the V_H maneuver flight profile at Station 60 are shown in Table 38.

The loads due to unsymmetrical maneuvers, autorotation, pull-ups, etc., were examined (Reference 13) and were found to be less critical than the loads assumed by linear load growth versus load factor shown in Table 38. Therefore, these conditions are contained in the maneuver V_H load profile presented in this table.

The loads for sidewards/rearward flight and for the control reversal conditions are shown in Table 39. These loads shown result from the maximum measured loads of Reference 13 modified for the gross weight and configuration differences as noted before. Ground-air-ground loads were examined and found to be uncritical and nondamaging.

Span steady flap bending moments are plotted in Figure 112. Since the composite blade has a lower bending stiffness, the lower steady moments are anticipated. However, the higher loads will be used in the analysis for conservatism. The steady chordwise moments shown in Figure 113 reflect the influence of

---

16. YUH-61A HELICOPTER FLIGHT LOADS SURVEY REPORT, Contract DAAJ01-72-C-0007 (PGA), Boeing Vertol Company, T179-10142-2.

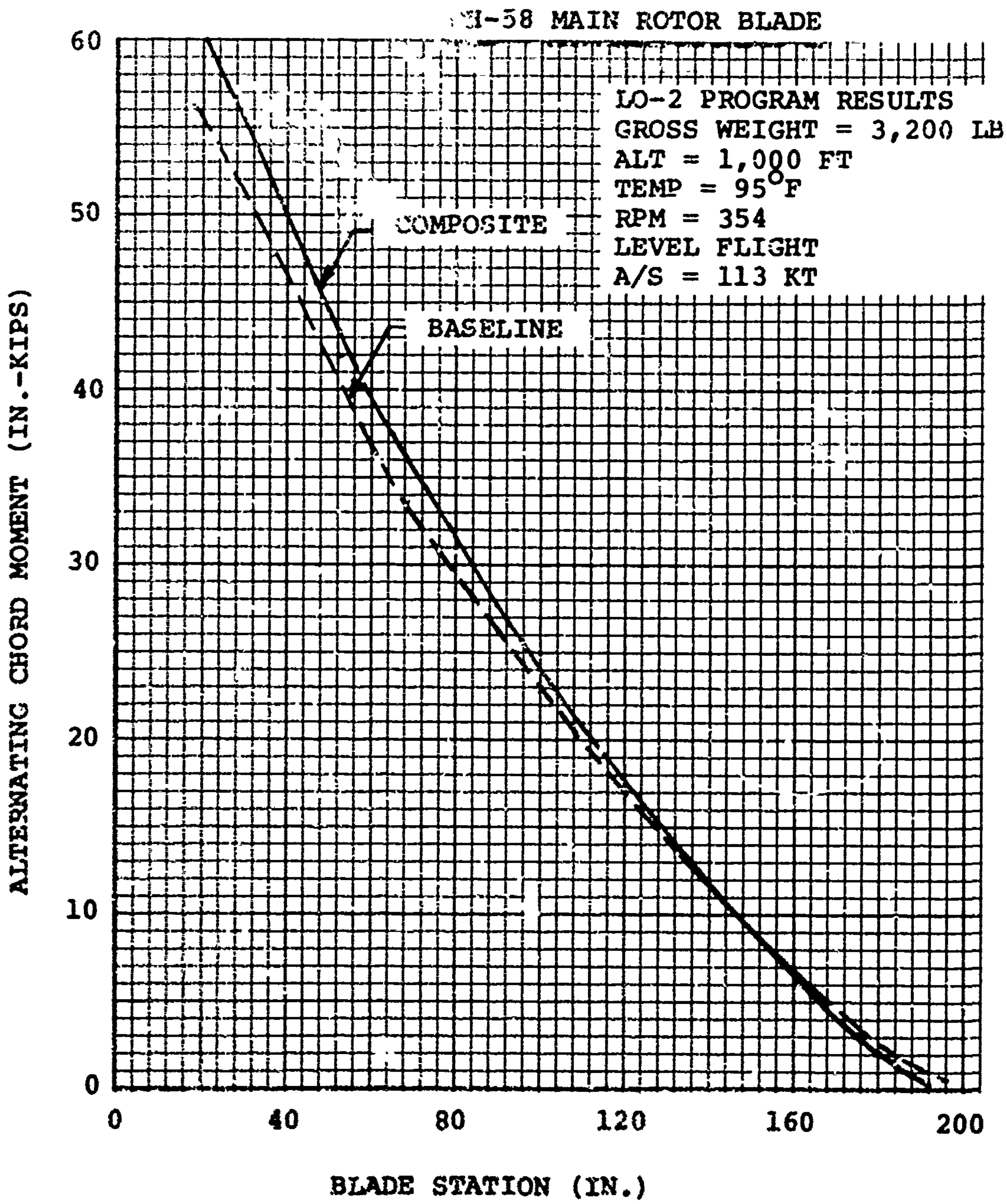

Figure 110. Calculated Alternating Chordwise Bending Moments

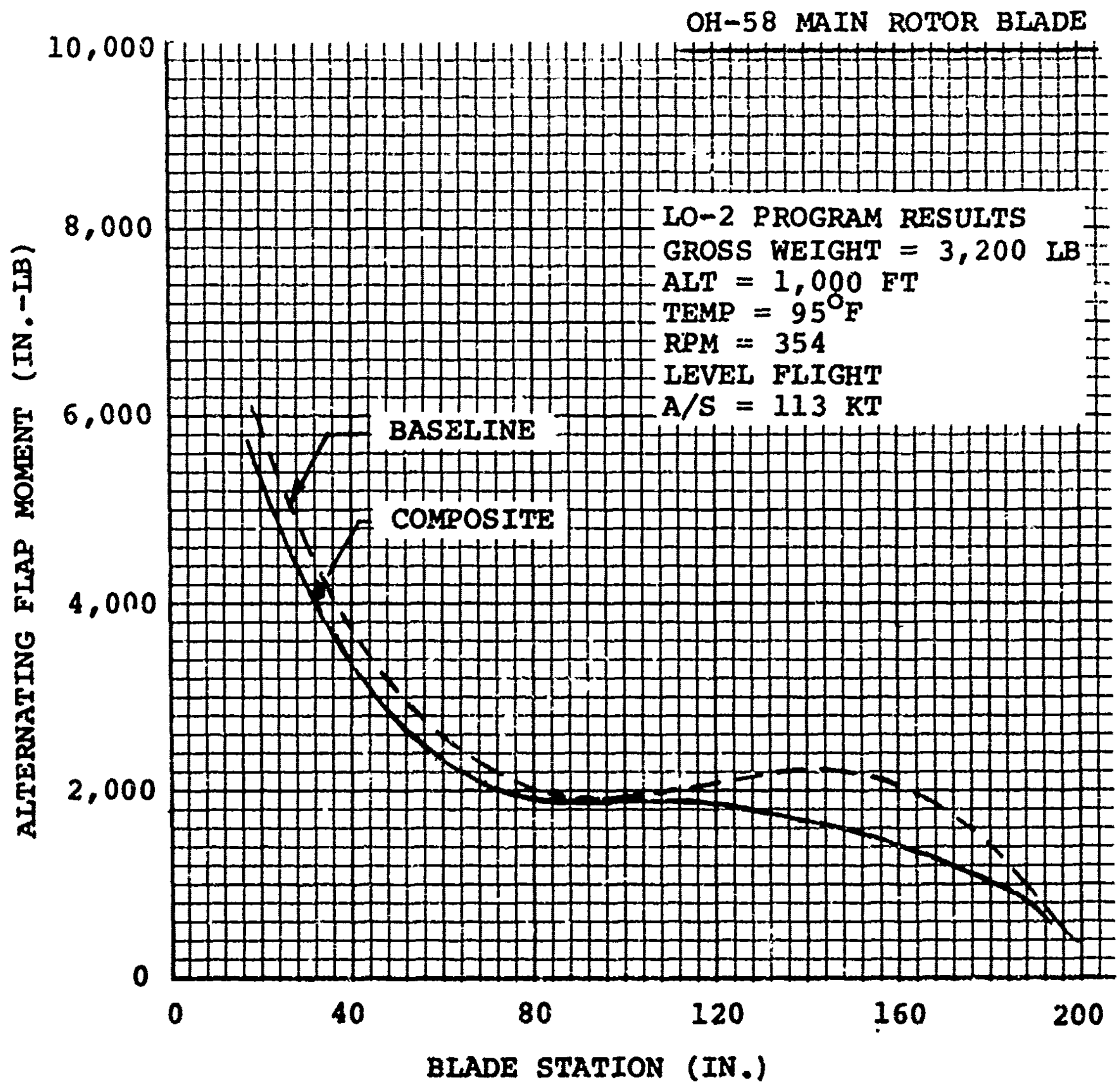

Figure 111. Calculated Alternating Flapwise Bending Moments

TABLE 38. FATIGUE LOADS FOR FLIGHT PROFILE

	Airspeed % V_H	Baseline Moment 1G	Composite Moment 1G	Bending Moment (in.-lb) for Flight Load Factors, g's											
				0.0 (2.0)	0.2 (1.8)	0.4 (1.6)	0.6 (1.4)	0.8 (1.2)	1.2	1.3	1.4	1.5	1.75	2.0	2.5
Flap Moment (3)	0	400	380 (1)	-	-	-	-	-	-	-	-	-	-	-	-
	10	600	570	-	-	-	800	684	684	740	800	855	1000	1140	-
	20	700	665	-	-	1050	920	786	786	850	920	980	1150	1310	-
	30	650	620	-	1120	990	870	744	744	810	870	930	1090	1240	1550
	50	900	855	1[illegible]10	1540	1370	1200	1030	1030	1110	1200	1280	1500	1710	2140
	70	1250	1190	-	2140	1900	1670	1430	1430	1550	1670	1790	2080	2380	2980
	80	1520	1440	-	-	2300	2020	1730	1730	1870	2020	2160	2520	2680	3600
	90	1850	1760	-	-	2820	2460	2110	2110	2290	2460	2640	3080	3520	-
	100	2300	2180	-	-	-	3050	2620	2620	2830	3050	3270	3820	4360	-
	110	2550	2420	-	-	-	-	2900	2900	3150	3390	3630	4240	-	-
Chord Moment (3)	0	11400	13020 (2)	-	-	-	-	-	-	-	-	-	-	-	-
	10	10100	12220	-	-	-	17110	14470	14470	15890	17110	18330	21390	24440	-
	20	10200	11650	-	-	18640	16310	13980	13980	15150	16310	17480	20390	23300	-
	30	9400	10730	-	19310	17170	15020	12880	12880	13950	15020	16100	18780	21460	26830
	50	9000	10280	20560	18500	15450	14390	12340	12340	13360	14390	15420	17990	20560	25700
	70	9800	11200	-	20160	17920	15680	13440	13440	14560	15680	16800	19600	22400	28000
	80	10400	11880	-	-	19010	16630	14260	14260	15440	16630	17820	20790	23760	29700
	90	11400	13020	-	-	20830	18230	15620	15620	16930	18230	19530	22790	26040	-
	100	13000	14840	-	-	-	20780	17810	17810	19290	20780	22260	25970	29680	-
	110	15000	17130	-	-	-	-	20500	20560	22270	23980	25700	29980	-	-

(1) Baseline x 1.067 x 0.89
(2) Baseline x 1.067 x 1.07
(3) Reference Station 60

TABLE 39. MISCELLANEOUS LOADS

Condition		Chord BM (in.-lb)	Flap BM (in.-lb)
Sideward Flight		17030	1220
Rearward Flight		14580	1030
Control Reversals			
Hover	Long.	16300	465
	Lat	8010	365
	Dir	6410	425
V_H	Long.	22800	2220
	Lat	27290	2165
	Dir	14230	1685
Auto Rotational	Long.	7720	1185
	Lat	16460	1010
	Dir	4380	805

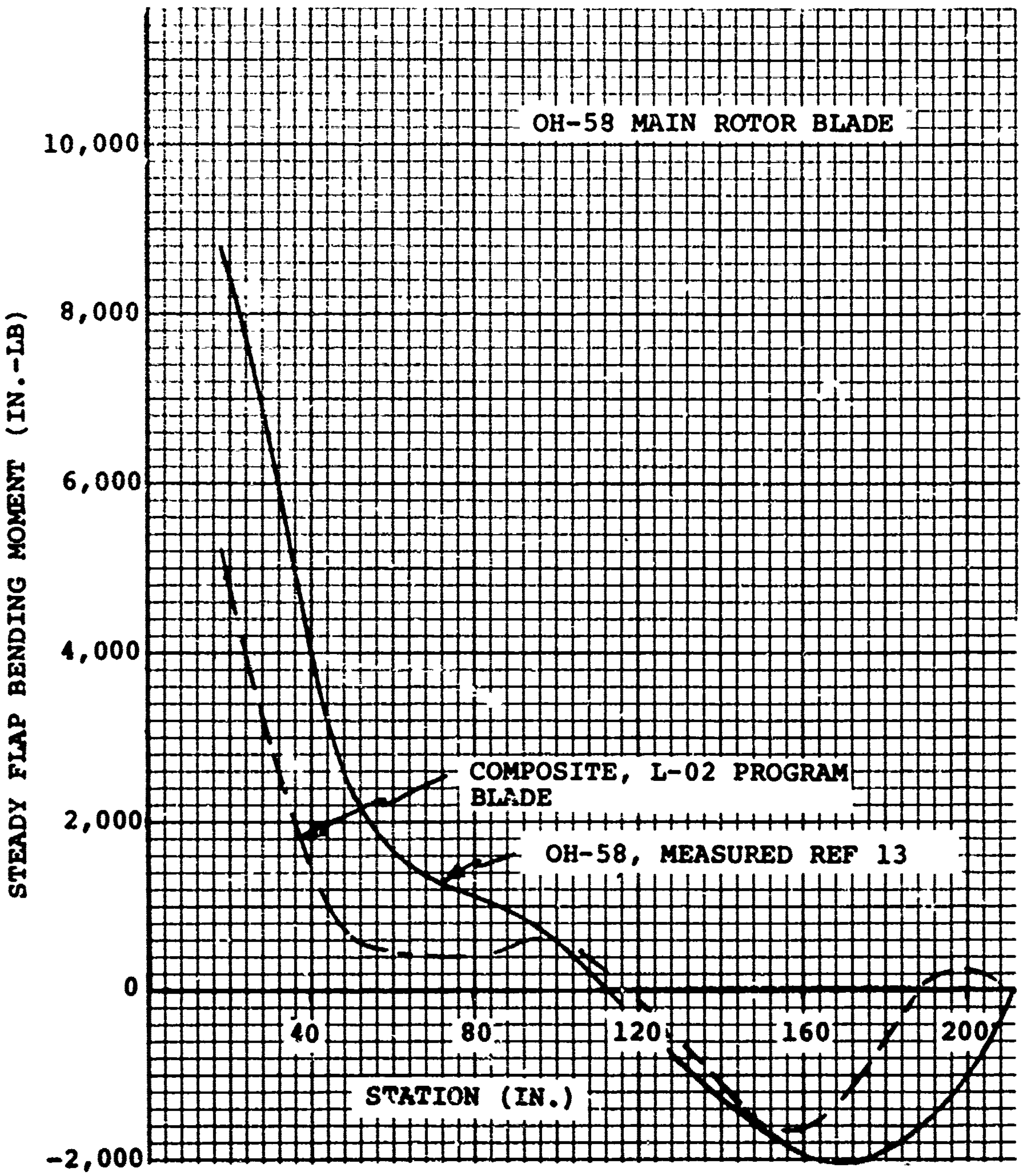

Figure 112. Steady Flap Bending Moment-Spanwise Distribution

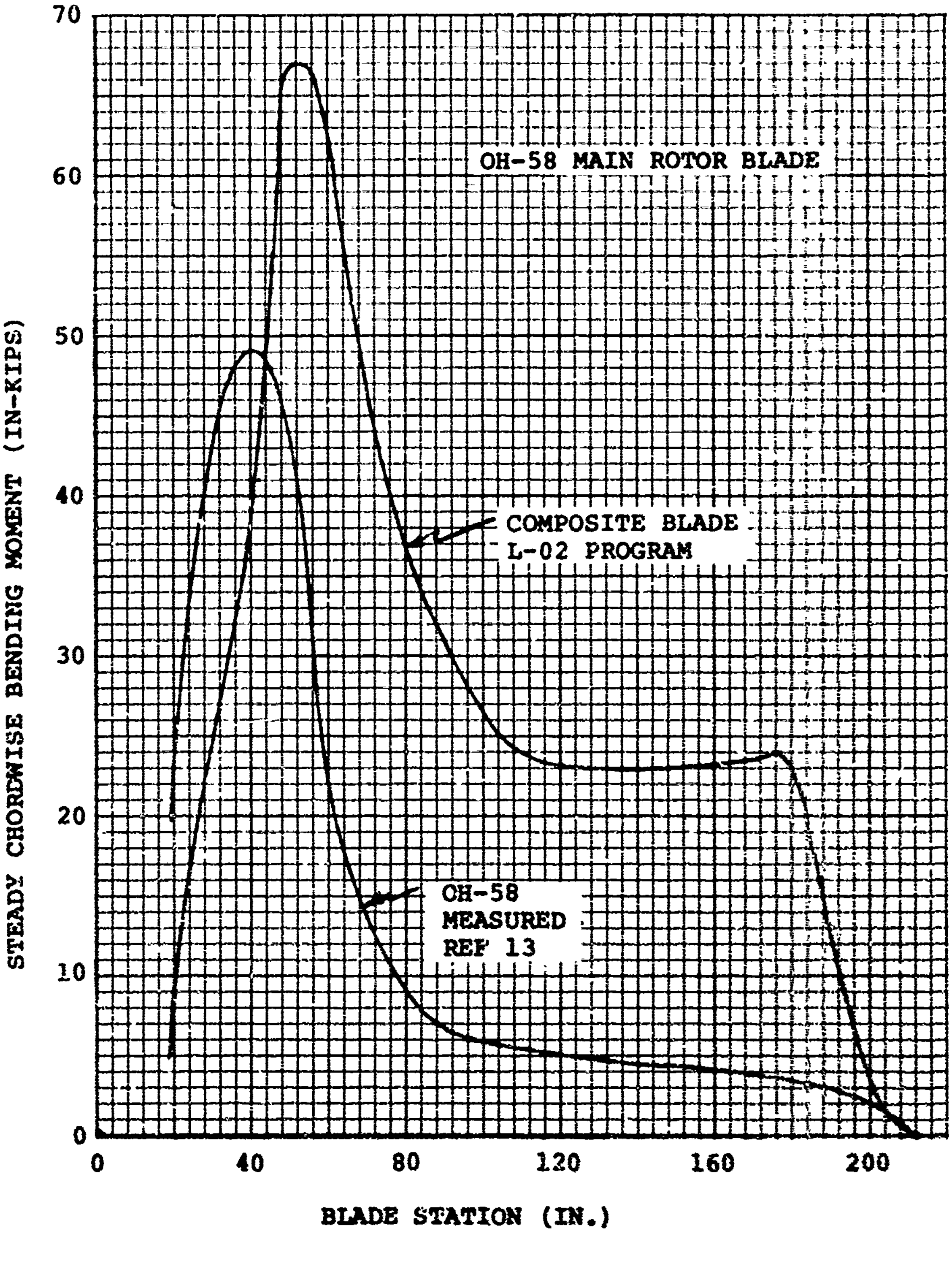

Figure 113. Steady Chord Bending Moment Spanwise Distribution

the further-aft neutral axis of the composite blade. Again for conservatism, the higher of the two is used for design substantiation. Centrifugal force is shown in Figure 114.

Life versus endurance limit trends have been calculated using the flight profile (Table 36), the fatigue loads (Table 38) and the fatigue curve shapes for S-Glass and Kevlar 49 (Figure 115). The plots of life versus endurance limit are shown in Figure 116. A design fatigue load factor of 1.25 is chosen for both materials and loading modes.

4.7.4 Failsafety

The primary means of attaining fail-safety in the OH-58 C/A composite blade is by the proven soft failure mode of fiberglass. For the primary blade section and blade retention at the pin wrap, it is anticipated that unidirectional Kevlar will prove to have a similar soft failure mode.

All weights located within the spar are bonded with a mechanical backup system. The teeter weight canister and the inertia weights can be retained by the wedging action of the tapered spar at the tip. The mid-span turning weights are provided with a fiberglass stop just outboard of the weights.

The sweep balance weights are retained by three lugs, only two of which are required to retain the weights.

The tip section is bonded to the main blade assembly and provided with two through mechanical fasteners for redundancy.

Cracks in the aft fairing will propagate, at the 45° bias of the material, ending at the spar heel. The only nonredundant area is the bond of the aft fairing to the spar heel. However, Boeing Vertol composite blades built in this manner have never incurred a failure.

4.7.5 Stress Analyses

The following stress analyses are presented to substantiate structural integrity in sufficient detail to confirm the feasibility of the design concepts.

4.7.5.1 Basic Airfoil Section

The basic airfoil section extends from Station 80 outboard to the tip. From Station 80 inboard to Station 53, unidirectional Kevlar is added to the trailing-edge wedge to increase the chordwise stiffness. This results in an aftward shift in the neutral axis and a rapid increase in chord moment due to the increase C.F. offset. From Station 53 inboard, the spar packs

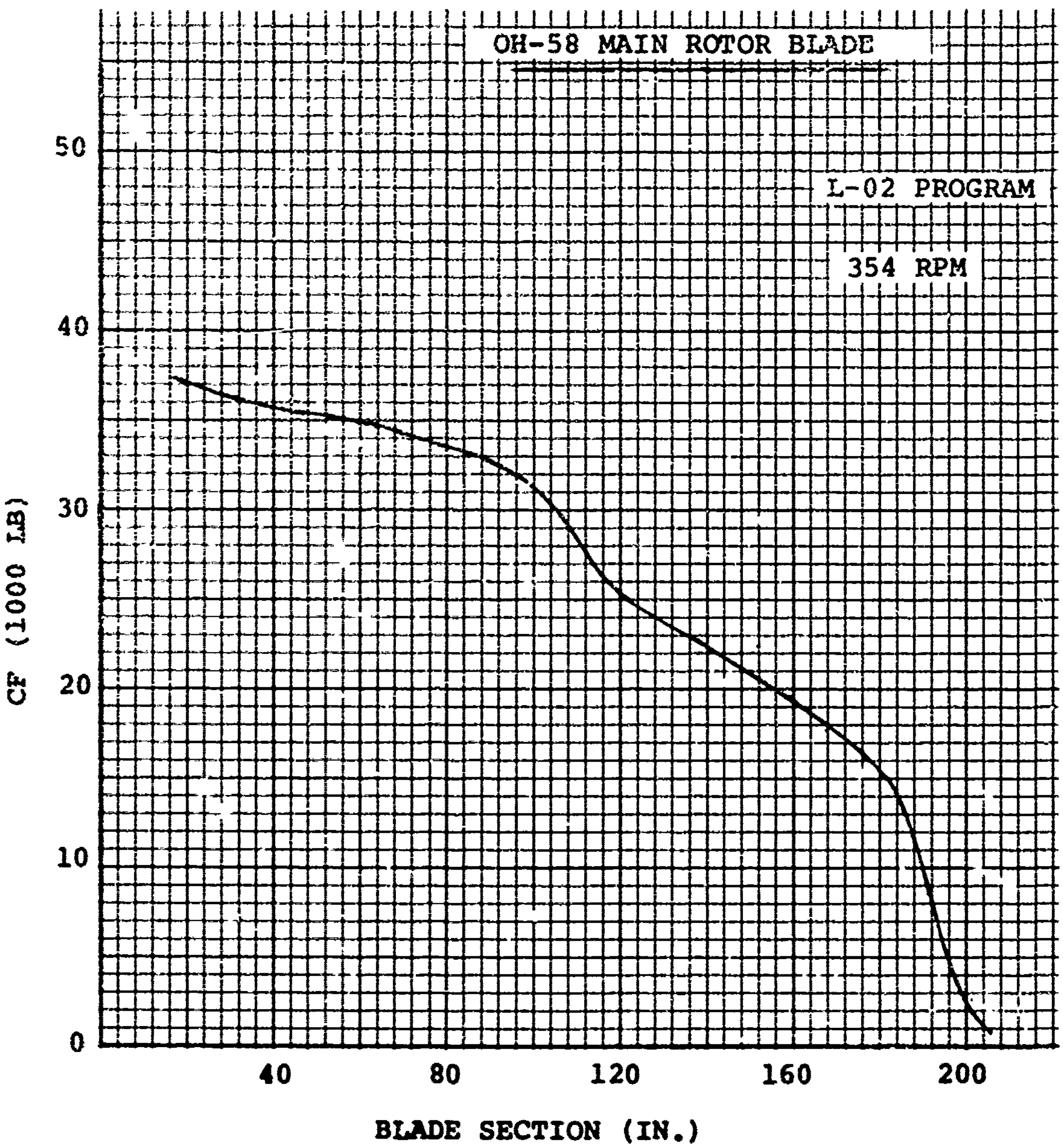

Figure 114. Spanwise Distribution of Centrifugal Force-Composite Blade

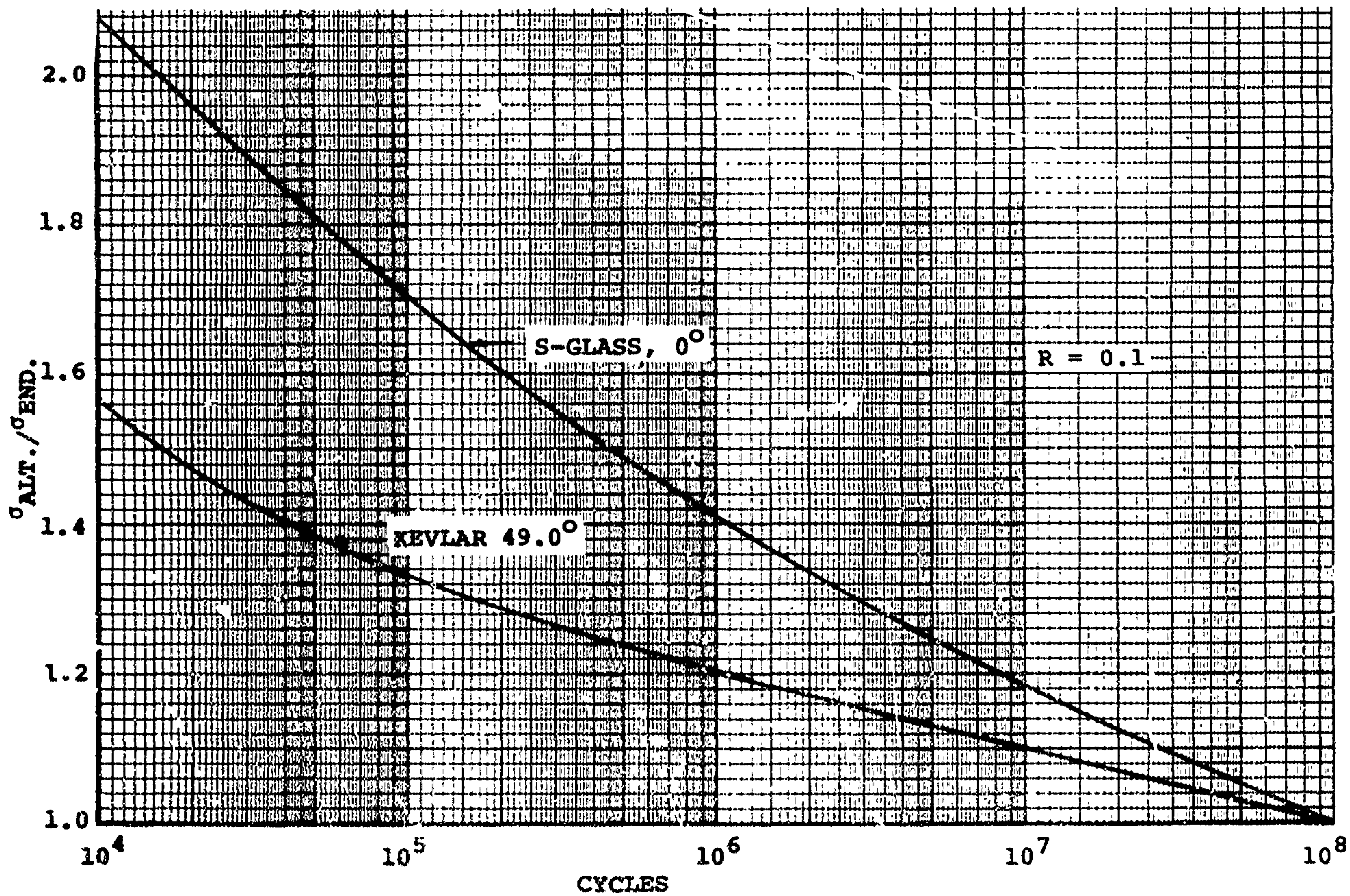

Figure 115. Fatigue Curve Shapes for S-Glass and Kevlar 49

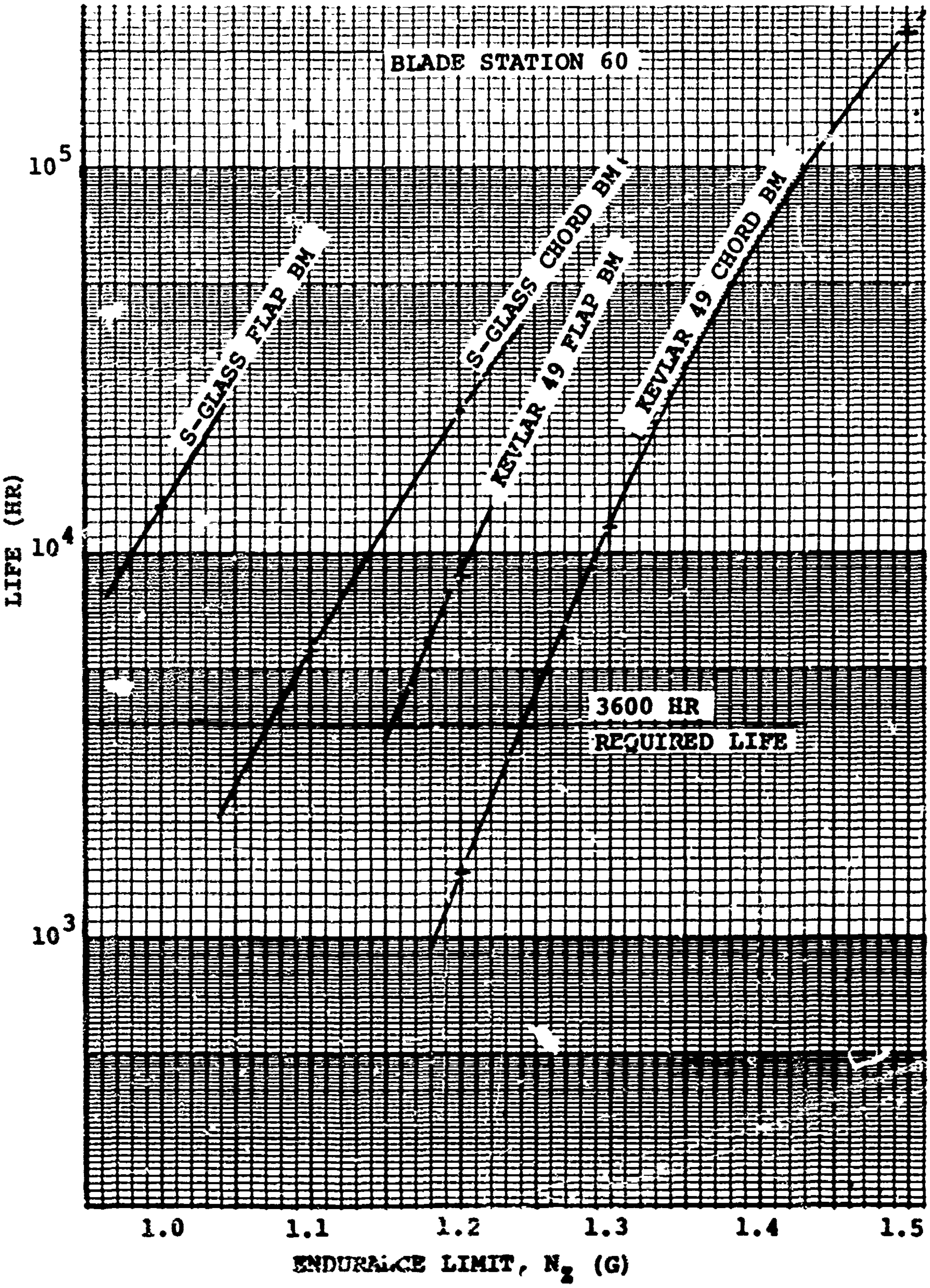

Figure 116. Life Vs. Endurance Limit Curves

are increased for flapwise stiffness and strength to attain the material required for a positive structural margin at the retaining pin.

Two blade sections are examined for strength. Station 53 is checked for the static limit load cases. Station 60 is checked for fatigue, conservatively, using Station 80 properties (i.e., no TE buildup) and Station 60 loads. The upper surface of the spar is analyzed for the effects of local pressure which causes stresses transverse to the primary direction of the spar pack filaments.

The aft fairing is a full-depth sandwich wedge extending aft of the spar heel at 42% chord. The core and faces are analyzed for the net upper and lower surface steady and alternating loads.

Large margins of safety are calculated for static strength and for the 3600-hour fatigue requirement, using the conservative methods and assumptions previously stated. Based on the margins calculated, an unlimited life of the basic blade section is anticipated.

4.7.5.2 Blade Retention Area

The blade is attached to the hub in the same manner as the baseline OH-58 blade. The flap bending moment and centrifugal force loads are reacted at the main pin through the pin wrap of S-Glass material that builds up from the upper and lower spar packs. The chord bending moment is reacted as a couple between the latches and the main retention pin. The Kevlar 49 nose and heel material is extended inboard of the main pin to the blade latch at Station 12.5.

The large margins of safety for the fatigue conditions indicate a probable unlimited life. The relatively low margins of safety for the ultimate loads result from the low compression strength of Kevlar 49. These strengths are derived from small coupon tests. Bending strengths of large thick sections have historically shown higher strengths in tests of composite materials.

5.0 CONCLUSIONS

1. Most of the features desired in a composite replacement blade can be attained. Among them are compatibility with existing hardware, and the objectives stipulated for structures, dynamics, performance, reliability and maintainability, and survivability. A 6% reduction in hover power required can be attained without a significant reduction in forward flight performance. All areas of the blade are invulnerable to the defined ballistic threats.

2. Some of the desired features can be achieved in part. Among them are the cost and the radar reflectivity objectives. It is felt that the $3400/blade recurring cost is unachievable, but a life cycle cost saving, based on a realistic blade cost, can be achieved by increasing the planned service period beyond the projected 10 year period or with an increase in the projected 13 hours/month utilization rate. A considerable improvement can be achieved in radar cross section (RCS), approaching, but falling short of, the desired levels.

3. The selected blade concept does not include some of the desired features. Among them are increased rotor inertia, and the least risk approach of matching all existing blade physical properties, without sacrificing the other desired objectives. An increase in rotor inertia is limited by reduced fatigue life of the tie bar assembly. Matching all existing blade physical properties is the lowest risk approach, but it requires extensive use of graphite, which adds to the cost, reduces reliability and maintainability, and prohibits any improvement in radar reflectivity.

4. Although the radar reflectivity objectives are nearly achievable, their inclusion significantly influences the choice of the design concept, sacrificing other objectives to a limited extent. Consideration should be given to retaining this requirement in the production proposal based on how much RCS significant improvement is to be accomplished on the rest of the helicopter, particularly on the hub, and what an improved RCS blade will mean to the total aircraft RCS.

5. A development program is recommended for the Estane/pneumatic leading edge boot. This should include an erosion test to verify the 1200-flight-hour requirement and functional testing to resolve any problems which may result from using this system on a helicopter rotor blade.

6.0 REFERENCES

1. MAY 1973 WIND TUNNEL TEST OF A 1/9 SCALE YUH-61A DYNAMIC MODEL FOR AEROELASTIC STABILITY, Boeing Vertol Company, D179-10395-1, August 14, 1973.

2. Saaty, T.L., A SCALING METHOD FOR PRIORITIES IN HIERARCHICAL STRUCTURES, Journal of Mathematical Psychology 15, 111-111, 1977.

3. Saaty, T.L., HIERARCHIES AND PRIORITIES - EIGENVALUE ANALYSIS, University of Pennsylvania, 1975.

4. Saaty, T.L. and Khouja, M., A MEASURE OF WORLD INFLUENCE, Peace Science, June 1976.

5. Stevens, W.A., Goradia, S.H., and Braden, J.A., MATHEMATICAL MODEL FOR TWO-DIMENSIONAL MULTI-COMPONENT AIRFOILS IN VISCOUS FLOW, NASA CR-1843, July 1971.

6. Bauer, F., Garabedian, P., Korn, D., and Jameson, A., SUPERCRITICAL WING SECTIONS II, Lecture Notes in Economics and Mathematical Systems, Volume 108, Springer-Verlag, New York, 1975.

7. Dadone, L., and McMullen, J., HLH/ATC ROTOR SYSTEM TWO-DIMENSIONAL AIRFOIL TEST, Boeing Vertol Company, D301-10071-1, December 1971.

8. Dadone, L. U., U.S. ARMY HELICOPTER DATCOM, VOLUME 1 - AIRFOILS, USAAMRDL CR 76-2, September 1976, AD A033425.

9. Blewitt, S.J., PRODUCT IMPROVEMENT PROGRAM EVALUATION, USAAMRDL-TR-77-17, U.S. Army Air Mobility Research and Development Laboratory, Ft. Eustis, Virginia, June 1977, ADA042134.

10. DESIGN DATA FOR COMPOSITE STRUCTURE SAFE LIFE PREDICTION Boeing Vertol Company, AFML-TR-73-223.

11. EVALUATION OF BALLISTIC DAMAGE RESISTANCE AND FAILURE MECHANISMS OF COMPOSITE MATERIALS, AVCO Corporation, AFML-TR-72-79.

12. PROPOSAL FOR A TRADE STUDY AND PRELIMINARY DESIGN OF AN ADVANCED COMPOSITE ROTOR BLADE FOR THE OH-58C/A HELICOPTER, Boeing Vertol Company, D210-11287-1, in response to RFQ DAAJ02-77-Q-0143.

13. MODEL 206A-1 CERTIFICATION FLIGHT LOAD SURVEY (6 Volumes), Bell Helicopter Company, 206-194-062, August 1969.

14. LOAD DETERMINATION AND STRUCTURAL ANALYSIS OF THE 206-011-001-3 MAIN ROTOR HUB AND BLADE ASSEMBLY FOR THE 206A-1 HELICOPTER Rev. C, Bell Helicopter Company, 206-099-107, October 1977.

15. FATIGUE LIFE SUBSTANTIATION FOR THE DYNAMIC COMPONENTS OF THE MODEL 206A-1 HELICOPTER Rev. H, Bell Helicopter Company, 206-099-114.

16. YUH-61A HELICOPTER FLIGHT LOADS SURVEY REPORT, Contract DAAJ01-72-C-0007 (PGA), Boeing Vertol Company, T179-10142-2.

APPENDIX A
AIRFOIL DATA

VR-7, -3° Tab, OH-58A Reynolds Numbers

```
375 375  VR-7 (-3 DEG TAB), OH-58         RKM/LP  11/11/77

     190.       110.  MAX POS ALPHA,MAX NEG ALPHA

   CLINC        K1           K2           K3           K4       CONTROL NOS.
    0.0  9     1.000       1.0000       1.0000       1.0000

     9 NO.OF MACH NUMBERS FOR CL VS ALPHA
      MACH NUMBERS
    0.000      0.300      0.400      0.500      0.600      0.710      0.740
    0.820      1.000

************************  LIFT TABLE  ******************************

  15        ALPHA-CL PAIRS FOR MACH NUM.=      0.000
ALPHA
     0.000      8.000     10.000     11.000     12.000     13.000     14.000
    16.000     20.000    340.000    350.000    352.000    356.000    358.000
   360.000
CL
  0.110000  0.960000  1.175000  1.260000  1.320000  1.360000  1.320000
  1.225000  1.120000 -0.800000 -0.760000 -0.660000 -0.320000 -0.110000
  0.110000

  15        ALPHA-CL PAIRS FOR MACH NUM.=      0.300
ALPHA
     0.000      8.000     10.000     11.000     12.000     13.000     14.000
    16.000     20.000    340.000    350.000    352.000    356.000    358.000
   360.000
CL
  0.110000  0.960000  1.175000  1.260000  1.320000  1.360000  1.320000
  1.225000  1.120000 -0.800000 -0.760000 -0.660000 -0.320000 -0.110000
  0.110000

  15        ALPHA-CL PAIRS FOR MACH NUM.=      0.400
ALPHA
     0.000      9.000     10.000     11.000     12.000     13.000     14.000
    17.000     20.000    340.000    350.000    352.000    356.000    358.000
   360.000
CL
  0.125000  1.025000  1.240000  1.325000  1.370000  1.370000  1.250000
  1.070000  0.970000 -0.800000 -0.750000 -0.670000 -0.330000 -0.100000
  0.125000

  12        ALPHA-CL PAIRS FOR MACH NUM.=      0.500
ALPHA
     0.000      9.700     10.000     11.000     11.800     12.000     20.000
   340.000    350.000    352.000    356.000    358.000    360.000
CL
  0.135000  1.290000  1.335000  1.430000  1.500000  1.350000  1.160000
 -0.800000 -0.760000 -0.660000 -0.330000 -0.090000  0.135000

  15        ALPHA-CL PAIRS FOR MACH NUM.=      0.600
ALPHA
     0.300      6.400      7.300      8.000      9.000     10.000     11.000
    12.000     20.000    340.000    350.000    352.000    356.000    358.000
   360.000
CL
  0.165000  1.050000  1.100000  1.150000  1.175000  1.210000  1.235000
```

THIS PAGE IS BEST QUALITY PRACTICABLE
FROM COPY FURNISHED TO DDC

```
 1.240000  1.200000 -0.800000 -0.720000 -0.670000 -0.330000 -0.095000
 0.165000

    9       ALPHA-CL PAIRS FOR MACH NUM.=      0.710
ALPHA
    0.000     3.200     8.500    20.000   340.000   350.000   355.000
  358.000   360.000
CL
 0.220000  0.700000  1.000000  1.470000 -0.800000 -0.750000 -0.500000
-0.095000  0.220000

   13       ALPHA-CL PAIRS FOR MACH NUM.=      0.740
ALPHA
    0.000     1.000     2.000     4.000    10.000    20.000   340.000
  350.000   352.000   354.000   355.000   356.000   360.000
CL
 0.270000  0.410000  0.500000  0.670000  1.050000  1.420000 -0.800000
-0.750000 -0.700000 -0.680000 -0.600000 -0.440000  0.270000

   11       ALPHA-CL PAIRS FOR MACH NUM.=      0.820
ALPHA
    0.000     1.100     8.000    15.200    20.000   340.000   350.000
  354.000   355.500   357.000   360.000
CL
 0.130000  0.300000  0.960000  1.400000  1.550000 -1.000000 -0.680000
-0.450000 -0.200000 -0.330000  0.130000

    6       ALPHA-CL PAIRS FOR MACH NUM.=      1.000
ALPHA
    0.000     4.000    20.000   340.000   356.000   360.000
CL
 0.110000  0.600000  0.600000 -0.300000 -0.300000  0.110000
```

```
375 375  VR-7 (-3 DEG TAB), OH-58        RKP/LD  11/11/77

********   *************  DRAG TABLE  ******************************

MAXIMUM POS-NEG ANGLES IN CD-M TABLES
     16.000   350.000

        21        ALPHA VALUES FOR CD VS M
         ALPHA
     0.000     1.000     2.000     3.000     4.000     5.000     6.000
     7.000     8.000     9.000    10.000    11.000    12.000    13.000
    16.000   350.000   355.000   357.000   358.000   359.000   360.000

   10          M-CD PAIRS FOR ALPHA =      0.000
 MACH
     0.000     0.300     0.404     0.505     0.610     0.660     0.710
     0.760     0.850     1.000
 CD
   0.010000  0.009000  0.008600  0.008400  0.008800  0.009200  0.011000
   0.035500  0.100000  0.100000

   10          M-CD PAIRS FOR ALPHA =      1.000
 MACH
     0.000     0.300     0.404     0.505     0.610     0.660     0.710
     0.760     0.832     1.000
 CD
   0.010000  0.009000  0.008600  0.008100  0.008800  0.009500  0.016400
   0.052500  0.100000  0.100000

   10          M-CD PAIRS FOR ALPHA =      2.000
 MACH
     0.000     0.300     0.404     0.505     0.610     0.660     0.710
     0.745     0.815     1.000
 CD
   0.010000  0.009000  0.008600  0.008100  0.008800  0.010200  0.032500
   0.055000  0.100000  0.100000

    9          M-CD PAIRS FOR ALPHA =      3.000
 MACH
     0.000     0.300     0.404     0.505     0.610     0.660     0.710
     0.785     1.000
 CD
   0.010500  0.009200  0.008700  0.008100  0.009000  0.013200  0.047500
   0.100000  0.100000

    8          M-CD PAIRS FOR ALPHA =      4.000
 MACH
     0.000     0.300     0.404     0.505     0.610     0.660     0.775
     1.000
 CD
   0.011500  0.009500  0.008900  0.008300  0.009450  0.020500  0.100000
   0.100000

    8          M-CD PAIRS FOR ALPHA =      5.000
 MACH
     0.000     0.300     0.404     0.505     0.610     0.660     0.750
     1.000
 CD
   0.012900  0.009800  0.009500  0.008800  0.010700  0.036500  0.100000
```

```
  0.100000

     8          M-CD PAIRS FOR ALPHA =      6.000
MACH
     0.000      0.300      0.404      0.505      0.610      0.660      0.705
     1.000
CD
  0.012500  0.010200  0.010100  0.009600  0.017500  0.065000  0.100000
  0.100000

     7          M-CD PAIRS FOR ALPHA =      7.000
MACH
     0.000      0.300      0.404      0.505      0.610      0.685      1.000
CD
  0.013000  0.011400  0.011300  0.010700  0.042500  0.100000  0.100000

     7          M-CD PAIRS FOR ALPHA =      8.000
MACH
     0.000      0.300      0.404      0.505      0.525      0.650      1.000
CD
  0.015000  0.012800  0.012600  0.011600  0.012500  0.100000  0.100000

     6          M-CD PAIRS FOR ALPHA =      9.000
MACH
     0.000      0.300      0.404      0.500      0.620      1.000
CD
  0.016000  0.014300  0.014500  0.014600  0.100000  0.100000

     6          M-CD PAIRS FOR ALPHA =     10.000
MACH
     0.000      0.300      0.404      0.475      0.596      1.000
CD
  0.017500  0.016200  0.018000  0.019000  0.100000  0.100000

     6          M-CD PAIRS FOR ALPHA =     11.000
MACH
     0.000      0.300      0.404      0.465      0.570      1.000
CD
  0.019000  0.018500  0.025000  0.028800  0.100000  0.100000

     6          M-CD PAIRS FOR ALPHA =     12.000
MACH
     0.000      0.300      0.404      0.467      0.540      1.000
CD
  0.023500  0.022500  0.037500  0.046700  0.100000  0.100000

     5          M-CD PAIRS FOR ALPHA =     13.000
MACH
     0.000      0.300      0.400      0.450      1.000
CD
  0.035000  0.032500  0.062000  0.100000  0.100000

     2          M-CD PAIRS FOR ALPHA =     16.000
MACH
     0.000      1.000
CD
  0.120000  0.100000

     2          M-CD PAIRS FOR ALPHA =    350.000
MACH
```

```
     0.9 0       1.000
CD
   0.150000   0.100000

     6          M-CD PAIRS FOR ALPHA =    355.000
MACH
     0.000       0.400       0.5 0       0.610       0.740       1.000
CL
   0.020000   0.027000   0.037000   0.045000   0.100000   0.120000

     9          M-CD PAIRS FOR ALPHA =    357.000
MACH
     0.000       0.300       0.4 0       0.5 0       0.610       0.710       0.760
     0.860       1.000
CD
   0.011000   0.009500   0.009400   0.011000   0.011500   0.022500   0.035000
   0.100000   0.100000

     9          M-CD PAIRS FOR ALPHA =    358.000
MACH
     0.000       0.300       0.400       0.500       0.610       0.710       0.760
     0.865       1.000
CD
   0.010000   0.009000   0.008900   0.009600   0.010000   0.013800   0.021000
   0.100000   0.100000

    10          M-CD PAIRS FOR ALPHA =    359.000
MACH
     0.000       0.300       0.404       0.505       0.610       0.660       0.710
     0.760       0.875       1.000
CD
   0.009500   0.009000   0.008700   0.008600   0.009200   0.009600   0.009800
   0.020000   0.100000   0.100000

    10          M-CD PAIRS FOR ALPHA =    360.000
MACH
     0.000       0.300       0.404       0.505       0.610       0.660       0.710
     0.760       0.850       1.000
CD
   0.010000   0.009000   0.008600   0.008400   0.008800   0.009200   0.011000
   0.035500   0.100000   0.100000
```

```
375 375  VR-7 (-3 DEG TAB), OH-58          RKM/LP  11/11/77

 *********************  PITCHING MOMENT TABLE  **************************

 VALUES OF CM FOR MAXIMUM POS-NEG ANGLES
     -0.200       0.140

        19        ALPHA VALUES FOR CM VS M
          ALPHA
      0.000      1.000      2.000      3.000      4.000      6.000      7.000
      8.000     10.000     11.800     12.000     14.000     15.000     16.000
    344.000    354.000    356.000    358.000    360.000

    11          M-CM PAIRS FOR ALPHA =        0.000
 MACH
      0.000      0.300      0.400      0.500      0.550      0.610      0.680
      0.740      0.800      0.900      1.000
 CM
  -0.009000 -0.009000 -0.010000 -0.012000 -0.014000 -0.015000 -0.018000
  -0.040000 -0.108000 -0.100000 -0.092000

    11          M-CM PAIRS FOR ALPHA =        1.000
 MACH
      0.000      0.300      0.400      0.500      0.550      0.610      0.680
      0.740      0.800      0.900      1.000
 CM
  -0.011000 -0.011000 -0.012000 -0.015000 -0.018000 -0.018000 -0.021000
  -0.062000 -0.109000 -0.130000 -0.151000

    11          M-CM PAIRS FOR ALPHA =        2.000
 MACH
      0.000      0.300      0.400      0.500      0.550      0.610      0.680
      0.740      0.800      0.900      1.000
 CM
  -0.014000 -0.014000 -0.015000 -0.017500 -0.020000 -0.021000 -0.027000
  -0.075000 -0.112000 -0.150000 -0.186000

    11          M-CM PAIRS FOR ALPHA =        3.000
 MACH
      0.000      0.300      0.400      0.500      0.550      0.610      0.680
      0.740      0.800      0.900      1.000
 CM
  -0.017000 -0.017000 -0.018000 -0.021000 -0.023000 -0.024000 -0.035000
  -0.082000 -0.120000 -0.178000 -0.236000

    11          M-CM PAIRS FOR ALPHA =        4.000
 MACH
      0.000      0.300      0.400      0.500      0.550      0.610      0.680
      0.740      0.800      0.900      1.000
 CM
  -0.020000 -0.020000 -0.022000 -0.023000 -0.025500 -0.026500 -0.055000
  -0.089000 -0.128000 -0.200000 -0.270000

    10          M-CM PAIRS FOR ALPHA =        6.000
 MACH
      0.000      0.300      0.400      0.500      0.550      0.610      0.680
      0.740      0.800      1.000
 CM
  -0.028000 -0.028000 -0.027000 -0.028000 -0.029000 -0.028000 -0.077000
```

```
 -0.100000 -0.148000 -0.310000

   10         M-CM PAIRS FOR ALPHA =      7.000
MACH
     0.000      0.300      0.400      0.500      0.550.     0.610      0.680
     0.740      0.800      1.000
CM
 -0.032000 -0.032000 -0.030000 -0.030000 -0.029000 -0.034000 -0.086000
 -0.109000 -0.158000 -0.320000

   10         M-CM PAIRS FOR ALPHA =      8.000
MACH
     0.000      0.300      0.400      0.500      0.550      0.610      0.680
     0.740      0.800      1.000
CM
 -0.035000 -0.035000 -0.032000 -0.032000 -0.027000 -0.051000 -0.092000
 -0.114000 -0.170000 -0.350000

   10         M-CM PAIRS FOR ALPHA =     10.000
MACH
     0.000      0.300      0.400      0.500      0.550      0.610      0.680
     0.740      0.800      1.000
CM
 -0.039000 -0.039000 -0.035000 -0.029000 -0.022000 -0.072000 -0.105000
 -0.127000 -0.190000 -0.350000

   10         M-CM PAIRS FOR ALPHA =     11.800
MACH
     0.000      0.300      0.400      0.500      0.550      0.610      0.680
     0.740      0.800      1.000
CM
 -0.042000 -0.042000 -0.036000 -0.017000 -0.045000 -0.084000 -0.115000
 -0.139000 -0.210000 -0.350000

   10         M-CM PAIRS FOR ALPHA =     13.000
MACH
     0.000      0.300      0.400      0.500      0.550      0.610      0.680
     0.740      0.800      1.000
CM
 -0.045000 -0.045000 -0.058000 -0.045000 -0.066000 -0.092000 -0.121000
 -0.145000 -0.220000 -0.350000

    4         M-CM PAIRS FOR ALPHA =     14.000
MACH
     0.000      0.400      0.800      1.000
CM
 -0.044000 -0.064000 -0.280000 -0.380000

   10         M-CM PAIRS FOR ALPHA =     15.000
MACH
     0.000      0.300      0.400      0.500      0.550      0.610      0.680
     0.740      0.800      1.000
CM
 -0.078000 -0.078000 -0.075000 -0.089000 -0.099000 -0.118000 -0.141000
 -0.176000 -0.250000 -0.350000

    2         M-CM PAIRS FOR ALPHA =     16.000
MACH
     0.000      1.000
CM
```

```
 -0.080000 -0.080000

    2          M-CM PAIRS FOR ALPHA =     344.000
MACH
     0.000      1.000
CM
  0.140000  0.140000

   11          M-CM PAIRS FOR ALPHA =     354.000
MACH
     0.000      0.300      0.400      0.500      0.550      0.610      0.680
     0.740      0.800      0.900      1.000
CM
 -0.002000 -0.002000 -0.00[illegible] -0.006000 -0.006000 -0.005000  0.005000
  0.010000  0.012000  0.020000  0.040000

   11          M-CM PAIRS FOR ALPHA =     356.000
MACH
     0.000      0.300      0.400      0.500      0.550      0.610      0.680
     0.740      0.800      0.900      1.000
CM
 -0.001000 -0.001000 -0.003000 -0.007000 -0.011000 -0.014000 -0.021000
 -0.024000 -0.032000 -0.015000  0.002000

   11          M-CM PAIRS FOR ALPHA =     358.000
MACH
     0.000      0.300      0.400      0.500      0.550      0.610      0.680
     0.740      0.800      0.900      1.000
CM
 -0.0[illegible] -0.0[illegible] -0.006000 -0.008000 -0.010000 -0.011000 -0.016000
 -0.024000 -0.0[illegible] -0.056000 -0.062000

   11          M-CM PAIRS FOR ALPHA =     360.000
MACH
     0.000      0.300      0.400      0.500      0.550      0.610      0.680
     0.740      0.800      0.900      1.000
CM
 -0.009000 -0.009000 -0.010000 -0.012000 -0.014000 -0.015000 -0.018000
 -0.040000 -0.106000 -0.[illegible] -0.092000
```

0012 Baseline Data Corrected to Turbulence Level of VR-7/VR-8 Data

37(37F (012 (T374) CORR. TO OH-58 LEVEL IN RSVT(RY Y-30) 11/77

INC. INC. MAX POS ALPHA.MAX NEG ALPHA

CHORD	K1	K2	K3	K4	CONTROL NOS.
0.0000	1.0000	1.0000	1.0000	1.0000	

11 NO.OF MACH NUMBERS FOR CL VS ALPHA
MACH NUMBERS

0.000	0.200	0.300	0.400	0.500	0.600	0.700
0.750	0.800	0.900	1.000			

************************ LIFT TABLE ******************************

26 ALPHA-CL PAIRS FOR MACH NUM.= 0.000

ALPHA

0.000	2.000	4.000	6.000	8.000	10.000	11.000
12.000	13.000	14.000	15.000	16.500	20.000	340.000
343.500	345.000	346.000	347.000	348.000	349.000	350.000
352.000	354.000	356.000	358.000	360.000		

CL

0.000000	0.230000	0.450000	0.700000	0.890000	1.080000	1.150000
1.210000	1.230000	1.250000	1.140000	1.007000	0.850000	-0.850000
-1.007000	-1.140000	-1.250000	-1.230000	-1.210000	-1.15[illegible]	-1.080000
-0.890000	-0.700000	-0.450000	-0.230000	0.000000		

26 ALPHA-CL PAIRS FOR MACH NUM.= 0.200

ALPHA

0.000	2.000	4.000	6.000	8.000	10.000	11.000
12.000	13.000	14.000	15.000	16.500	20.000	340.000
343.500	345.000	346.000	347.000	348.000	349.000	350.000
352.000	354.000	356.000	358.000	360.000		

CL

0.000000	0.230000	0.450000	0.700000	0.890000	1.080000	1.161000
1.255000	1.334000	1.333000	1.140000	1.007000	0.850000	-0.850000
-1.007000	-1.140000	-1.333000	-1.334000	-1.255000	-1.161000	-1.080000
-0.890000	-0.700000	-0.450000	-0.230000	0.000000		

26 ALPHA-CL PAIRS FOR MACH NUM.= 0.300

ALPHA

0.000	2.000	4.000	6.000	8.000	10.000	11.000
12.000	13.000	14.000	15.000	16.500	20.000	340.000
343.500	345.000	346.000	347.000	348.000	349.000	350.000
352.000	354.000	356.000	358.000	360.000		

CL

0.000000	0.230000	0.450000	0.700000	0.890000	1.080000	1.190000
1.260000	1.280000	1.220000	1.140000	0.944000	0.840000	-0.840000
-0.944000	-1.140000	-1.220000	-1.280000	-1.260000	-1.190000	-1.080000
-0.890000	-0.700000	-0.450000	-0.230000	0.000000		

26 ALPHA-CL PAIRS FOR MACH NUM.= 0.400

ALPHA

0.000	2.000	4.000	6.000	8.000	10.000	11.000
12.000	13.000	14.000	15.000	16.500	20.000	340.000
343.500	345.000	346.000	347.000	348.000	349.000	350.000
352.000	354.000	356.000	358.000	360.000		

CL

0.000000	0.240300	0.491600	0.722400	0.941600	1.055300	1.120000
1.130000	1.120000	0.897500	1.010000	0.960000	0.860000	-0.860000

```
-[illegible] -1.11[illegible] -0.897[illegible] -1.12[illegible] -1.130[illegible]0 -1.120000 -1.033300
-0.941[illegible] -0.722400 -0.491600 -0.240300  0.000000

  26        ALPHA-CL PAIRS FOR MACH NUM.=       0.5[illegible]
ALPHA
   [illegible]    2.000     4.[illegible]     6.000     8.000    10.000    11.000
  12.[illegible]   13.[illegible]   14.[illegible]   15.000    16.500    20.000   340.000
 343.500   345.000   346.000   347.000   348.000   349.000   350.000
 352.000   354.000   356.000   358.000   360.000
CL
 0.000000  0.250000  0.510000  0.750000  0.922000  0.985000  0.994000
 1.000000  1.000000  1.000000  0.990000  0.965000  0.880000 -0.880000
-0.965000 -0.990000 -1.000000 -1.000000 -1.000000 -0.994000 -0.985000
-0.922000 -0.750000 -0.510000 -0.250000  0.000000

  26        ALPHA-CL PAIRS FOR MACH NUM.=       0.600
ALPHA
   0.000     2.000     4.000     6.000     8.000    10.000    11.000
  12.000    13.000    14.000    15.000    16.500    20.000   340.000
 343.500   345.000   346.000   347.000   348.000   349.000   350.000
 352.000   354.000   356.000   358.000   360.000
CL
 0.000000  0.271000  0.573100  0.796700  0.871100  0.880200  0.930000
 0.947000  0.960000  0.970000  0.9[illegible]  0.965000  0.875000 -0.875000
-0.965000 -0.960000 -0.970000 -0.960000 -0.947000 -0.930000 -0.880200
-0.871100 -0.796700 -0.573100 -0.271000  0.000000

  26        ALPHA-CL PAIRS FOR MACH NUM.=       0.700
ALPHA
   0.000     2.000     4.000     6.000     8.000    10.000    11.000
  12.000    13.000    14.000    15.000    16.500    20.000   340.000
 343.500   345.000   346.000   347.000   348.000   349.000   350.000
 352.000   354.000   356.000   358.000   360.000
CL
 0.000000  0.324500  0.625200  0.736700  0.751300  0.860000  0.923000
 0.940000  0.960000  0.970000  0.980000  0.965000  0.875000 -0.875000
-0.965000 -0.980000 -0.970000 -0.960000 -0.940000 -0.923000 -0.860000
-0.751300 -0.736700 -0.625200 -0.324500  0.000000

  26        ALPHA-CL PAIRS FOR MACH NUM.=       0.750
ALPHA
   0.000     2.000     4.000     6.000     8.000    10.000    11.000
  12.000    13.000    14.000    15.000    16.500    20.000   340.000
 343.500   345.000   346.000   347.000   348.000   349.000   350.000
 352.000   354.000   356.000   358.000   360.000
CL
 0.000000  0.341700  0.636800  0.716900  0.707100  0.845000  0.850000
 0.850000  0.850000  0.840000  0.830000  0.795000  0.730000 -0.730000
-0.795000 -0.830000 -0.840000 -0.850000 -0.850000 -0.850000 -0.845000
-0.707100 -0.716900 -0.636800 -0.341700  0.000000

  26        ALPHA-CL PAIRS FOR MACH NUM.=       0.800
ALPHA
   0.000     2.000     4.000     6.000     8.000    10.000    11.000
  12.000    13.000    14.000    15.000    16.500    20.000   340.000
 343.500   345.000   346.000   347.000   348.000   349.000   350.000
 352.000   354.000   356.000   358.000   360.000
CL
 0.000000  0.367600  0.542800  0.643000  0.700000  0.805000  0.810000
 0.820000  0.815000  0.805000  0.790000  0.760000  0.700000 -0.700000
```

```
-0.760000 -0.790000 -0.805000 -0.815000 -0.820000 -0.810000 -0.805000
-0.700000 -0.643000 -0.542800 -0.367600  0.000000

  26        ALPHA-CL PAIRS FOR MACH NUM.=      0.900
ALPHA
    0.000     2.000     4.000     6.000     8.000    10.000    11.000
   12.000    13.000    14.000    15.000    16.500    20.000   340.000
  343.500   345.000   346.000   347.000   348.000   349.000   350.000
  352.000   354.000   356.000   358.000   360.000
CL
  0.000000  0.124500  0.465000  0.593000  0.695000  0.730000  0.740000
  0.740000  0.735000  0.730000  0.720000  0.700000  0.650000 -0.650000
 -0.700000 -0.720000 -0.730000 -0.735000 -0.740000 -0.740000 -0.730000
 -0.695000 -0.593000 -0.465000 -0.124500  0.000000

  26        ALPHA-CL PAIRS FOR MACH NUM.=      1.000
ALPHA
    0.000     2.000     4.000     6.000     8.000    10.000    11.000
   12.000    13.000    14.000    15.000    16.500    20.000   340.000
  343.500   345.000   346.000   347.000   348.000   349.000   350.000
  352.000   354.000   356.000   358.000   360.000
CL
  0.000000  0.124500  0.465000  0.593000  0.695000  0.730000  0.740000
  0.740000  0.735000  0.730000  0.720000  0.700000  0.650000 -0.650000
 -0.700000 -0.720000 -0.730000 -0.735000 -0.740000 -0.740000 -0.730000
 -0.695000 -0.593000 -0.465000 -0.124500  0.000000
```

```
376 376  2012 (T374) CORR. TO OH-58 LEVEL IN RSWT(BY Y-39)  11/77

    ************************  DRAG TABLE  ********************************

    MAXIMUM POS-NEG ANGLES IN CD-M TABLES
        15.000    351.000

          26        ALPHA VALUES FOR CD VS M
             ALPHA
         0.000       1.000      2.000      3.000      4.000      5.000      6.000
         7.000       8.000      9.000     10.000     11.000     12.000     13.000
        14.000      15.000    351.000    352.000    353.000    354.000    355.000
       356.000     357.000    358.000    359.000    360.000

          9         M-CD PAIRS FOR ALPHA =      0.000
    MACH
         0.300       0.400      0.500      0.600      0.700      0.750      0.800
         0.900       1.000
    CD
      [illegible]  [illegible]  0.008100  0.008200  0.008700  0.009200  0.010900
      0.045800    0.045800

          9         M-CD PAIRS FOR ALPHA =      1.000
    MACH
         0.300       0.400      0.500      0.600      0.700      0.750      0.800
         0.900       1.000
    CD
      0.008100    0.008100   0.008200  0.008200  0.008800  0.009600  0.015400
      [illegible]  [illegible]

          9         M-CD PAIRS FOR ALPHA =      2.000
    MACH
         0.300       0.400      0.500      0.600      0.700      0.750      0.800
         0.900       1.000
    CD
      [illegible]  [illegible]  0.008300  0.008300  [illegible]  0.013700  0.030330
      [illegible]  [illegible]

          8         M-CD PAIRS FOR ALPHA =      3.000
    MACH
         0.300       0.500      0.600      0.700      0.750      0.800      0.900
         1.000
    CD
      0.008570    0.008570   0.008870  0.015870  0.031670  0.047270  0.087770
      0.103770

          8         M-CD PAIRS FOR ALPHA =      4.000
    MACH
         0.300       0.500      0.600      0.700      0.750      0.800      0.900
         1.000
    CD
      0.009150    0.009150   0.009650  0.027950  0.050150  0.065350  0.097050
      0.114050

         10         M-CD PAIRS FOR ALPHA =      5.000
    MACH
      [illegible]    0.300      0.400      0.500      0.600      0.700      0.750
         0.800       0.900      1.000
    CD
```

```
[illegible]  [illegible]  [illegible]  [illegible]  [illegible]  0.053380  0.067880
0.074680  0.113280  0.142280

  9          M-CD PAIRS FOR ALPHA =      6.000
MACH
      0.000      0.400      0.500      0.600      0.700      0.750      0.800
      0.900      1.000
CD
   0.010700  0.010700  0.011000  0.023000  0.067100  0.082900  0.084300
   0.142500  0.172500

  9          M-CD PAIRS FOR ALPHA =      7.000
MACH
      0.000      0.400      0.500      0.600      0.700      0.750      0.800
      0.900      1.000
CL
   0.011550  0.011550  0.016850  0.033650  0.083150  0.103750  0.141750
   0.171750  0.194750

 10          M-CD PAIRS FOR ALPHA =      8.000
MACH
      0.000      0.300      0.400      0.500      0.600      0.700      0.750
      0.800      0.900      1.000
CD
   0.012700  0.012700  0.013600  0.025000  0.044500  0.103900  0.156300
   0.158000  0.186000  0.217000

 10          M-CD PAIRS FOR ALPHA =      9.000
MACH
      0.000      0.300      0.400      0.500      0.600      0.700      0.750
      0.800      0.900      1.000
CD
   0.013200  0.013200  0.016500  0.038100  0.059100  0.118200  0.162000
   0.175000  0.202000  0.235000

 10          M-CD PAIRS FOR ALPHA =     10.000
MACH
      0.000      0.300      0.400      0.500      0.600      0.700      0.750
      0.800      0.900      1.000
CD
   0.018000  0.018000  0.020500  0.056000  0.074000  0.133200  0.179000
   0.189000  0.216000  0.257000

 11          M-CD PAIRS FOR ALPHA =     11.000
MACH
      0.000      0.200      0.300      0.400      0.500      0.600      0.700
      0.750      0.800      0.900      1.000
CD
   0.022600  0.022600  0.026200  0.041000  0.058500  0.138000  0.173000
   0.195000  0.205000  0.235000  0.278000

 11          M-CD PAIRS FOR ALPHA =     12.000
MACH
      0.000      0.200      0.300      0.400      0.500      0.600      0.700
      0.750      0.800      0.900      1.000
CD
   0.025000  0.025000  0.033000  0.037600  0.071000  0.167000  0.201000
   0.214000  0.223000  0.255000  0.294000

 11          M-CD PAIRS FOR ALPHA =     13.000
```

MACH
0.000 0.200 0.300 0.400 0.500 0.600 0.700
0.750 0.800 0.900 1.000
CD
0.029400 0.029400 0.048500 0.059000 0.151000 0.194000 0.219000
0.234000 0.242000 0.275000 0.295000

11 M-CD PAIRS FOR ALPHA = 14.000
MACH
0.000 0.200 0.300 0.400 0.500 0.600 0.700
0.750 0.800 0.900 1.000
CD
0.041000 0.041000 0.083500 0.087500 0.183000 0.215000 0.236000
0.252000 0.253000 0.296000 0.296000

11 M-CD PAIRS FOR ALPHA = 15.000
MACH
0.000 0.200 0.300 0.400 0.500 0.600 0.700
0.750 0.800 0.900 1.000
CD
0.105000 0.105000 0.151000 0.184000 0.212000 0.236000 0.255000
0.274000 0.285000 0.301000 0.301000

10 M-CD PAIRS FOR ALPHA = 351.000
MACH
0.000 0.300 0.400 0.500 0.600 0.700 0.750
0.800 0.900 1.000
CD
0.013200 0.013200 0.016500 0.038100 0.059100 0.118200 0.162000
0.175000 0.202000 0.235000

10 M-CD PAIRS FOR ALPHA = 352.000
MACH
0.000 0.300 0.400 0.500 0.600 0.700 0.750
0.800 0.900 1.000
CD
0.012700 0.012700 0.013600 0.025000 0.044200 0.103900 0.156300
0.158000 0.186000 0.217000

9 M-CD PAIRS FOR ALPHA = 353.000
MACH
0.000 0.400 0.500 0.600 0.700 0.750 0.800
0.900 1.000
CD
0.011550 0.011550 0.016850 0.033650 0.083150 0.103750 0.141750
0.171750 0.194750

9 M-CD PAIRS FOR ALPHA = 354.000
MACH
0.000 0.400 0.500 0.600 0.700 0.750 0.800
0.900 1.000
CD
0.010700 0.010700 0.011000 0.023000 0.067100 0.082980 0.084300
0.142500 0.172500

10 M-CD PAIRS FOR ALPHA = 355.000
MACH
0.000 0.300 0.400 0.500 0.600 0.700 0.750
0.800 0.900 1.000
CD

```
  0.009880  0.009880  0.009780  0.009880  0.012780  0.053380  0.067880
  0.074680  0.113280  0.142280

     8        M-CD PAIRS FOR ALPHA =    356.000
MACH
      0.000     0.500     0.600     0.700     0.750     0.800     0.900
      1.000
CD
  0.005150  0.009150  0.009650  0.027950  0.050150  0.065350  0.097050
  0.114050

     8        M-CD PAIRS FOR ALPHA =    357.000
MACH
      0.000     0.500     0.600     0.700     0.750     0.800     0.900
      1.000
CD
  0.008570  0.008570  0.008870  0.015870  0.031670  0.047270  0.087770
  0.103770

     9        M-CD PAIRS FOR ALPHA =    358.000
MACH
      0.000     0.400     0.500     0.600     0.700     0.750     0.800
      0.900     1.000
CD
  0.0082[illegible]  0.008200  0.008300  0.008300  0.009600  0.013700  0.030300
  0.085[illegible]  0.085200

     9        M-CD PAIRS FOR ALPHA =    359.000
MACH
      0.000     0.400     0.500     0.600     0.700     0.750     0.800
      0.900     1.000
CD
  0.008100  0.008100  0.008200  0.008200  0.008800  0.009600  0.015400
  0.062800  0.062800

     9        M-CD PAIRS FOR ALPHA =    360.000
MACH
      0.000     0.400     0.500     0.600     0.700     0.750     0.800
      0.900     1.000
CD
  0.008000  0.008000  0.008100  0.008200  0.008700  0.009200  0.010900
  0.045800  0.045800
```

```
376 376  0012 (T774) CORR. TO OH-58 LEVEL IN PSWT(BY Y-39)  11/77

    ********************  PITCHING MOMENT TABLE  ************************

    VALUES OF CM FOR MAXIMUM POS-NEG ANGLES
        -0.128      0.128

            26        ALPHA VALUES FOR CM VS M
              ALPHA
         0.000     1.000     2.000     3.000     4.000     5.000     6.000
         7.000     8.000     9.000    10.000    11.000    12.000    13.000
        14.000    15.000    15.500    16.000   244.000   354.000   355.000
       356.000   357.000   358.000   359.000   360.000

        2          M-CM PAIRS FOR ALPHA =       0.000
    MACH
         0.000     1.000
    CM
      0.000000  0.000000

        5          M-CM PAIRS FOR ALPHA =       1.000
    MACH
         0.000     0.750     0.800     0.900     1.000
    CM
      0.000000  0.000000 -0.000300 -0.005900 -0.005900

        6          M-CM PAIRS FOR ALPHA =       2.000
    MACH
         0.000     0.700     0.750     0.800     0.900     1.000
    CM
      0.000000  0.000000  0.006300 -0.005800 -0.107200 -0.107200

        7          M-CM PAIRS FOR ALPHA =       3.000
    MACH
         0.000     0.600     0.700     0.750     0.800     0.900     1.000
    CM
      0.000000  0.000000  0.002500  0.018600 -0.018600 -0.087000 -0.087000

        7          M-CM PAIRS FOR ALPHA =       4.000
    MACH
         0.000     0.600     0.700     0.750     0.800     0.900     1.000
    CM
      0.000000  0.000000 -0.005100  0.020100 -0.023700 -0.102000 -0.102000

        7          M-CM PAIRS FOR ALPHA =       5.000
    MACH
         0.000     0.600     0.700     0.750     0.800     0.900     1.000
    CM
      0.000000  0.000000  0.011900  0.010700 -0.025600 -0.030700 -0.030700

        8          M-CM PAIRS FOR ALPHA =       6.000
    MACH
         0.000     0.500     0.600     0.700     0.750     0.800     0.900
         1.000
    CM
      0.000000  0.000000  0.002300 -0.000900 -0.000600 -0.011800 -0.125000
     -0.125000

        8          M-CM PAIRS FOR ALPHA =       7.000
```

```
MACH
     0.000      0.500      0.600      0.700      0.750      0.800      0.900
     1.000
CM
  0.000000  [illegible]  0.027700 -0.001100  0.000500 -0.112500 -0.136000
 -0.1[illegible]

   9        M-CM PAIRS FOR ALPHA =       8.000
MACH
     0.000      0.400      0.500      0.600      0.700      0.750      0.800
     0.900      1.000
CM
  0.000000  0.000000  [illegible]  0.025500 -0.031100  [illegible] -0.123000
 -0.145000 -0.145000

   9        M-CM PAIRS FOR ALPHA =       9.000
MACH
     0.000      0.400      0.500      0.600      0.700      0.750      0.800
     0.900      1.000
CM
  0.000000  0.000000  0.033000  0.014900 -0.004100 -0.089000 -0.132000
 -0.154000 -0.154000

  10        M-CM PAIRS FOR ALPHA =      10.000
MACH
     0.000      0.300      0.400      0.500      0.600      0.700      0.750
     0.800      0.900      1.000
CM
  0.000000  0.000000  0.001500 -0.002000  0.014000 -0.004100 -0.100000
 -0.142000 -0.163000 -0.163000

  10        M-CM PAIRS FOR ALPHA =      11.000
MACH
     0.000      0.300      0.400      0.500      0.600      0.700      0.750
     0.800      0.900      1.000
CM
  0.000000  0.000000  0.003000 -0.014000 -0.046000 -0.079000 -0.1[illegible]
 -0.149000 -0.170000 -0.170000

  10        M-CM PAIRS FOR ALPHA =      12.000
MACH
     0.000      0.300      0.400      0.500      0.600      0.700      0.750
     0.800      0.900      1.000
CM
  0.000000  0.000000 -0.002000  0.015000 -0.060000 -0.083000 -0.116000
 -0.157000 -0.176000 -0.176000

  10        M-CM PAIRS FOR ALPHA =      13.000
MACH
     0.000      0.300      0.400      0.500      0.600      0.700      0.750
     0.800      0.900      1.000
CM
  0.000000  0.000000  0.009700 -0.050000 -0.074000 -0.093000 -0.122000
 -0.163000 -0.184000 -0.184000

  11        M-CM PAIRS FOR ALPHA =      14.000
MACH
     0.000      0.200      0.300      0.400      0.500      0.600      0.700
     0.750      0.800      0.900      1.000
CM
```

```
 [illegible]  [illegible] -0.127000  0.0 9700 -0.068000 -0.086000 -0.103000
-0.127000 -0.147000 -0.189000 -0.189000

    11          M-CM PAIRS FOR ALPHA =      15.000
MACH
      [illegible]     .200     [illegible]     0.400     0.500     0.600     0.700
      0.750     [illegible]     [illegible]     1.000
CM
  0.000000 -0.054000 -0.065000 -0.073000 -0.084000 -0.097000 -0.111000
-0.173000 -0.173000 - .195000 -0.195000

    11          M-CM PAIRS FOR ALPHA =      15.[illegible]00
MACH
      0.000     0.200     0.300     0.400     0.500     0.600     0.700
      0.750     0.800     0.900     1.000
CM
  0.090000 -0.073000 -0.078000 -0.086000 -0.097000 -0.108000 -0.117000
-0.157000 -0.176000 -0.200000 -0.200000

     2          M-CM PAIRS FOR ALPHA =      16.000
MACH
      0.000     1.000
CM
-0.108000 -0.108000

     2          M-CM PAIRS FOR ALPHA =     344.000
MACH
      0.000     1.000
CM
  0.138000  0.138000

     8          M-CM PAIRS FOR ALPHA =     354.000
MACH
      0.000     0.500     0.600     0.700     0.750     0.800     0.900
      1.000
CM
  0.000000  0.000000 -0.003000  0.016000  0.062500  0.100000  0.125000
  0.125000

     7          M-CM PAIRS FOR ALPHA =     355.000
MACH
      0.000     0.600     0.700     0.750     0.800     0.900     1.000
CM
  0.000000  0.000000  0.005000  0.040000  0.076000  0.102000  0.102000

     8          M-CM PAIRS FOR ALPHA =     356.000
MACH
      0.000     0.500     0.600     0.700     0.750     0.800     0.900
      1.000
CM
  0.000000  0.000000 -0.010400 -0.025400 -0.020300  0.011800  0.102000
  0.102000

     8          M-CM PAIRS FOR ALPHA =     357.000
MACH
      0.000     0.500     0.600     0.700     0.750     0.800     0.900
      1.000
CM
  0.000000  0.000000 -0.007500 -0.012000 -0.013000 -0.016500  0.087000
  0.087000
```

```
    8          M-CM PAIRS FOR ALPHA =     358.000
MACH
     0.000      0.500      0.600      0.700      0.750      0.800      0.900
     1.000
CM
  0.000000  0.000000 -0.000600 -0.007700 -0.009400  0.008100  0.031800
  0.031800

    5          M-CM PAIRS FOR ALPHA =     359.000
MACH
     0.000      0.750      0.800      0.900      1.000
CM
  0.000000  0.000000  0.000400  0.000500  0.000500

    2          M-CM PAIRS FOR ALPHA =     360.000
MACH
     0.000      1.000
CM
  0.000000  0.000000
```

VR-8, 0° Tab, OH-58 Reynolds Number

```
382 382  VR-8 0+ TAB  OH-58 REYNOLDS NUMBER  RKP/LD  12/6/77

      180.       180.  MAX POS ALPHA,MAX NEG ALPHA

    CLIFC       K1          K2          K3          K4      CONTROL NOS.
    [illegible]  1.0000      1.0000      1.0000      1.0000

         10 NO.OF MACH NUMBERS FOR CL VS ALPHA
           MACH NUMBERS
     0.300       0.300       0.400       0.510       0.610       0.710       0.760
     [illegible] [illegible] 1.000

************************  LIFT TABLE  ******************************

    16        ALPHA-CL PAIRS FOR MACH NUM.=      0.000
  ALPHA
     [illegible]  4.000       6.000       8.000       9.000       10.000      12.000
     14.000      [illegible] 340.000     350.000     352.000     354.000     356.000
     358.000     360.000
  CL
   [illegible] 0.510000   0.725000   0.940000   1.010000   1.040000   1.060000
   1.060000   0.950000  -0.650000  -0.810000  -0.705000  -0.540000  -0.350000
  -0.135000   [illegible]

    16        ALPHA-CL PAIRS FOR MACH NUM.=      0.300
  ALPHA
     0.000       4.000       6.000       8.000       9.000       10.000      12.000
     14.000      20.000      340.000     350.000     352.000     354.000     356.000
     358.000     360.000
  CL
   0.080000   0.510000   0.725000   0.940000   1.010000   1.040000   1.060000
   1.060000   0.950000  -0.650000  -0.810000  -0.705000  -0.540000  -0.350000
  -0.135000   [illegible]

    17        ALPHA-CL PAIRS FOR MACH NUM.=      0.400
  ALPHA
     0.000       4.000       6.000       7.000       8.000       9.000       10.000
     11.000      12.000      20.000      340.000     350.000     352.000     354.000
     356.000     358.000     360.000
  CL
   0.090000   0.540000   0.760000   0.860000   0.950000   1.000000   1.030000
   1.040000   1.030000   0.960000  -0.850000  -0.805000  -0.730000  -0.575000
  -0.340000  -0.145000   0.090000

    17        ALPHA-CL PAIRS FOR MACH NUM.=      0.510
  ALPHA
     [illegible] 4.000       6.000       7.000       8.000       9.000       10.000
     12.000      14.000      20.000      340.000     350.000     352.000     354.000
     356.000     358.000     360.000
  CL
   0.095000   0.580000   0.815000   0.920000   1.010000   1.045000   1.060000
   1.050000   1.080000   1.000000  -0.850000  -0.820000  -0.740000  -0.590000
  -0.380000  -0.140000   0.095000

    17        ALPHA-CL PAIRS FOR MACH NUM.=      0.610
  ALPHA
     0.000       4.000       6.000       7.000       8.000       8.500       9.000
     10.000      12.000      20.000      340.000     350.000     352.000     354.000
     [illegible] 358.000     360.000
```

```
CL
  0.100000  0.640000  0.910000  1.050000  1.150000  1.175000  1.150000
  1.170000  1.170000  1.060000 -1.000000 -0.820000 -0.785000 -0.650000
 -0.430000 -0.180000  0.100000

   18        ALPHA-CL PAIRS FOR MACH NUM.=      0.710
ALPHA
     0.000     2.000     4.000     5.000     6.000     7.000     8.000
    10.000    11.000    12.000    20.000   340.000   350.000   352.000
   354.000   356.000   358.000   360.000
CL
  0.140000  0.450000  0.750000  0.900000  0.960000  0.990000  1.080000
  1.230000  1.240000  1.220000  1.370000 -1.190000 -0.900000 -0.[illegible]0000
 -0.800000 -0.540000 -0.185000  0.140000

   12        ALPHA-CL PAIRS FOR MACH NUM.=      0.760
ALPHA
     0.000     2.000     4.000     8.000    15.000    20.000   340.000
   350.000   352.000   354.000   356.000   360.000
CL
  0.140000  0.690000  0.783000  0.932300  1.684000  2.450000 -1.000000
 -0.946000 -0.951000 -0.837000 -0.562300  0.140000

    9        ALPHA-CL PAIRS FOR MACH NUM.=      0.8[illegible]0
ALPHA
     0.000     1.000     2.000     5.000    20.000   340.000   356.000
   358.000   360.000
CL
  0.265000  0.470000  0.570000  0.790000  2.450000 -1.500000 -0.690000
 -0.272500  0.265000

    8        ALPHA-CL PAIRS FOR MACH NUM.=      0.900
ALPHA
     0.000     5.000     8.000    20.000   340.000   354.000   356.000
   360.000
CL
  0.075000  0.455000  1.350000  2.450000 -2.000000 -0.670000 -0.430000
  0.075000

    8        ALPHA-CL PAIRS FOR MACH NUM.=      1.000
ALPHA
     0.000     2.000     4.000    20.000   340.000   355.000   358.000
   360.000
CL
  0.090000  0.370000  0.750000  0.750000 -0.500000 -0.470000 -0.170000
  0.090000
```

```
362 382   VP-R 0+ TAB   OH-58 REYNOLDS NUMBER   RKM/LD   12/6/77

     ***********************  DRAG TABLE  ******************************

     MAXIMUM POS-NEG ANGLES IN CD-M TABLES
          16.000    350.000

             16        ALPHA VALUES FOR CD VS M
               ALPHA
           0.000      1.000      2.000      3.000      4.000      5.000      6.000
           8.000     10.000     12.000     16.000    350.000    356.000    358.000
         359.000    360.000

        7          M-CD PAIRS FOR ALPHA =        0.000
     MACH
           0.000      0.400      0.500      0.610      0.710      0.810      1.000
     CD
        0.009300   0.008430   0.007930   0.008200   0.008270   0.020000   0.050000

        7          M-CD PAIRS FOR ALPHA =        1.000
     MACH
           0.000      0.400      0.500      0.610      0.710      0.810      1.000
     CD
        0.009300   0.008630   0.007930   0.007900   0.007970   0.030000   0.070000

        6          M-CD PAIRS FOR ALPHA =        2.000
     MACH
           0.000      0.400      0.500      0.610      0.710      1.000
     CD
        0.009300   0.008030   0.007930   0.007900   0.007770   0.090000

        6          M-CD PAIRS FOR ALPHA =        3.000
     MACH
           0.000      0.400      0.500      0.610      0.710      1.000
     CD
        0.009300   0.008030   0.007930   0.007900   0.009470   0.110000

        6          M-CD PAIRS FOR ALPHA =        4.000
     MACH
           0.000      0.400      0.500      0.610      0.710      1.000
     CD
        0.009000   0.008030   0.007930   0.008300   0.016800   0.110000

        6          M-CD PAIRS FOR ALPHA =        5.000
     MACH
           0.000      0.400      0.500      0.610      0.710      1.000
     CD
        0.009000   0.008030   0.008330   0.009400   0.038300   0.130000

        6          M-CD PAIRS FOR ALPHA =        6.000
     MACH
           0.000      0.400      0.500      0.610      0.710      1.000
     CD
        0.009000   0.008530   0.009130   0.012900   0.060800   0.150000

        6          M-CD PAIRS FOR ALPHA =        8.000
     MACH
           0.000      0.400      0.500      0.610      0.710      1.000
     CD
```

```
 0.025000  0.021000  0.020900  0.045900  0.100000  0.150000

     6        M-CD PAIRS FOR ALPHA =    10.000
MACH
     0.000      0.400      0.500      0.610      0.710      1.000
CD
 0.075000  0.071000  0.086000  0.156100  0.120000  0.150000

     6        M-CD PAIRS FOR ALPHA =    12.000
MACH
     0.000      0.400      0.500      0.610      0.710      1.000
CD
 0.151000  0.151000  0.166000  0.181000  0.150000  0.150000

     6        M-CD PAIRS FOR ALPHA =    16.000
MACH
     0.000      0.400      0.500      0.610      0.710      1.000
CD
 0.281000  0.281000  0.281000  0.300000  0.150000  0.150000

     6        M-CD PAIRS FOR ALPHA =   350.000
MACH
     0.000      0.400      0.500      0.610      0.710      1.000
CD
 0.141000  0.141000  0.151000  0.161000  0.171000  0.150000

     7        M-CD PAIRS FOR ALPHA =   356.000
MACH
     0.000      0.400      0.500      0.610      0.710      0.810      1.000
CD
 0.017030  0.017030  0.021000  0.023000  0.028000  0.025000  0.130000

     7        M-CD PAIRS FOR ALPHA =   358.000
MACH
     0.000      0.400      0.500      0.610      0.710      0.810      1.000
CD
 0.011000  0.009030  0.008530  0.008500  0.008270  0.011000  0.070000

     7        M-CD PAIRS FOR ALPHA =   359.000
MACH
     0.000      0.400      0.500      0.610      0.710      0.810      1.000
CD
 0.009300  0.008530  0.008430  0.008400  0.008270  0.011000  0.050000

     7        M-CD PAIRS FOR ALPHA =   360.000
MACH
     0.000      0.400      0.500      0.610      0.710      0.810      1.000
CD
 0.009000  0.008430  0.007730  0.008200  0.008270  0.020000  0.050000
```

382 382 VR-8 0* TAB OH-58 REYNOLDS NUMBER RKM/LD 12/6/77

******************** PITCHING MOMENT TABLE ************************

VALUES OF CM FOR MAXIMUM POS-NEG ANGLES
-0.160 0.120

18 ALPHA VALUES FOR CM VS M
ALPHA

0.000	2.000	4.000	6.000	8.000	10.000	11.000
12.000	14.000	15.000	16.000	344.000	350.000	352.000
354.000	356.000	358.000	360.000			

6 M-CM PAIRS FOR ALPHA = 0.000

MACH					
0.000	0.710	0.776	0.850	0.900	1.000
CM					
-0.013500	-0.015100	-0.019200	-0.125000	-0.066000	-0.046000

7 M-CM PAIRS FOR ALPHA = 2.000

MACH						
0.000	0.660	0.753	0.820	0.850	0.900	1.000
CM						
-0.016870	-0.018400	-0.021800	-0.110000	-0.156000	-0.108000	-0.092000

7 M-CM PAIRS FOR ALPHA = 4.000

MACH						
0.000	0.610	0.660	0.718	0.850	0.900	1.000
CM						
-0.019000	[illegible]	-0.017000	-0.025500	-0.205000	0.170000	0.160000

6 M-CM PAIRS FOR ALPHA = 6.000

MACH					
0.000	0.560	0.610	0.670	0.850	1.000
CM					
[illegible]	-0.019500	-0.011000	-0.010000	-0.245000	-0.205000

6 M-CM PAIRS FOR ALPHA = 8.000

MACH					
0.000	0.485	0.580	0.623	0.850	1.000
CM					
-0.029500	-0.017000	[illegible]	-0.004000	-0.245000	-0.255000

7 M-CM PAIRS FOR ALPHA = 10.000

MACH						
0.000	0.200	0.390	0.585	0.750	0.850	1.000
CM						
-0.029500	-0.024000	-0.024000	-0.046000	-0.140000	-0.245000	-0.305000

7 M-CM PAIRS FOR ALPHA = 11.000

MACH						
0.000	0.300	0.500	0.710	0.750	0.850	1.000
CM						
-0.035000	-0.040000	[illegible]	-0.116000	-0.140000	-0.245000	-0.330000

6 M-CM PAIRS FOR ALPHA = 12.000

MACH					
0.000	0.300	0.590	0.750	0.850	1.000
CM					

-0.065000 -0.065000 -0.095000 -0.140000 -0.245000 -0.355000

7 M-CM PAIRS FOR ALPHA = 14.000
MACH
0.000 0.230 0.310 0.585 0.770 0.850 1.000
CM
-0.118000 -0.118000 -0.131000 -0.131000 -0.159000 -0.245000 -0.410000

5 M-CM PAIRS FOR ALPHA = 15.500
MACH
0.000 0.575 0.660 0.850 1.000
CM
-0.155000 -0.145000 -0.162000 -0.245000 -0.435000

2 M-CM PAIRS FOR ALPHA = 16.000
MACH
0.000 1.000
CM
-0.160000 -0.160000

2 M-CM PAIRS FOR ALPHA = 344.000
MACH
0.000 1.000
CM
0.120000 0.120000

4 M-CM PAIRS FOR ALPHA = 350.000
MACH
0.000 0.400 0.760 1.000
CM
0.058000 0.058000 0.095000 0.305000

4 M-CM PAIRS FOR ALPHA = 352.000
MACH
0.000 0.457 0.710 1.000
CM
0.040000 0.040000 0.052000 0.270000

7 M-CM PAIRS FOR ALPHA = 354.000
MACH
0.000 0.610 0.695 0.860 0.900 0.950 1.000
CM
-0.010000 -0.010000 -0.024000 0.110000 0.160000 0.100000 0.100000

7 M-CM PAIRS FOR ALPHA = 356.000
MACH
0.000 0.550 0.660 0.750 0.850 0.900 1.000
CM
-0.010000 -0.010000 -0.017000 -0.030000 0.105000 0.040000 0.052000

7 M-CM PAIRS FOR ALPHA = 358.000
MACH
0.000 0.460 0.610 0.820 0.850 0.900 1.000
CM
-0.017400 -0.013000 -0.011000 -0.016000 0.025000 -0.011000 0.001000

6 M-CM PAIRS FOR ALPHA = 360.000
MACH
0.000 0.710 0.776 0.850 0.900 1.000
CM

-0.013500 -0.015000 -0.019230 -0.125000 -0.066000 -0.046000